Advancing the Mimetic Spectral Element Method

Towards Continuum Mechanics Applications

Joël Marius Fisser

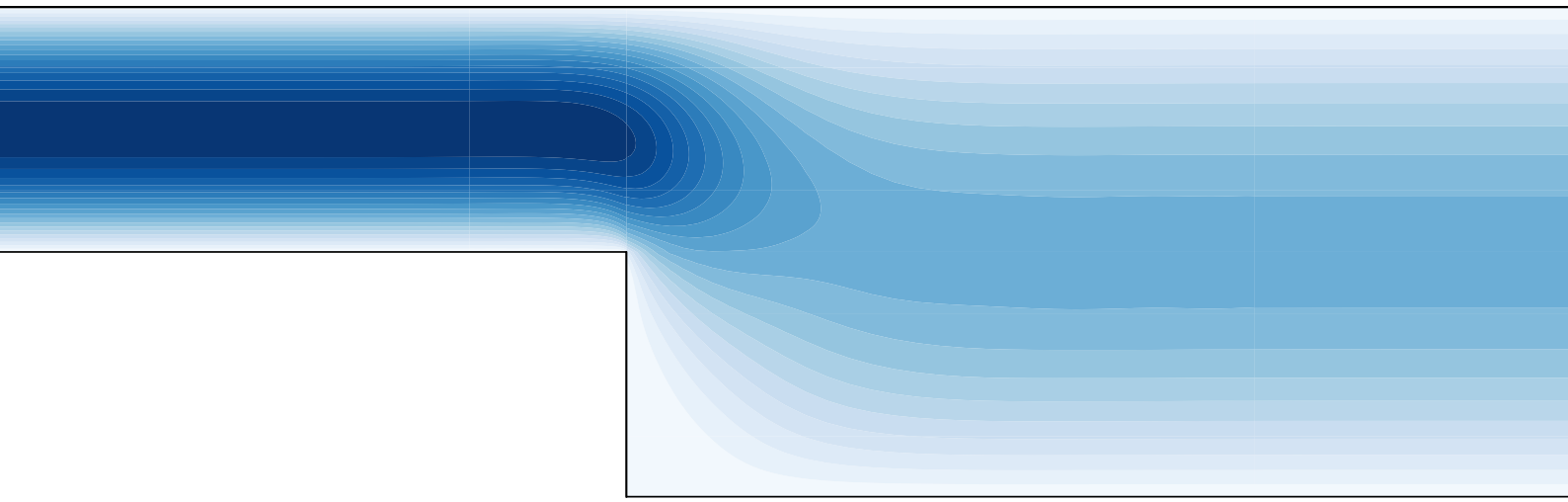

TU Delft

Aerodynamics

Advancing the Mimetic Spectral Element Method

Towards Continuum Mechanics Applications

by

Joël Marius Fisser

to obtain the degree of Master of Science in Aerospace Engineering
at the Delft University of Technology,
to be defended publicly on Thursday February 21, 2019 at 4:00 PM.

Student number:	4290089	
Project duration:	May, 2018 – February, 2019	
Supervisor:	Dr. ir. M. I. Gerritsma	TU Delft
Thesis committee:	Prof. dr. S. Hickel	TU Delft
	Dr. M. Möller	TU Delft
	Ir. V. Jain	TU Delft

An electronic version of this thesis is available at `http://repository.tudelft.nl/`.

TU Delft

Acknowledgements

This thesis is the result of a nine month journey, from which I learned to look in a fundamentally different way at physics and simulations. My interest for the topic of mimetic discretisation was sparked during the course taught by Dr. Marc Gerritsma on discretisation techniques for computational fluid dynamics. His clear way of introducing and motivating these techniques led me to perform my thesis work on the mimetic spectral element method.

I want to thank Dr. Marc Gerritsma for always taking the time to help me with the problems I faced. This thesis work would not have been possible without his dedication and the opportunities he offered. I also want to thank the PhD candidates Varun Jain and Yi Zhang for the insightful discussions and willingness to help, for explaining me the basics and helping me out with the implementation of the method.

Although it was often the subject of jokes or criticism, the basement was a very nice place to work at during the thesis. Many thanks to all the fellow students working there for making that possible and for the interesting discussions and fun we had during lunch and coffee breaks.

Finally, I want to thank my girlfriend, Vibeke, my parents, Ben & Ida, and my brothers and sisters-in-law, Job & Mieneke and Hanjo & Lisa, for the support and good times during my studies. A special mention should go to Arent for the five years of companionship. Who would have thought back then that we would finish the same studies at the same time.

I am truly happy to have come this far and look forward to what the future brings.

Joël Marius Fisser
Delft, February 2019

Abstract

Mimetic discretisation techniques are a growing field in computational physics research. Among these techniques, the recently developed mimetic spectral element method allows for exact discretisation of metric independent relations. This has been proven numerically in various mixed formulations, for instance the mixed velocity-vorticity-pressure formulation for Stokes flow, where mass conservation was point-wise strongly satisfied by the solution in the computational domain. Another example is the mixed stress-displacement formulation for the linear elasticity equations, where the balance law of linear momentum was point-wise strongly satisfied as well. A recent extension to a hybrid method leads to additional attractive features, such as the ability to decompose a large part of the computation of the solution into smaller problems. The aim of the research is to find a formulation for linear elasticity that is hybridisable while strongly satisfying conservation of linear and angular momentum as well, where the combination of linear momentum conservation and symmetry of the stress tensor is equivalent to angular momentum conservation. The proposed formulation has a mixed basis of both primal and algebraic dual nodal and edge basis functions. It fulfils the requirements as it is shown to be hybridisable, to satisfy point-wise linear momentum, and the discrete representation of the stress tensor is point-wise symmetric, hence angular momentum conservation is point-wise satisfied as well. The thesis furthermore functions as an overview of the method applied to elliptic problems, showing the results for previous formulations, and as a starting point for the next steps towards applying the method to fluids. A first step is proposed on extending the new formulation to a Stokes flow formulation with the stress as primary unknown, aimed at satisfying both linear and angular momentum conservation as well as mass conservation.

Contents

1 Introduction

The use of numerical simulation in engineering and research has been steadily increasing due to the developments in the computational power of computers [64]. The scope and complexity of these simulations has been increasing as well, ranging from coupling models from various disciplines to simulations using complex geometries or designs. Nowadays, these numerical simulations are used in many disciplines alongside experimental simulation, motivated by the decreased costs and time required to perform them. The importance of the accuracy and physical correctness of the results is therefore increasing as well, since designs and risk-assessments or decisions are increasingly dependent on these simulations. In recent years, there has been an increasing focus on developing discretisation techniques that are physics-compatible, symmetry-conserving, or mimetic [4, 33, 59]. These techniques take into account the geometric content of the equations describing physics in the process of converting a physical problem into a solvable system of equations. Moreover, the computed quantities are more connected to the geometry, as they not only represent values in points, but also integrated values over lines, surfaces, and volumes. In doing so, the intention is to mimic the relations between the considered discrete quantities and the mathematical relations as close as possible [33], to ultimately improve the accuracy and physical correctness of the results. The mimetic spectral element method [46] is one of the various methods that have been developed recently to achieve this goal.

1.1. Motivation

The main motivation for employing mimetic methods arises from the consequences of the limited extent to which conventional methods address the geometric content of the problem. Take for instance the simplest continuum mechanics problem, the problem of linear elasticity. Three mathematical relations describe the problem,

$$\nabla \cdot \underline{\underline{\sigma}} + \mathbf{f} = 0, \tag{1.1}$$

$$\underline{\underline{\sigma}} = \underline{\underline{\sigma}}^T, \tag{1.2}$$

$$\nabla \mathbf{u} = \frac{1}{2}\left(\nabla \mathbf{u} + (\nabla \mathbf{u})^T\right) + \frac{1}{2}\left(\nabla \mathbf{u} - (\nabla \mathbf{u})^T\right) = \underline{\underline{\epsilon}} - \underline{\underline{\mathrm{W}}}. \tag{1.3}$$

The first equation is the linear momentum balance equation, also called the equilibrium equation, stating that the divergence of the stress tensor $\underline{\underline{\sigma}}$ is equal to the body force $\mathbf{f}$. The second equation states that the stress tensor is symmetric. The third equation shows the compatibility relation between the strains and the displacements $\mathbf{u}$. These three equations describe the relation between displacements and strains on the one hand, and stresses and forces on the other hand. They can be considered as exact truth, completely known or topological, independent of the specific problem at hand.

One additional equation is required to relate the stresses to the strains,

$$C\underline{\underline{\sigma}} = \underline{\underline{\epsilon}}, \tag{1.4}$$

which is the constitutive relation or stress-strain relation, with C the compliance tensor and $\underline{\underline{\epsilon}}$ the strain tensor. In contrast, this physical relation linking the stresses to the strains represents an idealised model, a

generalisation of the real material, which depends on metric. The model may not be general but only valid for certain situations. Furthermore, the body forces may not be known exactly but come from measurements, and similarly, the boundary conditions may only be approximated.

When considering a numerical method to obtain a solution to these equations, it would be desirable that the only errors made arise from the uncertainty in the constitutive relation and inputs to the equations, since the other relations are known beforehand. Also, it would be best to solve the equations separate from each other, such that the constitutive relations stay separate from metric independent relations as well. However, this is not ensured from the outset by methods widely used for the discretisation of partial differential equations which arise in continuum mechanics problems [7]. Three of such methods are the finite difference, finite volume and finite element method, which differ mainly in their starting formulation but have central themes in common. These methods are considered here in particular because most of computational physics research and engineering is based on them [7], although there are of course many other methods not mentioned here. A brief general overview of these methods, in light of the framework at hand, now follows.

A finite difference method starts from the continuous partial differential equations. The derivatives are approximated directly using a local stencil, most conveniently on a structured mesh. Examples of stencils often used for one-dimensional problems are the upwind, downwind, and central difference schemes. Similar stencils for higher dimensional derivatives exist. The truncation error introduced for a particular stencil can be analysed with Taylor expansions, such that the choice of stencil determines the rate at which the truncation error decreases when the mesh is refined. Thus, the relations from vector calculus exactly known in the continuous formulation are represented by an approximated relation locally, which should converge to the continuous relation as the mesh is refined. In addition to the error introduced by the model and input, an error is made in representing the exact relations.

Alternatively, when considering the natural integral form of a partial differential equation directly, a finite volume method can be constructed, where the degrees of freedom are represented by volume averages at some chosen centre location in the cells, inducing fluxes between cells. The fluxes can be computed by means of numerical interpolation, based on the defined location of the centres of the cells. This has the advantage of approximating the divergence theorem more naturally, as the sum of the fluxes should be equal to the change in the volume. This indicates that the choice of degrees of freedom influences the way the equations are translated into a discrete setting, yet still errors are made in representing exact relations. For instance, the constitutive law may be inserted into the balance equations, such that the quantities solved for are field quantities like velocity, mixing the errors in the process. In addition, the computation of fluxes may introduce additional errors.

Finally, the finite element method is based on rewriting the equations using the Galerkin method in a weak form with test functions. In some cases, the weak form can be derived from an appropriately chosen Lagrangian functional. The trial and test functions are expanded using an appropriately chosen set of basis functions which have compact support, i.e. they are only non-zero locally (within the elements). The corresponding weights of these basis functions are the degrees of freedom, and together with the selected basis represent the solution. This method is easily applicable for both structured and unstructured meshes, hence it allows for mesh flexibility and thus handling complex geometries. Instead of taking local basis functions, in spectral methods one takes a basis that spans the full domain, trading mesh flexibility again for accuracy. The mimetic spectral element method is closely related to this method, but with emphasis on a choice of basis with geometric considerations in mind.

Some observations can be made with regard to the common use of these methods. First, the quantities of interest are more or less disconnected from the geometry [33]. The methods alone provide no guiding structure on the representation of computed variables. For example, arbitrary basis functions can be selected in the finite element method. The choice of how to represent the computed variables may however largely determine the performance [6]. A prime example of geometric consideration aiding stability is the staggered scheme in finite difference methods for fluid flows, in which the pressure and velocity are taken at different locations in a checkerboard formation ensuring a stable scheme [6]. Furthermore, it is known that stability issues such as non-physical modes arise when the discrete operators do not possess the same properties as the continuous operators they mimic [59].

In addition, the methods provide no clear separation between topological and metric aspects. As shown in the example of linear elasticity, the uncertainty in the continuous equations is clearly localised in the constitutive model and inputs. If this is not taken into account when discretising the equations, also no clear separation exists between the error contribution of modelling, discretisation, and stability error [40]. By contrast, the underlying geometrical description on which the mimetic methods are based, allows to separate

clearly which relations are topological or exact, and which relations depend on metric [6].

The most important consideration when dealing with problems in physics, e.g. continuum mechanics as considered in this work, is that the solution should capture the physics of the problem as well as possible. In other terms, fundamental laws such as the balance law of linear momentum seen in the example of linear elasticity or conservation of mass should always hold. When solving mathematical problems numerically, like the Poisson problem, the quality of the solution from the numerical method is usually assessed in terms of accuracy, stability, and consistency: An appropriately chosen method should be stable and consistent to converge to the right solution. However, while the method may still be convergent when applied directly to continuum mechanics problems, the fundamental laws are usually only weakly satisfied. In order to satisfy these laws strongly, an explicit constraint needs to be posed on the solution, separate from the constitutive law.

If the conservation laws are only weakly satisfied, fine meshes and thus more expensive simulations are in turn needed for a physical simulation. In fluid dynamics for example, conservation of mass is given by the continuity equation, which is one of the key concepts. When using the conventional numerical methods, this means that in case the mesh is not refined enough, mass conservation is not satisfied. In the example for linear elasticity, the force equilibrium may not hold locally [21, p. 3]. The results may then be non-physical without a clear indication from error analysis of the numerical implementation of the mathematical formulation alone. It is out of the question that extreme caution is needed when judging this to prevent that non-physical results are used [58].

To overcome the mentioned limitations, it is therefore considered important to reconsider the translation between the equations and their discrete representation. This is the true aim of the mimetic discretisation methods, to conserve as much as possible of the symmetry, and physical and geometrical structures in the translation of a continuous physical problem to a discrete formulation [46, p. 5]. By following this guiding framework, the correct steps to arrive at a physical discrete representation can be taken, which gives a clearer view on the limitations of this discrete representation as well.

1.2. Thesis outline

The aim of this research is to document the steps taken in the search for a formulation using the mimetic spectral element method, with an implementation based on linear elasticity, that can be extended to fluid problems such as Stokes flow. Such a formulation would be the first step towards solving the Navier-Stokes equations with desirable conservation properties that this method will be shown to have. The first steps to be taken in this direction are in the application of the mimetic spectral element method to linear elasticity and Stokes flow. The main question that will be answered is:

"Is it possible to find a formulation for the mimetic spectral element method applied to the linear elasticity problem, that is hybridisable and strongly conserves both linear momentum and angular momentum?"

The steps in the process of answering this question form the road map of this thesis. Several questions accompany these steps. The first question is, who have built the framework for the method to be derived, and which works are relevant to understand the reasoning behind using it? Then, what are the prerequisites for the implementation of the mimetic spectral element method? Furthermore, which problems have been considered already using this method until now, and what has been found? When can a formulation be hybridised? And, what are the considerations for the choice of solution representation in applying the method to continuum mechanics problems, keeping conservation properties in mind? In each part of this thesis, the answer to these questions is found. In Fig. 1.1, an overview of the parts in the thesis is shown.

This thesis starts with explaining the line of thinking that allows to eventually exploit the concepts from exterior calculus and algebraic topology in the construction of a mimetic discretisation method such as the mimetic spectral element method. This is done through presenting the main works studied and their findings. These concepts are described in Chapter 2. The discrete analogs to these concepts that lead to the mimetic spectral element method are studied conceptually here as well, and a brief overview of works in this field employing these concepts is given. The current state of application of these ideas using the method at hand is introduced. Finally, an elaboration is given on the relation between the recently developed hybrid method to other discontinuous methods.

Then, in Chapter 3, a summary of mathematical ingredients necessary to implement the mimetic spectral

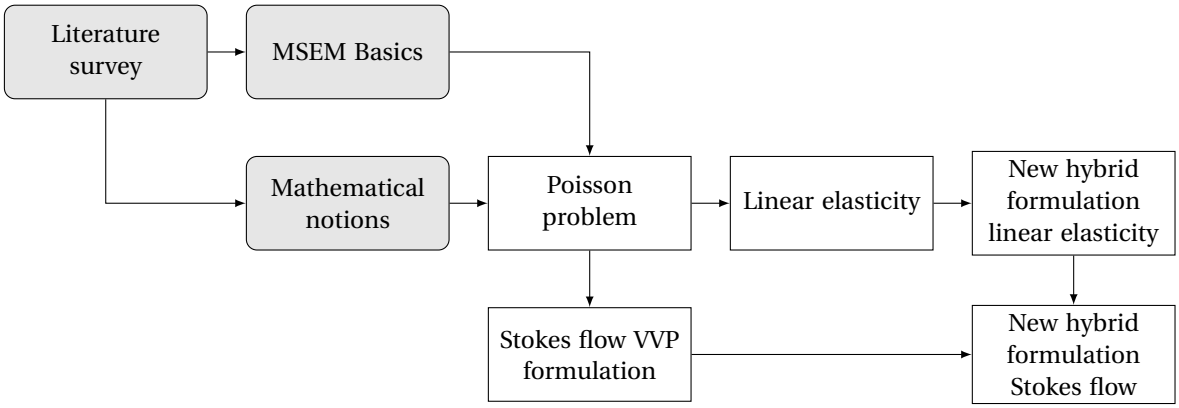

Figure 1.1: Road map of the thesis.

element method is given. It serves as an introduction to the most relevant basics of the method. Furthermore, other mathematical topics such as mappings, problem formulation in Lagrangian form, and error norms will be shortly elaborated on. The mixed formulations that are considered in this thesis comprise the Poisson equation, the Stokes Flow equations with vorticity introduced explicitly, and the linear elasticity equations. They are derived in Chapter 4, Chapter 5 and Chapter 6, respectively. A proposed new formulation is presented with initial results in Chapter 7, and it is extended to fluids in Chapter 8. The basic build-up of these chapters is motivated as follows.

First, the basics of the mimetic spectral element method have to be understood in more detail. This is done by reproduction of results for a basic problem, solving the Poisson problem. In this way, the general workings and implementation have been studied. Two test cases (the manufactured solution and L-shaped domain) then verify that the method is implemented correctly and converges as expected for both smooth and non-smooth solutions. Next, to reproduce the results for comparison of formulations later on, the problem of Stokes flow in the velocity-vorticity-pressure formulation, [47], has been implemented and tested on two test cases, verifying again that the implementation is correct. An additional test case was also performed, which showed new results for this formulation to be compared with other methods. The implementation of the problem of linear elasticity in a recent formulation was the last step in the process of verifying the method. At the start of this work, this formulation was still in development. The formulation is comparable to the existing documented formulation in [53], but it differs in the sense that the symmetry of the stress tensor is imposed by the constraint of angular momentum conservation instead. In the existing formulation, symmetry of the shear stresses was imposed. Therefore, this formulation is considered, documented, and examined in this work to provide a full overview. The new formulation for linear elasticity uses the symmetry constraint, but with a different use of basis. The conservation properties of this new method will be shown. Furthermore, it is shown that this new formulation is compatible with the hybrid method that will be discussed in Section 2.3.4, answering the research question at hand. Finally, a first attempt to extend the new formulation to fluids is taken. The constitutive law changes, and mass conservation is added as an extra constraint on the minimisation. It will be shown that also this formulation is hybridisable.

For these chapters, the results and error analysis of each of these formulations are presented separately in each chapter. To compare and verify the results, several test problems are considered. The problems for which analytic solutions are available aid in the verification of the method, and are necessary for evaluating the (predicted) error norms for convergence testing. The error convergence is studied in detail, while the conditions for point-wise conservation of mass, linear momentum, and angular momentum are elaborated on. The thesis ends with the conclusions drawn on the research question and formulations, and recommendations for directions in continuing the work on this method.

2

Literature Survey

This chapter is mainly based on overviews written on the reasons for the application of concepts from exterior calculus and algebraic topology to physics. The start and initial development of the mimetic discretisation methods is described and motivated. Furthermore, the application of algebraic topology to extend this to the discrete setting is discussed. Insights on operations on the differential forms from exterior calculus then lead to the ingredients for a mimetic discretisation. These are explained as they are implemented in the mimetic spectral element method. This method is further elaborated on through examples of recent applications. Some considerations and possibilities in the formulation of the Stokes flow and linear elasticity problems follow, and the survey is concluded with a short discussion on the development of the hybrid method.

2.1. Pioneers and development

The methods for mimetic discretisation are based on the framework of describing physics by means of notions from exterior calculus. The first work in this framework was performed by Tonti [68], and Dodziuk [26], and in recent years the concepts have been explored theoretically and motivated by Bossavit [11, 66], Mattiussi [51], Bochev & Hyman [7], Hiptmair [40], Robidoux & Steinberg [63], and the different implementations of mimetic discretisation by Perot & Zusi [59], Arnold, Falk & Winther [4, 5], Lipnikov, Manzini & Shashkov [49] and Brezzi & Buffa [14], Palha, Kreeft & Gerritsma [32, 47], amongst others.

Some of the first mathematicians to explore exterior calculus were Grassmann (exterior or Grassmann algebra), Poincaré (homology and duality), and Cartan (differential geometry). The concept of using exterior calculus to describe physics is certainly not new. Establishing this connection was for example explored early by Flanders [30].

In the theory of exterior calculus, relations between differential forms are studied, which are in essence field quantities associated to geometry, allowing for a geometric description of physics. Describing physics in terms of these differential forms can be argued to be advantageous over using vector or tensor calculus, which will be explained in this section. Additionally, through algebraic topology, the concepts of exterior calculus can be translated naturally into a discrete method [7].

This section contains the main findings of the first development in this line of thinking. It starts with a brief summary of the reasoning behind introducing an alternative to the normal vector calculus given in [70], followed by a brief introduction on the use of differential forms, an overview on the construction of a De Rham complex, and finally the link to discrete methods through algebraic topology.

2.1.1. Relating physics to geometry

In the differential formulation of a problem (e.g. a partial differential equation) an exact solution to the problem is possible in specific cases in the form of an analytic solution. This concept arises from the use of the mathematical notion of a limit. When dealing with reality and real problems, the solutions from numerical computations are only approximate and within some set tolerance. It is not possible to measure with perfect accuracy, let alone end up with an exact real number as is the case when taking a mathematical limit. There is thus a separation between physically relevant and mathematical solutions.

In this view, Tonti [70] gives a list of useful notions for this new starting point for computational physics. Of these, the classification of variables through the association to geometry, as well as the notion of cell com-

plexes and orientation and the association of variables to these, and a reformulation of a physical problem are highlighted here.

The quantities that are measured in experiments are domain variables, values assigned to geometry, such as displacement to points, force to surfaces or volumes, mass to volumes, etc. The necessary quantities for describing a system in differential formulation are field values, like density, velocity, or pressure. However, these are not directly measurable, but are a mathematical abstraction, arising only from a limiting process, something that is not possible with the approximate measurements. It is therefore argued better to work with the discrete quantities from the start, and use the geometrical and topological relations between them.

As explained, the global domain variables are assigned to geometry in the form of integral quantities. Furthermore, a distinction should be made between source and configuration variables. The source variables, such as forces, affect the configuration variables, such as velocity fields, introducing the need of a constitutive law, for example using an empirically determined constant. The relation between source variables and configuration variables is not topological and can only be represented by introducing metric [33]. The relations between source variables and between configuration variables is metric free.

In [68], one of the first comparisons is made of different physical theories that seem to have similar mathematical structure. The comparable quantities for computation, which are given different names in various applications such as fluid flow or electromagnetism, can be attributed to two different sets of geometry or *cell complexes*. These sets are called the primal and dual complex [70]. The positioning of various quantities (the domain and configuration variables) on the geometric components of a complex is called a classification diagram (or Tonti diagram). The addition of physical constitutive laws to a classification diagram is called a factorisation diagram [51]. The diagrams for numerous physics disciplines have been worked out in [69], and play an important role in capturing the symmetries of a physical system. Using these as guideline, the topological relations can be seen separate from the metric dependent, constitutive relations, which is of great advantage when the relations are considered at the discrete level.

The *orientation* of the complexes the variables are associated with plays an important role in the classification of the physical variables [70]. It is important to distinguish between two types of orientation, inner orientation and outer orientation. In Fig. 2.1, the orientation for objects in a two-dimensional domain is depicted. The two types of orientation are assigned to a primal and dual cell complex. Note that the names primal and dual are assigned arbitrarily, and apart from distinguishing between the two complexes, there is no predefined order. It can be seen that the inner orientation concerns the direction within or along geometric objects, while the outer orientation concerns directions through and around these objects.

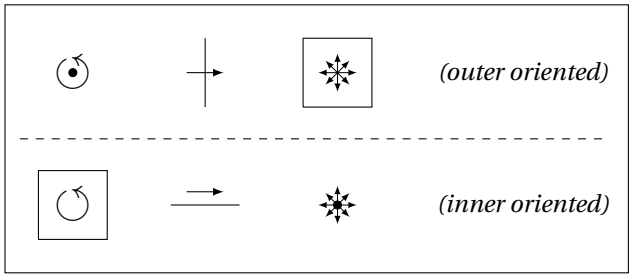

Figure 2.1: Inner and outer orientation of geometric objects in $\mathbb{R}^2$.

In three dimensions, there is a difference between vectors associated to lines such as circulation and vectors associated to surfaces such as fluxes, and between values in points such as temperature or displacement or density and values that represent a volume total such as energy or mass [59]. An argument from fluid mechanics for using the notions of orientation and cell complexes is the description of velocity. The velocity can be seen in inner orientation as the circulation, the integral of the velocity along a line. Alternatively, the velocity is found in an outer orientation as the flux, the integrated velocity through a surface. Considering orientation provides a tool to find the correct interpretations of a physical quantity.

This is important, because in this example, different quantities are related to the inner and outer oriented velocity. In the first, the rotation or vorticity, the curl of the velocity, should be taken as the total circulation (the inner oriented velocity) in a plane in the inner orientation, and represented by an integral quantity over a plane. The divergence of the velocity is taken in the outer orientation as the total flux in and out of a volume, but again represented by an integral quantity over a volume, which could be the mass flux. Note that it is possible to represent displacement or velocity as vector-valued quantities in points as well if stress is the

primary unknown, which will be done in Chapter 6.

2.1.2. Using differential forms to describe physics

Central to the mimetic discretisation framework is the relation between physical quantities and the geometric objects. By using the language of differential forms that exterior calculus provides, a clear distinction between physical quantities can be made from the geometry they are associated to, something which is not always the case for conventional vector calculus notation. Instead of considering point-wise quantities alone, quantities called differential forms can be used to represent physical quantities. Distinctions between the quantities that live on the two cell complexes in terms of orientation can be made in the language of differential forms easily as well. In this section, a short overview on differential forms is given that serves as a brief introduction, other more elaborate introductions to the topic with mimetic discretisation in mind can for instance be found in [6], [33], and [57].

What are these forms conceptually? Flanders introduces forms as "the things which occur under integral signs" [30, p. 1], while Hiptmair describes them more concretely as "mappings assigning values to oriented manifolds of different dimensions" [40, p. 266]. A manifold is the most general description of space in n dimensions, where Euclidean space is the most familiar particular case [31, p. 3]. The reason differential forms are associated to manifolds instead of Euclidean space is that in the definition of manifolds, there is no metric involved [31, p. 18]. Hence, the relations between forms are metric-independent. In some sense comparable to a vector field, a form does not represent a single component of geometry, but rather all components with the same dimension, e.g. points, lines, surfaces, etc. [57]. So in the description of a form, the functions associated to the geometric basis are called *vector proxies*, which are the only part normally considered in vector calculus [33].

It is important to distinguish between exterior forms and differential forms. Exterior k-forms are k-linear and anti-symmetric mappings from k-dimensional space (vectors) to the space of real numbers [6]. This assigns a value or proxy to the object spanned by the vectors. Next to addition and subtraction, multiplication of exterior forms is possible through the exterior product to create forms up to $k \leq n$. Exterior forms represent components of geometry spanned by vectors in Euclidean space. Differential forms are an application of these exterior forms to more general differentiable manifolds through the definition of the tangent vector. That means that the differential forms inherit the properties of exterior forms, including the exterior product, while introducing the operations of differentiation and integration. The differential form possesses an exterior form part, that transforms combinations of tangent vectors to values, and a proxy part that applies a spatially varying modification of the value [6].

A brief summary of the description of differential forms as explained in [57] follows, the notation used here is the same. By definition, any vector $\mathbf{v}$ in a vector space V located on a point p in a manifold $\mathcal{M}$ can be expanded using a basis of linear independent basis vectors from a vector space. A tangent vector is the derivative at p on a curve through p in $\mathcal{M}$. For an n-dimensional manifold, a basis of n tangent vectors is associated to n curves through this point, which form the tangent space $\mathcal{T}_p\mathcal{M}$, which is a linear vector space. A tangent bundle $\mathcal{T}\mathcal{M}$ is the collection of tangent spaces $\mathcal{T}_p\mathcal{M}$ at all points p in $\mathcal{M}$.

Then, given any linear vector space V, a dual vector space V' can be associated to it. This dual space contains co-vectors $\alpha \in V'$, linear functionals acting on the vectors $\mathbf{v} \in V$. These are the exterior forms, acting on the basis vectors. Co-vectors can be formulated in the dual space of the tangent space in a similar way as done for the vector space V, since the tangent space $\mathcal{T}_p\mathcal{M}$ is always a linear vector space. This is then called the cotangent space, $\mathcal{T}_p^*\mathcal{M}$. The collection of cotangent spaces of all points is called a cotangent bundle. A section of this cotangent bundle is a differentiable 1-form or basic 1-form [57], denoted in this report by $\mathrm{d}x$ and $\mathrm{d}y$ in $\mathbb{R}^2$.

A form that is differential and given for every point in $\mathcal{M}$ is called a k-form on $\mathcal{M}$ [6], where k is the dimension of the associated geometry. The k-forms are anti-symmetric tensors. To construct them, the wedge product that acts on basic 1-forms is needed. The space of k-forms in Ω is denoted by $\Lambda^{(k)}(\Omega)$. For example, the wedge product of two basic 1-forms creates a differential 2-form. In n dimensions, there are therefore $(n+1)$ different differential forms possible.

Multiplication of basis forms through the exterior product or *wedge product* is thus needed to construct differential k-forms [33]. The multiplication of forms in the same space is possible through this wedge product $\wedge$, a mapping that takes two forms and produces another form, where [33]

$$\wedge : \Lambda^{(k)}(\Omega) \times \Lambda^{(l)}(\Omega) \longrightarrow \Lambda^{(k+l)}(\Omega).$$

This operation is metric independent in case it is performed on forms on the same oriented manifold. The ex-

terior product is skew-symmetric, which means that it changes sign if the order changes and is zero whenever two components are equal, i.e. acting on the basis forms [33],

$$\begin{aligned} \mathrm{d}x \wedge \mathrm{d}x &= -\mathrm{d}x \wedge \mathrm{d}x = 0, \\ \mathrm{d}x \wedge \mathrm{d}y &= -\mathrm{d}y \wedge \mathrm{d}x. \end{aligned}$$

Note that it is common to write shorthand, $\mathrm{d}x\mathrm{d}y = \mathrm{d}x \wedge \mathrm{d}y$. The wedge product is furthermore multilinear, distributive, and associative [30, p. 9], thus the second relation follows directly from the first relation, as

$$0 = \big(\mathrm{d}x \wedge \mathrm{d}y\big) \wedge \big(\mathrm{d}x \wedge \mathrm{d}y\big) = \mathrm{d}x \wedge \mathrm{d}x + \mathrm{d}x \wedge \mathrm{d}y + \mathrm{d}y \wedge \mathrm{d}x + \mathrm{d}y \wedge \mathrm{d}y = \mathrm{d}x \wedge \mathrm{d}y + \mathrm{d}y \wedge \mathrm{d}x.$$

As this work only considers two-dimensions, in $\mathbb{R}^2$, inner oriented k-forms are denoted [33], for $k = 0,1,2$ respectively, with the basis forms $\mathrm{d}x$ and $\mathrm{d}y$, as

$$\begin{aligned} \alpha'^{(0)} &= \overline{a}(x,y), \\ \beta'^{(1)} &= \overline{b_1}(x,y)\mathrm{d}x + \overline{b_2}(x,y)\mathrm{d}y, \\ \gamma'^{(2)} &= \overline{c}(x,y)\mathrm{d}x \wedge \mathrm{d}y. \end{aligned}$$

The prime denotes that the space of inner oriented forms is considered to be the dual space here, this will be clarified later in Section 2.1.3. The functions of (x,y) are called vector proxies, since these are usually used only in vector calculus for representing physical quantities. The connection to the geometry is clear when integrating these forms, showing the concept of *duality pairing*. The integration of the forms is done over a series of points $\mathcal{P}$, a line $\mathcal{L}$ or a surface $\mathcal{S}$, and denoted by [33]

$$\begin{aligned} \int_{\mathcal{P}} \alpha'^{(0)} &= \sum_{\mathcal{P}} \overline{a} = \langle \alpha'^{(0)}, \mathcal{P} \rangle, \\ \int_{\mathcal{L}} \beta'^{(1)} &= \int_{\mathcal{L}} \overline{b_1}(x,y)\mathrm{d}x + \overline{b_2}(x,y)\mathrm{d}y = \langle \beta'^{(1)}, \mathcal{L} \rangle, \\ \int_{\mathcal{S}} \gamma'^{(2)} &= \int_{\mathcal{S}} \overline{c}(x,y)\mathrm{d}x \wedge \mathrm{d}y = \langle \gamma'^{(2)}, \mathcal{S} \rangle. \end{aligned}$$

2.1.3. The De Rham complex

Now, it will be shown that differential forms can be related with the theory from Tonti, where orientation and complexes are used to structure the physical quantities. The differentiation of forms allows to construct a De Rham complex that depicts the topological relations between physical quantities of the same orientation. With the introduction of the Hodge operator, the quantities of inner and outer orientation of different De Rham complexes can be related as well, though this relation is always metric dependent.

The differentiation of forms is possible through the *exterior derivative*. The exterior derivative applied to forms in $\mathbb{R}^n$ maps forms as [33]

$$\mathrm{d} : \Lambda^{(k)}(\Omega) \longrightarrow \Lambda^{(k+1)}(\Omega), \quad k < n.$$

It acts as the gradient, curl, and divergence operator depending on the form it is applied to, as it arises from the duality pairing of a form on a boundary and its derivative in the enclosed manifold by this boundary [57],

$$\int_{\mathcal{M}_{k+1}} \mathrm{d}\lambda^{(k)} = \int_{\partial\mathcal{M}_{k+1}} \lambda^{(k)}.$$

This pairing is formalised in the (Generalised) Stokes Theorem [33], also introduced in [30, p. 2] as the general Stokes' formula. The generalised Stokes theorem equivalently links the exterior derivative to the geometry through duality pairing by [33, 57]

$$\langle \mathrm{d}\lambda^{(k)}, \Omega \rangle = \langle \lambda^{(k)}, \partial\Omega \rangle.$$

It thus combines the well-known Newton-Leibniz or Gradient theorem, Gauss' or Divergence theorem, and the Kelvin-Stokes or Curl theorem into a unified theorem [47]. The exterior product is furthermore metric independent and nilpotent [57], for any differential form $\alpha^{(k)}$, $\mathrm{d}\mathrm{d}\alpha^{(k)} = 0$, which depending on the differential form can mean $\nabla \cdot \nabla \times \mathbf{a} = 0$ or $\nabla \times \nabla a = 0$, which are the well-known identities from vector calculus.

For the previously introduced inner-oriented forms in Section 2.1.2,

$$\begin{aligned}
\mathrm{d}\alpha'^{(0)} &= \frac{\partial \overline{a}}{\partial x}\mathrm{d}x + \frac{\partial \overline{a}}{\partial y}\mathrm{d}y,\\
\mathrm{d}\beta'^{(1)} &= \left(\frac{\partial \overline{b_2}}{\partial x} - \frac{\partial \overline{b_1}}{\partial y}\right)\mathrm{d}x\mathrm{d}y,\\
\mathrm{d}\gamma'^{(2)} &= 0.
\end{aligned}$$

The exterior derivative acts on forms in the same way the gradient, curl, and divergence operators act on scalars, vectors and pseudo-vectors. Applying the exterior derivative to the n-form leads to the null-space. Differential forms on a single cell complex are thus related topologically through the exterior derivative operator.

The differential forms are associated to the geometric components of the two complexes with the two type of orientation. Forms on both complexes can be related through the *Hodge operator*, which represents a constitutive law of physics [69]. This operator is approximate and metric dependent. It is the conversion by a Hodge operator between the primal and dual that introduces the metric part (and therefore approximation or discretisation error) of the equations. The Hodge-$\star$ operator maps k-forms onto $n-k$-forms [33],

$$\star : \Lambda'^{(k)} \longrightarrow \Lambda^{(n-k)}.$$

Here, the prime on the first form denotes that it is in the dual space of the latter form. Since there is no predefined order in the spaces, in the formulations discussed in Chapter 4, Chapter 5 and Chapter 6 the outer oriented space is taken as the primal space, hence a prime denotes an inner oriented variable. A full definition for the Hodge operator is given in [67, p. 436], where it is defined using the exterior product. The most relevant result is that this operator can be applied to the basis forms, such that in $\mathbb{R}^2$, $\star\,\mathrm{d}x = \mathrm{d}y$, $\star\,\mathrm{d}y = -\mathrm{d}x$, $\star\,\mathrm{d}x\mathrm{d}y = 1$, and $\star\,1 = \mathrm{d}x\mathrm{d}y$. The inner oriented forms can now be associated to the outer oriented forms, with

$$\begin{aligned}
\star\,\alpha'^{(0)} &= \overline{a}(x,y)\mathrm{d}x\mathrm{d}y = \alpha^{(n)} = \alpha^{(2)},\\
\star\,\beta'^{(1)} &= \overline{b_1}(x,y)\mathrm{d}y - \overline{b_2}(x,y)\mathrm{d}x = \beta^{(n-1)} = \beta^{(1)},\\
\star\,\gamma'^{(2)} &= \overline{c}(x,y) = \gamma^{(n-2)} = \gamma^{(0)}.
\end{aligned}$$

It is thus possible to describe a vector proxy in terms of forms of different order and orientation [40]. This is also clear in the example from fluid dynamics, where the velocity can be associated to both 1-forms (inner-oriented circulation) and $(n-1)$-forms (outer-oriented flux). Starting from points, one can draw up a *De Rham complex*, see Fig. 2.2 for two De Rham complexes, one for each orientation. It shows the relation between points and lines, and lines and surfaces through the same exterior derivative operator [66]. The double De Rham complex then summarises the actions of both the exterior derivative and Hodge operators. As the

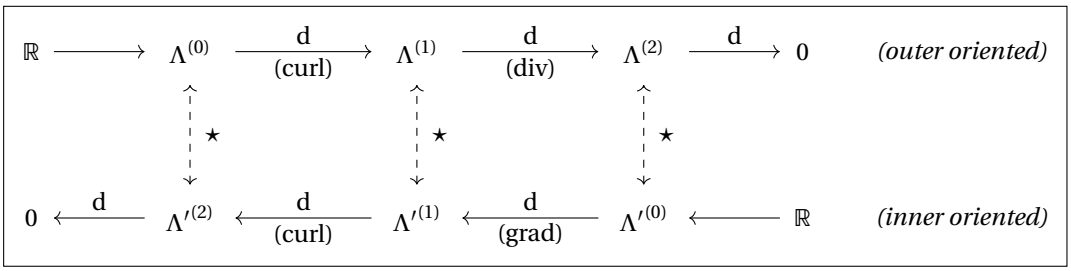

Figure 2.2: Double De Rham complex summarising the forms and operators in $\mathbb{R}^2$ [33].

complex changes in terms of relations for $\mathbb{R}^3$, since then volumes are added, Fig. 2.3 is shown that depicts this as well. Here, the full sequence (gradient, curl, divergence) is observed for both orientations.

2.1.4. Combining ideas from exterior calculus to algebraic topology

The insights of Tonti are combined with the introduced differential forms in Bossavit's Japanese papers (for instance [12]) in the context of electromagnetism, where it is introduced as a network of first order differential

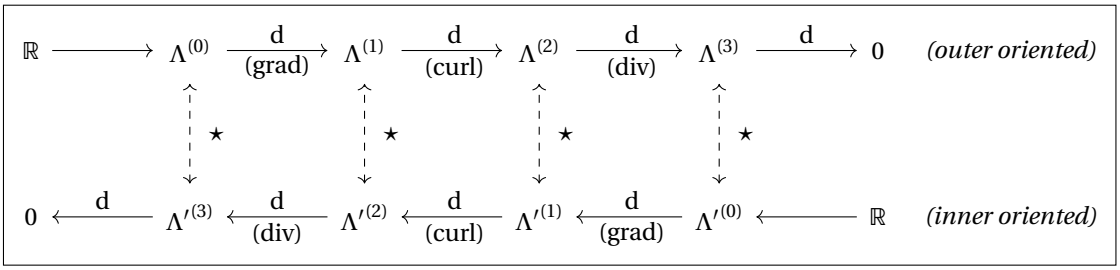

Figure 2.3: Double De Rham complex summarising the forms and operators in $\mathbb{R}^3$ [33].

equations. A distinction between the topological balance equations and the metric dependent constitutive relations is made clear. The topological equations inducing the exterior derivative in Fig. 2.3 can be described in a discrete sense by connectivity of the geometric components of a mesh only, a concept from algebraic topology. This gives rise to the concept of the topological incidence matrices discussed in Section 3.1.3. The concept of a dual mesh is also introduced. For triangular meshes, the dual mesh will be polygonal, where the cell centres can be taken as barycentric or by taking the dual mesh edges normal to the primal mesh edges. These result in the barycentric and Voronoi-Delaunay dual meshes, respectively. Note that for quadrilateral meshes considered in the mimetic spectral element method, the question on where to put the dual mesh remains. The fact that there is no unique way to construct a dual mesh is because there is metric involved to connect the primal and dual complex [12].

As discussed in [51], alike in network theory, the connectivity of the components of a discrete mesh gives rise to defining chains of these components. The co-chains are then the discrete projection of the differential forms on the chains. Co-chains act as weights on these chains, assigning values that represent the integrated value over the components. Or, as it is described more mathematically in [31, p. 638], it can also be stated as "chains correspond to vectors while co-chains correspond to co-vectors or 1-forms". Their implementation will be discussed in Section 3.1.2.

Mattiussi also continues on the theory from Tonti in the context of methods for solving numerical problems, focusing on electromagnetism as well. It is crucial to identify that different physical systems behave similarly. A deviation of the Tonti diagrams given in [51] arises from the fact that a distinction between chains and co-chains (the discrete representations of geometry and physics, respectively) is made. A qualitative comparison between popular numerical methods for partial differential equations and the mimetic approach is made. The conclusion is that the popular numerical methods have the tendency to adopt techniques adhering to the mimetic approach, an example is the staggered finite volume method. The combination of the best features of each method can be done by devising mimetic discretisation methods that maintain the distinction of topological and constitutive relations. With regard to error analysis, in the mimetic approach, the model error can be positioned with the discretisation error in the constitutive relations. The tendency of common approaches is to look at global errors, something that is natural for the co-chain-based field function approximation in a mimetic method. The boundary conditions and sources in a problem are identified as the modelling of external effects that are not considered in the problem description. The conclusion drawn on this is that the boundary conditions and sources too can be described in terms of topological and constitutive laws by physical reasoning [51].

This concludes an overview on the works and topics from which the ideas on mimetic discretisation have arisen. The specific requirements will be discussed in the next section.

2.2. Mimetic discretisation

The previously presented theory on exterior calculus is able to describe physical quantities and their relations in the continuous sense. Current research focuses mainly on how to arrive at the discrete representation that still strongly satisfy the same relations. It can be shown that the topological relations between the quantities of computation, which in classical vector calculus are called the gradient, curl, and divergence operations, have the advantage of being directly discretisable with the quantities they relate. These relations should hold for the discrete projections of forms, or co-chains, onto collections of geometric components of a discretised domain, or chains, and therefore be exact in the discrete setting as well.

This means that, in the case of incompressible flow for example, the conservation of mass (divergence of the velocity) can be exactly satisfied in the discrete formulation. It was also seen that working with this

framework allows to clearly separate the metric and topological parts before discretisation, allowing for the preservation of topological laws at the discrete level. The strength of the mimetic discretisation methods that are derived from this framework lies therefore in introducing the error in the approximate part of the physical model, the constitutive laws, where the discrete Hodge operator is introduced.

This is further discussed in this section. First, the requirements taken from literature on a mimetic discretisation method are denoted, and elaborated on. The next question is the discretisation of the metric dependent Hodge operators, and finally an overview on mimetic discretisation methods is given.

2.2.1. Requirements

In [7], a clear overview of the essential considerations in establishing a mimetic discretisation method is given. To arrive at a mimetic discretisation method, there are five requirements [63]:

1. a discretisation of integrals over geometry components,
2. a discrete analog of the fundamental theorems of calculus,
3. a discretisation of differential operators,
4. a discrete analog of commuting diagrams,
5. a discrete analog of product rules.

In the following, operators are described with some examples on the implementation from the mimetic spectral method. The requirements will be fulfilled step by step.

The first requirement is the discretisation of differential forms to co-chains associated to chains. A reduction operation is required to map the forms to co-chains [7] by discretising the known field variables that are generally the given quantities in a problem. As mentioned before, the quantities that are computed represent discrete integral quantities, which may not directly be the quantities of interest in a physical problem. However, any related quantities can in general be reconstructed from the degrees of freedom. To obtain field variables again from the computed integral quantities after solving a problem, a reconstruction operation that maps the co-chains back to forms [7] is necessary to represent them as such. The reconstruction in the mimetic spectral element method is implemented by performing interpolation, which can be done by sampling from the weighted basis functions.

The second requirement involves the generalised Stokes theorem by duality pairing, which must hold discretely for the co-chains as well. The third requirement translates to the co-boundary operator. The co-boundary operator is then the discrete analog of the exterior derivative, which relates the co-chains, the discrete projections of forms on mesh elements, within a complex exactly. This can be compared to Kirchhoff's laws in circuit analysis [31, p. 643]. In a discrete setting, applying this operator on a co-chain is done by the incidence matrices. The incidence matrices consist of only plus one, minus one, and zeros elsewhere [7, 33]. Hence, they are very sparse, which is a favourable property from a computational perspective. Furthermore, the incidence matrices are based only on the connectivity of the mesh but not on the metric properties (such as lengths and areas), and can thus be constructed for any type of mesh. This also means that these matrices remain invariant when the mesh is stretched or rotated, as long as the connections stay the same.

In general, *commutation diagrams* are used to represent the fact that many of these operations can be applied in different orders to achieve the same result, a property that is very useful when maintained at the discrete level. The fourth requirement therefore entails most importantly that the co-boundary operator commutes with the projection operator, the combined operation of reduction and reconstruction. This results in a discrete De Rham complex that involves the co-boundary operator, and also a discrete Hodge operator. Furthermore, reduction and reconstruction should be implemented such that consequent application on a co-chain should result in the same co-chain [7, 33].

And finally, for the last requirement, the wedge product should have a discrete version, such that products between co-chains resemble wedge products between forms. Furthermore, the choice of a discrete inner product then leads to an important consideration. Although the aim for the discrete versions of the operators on forms is to mimic the continuous operators as closely as possible, depending on the selection of reduction and reconstruction this can be difficult to achieve. The choice of primary operation, for instance the inner product or the discrete Hodge operator, affects whether the other operations are natural or derived from this primary operation. Choosing the inner product has several advantages, as it is easier to construct and leads to well-behaved discrete structures [7]. This is also done in the mimetic spectral element method.

2.2.2. Discrete Hodge operators

To separate the metric part from the topological part in the mimetic spectral element method when considering elliptic second order partial differential equations, either a system of first order equations called the mixed formulation (like in the mixed finite element method) can be constructed, or the equations are solved directly (by eliminating one of the first order equations again) but with explicit definition of a dual grid (like in a staggered finite volume method). A discrete Hodge operator is necessary in both cases. in the first case it appears in the inner product and thus in the mass matrices, that approximately relate the explicit primal variables to the implicit dual variables. In the second case, the Hodge-matrices to map from the primal to the dual grid (and vice versa) act as discrete Hodge operators [57].

The discretisation of Hodge operators is a key feature that distinguishes the mimetic approaches. As opposed to the discrete differential operator, discrete Hodge operators cannot be constructed using algebraic topology [33]. In other words, there are various options to choose from. This is in line with the findings in [40], where it is additionally stated that the choice of dual mesh is irrelevant, and furthermore information is lost when this elimination process is used. The mixed formulation leads to a saddle-point problem with a unique solution. In [66], the relation between the explicit definition of a Hodge operator or introduction by the Galerkin method was pointed out as well, stating that both the mass matrices and Hodge matrices, although different, represent a discrete Hodge operator.

There are three requirements on these Hodge or mass matrices [40]: They should be square, symmetric, positive definite, they should follow the property of the skew-symmetry of the wedge product when switching the arguments, and they should satisfy a discrete integration by parts rule. In the mimetic spectral element method, the introduction of discrete Hodge operators indeed results in diagonal or full square, symmetric, positive definite mass matrices. Furthermore, for the mimetic spectral element the discrete wedge product satisfies the skew-symmetry property, and the inner product between a form and a form on which a co-differential acts, which is a combination of the exterior derivative and the Hodge operator, satisfies a discrete integration by parts rule [57].

As the mass matrices are dependent on the metric, they have to be generated for every mesh constructed. However, one of the advantages of the method is that they can be constructed on a reference domain. That is because of another important commuting diagram for mappings, where the pull-back operator commutes with the exterior derivative. In numerical simulations, it is then possible to describe globally all elements in terms of a reference element through this mapping. The pull-back operator thus enables to use a mapping, such that computations can be conveniently done in a reference domain. This is convenient, since the mass matrices have to be determined once for the reference domain, and can be multiplied with the local pull-back for every part of the physical domain [33]. This is further discussed in Section 3.3.

This concludes the ingredients necessary for the method to be implemented. These are the construction of mass matrices and incidence matrices, the reduction of known simulation inputs to a right-hand-side vector (boundary conditions and forcing functions), and the reconstruction of the solution.

2.2.3. Development of related mimetic discretisation methods

In the mimetic discretisation framework, there are several distinct approaches designed for various applications. Next to the mimetic spectral element method, which will be discussed elaborately in the next section, related methods are mentioned here for completeness. These are the finite element exterior calculus and mimetic finite differences methods, which will be discussed in the following. Further areas to mention are on unstructured triangular staggered meshes preserving symmetries [58], extensions to general polyhedral meshes [10, 15], a most geometric approach that is discrete exterior calculus [25], covolume methods [52], and mimetic isogeometric discretisations [16, 28, 39].

The finite element exterior calculus [4, 5] is based directly on the conventional finite element method. It aims at "the development of finite element subcomplexes of certain elliptic differential complexes and co-chain projections onto them, and their implications and applications in numerical PDEs" [4, p. 4]. The ingredients for the method come from differential geometry, algebraic topology and homological algebra, with finite element de Rham subcomplexes and co-chain projections seen as key tools in the method. As in the conventional finite element method, the domain is divided in an unstructured mesh of elements, on which the solution is characterised by a weak or variational formulation. The solution exists in suitable function spaces, which are decomposed in finite dimensional subspaces, allowing for directly comparing to the exact solution through the same mathematical tools, such as norms or functionals. Central to the method are the Koszul operator and the Koszul complex in the construction and analysis of the finite element subspaces. By considering solutions only in finite-dimensional subspaces of the space in which the exact solution is sought,

the solution in this method inherits the co-homology and other features of the exact complexes through co-chain projections [4]. Recent work on the method is for example on the effect of lower order terms on stability and convergence rates for both scalar and vector Laplacian problems [1], an application to the rotating shallow-water equations [19], and a posteriori error estimates with bounds for the computational error computed from the discrete solution and problem data [24].

Another major framework is the mimetic finite differences, a recent extensive review of the 50-year history of the method is given in [49]. These have arisen from support operator methods, which are finite difference methods containing a discrete vector and tensor calculus with discrete analogs of the vector operators gradient, curl, and divergence [42, 65]. The degrees of freedom, which represent scalar, vector or tensor field, are associated to mesh objects, and collections of degrees of freedom are called grid functions, that function as a nodal or edge basis. The association to mesh objects can be well understood in terms of algebraic topology. The fact that the differential operators can be discretised directly is convenient when working with conservation laws, since the gradient and divergence operators are negatively adjoint, which means for instance that conservation of mass is ensured by the framework. The introduction of parasitic or spurious modes in discretisation methods in general is attributed to the fact that the differential operators possess null-spaces that are too large [49]. In addition, using the method simplifies the convergence analysis through symmetric discretisation [14]. The mimetic finite differences has been compared and shown to be almost identical to hybrid and mixed (staggered) finite volume methods [27]. It is applied to elliptic problems on polyhedral meshes in [14]. Other recent work on application are for example on using mimetic finite differences for solving the Stokes equations on unstructured polygonal meshes [20] and the extension to parabolic problems [50].

2.3. Applications of the mimetic spectral element method

Now that the basic ingredients for the mimetic spectral element method and their origin have been explained, the question remains on the current state of the method. To answer this question, a short history of the method will follow. The application of the method to Stokes flow and linear elasticity will then be discussed, and finally the hybrid method will be introduced further.

2.3.1. An overview

As mentioned, the work on the mimetic spectral element method is relatively new. The aim of this method is to have a high order mixed finite element method with exact conservation for topological relations, while also having optimal convergence. In this method, the quantities of interest are projected on components of the mesh with different dimensions, through the use of appropriate basis functions. This is possible with two types of basis, a nodal basis constructed from Lagrange polynomials, and an edge basis constructed with the edge functions proposed in [32]. These bases are constructed on a structured quadrilateral mesh, and satisfy the Kronecker delta property in their respective dimensions: the nodal basis on the nodes, and the edge basis on the edges. Through tensor products, these one-dimensional definitions can be extended to arbitrary dimension. A full introduction on the ideas implemented in the mimetic spectral element method is given in [33].

Some first works focusing on this method can be found in the conference papers [13, 32, 48, 55]. Here, the method was first presented to solve the Poisson equation on multiple continuous spectral elements. Later, several journal papers gave a full overview on the method [39, 47, 57], with applications to (anisotropic) diffusion and Stokes flow. A possible extension to advection problems is discussed in [56], and momentum conservation [71], followed by the development of a Navier-Stokes solver on simplicial meshes with conservative properties [54], conserving mass, energy, enstrophy, and vorticity. Discrete Lie derivatives to compute convection terms have been proposed in [35, 48, 55]. Recently, the algebraic dual polynomials have been derived and applied, which are described in the not yet published documents [36, 43]. These polynomials allow for the setup of sparse systems to solve due to the topological discretisation of the conservation laws, while only a single mesh has to be defined for all computations.

Additionally, effort is put to extend this method to hybrid elements with domain decomposition [73]. Applying the mimetic spectral element method in this hybrid formulation is promising. This is done by dividing the domain into multiple hybrid elements, the quantities for the hybrid elements can be solved for each domain independently. This in short involves setting up operators acting on the quantities on the boundaries, to ensure that conservation or equilibrium of the quantities hold at these locations. By doing so, the problem may be divided into separate domains for computation, which can be evaluated in parallel after the interface

relations have been computed. This is an attractive property for large systems of equations, which are generally the result of problems which require high accuracy and where many unknowns have to been found. Instead of having to solve the complete system at once, which is generally the case for continuous elements, it can be solved in parts more efficiently.

2.3.2. Stokes flow

In [47], the mimetic spectral element method is applied to Stokes flow. The Stokes flow equations arise in the case of very low Reynolds number flows, called creeping flows, where the inertial effects are negligible. Examples include the flows of highly viscous fluids, such as oils or resin. This means that the convection can be removed from the Navier-Stokes equations, which leaves the linear elliptic Stokes flow equations. The equations are then comparable to those of linear elasticity, but fluids possess a different stress-strain relation, hence the constitutive law changes. In addition, the stress tensor comprises an isotropic pressure term and shear stresses. For a physical flow, the mass conservation constraint results in an extra equation.

In the velocity-vorticity-pressure (VVP) formulation, a system of first order equations is solved for the velocity, vorticity, and pressure. This is done by assuming constant viscosity and using the relation for the vector Laplacian. The vorticity is then introduced as a third unknown, related to the velocity by the curl operator. The three equations are discretised by assigning the vorticity and velocity to the primal grid, as projections of 0-form and 1-form, respectively, and finally the pressure as a 2-form, since it is then dual to the 0-form in the dual space. The point here is that the velocity and vorticity are the primal variables, while the pressure (or stress) is the dual variable. The scheme is applied to a manufactured solution test case, and the lid-driven cavity flow in two and three dimensions. By construction, the method satisfies conservation of mass point-wise, and the error converges optimally [47]. In [39], the same results are found for Stokes flow in the VVP formulation when using B-spline basis functions. Furthermore, the topological relations should hold for any basis that "forms a partition of unity and allows a tensor product structure" [39, p. 1464].

Although the problem of Stokes flow has been considered in [39, 47], the formulation used was based on reducing the momentum equation to a system of first order equations through the introduction of the vorticity. The assumption here is constant viscosity, which is a restriction on generality. Moreover, the linear momentum balance is at most conserved weakly, since it is not imposed topologically. Introducing the constraint of mass conservation to a linear elasticity formulation can allow for a Stokes flow formulation which conserves both mass and linear momentum, which is shown in Chapter 8. It is necessary to find a formulation for linear elasticity that conserves linear and angular momentum first, where the latter is a combination of linear momentum and symmetry of the stress tensor. This will be shown in Chapter 6.

2.3.3. Linear elasticity

Until now, the results have been mostly gathered from mixed formulations of systems of first order equations. Continuum mechanics applications generally require the representation of higher order tensor quantities than vectors. A first step for the mimetic spectral element methods towards the discretisation of tensor quantities was performed on linear elasticity [53], where linear momentum was shown to be conserved exactly point-wise but the stress tensor was not symmetric. As opposed to the more mathematical VVP formulation, by using a stress based formulation for the Stokes problem, linear momentum could be conserved strongly. This in turn motivates the search for a better formulation for linear elasticity first, which should satisfy strongly the symmetry of the stress tensor.

The problem of linear elasticity arises in the analysis of solid structures and materials. It is valid only for small displacements, but can still be widely applied. In [53], a formulation within the mixed spectral element method for linear elasticity is proposed. The stress is here the primal variable, while the displacement and rotation are Lagrange multipliers that enforce linear momentum and symmetry of the stress tensor, respectively. The conservation of linear momentum, which originates from equilibrium of forces, is satisfied point-wise in this formulations. While symmetry on the stress tensor is strongly imposed, the presented approach results in only a weakly satisfied equilibrium of moments on curvilinear grids. The points for discretisation also play a role in the properties of the solution. Due to computing physical quantities as Lagrange multipliers in a mixed formulation, the amount of degrees of freedom and thus the system size is increased. However, this is compensated by the fact that no post-processing step is necessary to obtain the traction from the displacement, which is generally necessary in the traditional finite element method, but they are directly available.

A remaining problem is that the equilibrium of moments should be satisfied point-wise, without introducing spurious kinematic modes. This will be shown to be the case for the new formulation in Chapter 7. To

understand where these come from, it is important to know the properties of a mixed finite element method. In a mixed finite element method, the problem is formulated as a saddle-point problem, which results in a system of equations solved for two quantities separately. This means that, In the case of linear elasticity, both the stresses and displacements are solved for at the same time. In the case of the Stokes flow, not only the velocity is solved for but also the pressure [9, p. 16-21]. In case a minimisation problem is considered, Lagrange multipliers are introduced to ensure the conservation laws in addition to the energy minimisation, which then leads to a mixed formulation.

To correctly set up mixed methods, there are two different approaches. These either circumvent or satisfy the Ladyshenskaya–Babuška–Brezzi stability condition, also called the inf-sup condition. Circumvention of this condition led to stabilised methods and minimisation methods or least squares methods. Satisfaction of this condition is possible through the so-called compatible methods [47]. Discrete vector spaces that satisfy this condition have been constructed: Nedelec spaces (curl conforming), Raviart-Thomas spaces (divergence conforming), and Brezzi-Douglas-Marini spaces (divergence conforming) [47]. A well known mixed formulation for Stokes flow in terms of pressure and velocity and stable elements for it are given in [2]. The mimetic methods are a subclass of the compatible methods, and as such will lead to stable solutions for elliptic problems such as the Stokes flow problem, proven for the mimetic spectral element method applied to Stokes flow in the VVP formulation [46, p. 199-202]. However, the linear elasticity problem will introduce another saddle point system, and hence it is in general required to prove well-posedness as well for new formulations.

2.3.4. The hybrid method

In the introduction, the recent extension of the mimetic spectral element method to a hybrid method was noted. It is further introduced here and compared to other methods in this area.

The discretised equations of a problem can be computed on a single domain with the mimetic spectral element method, where the order of the basis may be increased to reduce the interpolation error up to machine precision (thus by a spectral element method). However, for a more flexible method that is more generally applicable to arbitrary geometries, it is important to apply the method on multiple elements. This can be done for low order polynomials in a large number of elements (which can then be considered to be a finite element method). To divide a domain in multiple elements, three different approaches are considered here, continuous Galerkin methods, discontinuous Galerkin methods, and the hybrid method in the framework of the mimetic spectral element method.

In continuous Galerkin methods for conventional finite element methods, the domain is divided in elements, on which basis functions are defined only within the elements. The edges are shared by neighbouring elements, such that only a single unknown is placed here. The structure of the sparse matrix then depends on the numbering of the elements and edges. These continuous methods are conforming, such that solutions are sought in a subset of the original solution space of the continuous problem. The conservation properties of these methods are re-examined in [41].

As opposed to the continuous methods, using domain decomposition with non-overlapping, discontinuous domains, the global problem is divided into sub-problems. This is the case in discontinuous Galerkin methods, as well as in the hybrid finite element method. As the name suggests, the numbering of unknowns (resulting in degrees of freedom) globally is then practically done as if the edges of elements are disconnected.

An overview of discontinuous Galerkin methods is given in [3]. The distinction between methods made there is based on the imposed numerical fluxes between elements. The term numerical flux reveals that these do not necessarily represent physical relations. The consequences of this choice results in the variety of methods, since it affects stability, accuracy, and the sparsity and symmetry of the stiffness matrix [3]. A clear motivation for using these methods is given in [18], where their applicability as finite element alternative to high resolution finite difference and finite volume methods for convection dominated problems with physical discontinuities is highlighted. Further advantages of the discontinuous methods are that they are highly parallelisable, provide a high mesh flexibility for complex geometries, and are easily compatible with adaptive refinement strategies.

The recent discontinuous Petrov-Galerkin method has improved stability [23] by first searching optimal test function spaces for each problem considered, and then solving using these test functions. This does not involve an extra solution step but can be computed during the setup of the element matrices. However, conservation laws do not hold on element level in general for the discontinuous Petrov-Galerkin method, although it is proposed to be possible at the expense of introducing another scalar unknown [23]. The method is more expensive than continuous Galerkin or other discontinuous Galerkin methods, but in return improved stability is obtained. Alternatively, combining ideas from the hybrid finite element method and discontin-

uous Galerkin methods, the hybridisable discontinuous Galerkin method [17] has been developed, which is based on a mixed formulation discussed later. Hybridisable discontinuous Galerkin methods are by construction discontinuous Galerkin methods which allow for static condensation, shown for steady state diffusion problem in [17].

The hybrid method that is used in [73] involves separate elements, where the bordering edges are constrained with an interface operator that is enforcing continuity as a Lagrange multiplier. This means that, although the edges of every element boundary have two degrees of freedom, the solution will be continuous across the elements. This is different from the discontinuous Galerkin methods, where the solution in general jumps between the elements. In addition, the Lagrange multipliers become in a sense part of the solution in the form of physical boundary conditions for each element. The method is comparable to the primal hybrid finite element methods from [61].

Although the method introduces extra unknowns at the edges, for higher order methods, the number of unknowns inside the elements will be higher than those at the edges, hence this is not an issue. The elements are separated by introducing separate degrees of freedom at the element edges results in independent blocks for each element in the system matrix. The pairing of edges at the same location can be performed using an interface operator, which introduces extra equations relating the edges at the same location. An example of such an operator is the Steklov-Poincare operator [60]. The computation of the interface quantity relations can then be performed separately by means of the method of static condensation, see [9, p. 429]. The domains can be solved independently afterwards, allowing parallelisation of computation, which can be highly favourable for a large number of unknowns. These methods lead to a block diagonal mass matrix that can be solved in parallel for every element [17].

Thus, each of the mentioned methods has the advantage of domain decomposition, the discontinuous Galerkin methods and hybrid method are parallelisable. The distinction of the hybrid method for the mimetic spectral element method is in the continuity of the fluxes and the physical interpretation of the Lagrange multipliers. For steady state, elliptic problems, this method is promising, while for time dependent problems which introduce discontinuities, the other discontinuous methods may be a better alternative.

2.4. Summary

The goal of this chapter was to introduce the works that functioned as the starting point for the mimetic spectral element method. The combination of concepts from exterior calculus and the insights of Tonti lead to a geometric description of physics. The relations between differential forms can be summarised in a De Rham complex, which is the basis for the Tonti classification diagrams. Furthermore, concepts from algebraic topology can be used to discretise the forms and their relations. This framework leads thus to a natural discretisation of the differential forms that describe physics. The requirements for a mimetic discretisation are fivefold, and entail the direct discretisation of differential and integral operators, while preserving the properties of the continuous relations through discrete analogs. The operators necessary to implement the mimetic spectral element method are projection through reduction and reconstruction, the inner product which results in mass matrices, and the co-boundary operator which results in incidence matrices. Next to the mimetic spectral element method, the finite element exterior calculus and mimetic finite differences methods have been discussed. An overview on the mimetic spectral element method led to the conclusion that to move towards continuum mechanics applications, the problem of linear elasticity needs to be reconsidered. Finally, the hybrid method has been compared to other related methods for handling domain decomposition.

3

Mathematical Background

Although this chapter contains only a brief overview of the mathematical background needed to work with the mimetic spectral element method, it will shed light on the notation and application of the concepts from exterior calculus and algebraic topology discussed in the previous chapter. It further functions as an illustration for those who are not familiar with these concepts but want to have a brief introduction of the basics, with references to full texts devoted to the subjects.

The treated topics in this chapter are the basics of the method, the basis functions that are derived using the knowledge of these basics, mapping techniques for the method, the theory behind minimisation of Lagrangian functionals, and finally the corresponding calculation of errors.

3.1. Basics of the mimetic spectral element method

The first part of this section describes the notation that will be used throughout the thesis. Although many of the ideas here are also presented in literature, the notation varies. Therefore, the preferred notation is given here. Furthermore, the concepts from algebraic topology that allow for a natural discrete representation are translated to the operations needed for the projection of forms onto a mesh. Finally, the construction of the connectivity or incidence matrices is explained.

3.1.1. Notation

The following symbols and specific notation are reserved in this thesis, and their meaning is therefore clarified here. As usual, n denotes the dimension of space, while p denotes the polynomial degree of basis. Since the amount of degrees of freedom varies depending on the basis, N is reserved for the necessary points to describe a polynomial of degree p, such that $N = p+1$ for a one-dimensional function. For two-dimensional functions, it depends on the basis. In general, h represents the element size for an orthogonal mesh with linear spaced elements, and is therefore defined as $h \equiv \frac{1}{K}$, where K is the number of elements in one direction. The geometrical interpretation for h of element size will not hold for the deformed grids. Then, k denotes the dimension of a form. For numerical integration and interpolation, p_f is a suitable number larger than p such that the numerical error in numerical integration and interpolation is negligible.

Vectors are in boldface, e.g. $\mathbf{u}$. Tensors are underlined twice, e.g. $\underline{\underline{\sigma}}$. The k-forms are always denoted with their respective k, e.g. $\phi^{(k)}$. Dual spaces and objects defined in them are denoted with a prime, e.g. Ω'. System vectors (for in computations) are in italic boldface with the superscript h, e.g. $\boldsymbol{p}^h$. Vector proxies are denoted with an over-line, e.g. $\overline{u}$. Test functions are denoted with a tilde, e.g. $\tilde{p}$. The determinant of a matrix or operator A is denoted with $|A| \equiv \det(A)$. Inner products are denoted with $(a,b)_\Omega$, and will be discussed in Section 3.4.2.

3.1.2. Projection onto a mesh

The differential forms should now be discretised such that the discrete quantities still satisfy the relations of the continuous quantities. This can be done in a convenient way through the use of the algebraic topology of the mesh components. In Fig. 3.1, a simple orthogonal outer oriented cell complex is shown. This cell complex consists of three k-cells. The 0-cell comprises all $(p+1)^2$ points, the 1-cell comprises all $2p(p+1)$ edges, and the 2-cell comprises all p^2 surfaces. Simply put, the variables represented by differential forms,

such as $\omega^{(0)}$, $q^{(1)}$, and $p^{(2)}$, will be represented on these discrete cells. To arrive at a discrete representation of the differential forms, two operators are required. This is explained more elaborately in [57], here only the key concepts are discussed.

First, to reduce continuous forms to the mesh, the reduction or integration operator $\mathcal{R}$ is used. The reduction of a form results in a co-chain that is associated to a chain of mesh elements. This operation is not well defined in general, as there are several ways to do this. The co-chains are values associated to components of the discrete geometry. They are the weights of the solution representation, while the basis representing the mesh can be formed by (tensor combinations of) Lagrange polynomials and edge polynomials, which will be introduced in Section 3.2. The discretisation of field variables can be performed on the primal grid by means of integration, and comes explicitly into play later on, for example when dealing with boundary conditions and forcing functions for the formulations in Chapter 4, Chapter 5, and Chapter 6. This discretisation can in general also be done using the algebraic dual polynomials, these will be described in Section 3.2. This approach will be taken in the new formulations in Chapter 7 and Chapter 8. The reduction of any continuous field results in loss of information, hence an interpolation error is introduce when reconstructing this reduced field.

To extract values point-wise from the discrete solution, the reconstruction or interpolation operator $\mathcal{I}$ is used. As the name suggests, reconstruction involves the interpolation of values from the degrees of freedom with their weighted basis, which will be introduced in Section 3.2. The projection is then the subsequent application of reduction and reconstruction, $\pi_h = \mathcal{I}\mathcal{R}$. The operation $\mathcal{I}$ must be the right inverse of the reduction $\mathcal{R}$, since then the consistency condition $\mathcal{R}\mathcal{I} = I$ holds, with I the identity matrix. Vice versa, the reduction followed by a reconstruction will always lead to an interpolation error, $\mathcal{I}\mathcal{R} = I + \mathcal{O}(h^p)$, which can be shown to be the main error contribution if the convergence is optimal [57].

In $\mathbb{R}^2$, there are three possible co-chains. Their components are numbered along x and y using the indices (i, j). The first, $\omega^{(0)}$ is situated on the chain of $(p+1)^2$ nodes or 0-cells, with components ω_{ij}. The reduction for 0-forms is direct nodal sampling at the defined nodes. The next co-chain $q^{(1)}$ is situated on the chain of $2p(p+1)$ edges or 1-cells, which comprises two sets of components, u_{ij} and v_{ij}. To reduce a 1-form, which should be a co-vector, onto this 1-cell, the value must be integrated over each edge. Finally, the co-chain $p^{(2)}$ associated to a chain of p^2 surfaces or 2-cells, such that each quantity represents an integral over the surface, hence surface integration is necessary.

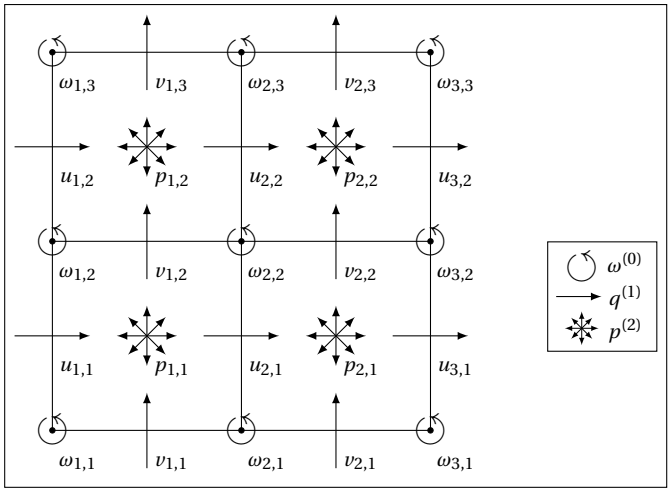

Figure 3.1: Cell complex for a low order element, with labeled degrees of freedom ($p = 2$).

3.1.3. The discrete exterior derivative

The co-boundary operator δ acts as the discrete counterpart of the exterior derivative, d, but acting on co-chains. It can relate the co-chains in the same way the exterior derivative relates the differential forms as shown in a De Rham complex in Fig. 2.2. As such, it is important to note that it commutes with both components of the projection [57],

$$\pi_h \mathrm{d} = \mathcal{I}\mathcal{R}\mathrm{d} = \mathcal{I}\delta\mathcal{R} = \mathrm{d}\mathcal{I}\mathcal{R} = \mathrm{d}\pi_h.$$

It is constructed as an incidence matrix depending on the co-chain it is acting on. To arrive at the co-chain on the 1-cells from the co-chain on the 0-cells, the positive or negative action of each component of the latter is used. Consider the cell complex in Fig. 3.1. Since ω is defined counter-clockwise positive here, the action of $\omega_{1,1}$ on $u_{1,1}$ is negative, while the action of $\omega_{1,1}$ on $v_{1,1}$ is positive. Similarly, if p is defined source-like, the action of $u_{1,1}$ on $p_{1,1}$ is negative, while the action of $v_{1,1}$ on $p_{1,1}$ is positive. This can be summarised in an incidence matrix. Note that any numbering and definition of positive sign is free to choose since it does not impact the sparsity properties of the incidence matrix, but it should of course be consistent everywhere in the setup of the system.

The incidence matrix $\mathbb{E}^{(1,0)}$ for the mesh in Fig. 3.1 is denoted for x-lexicographic numbering of the edges, first the vertical and then horizontal edges, as

$$\mathbb{E}^{(1,0)} = \begin{bmatrix} -1 & 0 & 0 & 1 & 0 & 0 & 0 & 0 & 0 \\ 0 & -1 & 0 & 0 & 1 & 0 & 0 & 0 & 0 \\ 0 & 0 & -1 & 0 & 0 & 1 & 0 & 0 & 0 \\ 0 & 0 & 0 & -1 & 0 & 0 & 1 & 0 & 0 \\ 0 & 0 & 0 & 0 & -1 & 0 & 0 & 1 & 0 \\ 0 & 0 & 0 & 0 & 0 & -1 & 0 & 0 & 1 \\ 1 & -1 & 0 & 0 & 0 & 0 & 0 & 0 & 0 \\ 0 & 1 & -1 & 0 & 0 & 0 & 0 & 0 & 0 \\ 0 & 0 & 0 & 1 & -1 & 0 & 0 & 0 & 0 \\ 0 & 0 & 0 & 0 & 1 & -1 & 0 & 0 & 0 \\ 0 & 0 & 0 & 0 & 0 & 0 & 1 & -1 & 0 \\ 0 & 0 & 0 & 0 & 0 & 0 & 0 & 1 & -1 \end{bmatrix}. \tag{3.1}$$

In this case, where $p = 2$, there are $(p+1)^2 = 9$ unknowns $\omega_{i,j}$ for $\omega^{(0)}$ and 12 unknowns for $q^{(1)}$, $(p+1)p = 6$ for $u_{i,j}$ and $p(p+1) = 6$ for $v_{i,j}$. The indices of $\omega_{i,j}$ have x-lexicographic numbering, i.e. for a single index ω_k, $k = i + (j-1)(p+1) \ \ \forall i, j \in [1, p+1]$. The indices of ω_k are in the horizontal direction of this matrix. Similarly for the unknowns for $u_{i,j}$ and $v_{i,j}$, along the vertical side of this matrix, i.e. for a single index u_k, $k = i + (j-1)(p+1) \ \ \forall i \in [1, p+1], j \in [1, p]$ and for a single index v_k, $k = i + (j-1)p \ \ \forall i \in [1, p], j \in [1, p+1]$. The indices of first u_k and then v_k are in the vertical direction of this matrix.

Similarly, the incidence matrix $\mathbb{E}^{(2,1)}$ can be denoted as

$$\mathbb{E}^{(2,1)} = \begin{bmatrix} -1 & 1 & 0 & 0 & 0 & 0 & -1 & 0 & 1 & 0 & 0 & 0 \\ 0 & -1 & 1 & 0 & 0 & 0 & 0 & -1 & 0 & 1 & 0 & 0 \\ 0 & 0 & 0 & -1 & 1 & 0 & 0 & 0 & -1 & 0 & 1 & 0 \\ 0 & 0 & 0 & 0 & -1 & 1 & 0 & 0 & 0 & -1 & 0 & 1 \end{bmatrix}. \tag{3.2}$$

There are $p^2 = 4$ unknowns $p_{i,j}$ for $p^{(2)}$, with single index p_k where $k = i + (j-1)p \ \ \forall i, j \in [1, p]$. In this matrix, the indices of first u_k and then v_k are in the horizontal direction while the indices of p_k are in the vertical direction.

In general, the incidence matrix $\mathbb{E}^{(n-1,n-2)}$ is the discrete equivalent of the curl operator and the exterior derivative acting on an outer oriented $n-2$-form in $\mathbb{R}^n$. The incidence matrix $\mathbb{E}^{(n,n-1)}$ is the discrete equivalent of the divergence operator, and the exterior derivative acting on an outer oriented $n-1$-form in $\mathbb{R}^n$. This readily shows the sparsity of these matrices.

3.2. Basis

As mentioned before, the co-chains are associated to mesh cells of different dimensions. To represent them in a finite element context, a basis is constructed with special properties. For this, a primal grid is selected which is found to be optimal for the representation of the mesh elements. Then, the basis for this primal grid is selected. From this primal grid and the definition of the inner product, the algebraic dual basis can be derived. Finally, the construction of basis in higher dimensions is summarised. Note that throughout Section 3.2.1 to Section 3.2.3, i, j, k are used as dummy indices. In Section 3.2.4, the variables i, j mean again the index in horizontal and vertical direction.

3.2.1. Grid construction

A Gauss-Lobatto-Legendre grid is preferably used [36], which is based on the root locations of the polynomial

$$\phi_{\mathrm{GLL}} = \left(1-\xi^2\right)\frac{\mathrm{d}L_p(\xi)}{\mathrm{d}\xi},$$

here $L_p(\xi)$ is a Legendre polynomial of degree p. This polynomial solves the Legendre's differential equation

$$\frac{\mathrm{d}}{\mathrm{d}\xi}\left((1-\xi^2)\frac{\mathrm{d}L_p(\xi)}{\mathrm{d}\xi}\right)+p(p+1)L_p(\xi)=0.$$

To obtain the points, instead of algebraically or numerically solving the ordinary differential equation, Bonnet's recurrence relation for the Legendre polynomials can be used, with $L_1(\xi)=1$ and $L_2(\xi)=\xi$, and for $k>2$,

$$(k+1)L_{k+1}(\xi)=(2k+1)\xi L_k(\xi)-kL_{k-1}(\xi).$$

Using an iterative method for root finding such as Newton-Raphson, the roots ξ_i of $L_p(\xi)$ can be found for any p.

3.2.2. Primal basis

To derive basis functions with the correct properties, it is convenient to define the nodal and edge degrees of freedom as $\mathcal{N}_i^0$ and $\mathcal{N}_i^1$, respectively. Note that the action of $\mathcal{N}_i^0(a^{(0)})$ and $\mathcal{R}(a^{(0)})$ are equivalent, different ways to write the same. Any 0-form $\phi^{(0)}$ or 1-form $\chi^{(1)}$ can be expanded using their corresponding degrees of freedom and basis, e.g.

$$\phi^{(0)}(\xi)=\sum_{i=1}^{p+1}\mathcal{N}_i^0(\phi)h_i(\xi),\quad \chi^{(1)}(\xi)=\sum_{i=1}^{p}\mathcal{N}_i^1(\chi)e_i(\xi).$$

Given the Gauss-Lobatto-Legendre nodes ξ_i, where $-1=\xi_1\leq\xi_2...\leq\xi_{p+1}=1$, the nodal and edge degrees of freedom are defined as [43]

$$\mathcal{N}_i^0(\phi)\equiv\phi^{(0)}(\xi_i),\qquad \mathcal{N}_i^1(\chi)\equiv\int_{\xi_i}^{\xi_{i+1}}\chi^{(1)}(\xi).$$

Here, $\mathcal{N}_i$ are linear functionals called local degrees of freedom, or co-chains, that act on the elements, evaluating on one node i. Note that this is only well-defined for smooth functions. Also, $\phi=\phi^{(0)}$ is denoted as a zero form here. The nodal basis functions should therefore satisfy

$$h_j(\xi_i)=\delta_{ij}=\begin{cases}1 & \text{if } j=i\\ 0 & \text{if } j\neq i\end{cases},\quad \forall i,j\in[1,p+1],$$

since then each nodal basis function represents the individual contribution of a node. Therefore, the Lagrange polynomials are used, which are constructed from $p+1$ data points with

$$h_i(\xi)\equiv\prod_{k=1,k\neq i}^{p+1}\frac{\xi-\xi_k}{\xi_i-\xi_k}.$$

The nodal basis functions are shown in Fig. 3.2a. At each node of the mesh, only one basis function has the value one, while the others are zero.

Similarly, the edge basis functions should satisfy the property

$$\int_{\xi_i}^{\xi_{i+1}}e_j=\delta_{ij}=\begin{cases}1 & \text{if } j=i\\ 0 & \text{if } j\neq i\end{cases},\quad \forall i,j\in[1,p].$$

The functions for the edge basis that will be used are the functions $e_j(\xi)$, called edge functions derived in [32]. On the same GLL-points, they are defined as the sum over the derivatives of the nodal basis functions over the grid,

$$e_j(\xi)\equiv-\sum_{k=1}^{j}\mathrm{d}h_k(\xi),$$

as these have the required property that [32]

$$\int_{\xi_i}^{\xi_{i+1}} e_j(\xi) = -\sum_{k=1}^{j} \int_{\xi_i}^{\xi_{i+1}} \mathrm{d}h_k(\xi) = -\sum_{k=1}^{j} \left[h_k(\xi_{i+1}) - h_k(\xi_i)\right] = \delta_{ij}, \quad \forall i,j \in [1,p].$$

A short note must be given on the fact that the edge basis functions actually include the basis form, since

$$e_j(x) \equiv -\sum_{k=1}^{j} \mathrm{d}h_k(x) = -\sum_{k=1}^{j} \frac{\mathrm{d}h_k(x)}{\mathrm{d}x}\mathrm{d}x = \epsilon_j(x)\mathrm{d}x.$$

However, in the remainder of this report, the basis $\mathrm{d}x$ will still be noted when performing the derivations. Hence, the edge functions denoted by e_j are in fact only the vector proxy part ϵ_j of the true edge functions, which are the basis forms derived in [32].

The edge functions are also depicted in Fig. 3.2b, where the shaded area equals one, while the integrals of the other two edge functions over this part of the domain are zero.

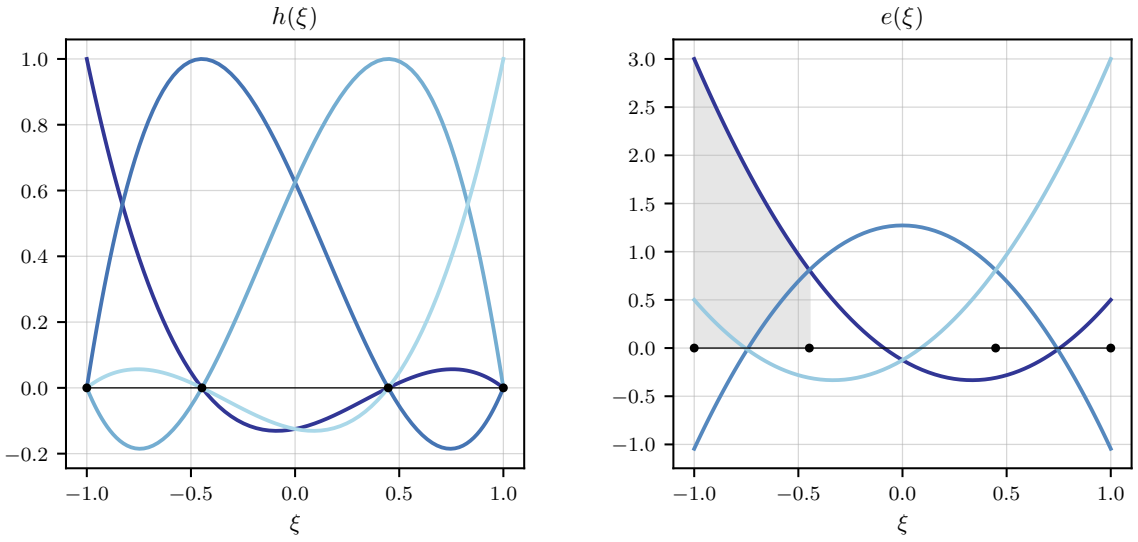

(a) Nodal basis functions, of order p.

(b) Edge basis functions, of lower order $p-1$.

Figure 3.2: The primal basis functions for an element in $\mathbb{R}^1$ of $p = 3$.

3.2.3. Dual basis

A thorough overview and proofs for the derivation of the algebraic dual basis functions discussed here can be found in [43]. The origin for defining this basis explicitly is that for the problems in the following chapters Chapter 4, Chapter 5, and Chapter 6, the system to solve usually involves full mass matrices, which can be mitigated by defining an algebraic dual basis and solving for degrees of freedom on this basis. This dual basis is orthonormal to the primal basis. Although the derivation and construction of these polynomials can be done explicitly, in an actual implementation this is not necessary. In the new formulation described in Chapter 7, the dual polynomials will be used explicitly.

Any polynomial $\phi \in \mathcal{P}$, with $\mathcal{P}$ the space of polynomials of degree p, can be represented by $p+1$ nodal degrees of freedom, i.e.

$$\phi(\xi) = \sum_{i=1}^{p+1} \mathcal{N}_i^0(\phi) h_i(\xi) = \Psi^0(\xi)\mathcal{N}^0(\phi),$$

where matrices holding the function values at each node for each function are defined,

$$\Psi^0(\xi) = \left[h_1(\xi), h_2(\xi), \ldots h_{p+1}(\xi)\right], \qquad \left(\mathcal{N}^0(\phi)\right)^T = \left[\mathcal{N}_1^0(\phi), \mathcal{N}_2^0(\phi), \ldots \mathcal{N}_{p+1}^0(\phi)\right].$$

Defining the one dimensional mass matrix

$$\mathbb{M}_{1D}^{(0)} = \int_\Omega \left(\Psi^0(\xi)\right)^T \Psi^0(\xi)\mathrm{d}\Omega,$$

the L^2-inner product of two elements $\phi, \pi \in \mathcal{P}$ leads to

$$(\phi,\pi)_{L^2(\Omega)} \equiv \int_\Omega \phi\pi \mathrm{d}\Omega = \int_\Omega \left(\mathcal{N}^0(\phi)\right)^T \left(\Psi^0(\xi)\right)^T \Psi^0(\xi)\mathcal{N}^0(\pi) = \left(\mathcal{N}^0(\phi)\right)^T \mathbb{M}^{(0)}_{1D}\mathcal{N}^0(\pi).$$

Then, defining the dual edge degrees of freedom, $\mathcal{N}'^1(\pi)$, with

$$\left(\mathcal{N}^0(\phi)\right)^T \mathcal{N}'^1(\pi) \equiv \left(\mathcal{N}^0(\phi)\right)^T \mathbb{M}^{(0)}_{1D}\mathcal{N}^0(\pi),$$

the dual basis functions $h'_j(\xi)$ must again satisfy the Kronecker-delta property, i.e. $\mathcal{N}'^1_i(h'_j) = \delta_{ij}$, hence they are found to be

$$\Psi'^1(\xi) = \Psi^0(\xi)\left(\mathbb{M}^{(0)}_{1D}\right)^{-1},$$

where

$$\Psi'^1(\xi) = \left[e'_1(\xi), e'_2(\xi), \ldots e'_{p+1}(\xi)\right].$$

In Fig. 3.3, these dual polynomials are shown. It can be seen that, while the Lagrange polynomials are nodal, the dual polynomials derived from them are more like edge polynomials.

Expressing the edge degrees of freedom again for any $\chi \in \mathcal{Q}$, with $\mathcal{Q}$ the space of polynomials of degree $p-1$,

$$\chi(\xi) = \sum_{i=1}^{p} \mathcal{N}^1_i(\chi) e_i(\xi) = \Psi^1(\xi)\mathcal{N}^1(\chi),$$

where

$$\Psi^1(\xi) = \left[e_1(\xi), e_2(\xi), \ldots e_p(\xi)\right], \qquad \left(\mathcal{N}^1(\chi)\right)^T = \left[\mathcal{N}^1_1(\chi), \mathcal{N}^1_2(\chi), \ldots \mathcal{N}^1_p(\chi)\right].$$

Then, following the same arguments as for the nodal basis, the L^2-inner product of two elements $\chi, \gamma \in \mathcal{Q}$ leads again to a mass matrix,

$$\mathbb{M}^{(1)}_{1D} = \int_\Omega \left(\Psi^1(\xi)\right)^T \Psi^1(\xi)\mathrm{d}\Omega,$$

and the dual edge functions are given by

$$\Psi'^0(\xi) = \Psi^1(\xi)\left(\mathbb{M}^{(1)}_{1D}\right)^{-1},$$

where

$$\Psi'^0(\xi) = \left[h'_1(\xi), h'_2(\xi), \ldots h'_p(\xi)\right].$$

In Fig. 3.3, these dual polynomials are also shown. It can be seen that the dual polynomials derived from the edge functions look more like (weighted) nodal polynomials.

3.2.4. Tensor products of basis functions

In two (or higher) dimensions, the co-chains are expanded in tensor products of the basis [57]. 0-forms are projected to 0-co-chains on nodal values, hence the basis will be

$$P(\xi,\eta) = \Psi^0(\xi) \otimes \Psi^0(\eta),$$

with individual components

$$P_{i,j}(\xi,\eta) = h_i(\xi)h_j(\eta).$$

Then, the basis of a projected 1-form is constructed from a mix of nodal and edge basis, for lines in ξ- and η-direction, respectively, as

$$\mathbf{L}(\xi,\eta) = \begin{bmatrix} \mathbf{L}_x(\xi,\eta) & 0 \\ 0 & \mathbf{L}_y(\xi,\eta) \end{bmatrix} = \begin{bmatrix} \Psi^1(\xi) \otimes \Psi^0(\eta) & 0 \\ 0 & \Psi^0(\xi) \otimes \Psi^1(\eta) \end{bmatrix},$$

with individual components

$$\left(\mathbf{L}_x\right)_{i,j}(\xi,\eta) = e_i(\xi)h_j(\eta),$$
$$\left(\mathbf{L}_y\right)_{i,j}(\xi,\eta) = h_i(\xi)e_j(\eta).$$

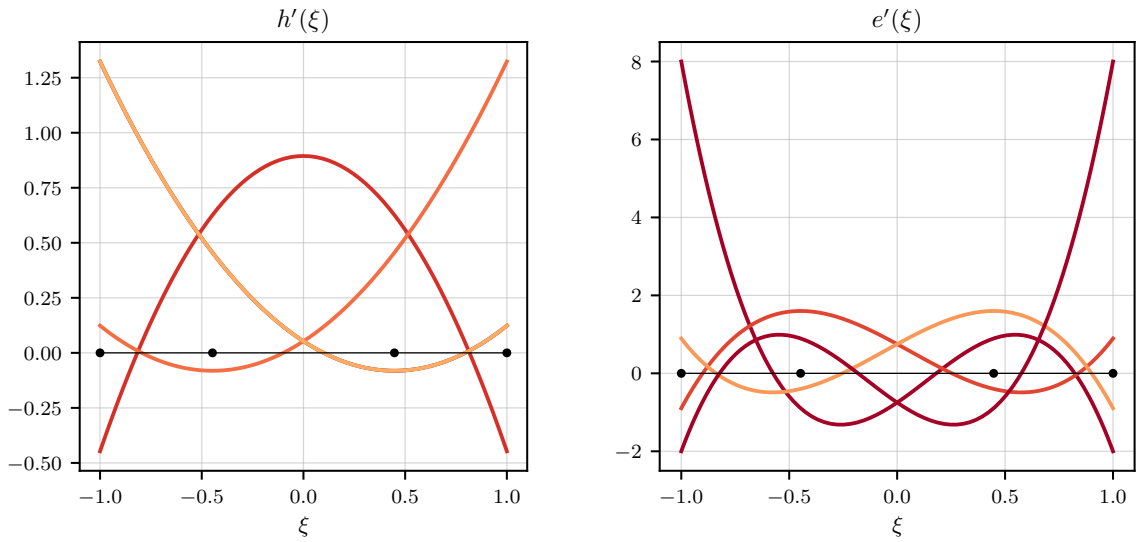

(a) Nodal basis functions, of lower order $p-1$.

(b) Edge basis functions of order p.

Figure 3.3: The algebraic dual basis functions for an element in $\mathbb{R}^1$ of $p=3$.

Finally, the basis of a projected 2-form is constructed of only edge basis, such that a surface basis is constructed,

$$S(\xi,\eta) = \Psi^1(\xi) \otimes \Psi^1(\eta),$$

with individual components

$$S_{i,j}(\xi,\eta) = e_i(\xi) e_j(\eta).$$

The algebraic dual basis for $\mathbb{R}^2$ is constructed in a similar manner as for the 1-dimensional basis. For an elaborate derivation including mappings (discussed in Section 3.3) of the mass matrices, see Appendix A.1. The (two-dimensional) mass matrices can be constructed in $\mathbb{R}^2$ with

$$\mathbb{M}^{(0)} = \int_\Omega P^T P \mathrm{d}\Omega, \quad \mathbb{M}^{(1)} = \int_\Omega \mathbf{L}^T \mathbf{L} \mathrm{d}\Omega, \quad \mathbb{M}^{(2)} = \int_\Omega S^T S \mathrm{d}\Omega$$

For the polynomials of a polynomials space of order p, denoted again by $\mathcal{P}^p$, with $\phi \in \mathcal{P}^p \otimes \mathcal{P}^p$, $\boldsymbol{\pi} \in \left(\mathcal{P}^p \otimes \mathcal{P}^{p-1}\right) \times \left(\mathcal{P}^{p-1} \otimes \mathcal{P}^p\right)$ and $\chi \in \mathcal{P}^{p-1} \otimes \mathcal{P}^{p-1}$, the nodal, edge, and surface degrees of freedom given by [43]

$$\mathcal{N}'^2(\phi) = \mathbb{M}^{(0)} \mathcal{N}^0(\phi), \quad \mathcal{N}'^1(\boldsymbol{\pi}) = \mathbb{M}^{(1)} \mathcal{N}^1(\boldsymbol{\pi}), \quad \mathcal{N}'^0(\chi) = \mathbb{M}^{(2)} \mathcal{N}^2(\chi).$$

The corresponding basis can be constructed using

$$P' = P^T \left(\mathbb{M}^{(0)}\right)^{-1}, \quad \mathbf{L}' = \mathbf{L}^T \left(\mathbb{M}^{(1)}\right)^{-1}, \quad S' = S^T \left(\mathbb{M}^{(2)}\right)^{-1}.$$

3.3. Mapping

Instead of directly computing quantities for the construction of the system matrix (mass matrices) and right-hand-side (boundary conditions and forcing functions) on the physical domain, it is convenient to compute on a reference domain, with $(\xi,\eta) \in \widehat{\Omega}$, and use a mapping to the physical domain $(x,y) \in \Omega$. The mapping of coordinates can be expressed in an operator $\Phi : \widehat{\Omega} \to \Omega$, such that $(x,y) = (f_1(\xi,\eta), f_2(\xi,\eta))$. This mapping is in general not invertible. The mapping of differential forms from the physical domain to the reference domain then happens with the pull-back operator Φ^*. The k-forms have the desired property that they are independent of metric, that is [47],

$$\int_{\widehat{\Omega}} \widehat{a}^{(k)} = \int_\Omega a^{(k)}.$$

It is then the pull-back operator that maps between $a^{(k)}$ and $\widehat{a}^{(k)}$, which is defined by [47]

$$\int_\Omega a^{(k)} = \int_{\Phi(\widehat{\Omega})} a^{(k)} = \int_{\widehat{\Omega}} \Phi^* a^{(k)} = \int_{\widehat{\Omega}} \widehat{a}^{(k)}.$$

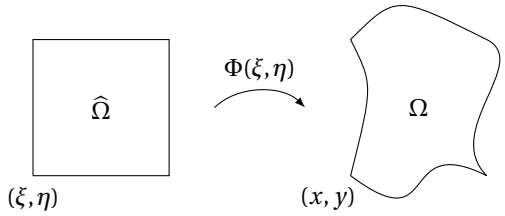

Figure 3.4: Mapping between reference and physical domain.

It is important to note that the pull-back operator commutes with the wedge product $\wedge$, denoted as

$$\Phi^*\left(a^{(k)} \wedge b^{(k)}\right) = \Phi^*\left(a^{(k)}\right) \wedge \Phi^*\left(b^{(k)}\right),$$

and the exterior derivative d [47, 57], denoted as $\Phi^* \mathrm{d} = \mathrm{d}\Phi^*$, two properties that will be used extensively in derivations of mapping terms. It also commutes with the projection operation π_h [47]. The pull-back operator involves computing components of the Jacobian matrix, for a two-dimensional problem the Jacobian matrix and its inverse can written as

$$\boldsymbol{\Phi}^* = \boldsymbol{J} = \begin{bmatrix} \frac{\partial x}{\partial \xi} & \frac{\partial x}{\partial \eta} \\ \frac{\partial y}{\partial \xi} & \frac{\partial y}{\partial \eta} \end{bmatrix}.$$

The determinant then follows as

$$\left|\boldsymbol{\Phi}^*\right| = |\boldsymbol{J}| = \frac{\partial x}{\partial \xi}\frac{\partial y}{\partial \eta} - \frac{\partial x}{\partial \eta}\frac{\partial y}{\partial \xi}.$$

To compute components of the inverse pull-back operation, a one-to-one correspondence can be used,

$$\boldsymbol{\Phi}^{-*} = \begin{bmatrix} \frac{\partial \xi}{\partial x} & \frac{\partial \xi}{\partial y} \\ \frac{\partial \eta}{\partial x} & \frac{\partial \eta}{\partial y} \end{bmatrix} = \frac{1}{|\boldsymbol{\Phi}^*|} \begin{bmatrix} \frac{\partial y}{\partial \eta} & -\frac{\partial x}{\partial \eta} \\ -\frac{\partial y}{\partial \xi} & \frac{\partial x}{\partial \xi} \end{bmatrix}.$$

The application of Φ^* on the physical differential basis $\mathrm{d}x$ and $\mathrm{d}y$ follow as

$$\Phi^*(\mathrm{d}x) = \frac{\partial x}{\partial \xi}\mathrm{d}\xi + \frac{\partial x}{\partial \eta}\mathrm{d}\eta, \qquad \Phi^*(\mathrm{d}y) = \frac{\partial y}{\partial \xi}\mathrm{d}\xi + \frac{\partial y}{\partial \eta}\mathrm{d}\eta,$$

as well as the application of Φ^{-*} on the reference differential basis $\mathrm{d}\xi$ and $\mathrm{d}\eta$ to map back to the physical domain,

$$\Phi^{-*}(\mathrm{d}\xi) = \frac{\partial \xi}{\partial x}\mathrm{d}x + \frac{\partial \xi}{\partial y}\mathrm{d}y = \frac{1}{|\boldsymbol{\Phi}^*|}\left(\frac{\partial y}{\partial \eta}\mathrm{d}x - \frac{\partial x}{\partial \eta}\mathrm{d}y\right),$$
$$\Phi^{-*}(\mathrm{d}\eta) = \frac{\partial \eta}{\partial x}\mathrm{d}x + \frac{\partial \eta}{\partial y}\mathrm{d}y = \frac{1}{|\boldsymbol{\Phi}^*|}\left(-\frac{\partial y}{\partial \xi}\mathrm{d}x + \frac{\partial x}{\partial \xi}\mathrm{d}y\right).$$

In the second line, the correspondence of the inverse pull-back is used.

The mapping has an important consequence for the solution representation, as the solution is represented on quadrature points, which cannot be freely selected on the physical domain, but are determined by the mapping. For the application of the mimetic spectral element method on arbitrary domains, the transfinite mappings discussed in [37, 38] may be used.

3.4. Minimisation problems

There are different ways to rewrite a problem to arrive at a weak formulation that can be solved. Following the Galerkin method, any partial differential equation can be directly rewritten in the weak form, by multiplying all terms with a test function and integrating over the domain, and applying integration by parts to introduce the boundary condition [9, p. 1-3]. For some problems, a different formulation than the partial differential equations and the corresponding weak form notations is possible. This involves a minimisation problem, which is posed such that the minimum of a given functional is sought for. The solution can be

constrained beforehand by the essential boundary condition on the variables. This minimisation is done by taking variations. From this, the weak formulation is then obtained [72, p. 75-77]. If the exact solution is smooth enough, the weak formulation leads to the partial differential equations to solve, which can be done by adding explicitly additional boundary conditions, called natural boundary conditions.

The latter procedure will be explained in this section in more detail. Then, the inner product of differential forms is defined, and finally the function spaces in which the test and trial basis will be defined, and which will also allow for the proper error evaluation are shortly elaborated on.

3.4.1. Deriving the weak form

When starting from the minimisation problem, the resulting system of equations can lead to a symmetric matrix to solve. It is possible to write the Poisson problem, the linear elasticity problem and the Stokes flow problem in this form. These start from the principle of minimisation of energy. For the Poisson problem, the energy in the system is given, with $\mathbf{q} = \nabla p$, by

$$J(p) = \int_\Omega \frac{1}{2}\left|\mathbf{q}\right|^2 - pf\,\mathrm{d}\Omega = \int_\Omega \frac{1}{2}\left|\nabla p\right|^2 - pf\,\mathrm{d}\Omega.$$

Furthermore, $p = 0$ is prescribed on the boundary. The minimum of energy can be found by considering a small change, here α, taking the derivative and setting zero,

$$\begin{aligned}
0 = \left.\frac{\mathrm{d}J(p+\alpha\tilde{p})}{\mathrm{d}\alpha}\right|_{\alpha=0} &= \int_\Omega \left.\frac{\mathrm{d}\left\{\frac{1}{2}\left|\nabla p + \alpha\nabla\tilde{p}\right|^2 - f\left(p+\alpha\tilde{p}\right)\right\}}{\mathrm{d}\alpha}\right|_{\alpha=0} \mathrm{d}\Omega \\
&= \int_\Omega \left.\left\{\frac{1}{2}\left(2\nabla\tilde{p}\cdot\left(\nabla p + \alpha\nabla\tilde{p}\right)\right) - \tilde{p}f\right\}\right|_{\alpha=0} \mathrm{d}\Omega \\
&= \int_\Omega \left(\nabla\tilde{p}\cdot\nabla p\right) - \tilde{p}f\,\mathrm{d}\Omega \\
&= \left(\nabla\tilde{p},\nabla p\right)_\Omega - \left(\tilde{p},f\right)_\Omega,
\end{aligned}$$

where α is set zero, and the inner product was written in shorthand. This procedure is called taking variations. Using integration by parts,

$$\left(\nabla\tilde{p},\nabla p\right)_\Omega - \left(\tilde{p},f\right)_\Omega = \left(\tilde{p},\nabla\cdot\left(\nabla p\right)\right)_\Omega - \left(\tilde{p},f\right)_\Omega = 0.$$

Since this must hold $\forall\tilde{p}$, the result is the Poisson equation, $\nabla\cdot\left(\nabla p\right) = \Delta p = f$.

To pose additional constraints on the solution, the energy functional can be restricted by imposing constraints on the solution. This is called constrained minimisation [6]. To do so, one or more Lagrange multipliers (here λ) can be used, such that the functional to be minimised becomes

$$J(\mathbf{q},\lambda) = \int_\Omega \frac{1}{2}\left|\mathbf{q}\right|^2 \mathrm{d}\Omega + \int_\Omega \lambda L\left(\mathbf{q}\right)\mathrm{d}\Omega.$$

Here, $L(\mathbf{q}) = \nabla\cdot q - f$ is a linear operator, which is the case for the other constraints used in Lagrangian formulations in this report. It will turn out that such a minimisation problem will lead to a mixed formulation, and that if a physical constraint is enforced by a Lagrange multiplier, the latter also has physical meaning. In this case, $\lambda = p$. For an elaborate discussion and comparison of the different properties of formulations arising from unconstrained and constrained optimisation problems and formulations derived using the Galerkin method, see [6].

3.4.2. The inner product

To be able to construct weak-form based solutions, it is necessary to formulate an inner product in terms of the exterior product and a Hodge operator [40]. The inner product on forms on the same oriented manifold is always metric dependent.

For two k-forms $a^{(k)}$ and $b^{(k)}$ associated to the same geometry, the inner product is defined as [47, 57]

$$\left(a^{(k)},b^{(k)}\right)_\Omega = \int_\Omega a^{(k)} \wedge \star\, b^{(k)}.$$

The inner product is a bilinear form, mapping two differential forms to a scalar. This form which is symmetric and thus results in a symmetric mass matrix. In the case the two forms are in dual spaces to each other, the

inner product becomes metric free, since the wedge product between two forms in the same space is metric free [33].

Furthermore, this inner product has the following identity when dealing with the co-differential operator, $\mathrm{d}^\star = (-1)^{n(k+1)+1} \star \mathrm{d} \star$ [57]. Like integration by parts [47], which is the Green's formula [7], the following holds,

$$\left(a^{(k-1)}, \mathrm{d}^\star b^{(k)}\right)_\Omega = \left(\mathrm{d}a^{(k-1)}, b^{(k)}\right)_\Omega - \int_{\partial\Omega} \mathrm{tr}\left(a^{(k-1)}\right) \wedge \mathrm{tr}\left(\star\, b^{(k)}\right).$$

3.4.3. Function spaces

The necessary function spaces for the solution will be stated here. To determine the properties of the solution of the problems considered, the function spaces should be defined beforehand. Here, Ω denotes a domain of computation, and $\partial\Omega$ denotes the boundary of that domain, and it is assumed for all problems that the boundary is Lipschitz continuous. The most general function space in Ω is the space of square integrable functions, $L^2(\Omega)$, formally defined as [9, p. 4]

$$L^2(\Omega) \equiv \left\{ f \;\middle|\; \int_\Omega |f|^2 \,\mathrm{d}\Omega = \|f\|^2_{L^2(\Omega)} < \infty \right\}.$$

Function spaces that ensure that the solution spaces contain suitable functions with appropriate derivatives [9, p. 4]

$$H^1(\Omega) \equiv \left\{ p \in L^2(\Omega) \;\middle|\; \nabla p \in \left[L^2(\Omega)\right]^n \right\}, \tag{3.3a}$$

$$H(\mathrm{div}, \Omega) \equiv \left\{ \mathbf{q} \in \left[L^2(\Omega)\right]^n \;\middle|\; \nabla \cdot \mathbf{q} \in L^2(\Omega) \right\}, \tag{3.3b}$$

$$H(\mathrm{curl}, \Omega) \equiv \left\{ \mathbf{q} \in \left[L^2(\Omega)\right]^n \;\middle|\; \nabla \times \mathbf{q} \in \left[L^2(\Omega)\right]^n \right\}. \tag{3.3c}$$

The selected function spaces for a problem should always ensure that variational analysis of a minimisation problem is well-defined.

3.5. Error computation

Although the solution can be visualised qualitatively by point-wise evaluation in contour plots and plots of cross-sections, it is also important to compare to the exact solution and compute the error at many points to verify the method. This is done by computing the error with appropriate norms. By measuring the error quantitatively with these norms, the convergence of the solution when refining the mesh can then be determined.

3.5.1. Norms

The error is evaluated using norms introduced earlier. The most commonly used norm is the L^2-error norm, which for a scalar (here p) is given by

$$\|\epsilon_p\|_{L^2(\Omega)} = \sqrt{\int_\Omega \left(p^{\mathrm{ex}}(x,y) - p^h(x,y)\right)^2 \mathrm{d}\Omega}, \tag{3.4}$$

which can be numerically approximated by introducing quadrature, taking a weighted sum over a large number of points,

$$\|\epsilon_p\|^2_{L^2(\Omega)} \approx \sum_r \sum_s \left(p^{\mathrm{ex}}(x_r, y_s) - p^h(x_r, y_s)\right)^2 w_r w_s. \tag{3.5}$$

For mapped domains, it is noted that the norm changes since the size of the domain changes. The determinant of the pull-back operator or Jacobian J is applied to the integration, such that

$$\|\epsilon_p\|^2_{L^2(\Omega)} = \sum_r \sum_s \left(p^{\mathrm{ex}}(x_r, y_s) - p^h(x_r, y_s)\right)^2 J(x_r, y_s) w_r w_s.$$

For a vector (here the flux $\mathbf{q}$), that is projected as a 1-form onto the grid, to compute the total error, a Pythagorean sum of the two components should be taken,

$$\|\epsilon_{\mathbf{q}}\|^2_{L^2(\Omega)} = \|\epsilon_{q_x}\|^2_{L^2(\Omega)} + \left\|\epsilon_{q_y}\right\|^2_{L^2(\Omega)}.$$

The same holds for a tensor. Other norms that also take into account the derivative can be used. These norms are stronger, since local oscillations with low values may have high valued derivatives, hence these are ruled out even more by these norms. First, there is the divergence norm based on the space $H(\text{div})$ from (3.3b) that takes into account the residual of the discrete divergence equation. For a vector $\mathbf{q}$ and a tensor $\underline{\underline{\sigma}}$,

$$\left\|\epsilon_{\mathbf{q}}\right\|^2_{H(\text{div};\Omega)} = \left\|\epsilon_{\mathbf{q}}\right\|^2_{L^2(\Omega)} + \left\|\epsilon_{\text{div}\mathbf{q}}\right\|^2_{L^2(\Omega)}, \tag{3.6a}$$

$$\left\|\epsilon_{\underline{\underline{\sigma}}}\right\|^2_{[H(\text{div};\Omega)]^n} = \left\|\epsilon_{\underline{\underline{\sigma}}}\right\|^2_{L^2(\Omega)} + \left\|\epsilon_{\text{div}\underline{\underline{\sigma}}}\right\|^2_{L^2(\Omega)}. \tag{3.6b}$$

Similarly, the curl norm based on the space $H(\text{curl})$ from (3.3c) that takes into account the residual of the discrete curl equation,

$$\|\epsilon_\omega\|^2_{H(\text{curl};\Omega)} = \|\epsilon_\omega\|^2_{L^2(\Omega)} + \|\epsilon_{\text{curl}\omega}\|^2_{L^2(\Omega)}. \tag{3.7}$$

Finally, the gradient norm for the space H^1 from (3.3a) is used to take into account the residual of the discrete gradient of the solution, here for a scalar p and a vector $\mathbf{u}$,

$$\left\|\epsilon_p\right\|^2_{H^1(\Omega)} = \left\|\epsilon_p\right\|^2_{L^2(\Omega)} + \left\|\epsilon_{\text{grad}p}\right\|^2_{L^2(\Omega)}, \tag{3.8a}$$

$$\|\epsilon_{\mathbf{u}}\|^2_{[H^1(\Omega)]^n} = \|\epsilon_{\mathbf{u}}\|^2_{L^2(\Omega)} + \left\|\epsilon_{\text{grad}\mathbf{u}}\right\|^2_{L^2(\Omega)}. \tag{3.8b}$$

The divergence, curl and gradient part of the norms will be specified for each problem in the relevant results sections. Apart from the L^2-norm, the L^∞ norm can additionally be used to identify or rule out the presence of local (large) oscillations in the solution. It is defined as

$$\left\|\epsilon_p\right\|_{L^\infty(\Omega)} = \max_{r,s}\left|p^{\text{ex}}(x_r, y_s) - p^h(x_r, y_s)\right|. \tag{3.9}$$

Since the case of a single point with high error would be weighted out in an L^2-norm, using the L^∞ in addition guarantees that local errors are always lower than the obtained error-norm value. This is useful to prove that the error is up to machine precision, as should be the case for topological relations.

3.5.2. Convergence

As discussed in Section 3.1, the interpolation error is of order $\mathcal{O}(h^p)$. When computing the norms described in Section 3.5.1, it is relevant to see what the influence is of refinements in polynomial order p of the elements, or refinements in the number of elements K through $h = 1/K$. The error can be expressed as

$$\epsilon = Ch^{\alpha p}, \tag{3.10}$$

where C and α are positive non-zero constants, $0 < \alpha < 1$. By refinement of polynomial order p, it is thus expected that for a linear increase in p, the error decreases exponentially. This can be shown in a plot with a linear scale for p and a logarithmic scale for the error, where a straight line can be expected. By refinement of the element size, done for a set domain by increasing the number of elements K, the convergence will be of the order αp. The optimal convergence is then characterised in a plot with a logarithmic scale for both the error and element size by a straight line with slope p. The constant C only determines the height of the line in this plot, which can be influenced by the quality of the mesh.

It is valuable to compare the error of the solution to the interpolation error. This directly indicates sub-optimal performance, e. g. $\alpha < \alpha_{\text{opt}} < 1$. The interpolation error, with the exact solution projected on the mesh denoted by $\left(f^{\text{ex}}\right)^h$, is computed with

$$\|\epsilon_{\mathcal{I}}\|^2_{L^2(\Omega)} = \int_\Omega \left(f^{\text{ex}}(x,y) - \left(f^{\text{ex}}\right)^h(x,y)\right)^2 \mathrm{d}\Omega. \tag{3.11}$$

3.6. Summary

With the defined connectivity of the mesh, a means of projecting the continuous quantities and their relations on them, the basis functions for the solution and test functions, and the definitions for the solution, it is possible to construct the necessary matrices to solve problems using the mimetic spectral element method. Using reconstruction, the results can then be quantitatively analysed. Using the mapping, this is then possible for any quadrilateral mesh. Finally, the error norms defined will allow a quantitative analysis of the results, which can be expressed in convergence plots. Note that the procedure for implementation is shown schematically in Appendix C.

4

The Poisson Problem

In this chapter, a first look is taken at a simple problem, the Poisson problem, to gradually introduce the techniques used in the mimetic spectral element method. First, the derivation of the weak form and the implementation using a discrete system to solve will be shown. Then, the results for this implementation will be shown for two test cases.

4.1. Derivation and implementation

After introducing the Poisson problem in its common form, the equations are rewritten in differential forms, giving a motivation for this different way of writing. Then, the weak form is derived from a minimisation problem, leading to the system matrix to find the solution for the problem. Finally, a note is given on multiple elements, and on how to compute the solution.

4.1.1. Problem introduction

The scalar Poisson problem with Dirichlet boundary conditions is given by

$$\Delta p = f \qquad \text{in } \Omega, \tag{4.1a}$$
$$p = g \qquad \text{on } \partial\Omega. \tag{4.1b}$$

Here, p is a potential, and f a forcing function. For Neumann boundary conditions, the second part generally reads $\nabla p \cdot \mathbf{n} = g \in \partial\Omega$. If only Neumann boundary conditions are prescribed, this poses the constraint on the choice of f and g,

$$\int_\Omega f \mathrm{d}\Omega = \int_\Omega \Delta p \mathrm{d}\Omega = \int_{\partial\Omega} \nabla p \mathrm{d}\Gamma = \int_{\partial\Omega} g \mathrm{d}\Gamma,$$

and that an additional constraint is needed for p, since it is only determined up to a constant. The additional constraint is either setting one value in the domain, or setting $\int_\Omega p \mathrm{d}\Omega = 0$.

In differential forms, the Poisson problem can be written for $\mathbb{R}^n$ as, [33]

$$\mathrm{d}q^{(n-1)} = f^{(n)} \quad \text{in } \Omega,$$

with q the flux or normal velocity, and

$$\begin{aligned} q^{(n-1)} &= \star\, u^{(1)} \\ &= \star\, \mathrm{d}p^{(0)} \\ &= \star\, \mathrm{d} \star p^{(n)} \\ &= -\mathrm{d}^\star p^{(n)}, \end{aligned}$$

since $u^{(1)} = \mathrm{d}p^{(0)}$, and for $n = 2$ applying $\mathrm{d}^\star$ to a 2-form sets $k = 2$, and $\mathrm{d}^\star = (-1)^{n(k+1)+1} \star \mathrm{d} \star = - \star \mathrm{d} \star$ [33]. Here, $u^{(1)}$ is the circulation or tangential velocity. This can be rewritten to a system of first order equations,

such that

$$q^{(n-1)} + \mathrm{d}^\star p^{(n)} = 0 \qquad \text{in } \Omega, \tag{4.2a}$$

$$\mathrm{d}q^{(n-1)} = f^{(n)} \qquad \text{in } \Omega, \tag{4.2b}$$

$$\star p^{(n)} = p'^{(0)} = g'^{(0)} \qquad \text{on } \partial\Omega. \tag{4.2c}$$

The differential forms clarify which relations are approximate and which can be represented exactly. The relations between $q^{(n-1)}$ and $u^{(1)}$ involves a Hodge operation. The same holds for $f^{(n)} = \star f^{(0)}$, where $f^{(0)}$ can be seen as input data which may not be certain in practise. Finally, the boundary condition poses another uncertainty, and also here the metric dependency is seen. From this formulation, the separation of relations that are uncertain and the relations that are exactly known is clear.

As discussed in Section 3.1.2, these differential forms can be projected onto components of the cell complex. The projection on them are co-chains, and these values thus represent the weights of a basis that is defined on mesh elements. The associated geometry in $n = 2$ for the 1-form q and the dual 0-form for this specific problem is depicted in Fig. 3.1.

4.1.2. Lagrangian formulation

The derivation of the weak form from the Lagrangian formulation now follows. The Lagrangian formulation for the minimisation problem for the Poisson problem is posed as the saddle-point problem [9, p. 24-25]

$$\mathcal{L}\left(\mathbf{q}, \lambda; f, \lambda_P\right) = \int_\Omega \frac{1}{2}\mathbf{q}^T\mathbf{q} + \lambda\left(\nabla\cdot\mathbf{q} - f\right)\mathrm{d}\Omega - \int_{\partial\Omega} \lambda_P \mathbf{q}\cdot\mathbf{n}\mathrm{d}\Gamma. \tag{4.3}$$

Here, $\lambda_P = \mathrm{tr}\,(\lambda)$ is given on the boundary, and $f \in L^2(\Omega)$ in the domain. From this formulation, it is seen in which spaces the solution $(\mathbf{q}, \lambda)$ should be sought for: $\lambda \in L^2(\Omega)$, and $\mathbf{q} \in H(\mathrm{div}, \Omega)$. As explained in Section 3.4, the functional (4.3) can be minimised by considering small variations in the arguments, taking the derivative, and setting to zero. For example, now taking variations with respect to $\mathbf{q}$,

$$\left.\frac{\mathrm{d}\mathcal{L}\left(\mathbf{q} + \alpha\tilde{q}, \lambda + \beta\tilde{\lambda}; f, \lambda_P\right)}{\mathrm{d}\alpha}\right|_{\alpha=\beta=0} = 0,$$

gives

$$\left(\tilde{\mathbf{q}}, \mathbf{q}\right)_\Omega + \left(\lambda, \nabla\cdot\tilde{\mathbf{q}}\right)_\Omega = \int_{\partial\Omega} \lambda_P \tilde{\mathbf{q}}\cdot\mathbf{n}\mathrm{d}\Gamma, \quad \forall\tilde{\mathbf{q}} \in H(\mathrm{div}).$$

Next, taking variations with respect to λ results in the conservation law,

$$\left(\tilde{\lambda}, \nabla\cdot\mathbf{q}\right)_\Omega = \left(\tilde{\lambda}, f\right)_\Omega, \quad \forall\tilde{\lambda} \in L^2(\Omega).$$

The final system of equations in weak form is then described in the variational problem: Find $\lambda \in L^2(\Omega)$, and $\mathbf{q} \in H(\mathrm{div}, \Omega)$, such that

$$\left(\tilde{\mathbf{q}}, \mathbf{q}\right)_\Omega + \left(\lambda, \nabla\cdot\tilde{\mathbf{q}}\right)_\Omega = \int_{\partial\Omega} \lambda_P \tilde{\mathbf{q}}\cdot\mathbf{n}\mathrm{d}\Gamma, \tag{4.4a}$$

$$\left(\tilde{\lambda}, \nabla\cdot\mathbf{q}\right)_\Omega = \left(\tilde{\lambda}, f\right)_\Omega, \tag{4.4b}$$

$\forall\tilde{\mathbf{q}} \in H(\mathrm{div}, \Omega), \forall\tilde{\lambda}) \in L^2(\Omega)$. If the solution is sufficiently smooth in Ω, and if $\lambda \in H^1(\Omega)$, since this holds $\forall\tilde{\lambda} \in L^2(\Omega)$ and $\forall\tilde{\mathbf{q}} \in H(\mathrm{div}, \Omega)$, applying the main theorem of calculus results in the system of first order ordinary differential equation of the Poisson problem,

$$\mathbf{q} - \nabla\lambda = 0 \qquad \text{in } \Omega, \tag{4.5a}$$

$$\nabla\cdot\mathbf{q} = f \qquad \text{in } \Omega, \tag{4.5b}$$

$$\lambda = \lambda_P \qquad \text{on } \partial\Omega. \tag{4.5c}$$

In this case, it is seen that the Lagrange multiplier λ will have as physical interpretation the pressure p, while q has the physical interpretation of a flux.

4.1.3. Weak formulation

In finite element methods, an engineering approach to derive the weak form is to directly test the familiar differential equation (4.2) with suitable test functions. However, as seen in the previous section, in case of the Poisson problem, it is also possible to derive a weak formulation from a minimisation problem. The weak form (4.4) can be written with differential forms as

$$\left(\tilde{q}^{(n-1)}, q^{(n-1)}\right)_\Omega + \left(\mathrm{d}\tilde{q}^{(n-1)}, p^{(n)}\right)_\Omega = \int_{\partial\Omega} \mathrm{tr}\left(\tilde{q}^{(n-1)}\right) \wedge \mathrm{tr}\left(p^{(0)}\right), \tag{4.6a}$$

$$\left(\tilde{p}^{(n)}, \mathrm{d}q^{(n-1)}\right)_\Omega = \left(\tilde{p}^{(n)}, f^{(n)}\right)_\Omega. \tag{4.6b}$$

If the standard Galerkin method is followed, i.e. (4.2) is tested with test functions that have the same basis as the solution, then

$$\begin{aligned}\left(\tilde{q}^{(n-1)}, q^{(n-1)}\right)_\Omega + \left(\tilde{q}^{(n-1)}, \mathrm{d}^\star p^{(n)}\right)_\Omega &= 0,\\ \left(\tilde{p}^{(n)}, \mathrm{d}q^{(n-1)}\right)_\Omega &= \left(\tilde{p}^{(n)}, f^{(n)}\right)_\Omega.\end{aligned}$$

The system can be rewritten using integration by parts [47], as

$$\left(\tilde{q}^{(n-1)}, \mathrm{d}^\star p^{(n)}\right)_\Omega = \left(\mathrm{d}\tilde{q}^{(n-1)}, p^{(n)}\right)_\Omega - \int_{\partial\Omega} \mathrm{tr}\left(\tilde{q}^{(n-1)}\right) \wedge \mathrm{tr}\left(\star\, p^{(n)}\right),$$

hence (4.6) can be derived from either (4.2) or (4.3). Since this is a mixed formulation arising from a constrained optimisation, this setting is called mixed Galerkin [6]. The point made here is that starting from the Lagrangian formulation allows to more clearly select the necessary function spaces, and hence the correct basis for representing the solution.

4.1.4. The system to solve

The system (4.6) can be written in terms of matrices for the given basis functions as

$$\begin{bmatrix} \mathbb{M}^{(n-1)} & \left(\mathbb{M}^{(n)}\mathbb{E}^{(n,n-1)}\right)^T \\ \mathbb{M}^{(n)}\mathbb{E}^{(n,n-1)} & 0 \end{bmatrix} \begin{bmatrix} \boldsymbol{q}^h \\ \boldsymbol{p}^h \end{bmatrix} = \begin{bmatrix} \boldsymbol{g}^h \\ \mathbb{M}^{(n)}\boldsymbol{f}^h \end{bmatrix}, \tag{4.8}$$

with $\boldsymbol{g}^h$ a vector containing all boundary values at the same edges as $\boldsymbol{q}^h$, and $\boldsymbol{f}^h$ a vector containing the reduced co-chain values of f at the same locations as $\boldsymbol{p}^h$. The reduction of these quantities from their known continuous functions is discussed in detail in Appendix A.3 and Appendix A.4. The construction of mass matrices, and the derivation of the term leading to the incidence matrix, is discussed in detail in Appendix A.1 and Appendix A.2.

Using the algebraic dual basis from Section 3.2.3, it is possible to rewrite the system to eliminate the mass matrix $\mathbb{M}^{(n)}$ from the second row and make it part of the solution. Introducing $\left(\boldsymbol{p}'\right)^h \equiv \mathbb{M}^{(n)}\boldsymbol{p}^h$,

$$\begin{bmatrix} \mathbb{M}^{(n-1)} & \left(\mathbb{E}^{(n,n-1)}\right)^T \\ \mathbb{E}^{(n,n-1)} & 0 \end{bmatrix} \begin{bmatrix} \boldsymbol{q}^h \\ \left(\boldsymbol{p}'\right)^h \end{bmatrix} = \begin{bmatrix} \boldsymbol{g}^h \\ \boldsymbol{f}^h \end{bmatrix}, \tag{4.9}$$

since on the primal grid, where the fluxes are, the algebraic dual polynomials can be used as a basis for $\star\, p^{(2)}$ in the system. This means that the system to solve becomes sparser, and part of the solution, $\left(\boldsymbol{p}'\right)^h$ has to be solved for $\mathbb{M}^{(n)}$ in a post-processing step, e.g. $\boldsymbol{p}^h = \left(\mathbb{M}^{(n)}\right)^{-1}\left(\boldsymbol{p}'\right)^h$. This is done to be able to expand it in primal basis functions for p^h again. The sparsity of these two systems, in primal-primal and primal-dual formulation, is compared in Fig. 4.1. The effect of the full mass matrix $\mathbb{M}^{(n)}$ is clear from the sparsity in the primal-dual formulation.

4.1.5. Continuous and hybrid elements

To divide the domain in multiple spectral elements, there are generally two approaches, separating into continuous and hybrid elements. In continuous methods, the global unknown vector includes only one unknown for every edge, even if it is shared by two elements. In the hybrid method, the numbering globally is done as if the edges of elements are disconnected, such that adjacent boundaries of edges have two unknowns. The pairing of edges at the same location is then performed using an interface operator. This step can be performed separately and the domains can be solved independently afterwards. For the Poisson problem using

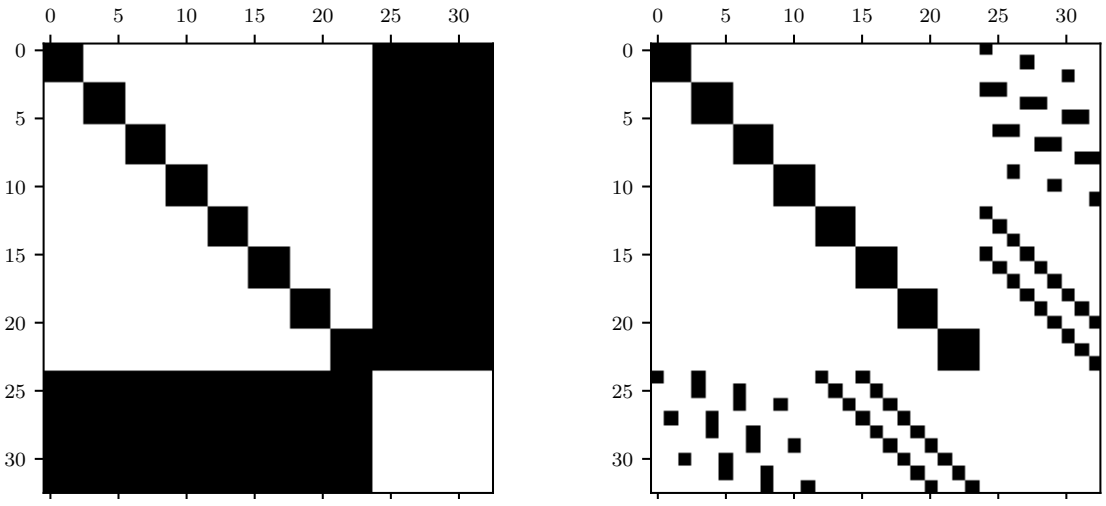

(a) Primal-primal formulation, from (4.8).

(b) Primal-dual formulation, from (4.9).

Figure 4.1: Sparsity patterns of the system matrix for the Poisson problem on a single orthogonal element, $p = 3$.

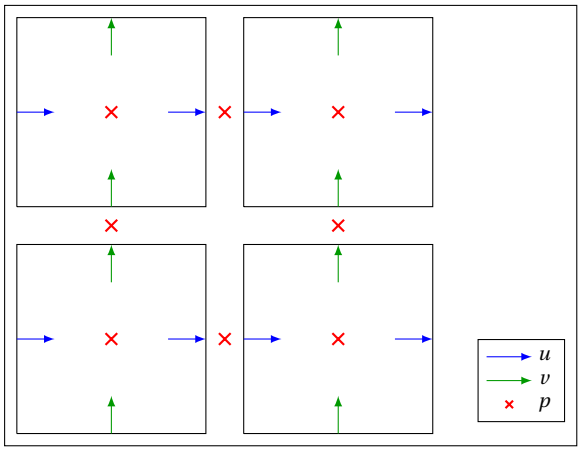

Figure 4.2: Coupling the hybrid elements of lowest order for the Poisson problem, $K = 2$, $p = 1$.

the hybrid method, the setup is visualised in Fig. 4.2. The practical implementation for coupling the shared edges at boundaries between elements is setting up a matrix that equates the two edges. For a global numbering index, the Poisson problem becomes

$$\begin{bmatrix} \mathbb{M}^{(n-1)} & \left(\mathbb{E}^{(n,n-1)}\right)^T & \mathbb{N}^T \\ \mathbb{E}^{(n,n-1)} & 0 & 0 \\ \mathbb{N} & 0 & 0 \end{bmatrix} \begin{bmatrix} \boldsymbol{q}^h \\ \mathbb{M}^{(n)}\boldsymbol{p}^h \\ \boldsymbol{\lambda}^h \end{bmatrix} = \begin{bmatrix} \boldsymbol{g}^h \\ \boldsymbol{f}^h \\ 0 \end{bmatrix}.$$

The matrix $\mathbb{N}$ is sparse, just like the incidence matrix. Due to the orientation of the edges, it will be composed of plus and minus one, and zero entries. A note on how to solve this particular system is given in Appendix B. For an elaborate derivation of the hybrid formulation of the Poisson problem and the derivation of a Lagrangian for the interface operator, see [73]. The results presented in this chapter are generated with continuous elements, since the result is the same.

The mass matrices can be generated for each element separately, as the element mass matrices include a local mapping of each element. This is a useful property for the hybrid method, since the inversion of the matrix can then be done for each element separately. For continuous elements, the whole system must be solved, such that the global numbering may alter the condition number of the system matrix, and therefore the computational effort needed to solve it. The numbering is a matter of using a consistent index.

The global matrix can be set up in different ways. Each element can be numbered such that a diagonal of

the element systems is created. This means that the vector on the left-hand side is built up directly by stacking the element unknown vectors. The right hand side must also be ordered in the same way. Another way is to order the whole matrix globally. This means assigning the entries in the matrix such that a global unknown vector is created. This will mean that the mass matrices are on a diagonal, with some sparse off-diagonal matrices and a large part is zero. The solution and right-hand side vector is then also ordered with a global numbering index.

4.1.6. Evaluating the solution

The solution vector contains discrete projections of the 1-form $q^{(1)}$ and 2-form $p^{(2)}$, which represent the integral value (or co-chain) of the fluxes q through the lines, and the integral value of p over a surface. To localise these values on any point in the domain, the solution can be interpolated by evaluating the solution at an amount of points larger than the polynomial order used.

Assuming an orthogonal square reference domain,

$$u^h(x,y) = \sum_{i=1}^{p+1}\sum_{j=1}^{p}(u)_{ij}h_i(x)e_j(y), \qquad v^h(x,y) = \sum_{i=1}^{p}\sum_{j=1}^{p+1}(v)_{ij}e_i(x)h_j(y),$$

where x, y are chosen on a fine grid. Similarly,

$$p^h(x,y) = \sum_{i=1}^{p}\sum_{j=1}^{p}p_{ij}e_i(x)e_j(y).$$

The errors are evaluated point-wise using these functions. For general domains that require mapping, the derived expressions are given in Appendix A.3.2.

Denoting the result vector of the application of the incidence matrix to the solution vector of the flux as $\left(\mathrm{d}q^{(1)}\right)^h = \mathbb{E}^{(n,n-1)}\boldsymbol{q}^h$, the resulting system vector can be reconstructed using the same basis as for p^h,

$$\left(\mathrm{d}q^{(1)}\right)^h(x,y) = \sum_{i=1}^{p}\sum_{j=1}^{p}\left(\mathrm{d}q^{(1)}\right)_{i,j}e_i(x)e_j(y).$$

4.2. Results

In this section, the results for the Poisson problem are presented. These results have been reproduced as a verification of the code implementation, but also serve as an overview of the key findings in previous works. The two test problems are a manufactured solution and a solution with a singularity which has an exact solution as well.

4.2.1. Manufactured solution

For all implementations, the first test case for verification is reproducing a manufactured solution. This can be done on an orthogonal mesh and a deformed, curvilinear mesh seen in Fig. 4.3. The spacing of the elements is linear, while the solution points inside an element are the Gauss-Lobatto-Legendre points. The mapping of reference coordinates (ξ,η) from the reference domain $[-1,1]^2$ to the deformed mesh coordinates (x,y), is given by, [57],

$$x(\xi,\eta) = \frac{1}{2}\left(1+\xi+c\sin(\pi\xi)\sin(\pi\eta)\right),$$
$$y(\xi,\eta) = \frac{1}{2}\left(1+\eta+c\sin(\pi\xi)\sin(\pi\eta)\right).$$

In this test case, the domain is rectangular, such that mappings are only needed on internal degrees of freedom, and the domain bounds can be freely chosen. The components of the Jacobian follow directly as

$$\frac{\partial x}{\partial\xi}(\xi,\eta) = \frac{1}{2}\left(1+\pi c\cos(\pi\xi)\sin(\pi\eta)\right), \qquad \frac{\partial x}{\partial\eta}(\xi,\eta) = \frac{1}{2}\left(\pi c\sin(\pi\xi)\cos(\pi\eta)\right),$$
$$\frac{\partial y}{\partial\xi}(\xi,\eta) = \frac{1}{2}\left(\pi c\cos(\pi\xi)\sin(\pi\eta)\right), \qquad \frac{\partial y}{\partial\eta}(\xi,\eta) = \frac{1}{2}\left(1+\pi c\sin(\pi\xi)\cos(\pi\eta)\right).$$

A smooth manufactured solution is chosen, where

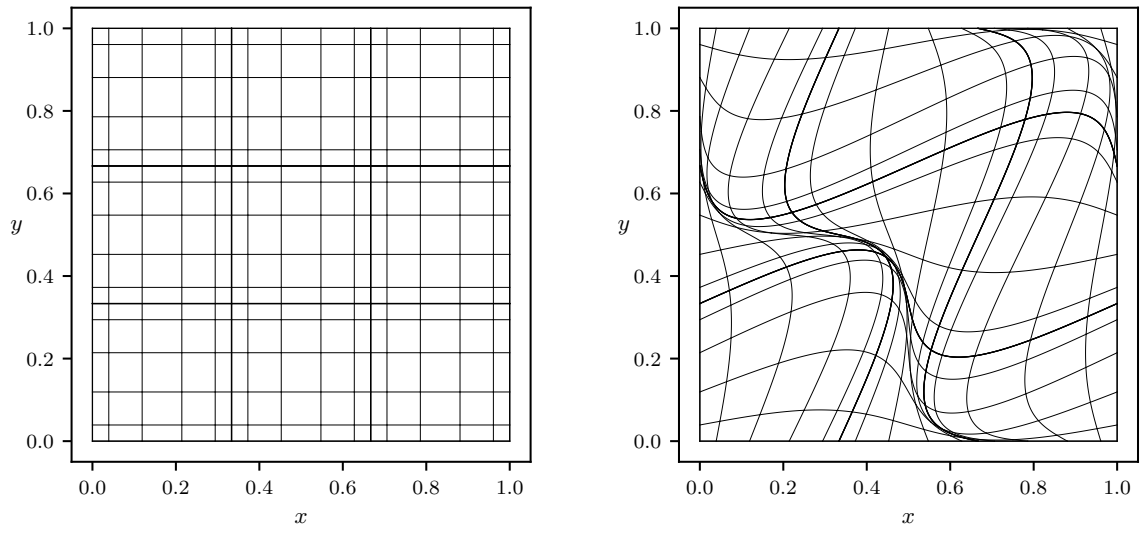

(a) Orthogonal mesh, $c = 0$.

(b) Deformed mesh, $c = 0.3$.

Figure 4.3: Meshes with $K^2 = 3^2$ elements of order $p = 5$ for different deformation coefficient c.

$$p^{\text{ex}} = \sin(2\pi x)\sin(2\pi y),$$

such that

$$\begin{aligned} u^{\text{ex}} &= 2\pi\cos(2\pi x)\sin(2\pi y), \\ v^{\text{ex}} &= 2\pi\sin(2\pi x)\cos(2\pi y), \\ f^{\text{ex}} &= -8\pi\cos(2\pi x)\cos(2\pi y). \end{aligned}$$

The solution for the potential p^h is zero on the boundary in this test case, as the test domain of $[0,1]^2$ is used. In Fig. 4.4, the solution and error contours are shown for three cases, where the meshes in Fig. 4.3 are used. The boundary conditions are all Dirichlet, so with prescribed pressure. Furthermore, continuous elements are used, such that elements share a degree of freedom on the boundaries between them. The errors in a solution on a deformed mesh for the same order are clearly larger. However, by refining the mesh, the solution converges to the exact solution.

This is shown quantitatively in Fig. 4.5 for both spectral or p-refinement, and mesh or h-refinement, respectively. The norms are as defined in Section 3.5.1. For the Poisson problem, the residual norm for (3.6a), the divergence part of the $H(\text{div})$ norm, should be computed as

$$\left\|\epsilon_{\text{div}\mathbf{q}}\right\|^2_{L^2(\Omega)} = \left\|\left(\mathrm{d}q^{(1)}\right)^h - f^{\text{ex}}\right\|^2_{L^2(\Omega)}.$$

The gradient part of $\left\|\epsilon_p\right\|^2_{H^1(\Omega)}$ in (3.8a), $\left\|\epsilon_{\text{grad}p}\right\|^2_{L^2(\Omega)}$, is computed by computing

$$\left(\text{grad}p\right)^h = \left(\mathbb{M}^{(1)}\right)^{-1}\left[-\left(\mathbb{E}^{(2,1)}\right)^T\left(\boldsymbol{p}'\right)^h + \boldsymbol{g}^h\right],$$

which has two components and is expanded in the same way as q^h.

The interpolation error for the solution components is plotted as well in Fig. 4.5, which, as explained in Section 3.5.2, shows that the error in the solution representation is almost entirely due to interpolation errors. Furthermore, the indicated slopes show that the solution follows the optimal convergence of order p. The order of convergence for a deformed mesh does not change, as evident from the slopes in the h-convergence plot. The value of the constant C in (3.10) is only increased for a deformed mesh. For p-convergence, it is seen that the constant α in (3.10) decreases with deformation. The solution is still optimal independent of deformation, evident from the proximity to the interpolation error.

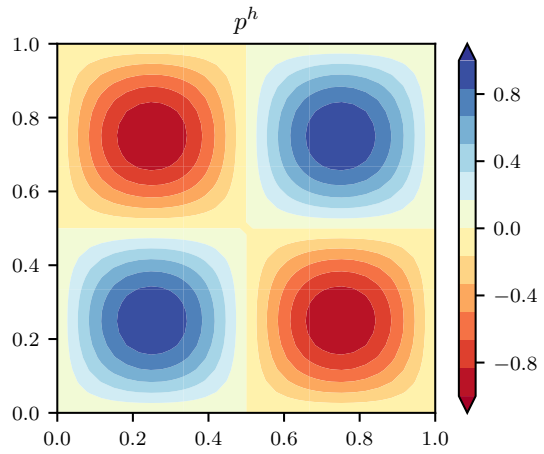

(a) Solution on orthogonal mesh (order $p = 5$).

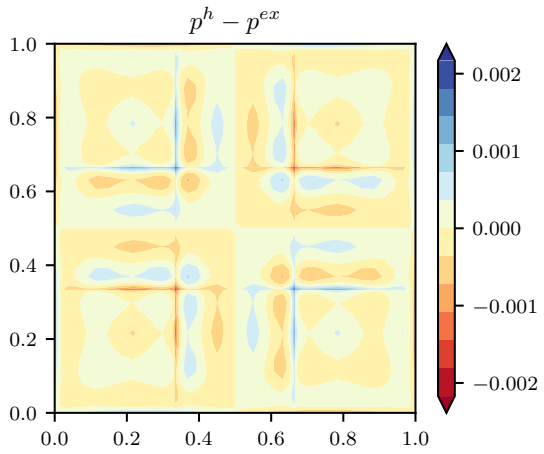

(b) Error on orthogonal mesh (order $p = 5$).

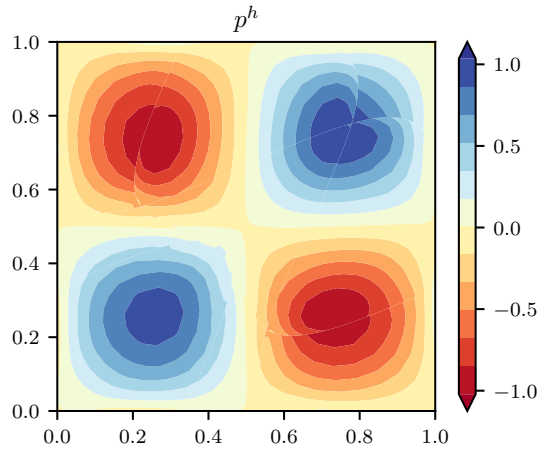

(c) Solution on deformed mesh with $c = 0.3$ (order $p = 5$).

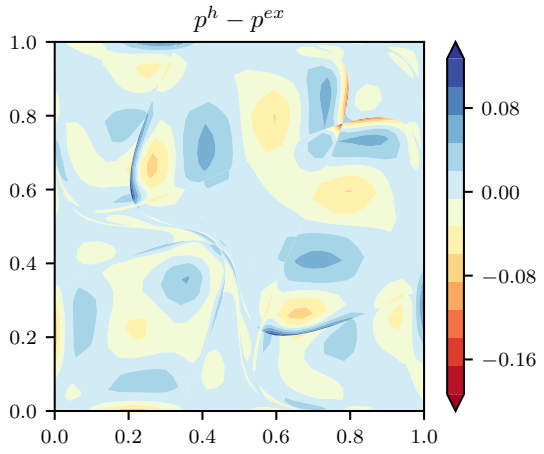

(d) Error on deformed mesh with $c = 0.3$ (order $p = 5$).

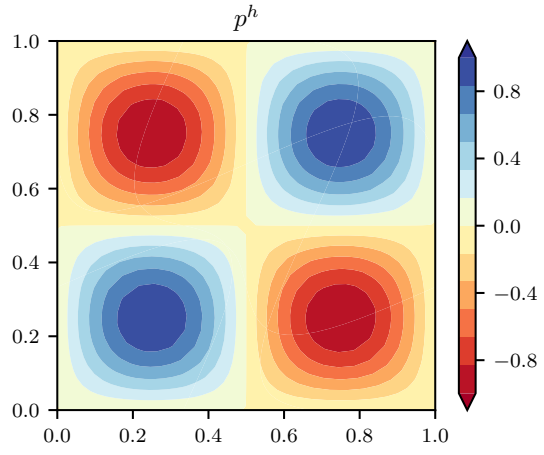

(e) Solution on deformed mesh with $c = 0.3$ (order $p = 10$).

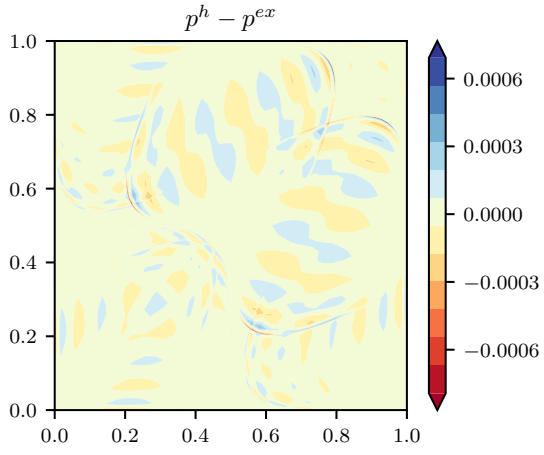

(f) Error on deformed mesh with $c = 0.3$ (order $p = 10$).

Figure 4.4: Solution for the potential p^h, computed with continuous elements on the element mesh of Fig. 4.3.

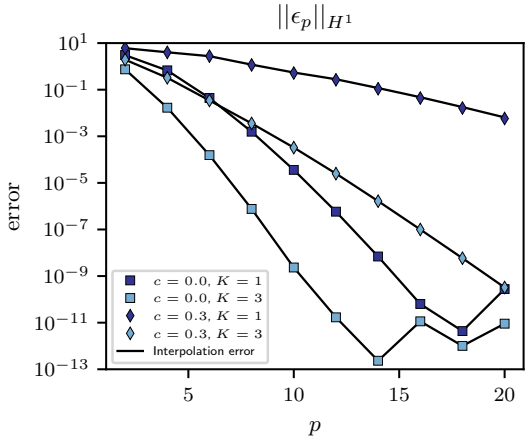

(a) p-convergence of the potential p.

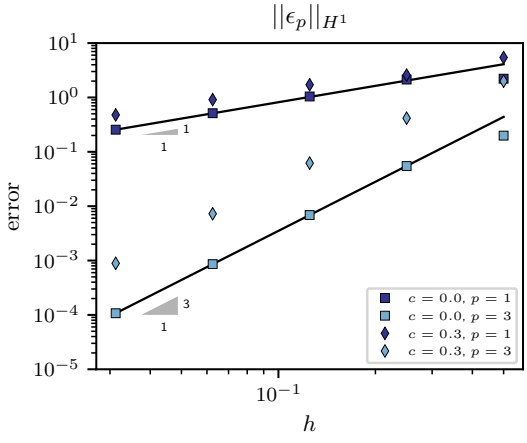

(b) h-convergence of the potential p.

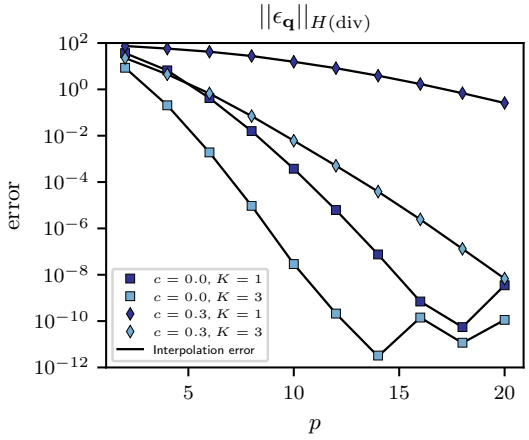

(c) p-convergence for the flux q.

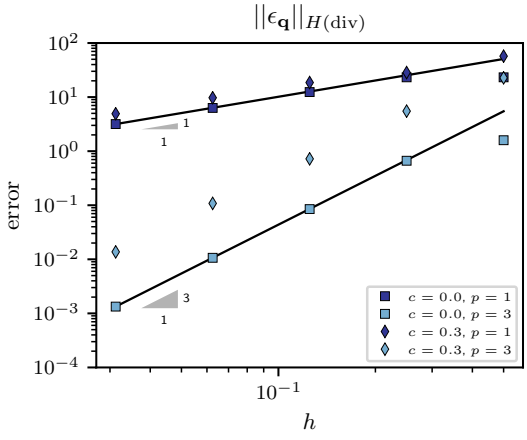

(d) h-convergence for the flux q.

Figure 4.5: Convergence trends for the Poisson manufactured solution on the domain $[0,1]^2$.

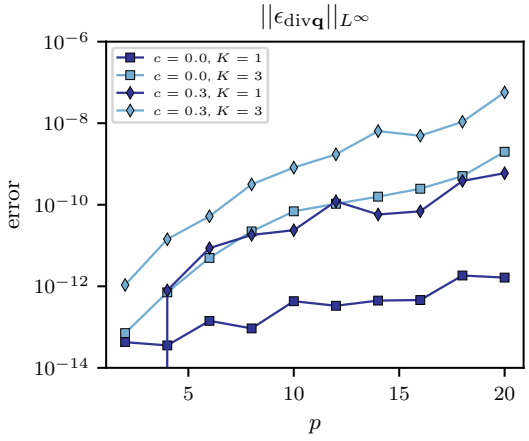

(a) Divergence of the velocity, varying resolution in p.

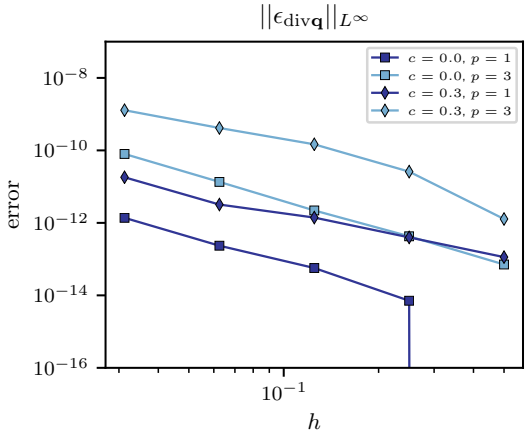

(b) Divergence of the velocity, varying resolution in h.

Figure 4.6: Conservation of mass for the Poisson manufactured solution on the domain $[0,1]^2$.

Furthermore, the point-wise error in the conservation law is shown in Fig. 4.6 for the same refinements in p and h, which can be said to be in the order of machine precision. If the force function is non-zero, it is not always possible to reduce it such that the reconstructed force is point-wise exact, as there is a loss of information if it cannot be resolved by the discrete representation. For the manufactured solution used in this section, the reduction of f is only approximate (it cannot be represented by polynomials), hence instead the reduced function f^h is used for computing the error in divergence of the velocity used for expressing mass conservation,

$$\left\|\epsilon_{\mathrm{div}\mathbf{q}}\right\|_{L^\infty}^2 = \left\|\left(\mathrm{d}q^{(1)}\right)^h - f^h\right\|_{L^\infty}^2. \tag{4.12}$$

The reason for this approach is that in real applications, the forcing function may only be a simple polynomial function. For instance, if gravity is the forcing function, it is nearly constant in the domain. In these cases, it can be fully represented in f^h. Therefore, the conservation law is point-wise satisfied up to the representation of f as f^h. Note that the coloured lines in Fig. 4.6 have no further meaning, as opposed to the black lines in Fig. 4.5. The next test problem will show that mass conservation is point-wise satisfied as well if the forcing function is zero.

4.2.2. L-shaped domain

An additional test case in an L-shaped domain is used to show the method performance on non-smooth solutions. As such, the L-shaped domain test case from [22] is used, see the geometry in Fig. 4.7a. Each of the three blocks contains K^2 elements, hence there are $3K^2$ elements in total for this problem. All boundaries

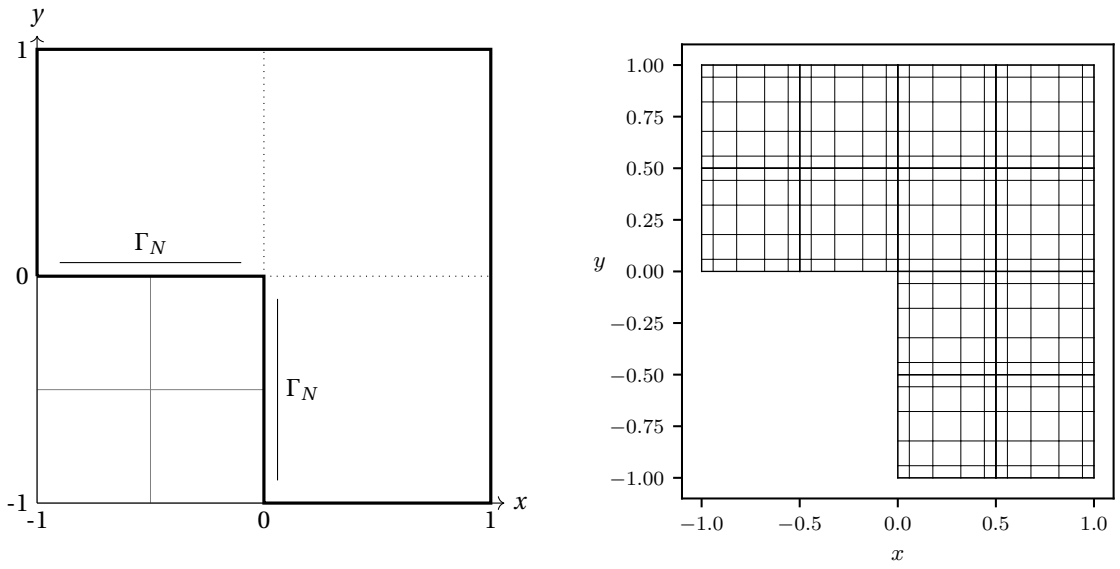

(a) L-shaped domain.

(b) Mesh for $3K^2 = 3(2^2)$ elements, $p = 5$.

Figure 4.7: L-shaped domain specifications and mesh used for generating the solution contour plots.

have a Dirichlet boundary condition, except for the inside boundaries from point $(-1,0)-(0,0)$ and $(0,-1)-(0,0)$ where the flux is prescribed directly with a Neumann boundary condition (see Appendix A.4.3 on how to implement this), these boundaries are indicated in Fig. 4.7a with Γ_N. The exact solution is given in polar coordinates by

$$\phi^{\mathrm{ex}}(r,\theta) = r^{2/3}\sin\left(\frac{2}{3}\left(\theta+\frac{\pi}{2}\right)\right),$$

such that the velocity components are given by

$$u^{\mathrm{ex}} = \frac{\partial\phi}{\partial x} = \frac{2}{3}r\cos(\theta)\sin\left(\frac{2}{3}\left(\theta+\frac{\pi}{2}\right)\right) - r^{-\frac{1}{3}}\sin(\theta)\cos\left(\frac{2}{3}\left(\theta+\frac{\pi}{2}\right)\right),$$
$$v^{\mathrm{ex}} = \frac{\partial\phi}{\partial y} = \frac{2}{3}r\sin(\theta)\sin\left(\frac{2}{3}\left(\theta+\frac{\pi}{2}\right)\right) - r^{-\frac{1}{3}}\cos(\theta)\cos\left(\frac{2}{3}\left(\theta+\frac{\pi}{2}\right)\right),$$

and the forcing term $f^{\mathrm{ex}} = 0$.

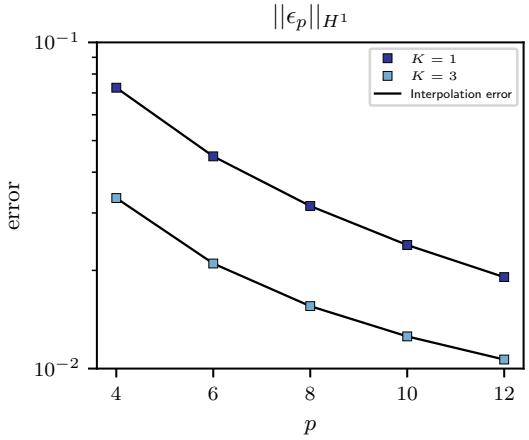

(a) p-convergence of the potential.

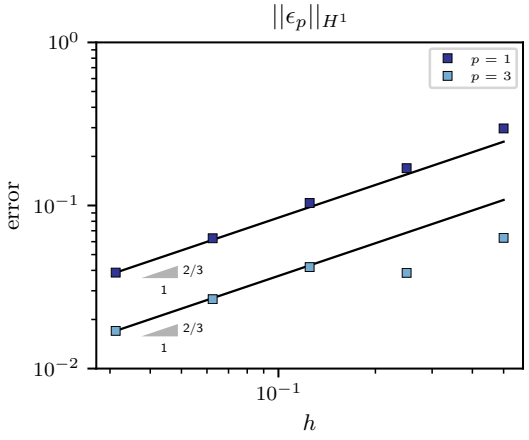

(b) h-convergence of the potential.

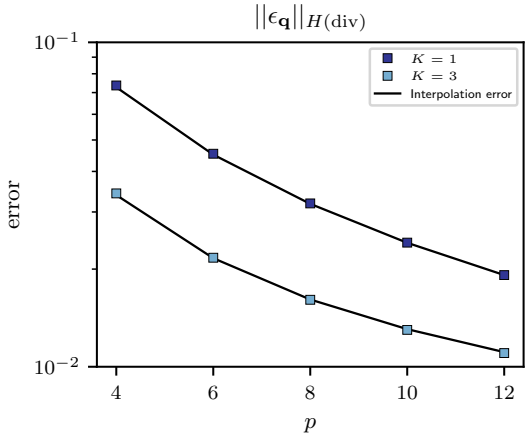

(c) p-convergence of the velocity.

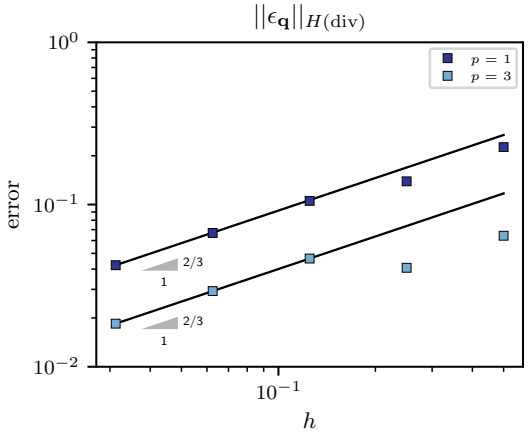

(d) h-convergence of the velocity.

Figure 4.8: Convergence trends for the solution on the L-shaped domain.

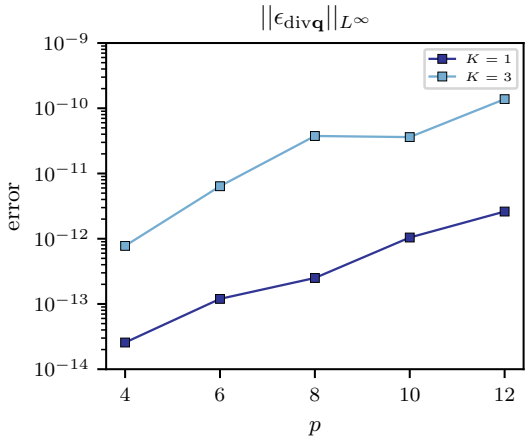

(a) Divergence of velocity for varying p.

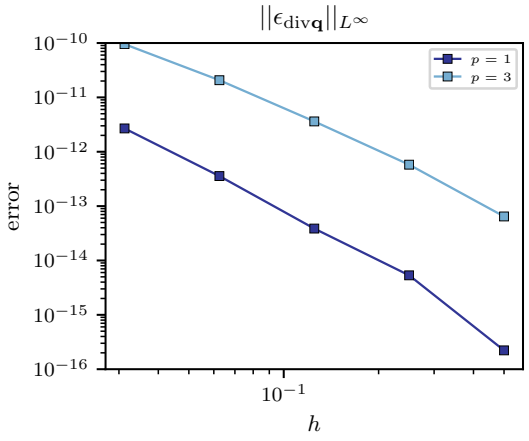

(b) Divergence of velocity for varying h.

Figure 4.9: Conservation of mass for the solution on the L-shaped domain.

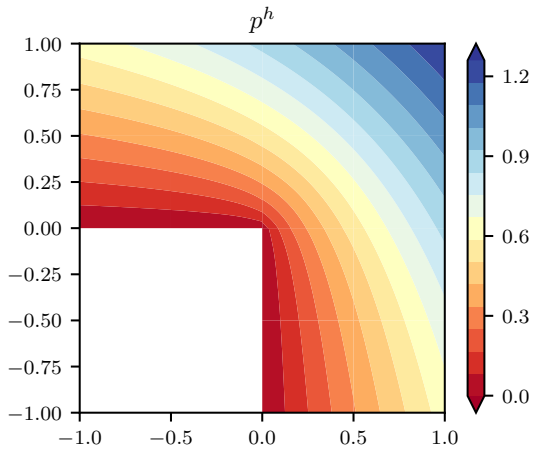

(a) Solution for the potential p.

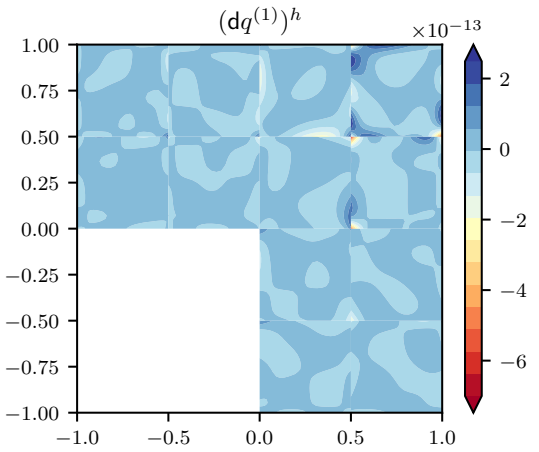

(b) Divergence of the velocity.

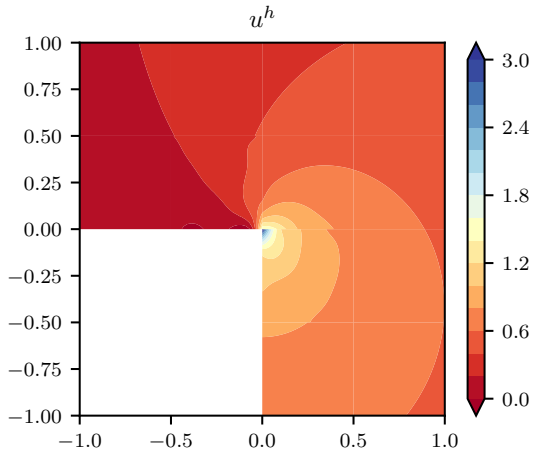

(c) Solution for velocity component u.

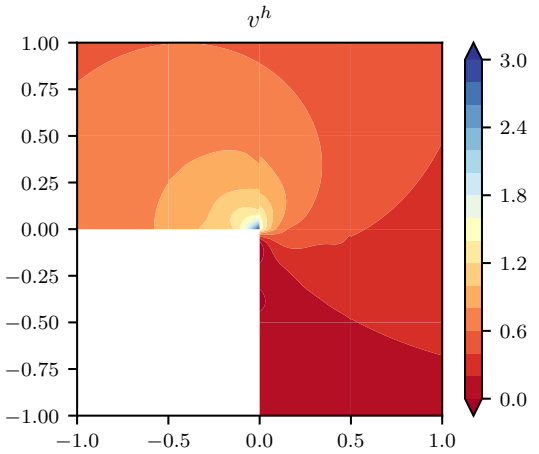

(d) Solution for velocity component v.

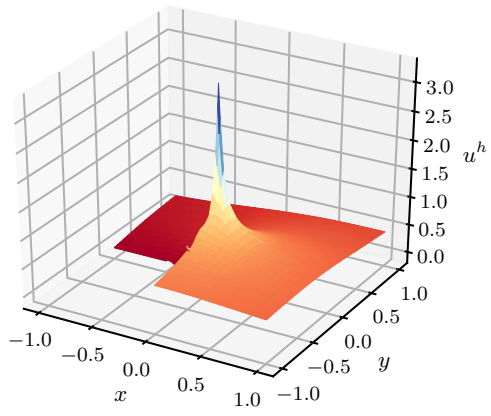

(e) Three dimensional plot of the velocity component u.

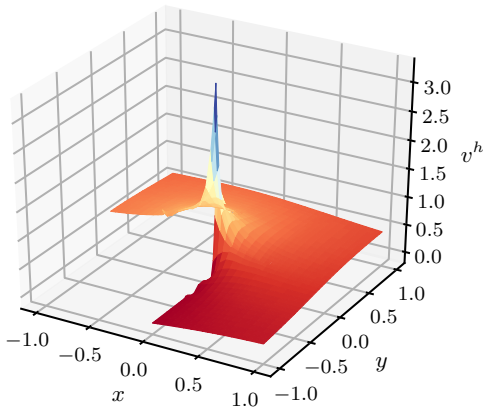

(f) Three dimensional plot of the velocity component v.

Figure 4.10: The solution on the L-shaped domain, for $K = 2$, $p = 5$.

The solution results using a mesh of continuous elements seen in Fig. 4.7b are shown in Fig. 4.10, where again, the conservation law is shown to be point-wise satisfied, even in this case where the forcing function is zero. The singularity at the point $(0,0)$ is clearly visible in the three-dimensional contour plots Fig. 4.10e and Fig. 4.10f. For this setup, the singularity poses no problem, since the solution of the velocities is represented by integral quantities over the edge instead of point-wise quantities. The discontinuity of the flux, for u^h in y-direction and for v^h in x-direction is also clearly visible in Fig. 4.10c and Fig. 4.10d. The convergence plots for this problem in Fig. 4.8 show sub-optimal p-convergence (i.e. no straight line), as expected for this non-smooth problem. The error is however close in value to the interpolation error, hence this is the best possible solution using this discrete representation. The h-convergence of reduced order $(2/3)$ is also observed in [22], attributed to the limited regularity of the solution. The maximum point-wise error for both refinements confirms again the conservation of mass.

4.3. Summary

The Poisson problem has been presented as a first introduction to the application of the mimetic spectral element method. From a Lagrangian formulation, it is possible to derive the weak formulation with the correctly selected function spaces. The weak formulation leads to a system with mass matrices, while the choice of the basis allows for discretising the divergence operator as an incidence matrix. To make the system more sparse, it is convenient to introduce the algebraic dual basis. The formulation was tested with two test problems. The first was a manufactured solution, that showed the convergence of the error to be optimal for the given basis for both h- and p refinement. In addition, the L-shaped domain test case allowed for proving again the point-wise exactness of the discrete divergence operator. This implementation of the method has now been verified.

5

The Stokes Problem

This chapter contains a verification of results for a previously studied formulation of the Stokes problem. A new problem is also treated using this formulation, which is the backwards facing step problem. The problem is first derived and new terms are elaborated on, and then the results for the three test cases are shown and discussed.

5.1. Derivation and implementation

The Stokes flow equations will be first introduced in this section in vector notation. The main line of thought from [47] to obtain the system of equations will be followed here. Then, as the constraint of constant viscosity allows to introduce the vector Laplacian, the vector Laplacian will be rewritten in differential forms, and the equations are rewritten as a system of first order equations. The weak formulation and system to solve follow, and a note on hybridisation then concludes this section.

5.1.1. The Stokes flow equations

The Stokes flow equations are

$$\nabla \cdot \underline{\underline{\tau}} + \mathbf{f} = 0, \tag{5.1}$$

$$\nabla \cdot \mathbf{u} = 0. \tag{5.2}$$

The first equation represents conservation of linear momentum, while the second equation represents conservation of mass. Here, the Cauchy stress tensor $\underline{\underline{\tau}}$ can be divided in the deviatoric stress tensor $\underline{\underline{\sigma}}$ and pressure p,

$$\underline{\underline{\tau}} = \underline{\underline{\sigma}} - p\underline{\underline{\mathrm{I}}},$$

where $\underline{\underline{\sigma}} = 2\nu\underline{\underline{\epsilon}}$, with $\underline{\underline{\epsilon}}$ the rate of deformation tensor

$$\underline{\underline{\epsilon}} = \frac{1}{2}\left(\nabla\mathbf{u} + (\nabla\mathbf{u})^T\right)$$

The tensors can hence be written out, with $\mathbf{u} = \begin{bmatrix} u \\ v \end{bmatrix}$, as

$$\underline{\underline{\sigma}} = \begin{bmatrix} \sigma_{xx} & \sigma_{yx} \\ \sigma_{xy} & \sigma_{yy} \end{bmatrix}, \qquad \underline{\underline{\epsilon}} = \frac{1}{2}\begin{bmatrix} 2\frac{\partial u}{\partial x} & \frac{\partial u}{\partial y} + \frac{\partial v}{\partial x} \\ \frac{\partial v}{\partial x} + \frac{\partial u}{\partial y} & 2\frac{\partial v}{\partial y} \end{bmatrix}. \tag{5.3}$$

Unless the pressure is prescribed on the boundaries, the pressure in this equation is determined up to a constant, such that the solution values for the pressure should be taken relative to a point or the average pressure should be set zero [47].

Taking $\nu = 1$ (or another constant), as $\nabla \cdot \mathbf{u} = \frac{\partial u}{\partial x} + \frac{\partial v}{\partial y} = 0$, and thus

$$\nabla \cdot (\nabla\mathbf{u})^T = \begin{bmatrix} \frac{\partial^2 u}{\partial x^2} + \frac{\partial^2 v}{\partial x \partial y} \\ \frac{\partial^2 u}{\partial x \partial y} + \frac{\partial^2 v}{\partial y^2} \end{bmatrix} = \begin{bmatrix} \frac{\partial}{\partial x}\left(\frac{\partial u}{\partial x} + \frac{\partial v}{\partial y}\right) \\ \frac{\partial}{\partial y}\left(\frac{\partial u}{\partial x} + \frac{\partial v}{\partial y}\right) \end{bmatrix} = \nabla\left(\nabla \cdot \mathbf{u}\right) = 0,$$

the vector Laplacian appears, since then,

$$\nabla \cdot \underline{\underline{\sigma}} = \nu \nabla \cdot \left(\nabla \mathbf{u} + (\nabla \mathbf{u})^T \right) = \nu \left(\nabla \cdot \nabla \right) \mathbf{u} = \nu \Delta \mathbf{u}.$$

Hence, the Stokes flow equations for constant viscosity are

$$\nu \Delta \mathbf{u} - \nabla p + \mathbf{f} = 0, \tag{5.4}$$

$$\nabla \cdot \mathbf{u} = 0. \tag{5.5}$$

5.1.2. The vector Laplacian

In vector calculus, the vector Laplacian has the identity

$$\begin{aligned} \Delta \mathbf{u} &= \nabla^\star (\nabla \cdot \mathbf{u}) - \nabla \times \left(\nabla^\star \times \mathbf{u} \right) \\ &= \text{grad}^\star (\text{div} \mathbf{u}) - \text{curl} \left(\text{curl}^\star \mathbf{u} \right). \end{aligned}$$

The stars are written in these equations, because it must be made clear that the gradient and the divergence operations are performed on different forms, as are the curl operations. These relations are seen as well on the double De Rham complex, see Fig. 2.2. Taking the grad* is equivalent of first applying the Hodge-$\star$, then the exterior derivative which is the gradient on a 0-form, and then again applying the Hodge-$\star$. The same can be done for the curl*. Using this complex, the Hodge Laplacian [7] for a 1-form in $\mathbb{R}^2$ is written as

$$\Delta q^{(1)} = \mathrm{d}^\star \mathrm{d} q^{(1)} - \mathrm{d}\mathrm{d}^\star q^{(1)}. \tag{5.6}$$

Here, the quantity $\nabla \times \mathbf{q}$ or $\mathrm{d}^\star q^{(1)}$ can be replaced by a different quantity, the vorticity, which should be a 0-form $\omega^{(0)}$,

$$\omega^{(0)} = \mathrm{d}^\star q^{(1)}. \tag{5.7}$$

The forms appearing in the equations in $\mathbb{R}^2$ are thus the outer-oriented $\Lambda^{(n-2)} = \omega^{(0)}$ and $\Lambda^{(n-1)} = q^{(1)}$.

5.1.3. System to solve

Now the previously found expression in (5.6) can be taken to rewrite the equations (5.1) in differential forms as

$$\begin{aligned} \mathrm{d}^\star \mathrm{d} q^{(n-1)} - \mathrm{d}\mathrm{d}^\star q^{(n-1)} - \mathrm{d}^\star p^{(n)} + f^{(n-1)} &= 0, \\ \mathrm{d} q^{(n-1)} &= 0. \end{aligned}$$

In the first line, the first term can be removed due to the second equation. The second term can be rewritten by introducing the vorticity explicitly, resulting in the system from [47],

$$\begin{aligned} \omega^{(n-2)} - \mathrm{d}^\star q^{(n-1)} &= 0, \\ \mathrm{d}\omega^{(n-2)} + \mathrm{d}^\star p^{(n)} &= f^{(n-1)}, \\ \mathrm{d} q^{(n-1)} &= 0. \end{aligned}$$

Using the standard Galerkin method, rewriting these equations for $\mathbb{R}^2$ in the weak formulation requires three test functions, $\widetilde{\omega}^{(0)}$, $\widetilde{q}^{(1)}$ and $\widetilde{p}^{(2)}$. Multiplying the terms in each line with the respective correct test function and integrating over the domain yields

$$\begin{aligned} \left(\widetilde{\omega}^{(0)}, \omega^{(0)} \right)_\Omega - \left(\widetilde{\omega}^{(0)}, \mathrm{d}^\star q^{(1)} \right)_\Omega &= 0, \\ \left(\widetilde{q}^{(1)}, \mathrm{d}\omega^{(0)} \right)_\Omega + \left(\widetilde{q}^{(1)}, \mathrm{d}^\star p^{(2)} \right)_\Omega &= \left(\widetilde{q}^{(1)}, f^{(1)} \right)_\Omega, \\ \left(\widetilde{p}^{(2)}, \mathrm{d} q^{(1)} \right)_\Omega &= 0. \end{aligned}$$

The terms with the co-differential can be rewritten as [47]

$$\begin{aligned} \left(\widetilde{\omega}^{(0)}, \mathrm{d}^\star q^{(1)} \right)_\Omega &= \left(\mathrm{d}\widetilde{\omega}^{(0)}, q^{(1)} \right)_\Omega - \int_{\partial\Omega} \mathrm{tr}\left(\widetilde{\omega}^{(0)} \right) \wedge \mathrm{tr}\left(\star\, q^{(1)} \right), \\ \left(\widetilde{q}^{(1)}, \mathrm{d}^\star p^{(2)} \right)_\Omega &= \left(\mathrm{d}\widetilde{q}^{(1)}, p^{(2)} \right)_\Omega - \int_{\partial\Omega} \mathrm{tr}\left(\widetilde{q}^{(1)} \right) \wedge \mathrm{tr}\left(\star\, p^{(2)} \right). \end{aligned}$$

Thus the final system becomes

$$\left(\widetilde{\omega}^{(0)}, \omega^{(0)}\right)_\Omega - \left(\mathrm{d}\widetilde{\omega}^{(0)}, q^{(1)}\right)_\Omega = -\int_{\partial\Omega} \operatorname{tr}\left(\widetilde{\omega}^{(0)}\right) \wedge \operatorname{tr}\left(\star\, q^{(1)}\right), \tag{5.12a}$$

$$\left(\widetilde{q}^{(1)}, \mathrm{d}\omega^{(0)}\right)_\Omega + \left(\mathrm{d}\widetilde{q}^{(1)}, p^{(2)}\right)_\Omega = \left(\widetilde{q}^{(1)}, f^{(1)}\right)_\Omega + \int_{\partial\Omega} \operatorname{tr}\left(\widetilde{q}^{(1)}\right) \wedge \operatorname{tr}\left(\star\, p^{(2)}\right), \tag{5.12b}$$

$$\left(\widetilde{p}^{(2)}, \mathrm{d}q^{(1)}\right)_\Omega = 0. \tag{5.12c}$$

Now, these terms can be evaluated similarly as before, resulting in a system with three unknown vectors,

$$\begin{bmatrix} \mathbb{M}^{(0)} & \left(\mathbb{E}^{(1,0)}\right)^T \mathbb{M}^{(1)} & 0 \\ \mathbb{M}^{(1)}\mathbb{E}^{(1,0)} & 0 & \left(\mathbb{E}^{(2,1)}\right)^T \mathbb{M}^{(2)} \\ 0 & \mathbb{M}^{(2)}\mathbb{E}^{(2,1)} & 0 \end{bmatrix} \begin{bmatrix} \boldsymbol{\omega}^h \\ \boldsymbol{q}^h \\ \boldsymbol{p}^h \end{bmatrix} = \begin{bmatrix} -\boldsymbol{b}^h \\ \mathbb{M}^{(1)}\boldsymbol{f}^h + \boldsymbol{g}^h \\ 0 \end{bmatrix}, \tag{5.13}$$

where the vector $\boldsymbol{f}^h$ results from reducing the forcing 1-form f, and $\boldsymbol{b}^h$ and $\boldsymbol{g}^h$ from boundary conditions posed on the tangential velocity component and the pressure, respectively [47]. The two newly introduced matrices are the mass matrix $\mathbb{M}^{(0)}$, which is derived as well in Appendix A.1 and the incidence matrix $\mathbb{E}^{(1,0)}$ shown in Appendix A.2. The derivation of components for $\boldsymbol{b}^h$ and $\boldsymbol{g}^h$ is given in Appendix A.4 and for $\boldsymbol{f}^h$ in Appendix A.3.

The system can be rewritten (increasing the sparsity) by dividing the last row by $\mathbb{M}^{(2)}$ and solving for an altered $\left(\boldsymbol{p}'\right)^h = \mathbb{M}^{(2)}\boldsymbol{p}^h$,

$$\begin{bmatrix} \mathbb{M}^{(0)} & \left(\mathbb{E}^{(1,0)}\right)^T \mathbb{M}^{(1)} & 0 \\ \mathbb{M}^{(1)}\mathbb{E}^{(1,0)} & 0 & \left(\mathbb{E}^{(2,1)}\right)^T \\ 0 & \mathbb{E}^{(2,1)} & 0 \end{bmatrix} \begin{bmatrix} \boldsymbol{\omega}^h \\ \boldsymbol{q}^h \\ \left(\boldsymbol{p}'\right)^h \end{bmatrix} = \begin{bmatrix} -\boldsymbol{b}^h \\ \mathbb{M}^{(1)}\boldsymbol{f}^h + \boldsymbol{g}^h \\ 0 \end{bmatrix}. \tag{5.14}$$

The expansions for the pressure p^h and flux q^h are the same as for the Poisson problem in Section 4.1.6. The expansion of the solution for ω is given by

$$\omega^h(x,y) = \sum_{i=1}^{p+1}\sum_{j=1}^{p+1} \omega_{ij} h_i(x) h_j(y). \tag{5.15}$$

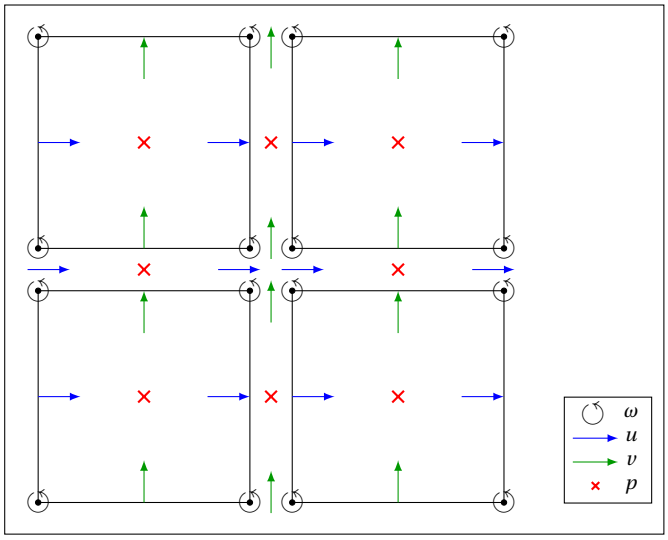

Figure 5.1: Coupling the hybrid elements of lowest order for the Stokes problem in VVP formulation, $K = 2$, $p = 1$.

5.1.4. Note on hybridisation

This formulation is not hybrid, and cannot be hybridised directly like the Poisson problem. In Fig. 5.1, the setup for the lowest order elements is given. The interface variables that couple the vorticity are visualised using arrows, since their physical interpretation is the circulation, which is the dual of the flux. At each intersection of four elements, four vorticity nodes meet, one for each corner. But if the top two vorticity nodes are coupled, i. e. set to the same value, and the same happens for the left two and the right two, the bottom two are automatically set equal by the first three constraints. This means that the last constraint does not add information, hence the system is under-determined.

5.2. Results

This section contains the results for the formulation presented in this chapter. Three test cases are considered, the manufactured solution, the lid-driven cavity flow, and the flow over a backwards facing step. The latter is a new result using this existing formulation. The results for this formulation are again generated using continuous elements.

5.2.1. Manufactured solution

The manufactured solution test case can be repeated again for the Stokes flow problem in VVP formulation. Taking the following standard exact solution for the pressure and velocity components, also used in [47],

$$p^{\text{ex}}(x,y) = \sin(\pi x)\sin(\pi y), \tag{5.16a}$$
$$u^{\text{ex}}(x,y) = -\sin(2\pi x)\cos(2\pi y), \tag{5.16b}$$
$$v^{\text{ex}}(x,y) = \cos(2\pi x)\sin(2\pi y), \tag{5.16c}$$

it is derived that

$$f_x^{\text{ex}}(x,y) = \pi\cos(\pi x)\sin(\pi y) - 8\pi^2\sin(2\pi x)\cos(2\pi y),$$
$$f_y^{\text{ex}}(x,y) = \pi\sin(\pi x)\cos(\pi y) + 8\pi^2\cos(2\pi x)\sin(2\pi y),$$
$$\omega^{\text{ex}}(x,y) = -4\pi\sin(2\pi x)\sin(2\pi y).$$

The maximum point-wise error of the divergence of the velocity for varying resolutions is shown in Fig. 5.2. Note that the (coloured) connecting lines here do not have further meaning. The convergence results are shown in Fig. 5.3.

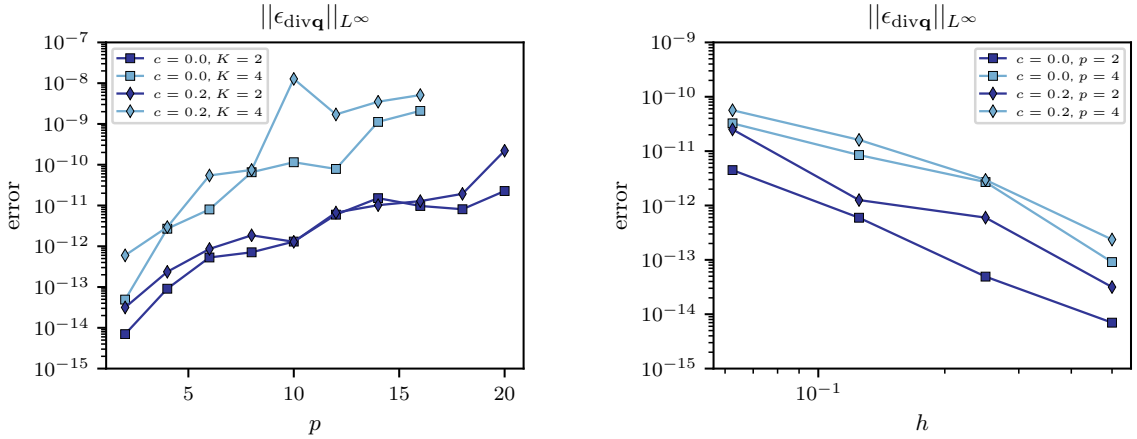

(a) Varying resolution in p.

(b) Varying resolution in h.

Figure 5.2: Point-wise maximum error in conservation law for the Stokes flow problem, for the manufactured solution on the domain $[0,1]^2$.

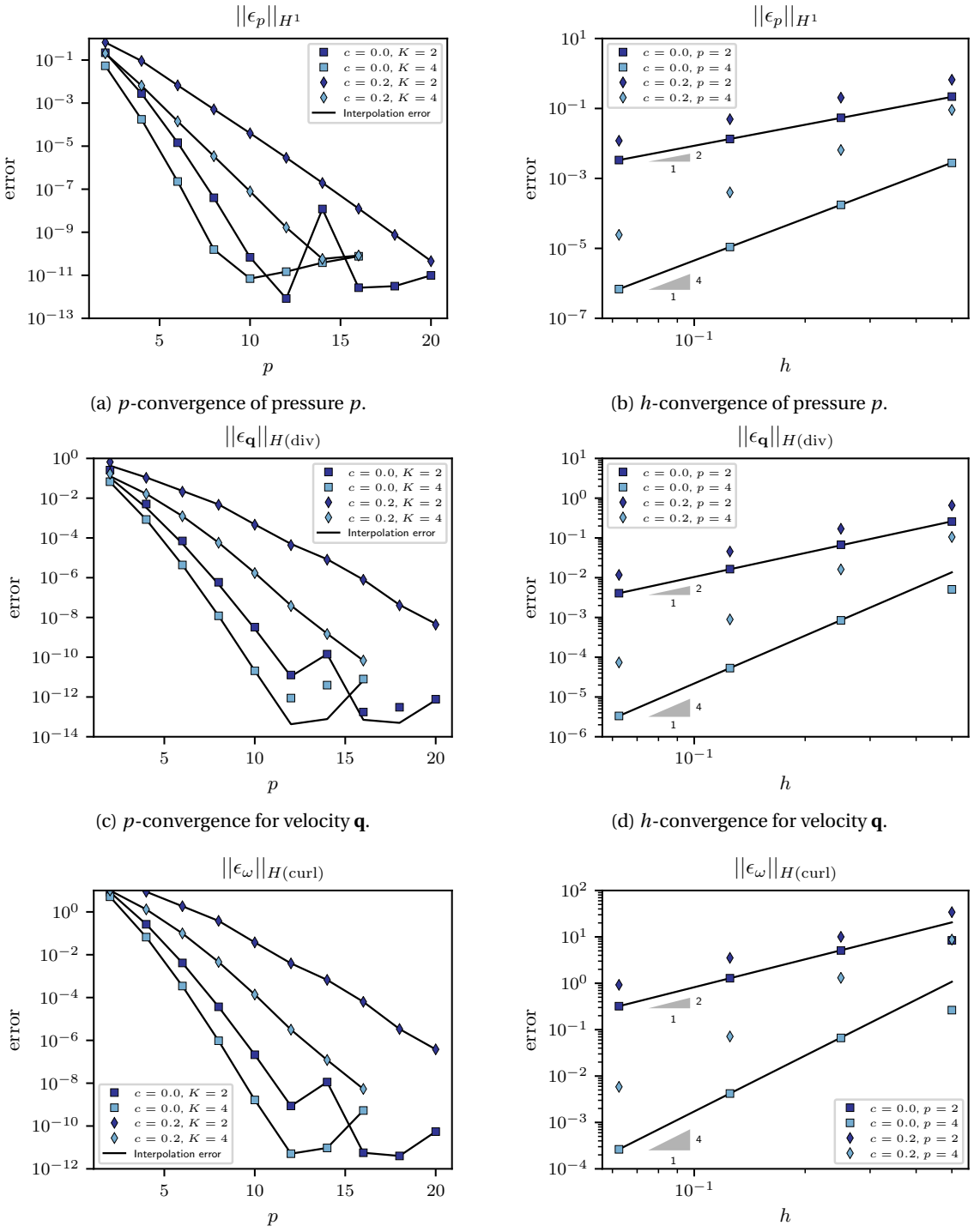

(a) p-convergence of pressure p.

(b) h-convergence of pressure p.

(c) p-convergence for velocity $\mathbf{q}$.

(d) h-convergence for velocity $\mathbf{q}$.

(e) p-convergence of vorticity ω.

(f) h-convergence of vorticity ω.

Figure 5.3: p- and h-convergence trends for the Stokes flow problem, for the manufactured solution on the domain $[0,1]^2$.

The norms used are computed as defined in Section 3.5.1, where here specifically,

$$\begin{aligned}
\left\|\epsilon_{\mathrm{div}\mathbf{q}}\right\|_{L^2} &= \left\|\left(\mathrm{d}q^{(1)}\right)^h\right\|_{L^2} \\
\|\epsilon_{\mathrm{curl}\omega}\|_{L^2}^2 &= \left\|\left(\mathrm{d}\omega^{(0)}\right)_x^h - \left(\frac{\partial\omega}{\partial x}\right)^{\mathrm{ex}}\right\|_{L^2}^2 + \left\|\left(\mathrm{d}\omega^{(0)}\right)_y^h - \left(\frac{\partial\omega}{\partial y}\right)^{\mathrm{ex}}\right\|_{L^2}^2 \\
\left\|\epsilon_{\mathrm{div}\mathbf{q}}\right\|_{L^\infty} &= \left\|\left(\mathrm{d}q^{(1)}\right)^h\right\|_{L^\infty}
\end{aligned}$$

The components of the norm $\|\epsilon_{\mathrm{curl}\omega}\|_{L^2}$ arises from the fact that $\mathrm{d}\omega^{(0)}$ is a 1-form, hence the co-chain $\mathbb{E}^{(1,0)}\boldsymbol{\omega}^h$ will have two components with the same expansion as q^h. The gradient part of $\left\|\epsilon_p\right\|_{H^1(\Omega)}$ is computed in the same way as in Section 4.2.1. The interpolation error is plotted separately as well in the p-refinement plots, and the slope of the optimal h-convergence is shown as black lines for the orthogonal mesh results. The fact that the slope for $\|\epsilon_\omega\|_{H(\mathrm{curl})}$ is the same as for the other solution components, comes from the fact that although ω^h has one order higher convergence it its L^2 norm, its derivative does not, hence the contribution of $\|\epsilon_{\mathrm{curl}\omega}\|_{L^2}$ is dominant. It is observed that for p-refinement, the results lie very close to the interpolation error, and furthermore follow the optimal trends very well. For h-refinement, the correct convergence rate is observed, even for the distorted meshes. Therefore, optimal convergence is confirmed for all solution components, and all error lies in the representation of the constitutive law.

5.2.2. Lid driven cavity flow

The second problem considered is the typical problem of lid driven cavity flow, of which reference results are found in [39], [45], and [47]. The problem is a challenging test case, since there are two singularities in the solution for the pressure and vorticity at the corners where the velocity jumps [47]. However, as flux is represented by the average over the edge, these singularities will not be a problem for this formulation. It has been recomputed for further verification of the implementation.

A square mesh on the domain $[0,1]^2$ is used, with a cosine spacing of the elements. Using this spacing greatly increases the resolution near the corners. The boundary conditions are unit velocity to the right at the top boundary, and all other boundary velocities set to zero as no-slip boundary conditions. As the normal velocity is prescribed on every boundary, the pressure is determined up to a constant, hence the average pressure is set to zero.

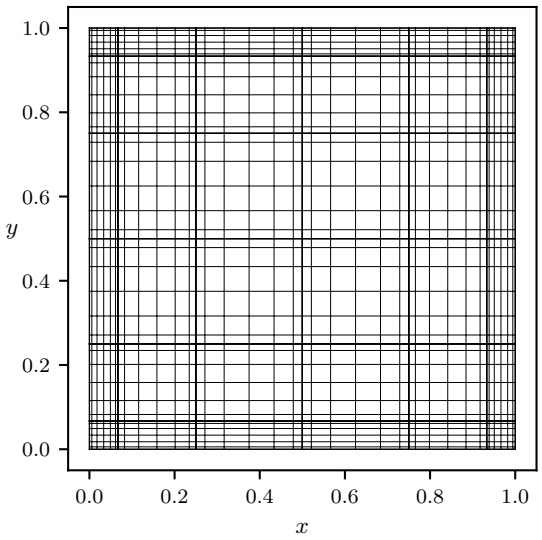

Figure 5.4: Orthogonal mesh with $K^2 = 6^2$ elements of order $p = 6$ used for the lid-driven cavity flow problem.

The mesh used for this test case is shown in Fig. 5.4. The results are summarised qualitatively in the contour plots in Fig. 5.5. These plots show the expected trends and a clear match with the results from the reference [47]. Also, the divergence of the velocity in this test problem confirms again exact point-wise mass conservation for this scheme.

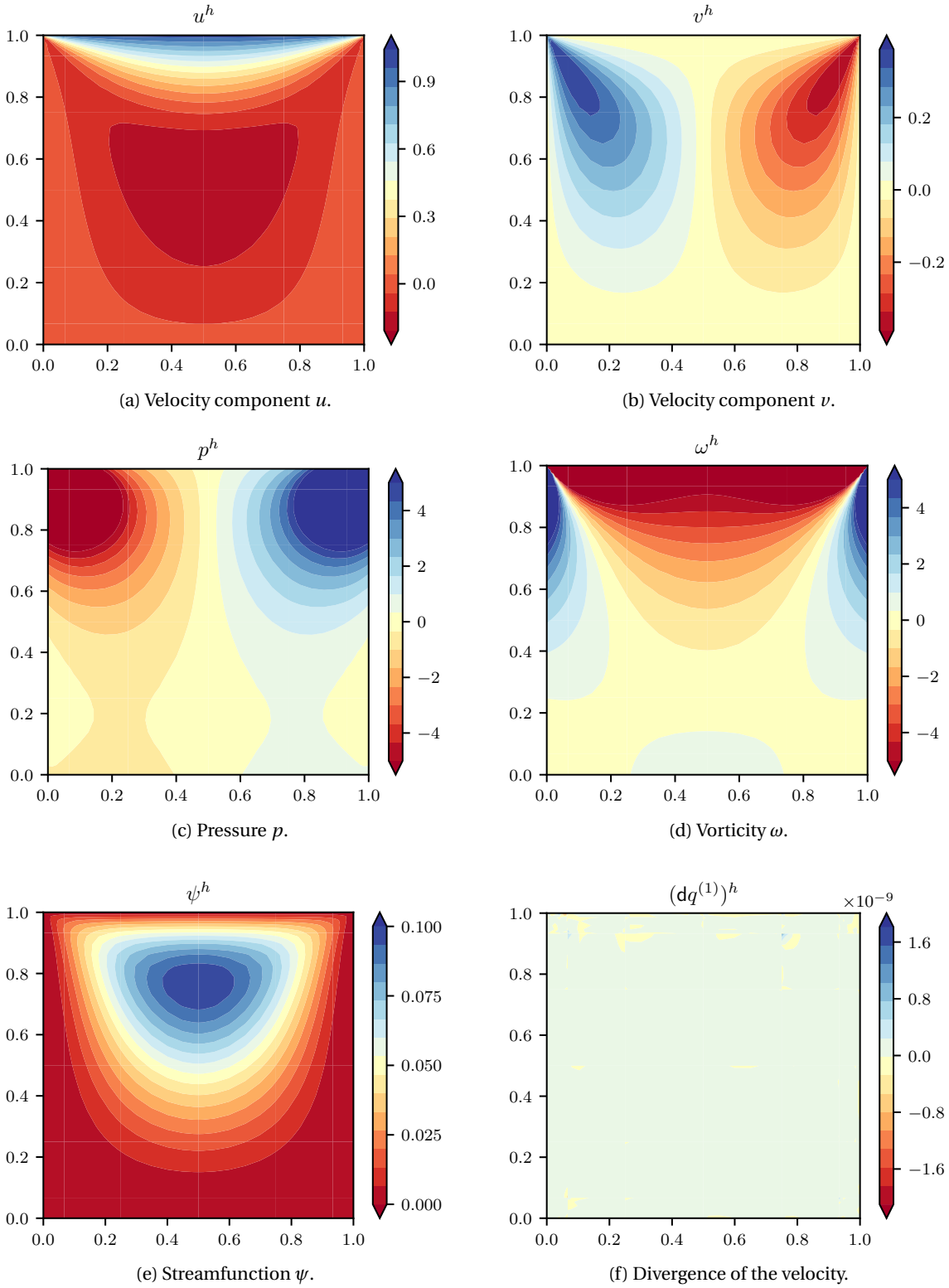

(a) Velocity component u.

(b) Velocity component v.

(c) Pressure p.

(d) Vorticity ω.

(e) Streamfunction ψ.

(f) Divergence of the velocity.

Figure 5.5: Solution for the lid driven cavity test problem, with $K^2 = 6^2$ cosine spaced elements of order $p = 6$.

5.2.3. Backwards facing step

Additionally, there is the backward-facing step flow, found in [8] and in [29]. In terms of connectivity, this same domain was used for the backwards facing step problem in Stokes flow, although the three blocks are sized differently. This final test problem is taken from [8], see Fig. 5.6. The boundary conditions are again

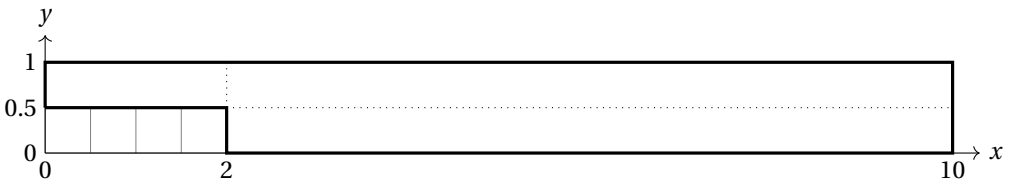

Figure 5.6: Domain for the backwards facing step problem.

set with normal and tangential velocity everywhere, such that the average pressure has to be set to zero. The inlet and outlet velocity u^{in} and u^{out} are respectively given by

$$u^{\text{in}} = 8(y-0.5)(1-y),$$
$$u^{\text{out}} = y(1-y).$$

All other walls have no-slip wall boundary conditions.

The backwards facing step problem results are shown here for two highly refined meshes. The element meshes used are shown in Fig. 5.7a and Fig. 5.8a, note that the grid inside the elements is not shown. A small number of high order elements is used in Fig. 5.7 and a large number of lower order elements in Fig. 5.8. In both cases, the solution has a comparable maximum error in mass conservation of machine precision, and the contours qualitatively agree to those in [8], which are shown in Fig. 5.9.

5.3. Summary

The Stokes flow equations can be rewritten in a system of first order equations. These equations, following the standard Galerkin procedure, can be rewritten in a weak form. This formulation is comparable to the Poisson problem formulation, the divergence of the velocity is however always set to zero. It was tested with a similar manufactured solution test case, producing optimal results with point-wise mass conservation. The formulation is also capable of simulating non-smooth cases such as the lid-driven cavity flow and the backwards facing step. Even for these cases, the mass conservation constraint can be said to be satisfied point-wise. However, as was pointed out before in Section 2.3.2, the linear momentum law cannot be discretised exactly in this formulation. Therefore, it is important to look at a first problem that explicitly introduces the linear momentum equation by computing the stresses, the problem of linear elasticity.

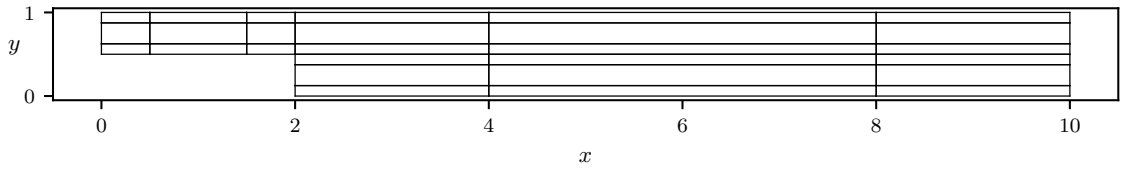

(a) Element mesh with $3K^2$ elements, $K = 10$ used. Note that only element boundaries are visible for clarity.

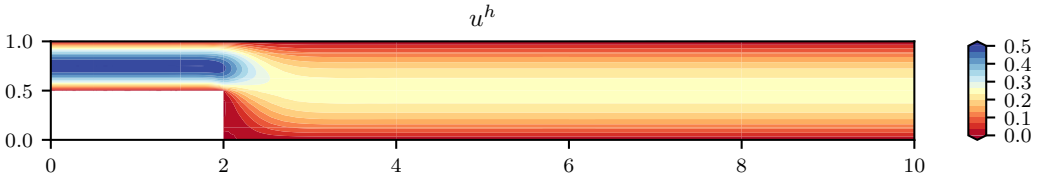

(b) Velocity components u.

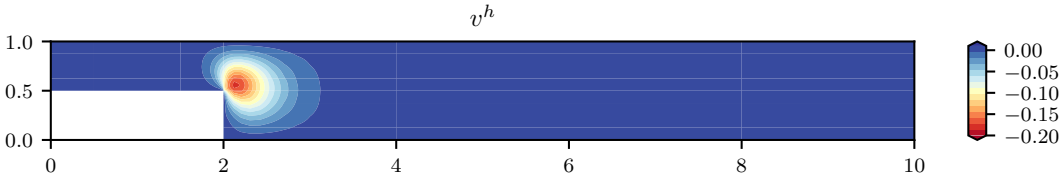

(c) Velocity component v.

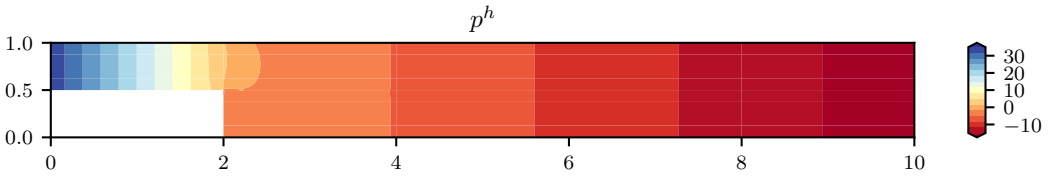

(d) Pressure p.

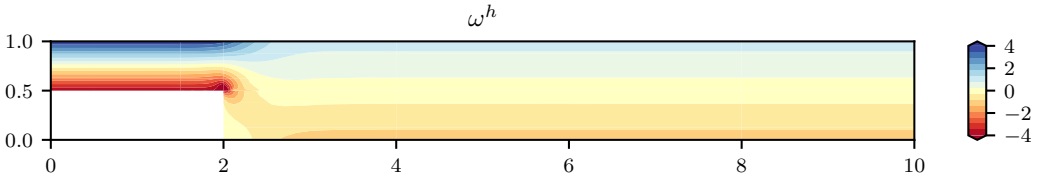

(e) Vorticity ω.

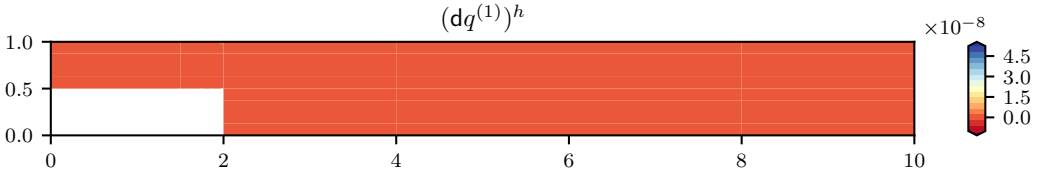

(f) Mass conservation.

Figure 5.7: Solution of the backwards facing step test problem, with $3K^2 = 3(3^2)$ elements of order $p = 10$.

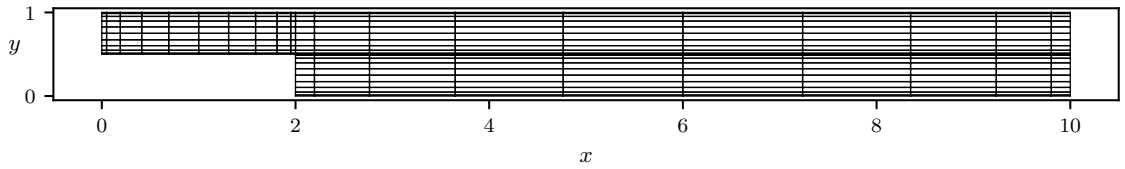

(a) Element mesh with $3K^2$ elements, $K = 10$ used. Note that only element boundaries are visible for clarity.

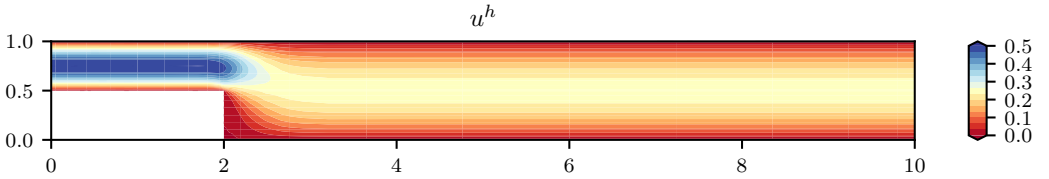

(b) Velocity component u.

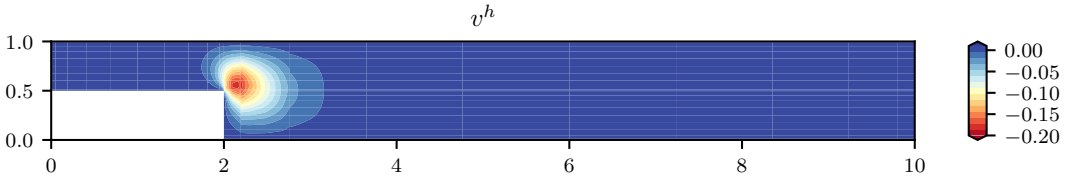

(c) Velocity component v.

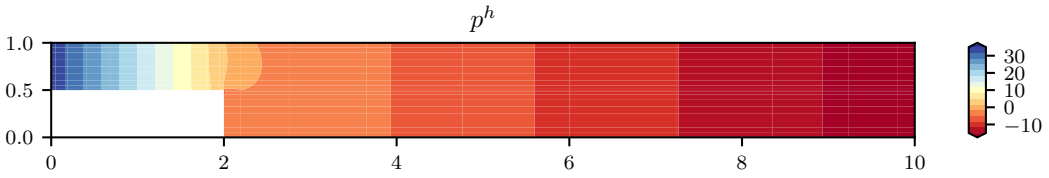

(d) Pressure p.

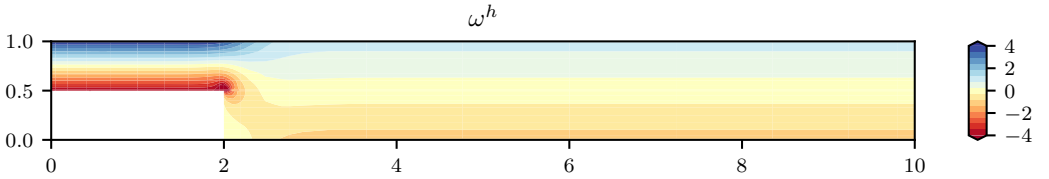

(e) Vorticity ω.

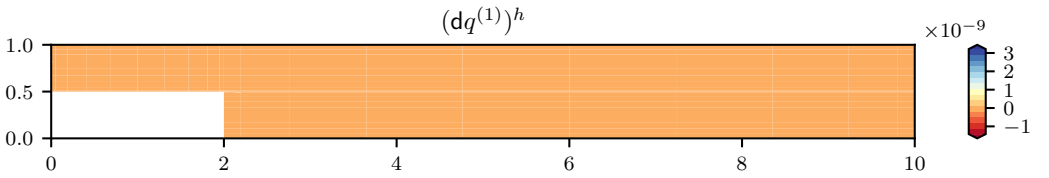

(f) Mass conservation.

Figure 5.8: Solution of the backwards facing step test problem, with $3K^2 = 3(10^2)$ elements of order $p = 3$.

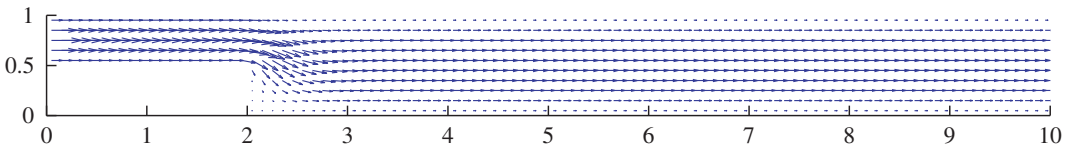

(a) Velocity.

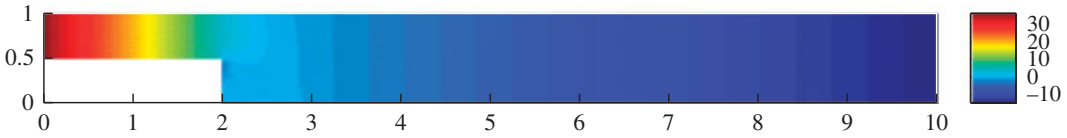

(b) Pressure p.

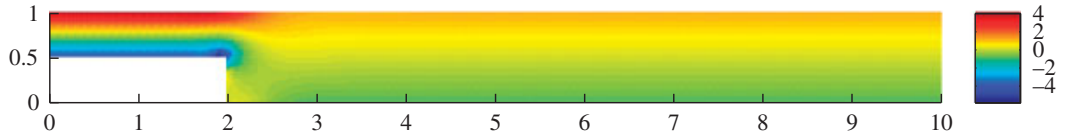

(c) Vorticity ω.

Figure 5.9: Solution of the backwards facing step test problem for the velocity field, the pressure and the vorticity, taken from [8] for comparison.

6

The Linear Elasticity Problem

The next problem, linear elasticity, will be considered twice in this thesis. This first formulation was still being developed at the start of this work. It was seen important to document and analyse this particular formulation, since it lead to key insights for the new formulation presented in the next chapter. This formulation build on the knowledge from the Poisson problem, where it actually solves two Poisson problems and couples them through the angular momentum balance law. The stresses as such are represented on the primal mesh (like the fluxes in Poisson), while the displacements are in the dual space, with a basis spanned by the algebraic dual polynomials.

6.1. Derivation and implementation

First, the problem is introduced in common notation, using vector calculus. The Lagrangian formulation will then be used to derive a weak form. This will lead again to the system to solve. In this section, the derivation of the mass matrix and the torque matrix is shown explicitly for completeness.

6.1.1. Problem introduction

The equations for linear elasticity are given by

$$\nabla \cdot \underline{\underline{\sigma}} + \mathbf{f} = 0, \tag{6.1}$$

with again the stress tensor $\underline{\underline{\sigma}}$ as defined in (5.3) and the body force $\mathbf{f}$. The constitutive law relates the stress tensor to the strain tensor $\underline{\underline{\epsilon}}$ by the inverse of the stiffness tensor, the compliance tensor C, as

$$C\underline{\underline{\sigma}} = \underline{\underline{\epsilon}}. \tag{6.2}$$

Here, $\underline{\underline{\epsilon}} = \frac{1}{2}\left(\nabla\mathbf{u} + (\nabla\mathbf{u})^T\right)$, which was written out in (5.3). If the stress tensor components are numbered as

$$\begin{bmatrix}\sigma_{xx} & \sigma_{yx} & \sigma_{xy} & \sigma_{yy}\end{bmatrix} = \begin{bmatrix}\sigma_1 & \sigma_2 & \sigma_3 & \sigma_4\end{bmatrix},$$

the constitutive law that is used in this report is Hooke's law for a simple linear isotropic medium in the case of plane stress, with E the stiffness and ν Poisson's ratio,

$$C = \begin{bmatrix} C_{11} & C_{12} & C_{13} & C_{14} \\ C_{21} & C_{22} & C_{23} & C_{24} \\ C_{31} & C_{32} & C_{33} & C_{34} \\ C_{41} & C_{42} & C_{43} & C_{44} \end{bmatrix} = \frac{1}{E}\begin{bmatrix} 1 & 0 & 0 & -\nu \\ 0 & 1+\nu & 0 & 0 \\ 0 & 0 & 1+\nu & 0 \\ -\nu & 0 & 0 & 1 \end{bmatrix}. \tag{6.3}$$

In the continuous formulation, the conservation of angular momentum is denoted by

$$\nabla \cdot \left(\mathbf{r} \times \underline{\underline{\sigma}}\right) + \mathbf{r} \times \mathbf{f} = 0, \tag{6.4}$$

with $\mathbf{r} \times \underline{\underline{\sigma}}$ shorthand for the column wise cross product, such that

$$\mathbf{T} = \mathbf{r} \times \underline{\underline{\sigma}} = \begin{bmatrix} x \\ y \end{bmatrix} \times \begin{bmatrix} \sigma_{xx} & \sigma_{yx} \\ \sigma_{xy} & \sigma_{yy} \end{bmatrix} = \begin{bmatrix} x\sigma_{xy} - y\sigma_{xx} \\ x\sigma_{yy} - y\sigma_{yx} \end{bmatrix}.$$

This can be clarified by writing out the terms in (6.4),

$$\begin{aligned} 0 &= \nabla \cdot \left(\begin{bmatrix} x \\ y \end{bmatrix} \times \begin{bmatrix} \sigma_{xx} & \sigma_{yx} \\ \sigma_{xy} & \sigma_{yy} \end{bmatrix} \right) + \begin{bmatrix} x \\ y \end{bmatrix} \times \begin{bmatrix} f_x \\ f_y \end{bmatrix} \\ &= \nabla \cdot \begin{bmatrix} x\sigma_{xy} - y\sigma_{xx} \\ x\sigma_{yy} - y\sigma_{yx} \end{bmatrix} + xf_y - yf_x \\ &= \frac{\partial}{\partial x}\left(x\sigma_{xy} - y\sigma_{xx}\right) + \frac{\partial}{\partial y}\left(x\sigma_{yy} - y\sigma_{yx}\right) + xf_y - yf_x \\ &= \sigma_{xy} + x\frac{\partial \sigma_{xy}}{\partial x} - y\frac{\partial \sigma_{xx}}{\partial x} + x\frac{\partial \sigma_{yy}}{\partial y} - \sigma_{yx} - y\frac{\partial \sigma_{yx}}{\partial y} + xf_y - yf_x \\ &= \sigma_{xy} - \sigma_{yx} + \mathbf{r} \times \left(\nabla \cdot \underline{\underline{\sigma}} + \mathbf{f} \right). \end{aligned} \tag{6.5}$$

Substituting (6.1) in this equation, the symmetry constraint is obtained,

$$\sigma_{xy} - \sigma_{yx} = 0.$$

Hence, in the continuous problem, satisfying conservation of angular momentum is equivalent to satisfying conservation of linear momentum with a symmetric stress tensor.

6.1.2. Lagrangian formulation

The minimisation problem is written as [1]

$$\mathcal{L}\left(\underline{\underline{\sigma}}, \boldsymbol{\lambda}_1, \lambda_2\right) = \int_\Omega \frac{1}{2} \underline{\underline{\sigma}}^T C \underline{\underline{\sigma}} + \boldsymbol{\lambda}_1 \left(\nabla \cdot \underline{\underline{\sigma}} + \mathbf{f} \right) + \lambda_2 \left(\nabla \cdot \left(\mathbf{r} \times \underline{\underline{\sigma}} \right) + \mathbf{r} \times \mathbf{f} \right) \mathrm{d}\Omega - \int_{\partial\Omega} \underline{\underline{\sigma}} \left(\mathbf{u}_P \cdot \mathbf{n} \right) \mathrm{d}\Gamma. \tag{6.6}$$

Here, $\underline{\underline{\sigma}} \in [H(\mathrm{div}, \Omega)]^n$, $\boldsymbol{\lambda}_1 \in \left[L^2(\Omega)\right]^n$, and $\lambda_2 \in L^2(\Omega)$. Taking variations with respect to $\underline{\underline{\sigma}}$ gives

$$\left(\underline{\underline{\tilde{\sigma}}}, C\underline{\underline{\sigma}}\right)_\Omega + \left(\boldsymbol{\lambda}_1, \nabla \cdot \underline{\underline{\tilde{\sigma}}}\right)_\Omega + \left(\lambda_2, \nabla \cdot \left(\mathbf{r} \times \underline{\underline{\tilde{\sigma}}}\right)\right)_\Omega = \int_{\partial\Omega} \underline{\underline{\tilde{\sigma}}} \left(\mathbf{u}_P \cdot \mathbf{n} \right) \mathrm{d}\Gamma, \qquad \forall \underline{\underline{\tilde{\sigma}}} \in [H(\mathrm{div}, \Omega)]^n.$$

Taking variations with respect to $\boldsymbol{\lambda}_1$ gives

$$\left(\tilde{\boldsymbol{\lambda}}_1, \nabla \cdot \underline{\underline{\sigma}}\right)_\Omega = -\left(\tilde{\boldsymbol{\lambda}}_1, \mathbf{f}\right)_\Omega, \qquad \forall \tilde{\boldsymbol{\lambda}}_1 \in \left[L^2(\Omega)\right]^n,$$

and with respect to λ_2 gives

$$\left(\tilde{\lambda}_2, \nabla \cdot \left(\mathbf{r} \times \underline{\underline{\sigma}}\right)\right)_\Omega = -\left(\tilde{\lambda}_2, \mathbf{r} \times \mathbf{f}\right)_\Omega, \qquad \forall \tilde{\lambda}_2 \in L^2(\Omega).$$

The final weak formulation is

$$\left(\underline{\underline{\tilde{\sigma}}}, C\underline{\underline{\sigma}}\right)_\Omega + \left(\boldsymbol{\lambda}_1, \nabla \cdot \underline{\underline{\tilde{\sigma}}}\right)_\Omega + \left(\lambda_2, \nabla \cdot \left(\mathbf{r} \times \underline{\underline{\tilde{\sigma}}}\right)\right)_\Omega = \int_{\partial\Omega} \underline{\underline{\tilde{\sigma}}} \left(\mathbf{u}_P \cdot \mathbf{n} \right) \mathrm{d}\Gamma, \tag{6.7a}$$

$$\left(\tilde{\boldsymbol{\lambda}}_1, \nabla \cdot \underline{\underline{\sigma}}\right)_\Omega = -\left(\tilde{\boldsymbol{\lambda}}_1, \mathbf{f}\right)_\Omega, \tag{6.7b}$$

$$\left(\tilde{\lambda}_2, \nabla \cdot \left(\mathbf{r} \times \underline{\underline{\sigma}}\right)\right)_\Omega = -\left(\tilde{\lambda}_2, \mathbf{r} \times \mathbf{f}\right)_\Omega, \tag{6.7c}$$

which must hold $\forall \underline{\underline{\tilde{\sigma}}} \in [H(\mathrm{div}, \Omega)]^n, \forall \tilde{\boldsymbol{\lambda}}_1 \in \left[L^2(\Omega)\right]^n, \forall \tilde{\lambda}_2 \in L^2(\Omega)$. The equality that was found in (6.5),

$$\nabla \cdot \left(\mathbf{r} \times \underline{\underline{\tilde{\sigma}}}\right) = \mathbf{r} \times \left(\nabla \cdot \underline{\underline{\tilde{\sigma}}}\right) + \tilde{\sigma}_{xy} - \tilde{\sigma}_{yx},$$

[1] This formulation was derived by V. Jain, PhD candidate at the faculty of Aerospace Engineering of the Delft University of Technology.

can be used to rewrite

$$\begin{aligned}\left(\lambda_2, \nabla\cdot\left(\mathbf{r}\times\underline{\underline{\widetilde{\sigma}}}\right)\right)_\Omega &= \left(\lambda_2, \mathbf{r}\times\left(\nabla\cdot\underline{\underline{\widetilde{\sigma}}}\right)\right)_\Omega + \left(\lambda_2, \widetilde{\sigma}_{xy}-\widetilde{\sigma}_{yx}\right)_\Omega \\ &= -\left(\begin{bmatrix} y\lambda_2 \\ -x\lambda_2\end{bmatrix}, \nabla\cdot\underline{\underline{\widetilde{\sigma}}}\right)_\Omega + \left(\lambda_2, \widetilde{\sigma}_{xy}-\widetilde{\sigma}_{yx}\right)_\Omega.\end{aligned}$$

If it is taken now that $\boldsymbol{\lambda}_1 = \mathbf{u} + \begin{bmatrix} y\lambda_2 \\ -x\lambda_2\end{bmatrix}$ with $\lambda_2 = \omega = \frac{1}{2}\left(\frac{\partial v}{\partial x} - \frac{\partial u}{\partial y}\right)$, for a sufficiently smooth solution in the domain, when $\boldsymbol{u} \in \left[H^1(\Omega)\right]^2$, it is possible to use integration by parts since the gradient of $\boldsymbol{u} = \boldsymbol{\lambda}_1 - \begin{bmatrix} y\lambda_2 \\ -x\lambda_2\end{bmatrix}$ is then defined,

$$\left(\boldsymbol{\lambda}_1, \nabla\cdot\underline{\underline{\widetilde{\sigma}}}\right)_\Omega - \left(\begin{bmatrix} y\lambda_2 \\ -x\lambda_2\end{bmatrix}, \nabla\cdot\underline{\underline{\widetilde{\sigma}}}\right)_\Omega - \int_{\partial\Omega}\underline{\underline{\widetilde{\sigma}}}\left(\mathbf{u}_P\cdot\mathbf{n}\right)\mathrm{d}\Gamma = -\left(\underline{\underline{\widetilde{\sigma}}}, \nabla\boldsymbol{\lambda}_1\right)_\Omega + \left(\underline{\underline{\widetilde{\sigma}}}, \nabla\begin{bmatrix} y\lambda_2 \\ -x\lambda_2\end{bmatrix}\right)_\Omega.$$

Hence, the weak form can be rewritten as

$$\left(\underline{\underline{\widetilde{\sigma}}}, C\underline{\underline{\sigma}}\right)_\Omega - \left(\underline{\underline{\widetilde{\sigma}}}, \nabla\boldsymbol{\lambda}_1\right)_\Omega + \left(\underline{\underline{\widetilde{\sigma}}}, \nabla\begin{bmatrix} y\lambda_2 \\ -x\lambda_2\end{bmatrix}\right)_\Omega + \left(\lambda_2, \widetilde{\sigma}_{xy}-\widetilde{\sigma}_{yx}\right)_\Omega = 0, \tag{6.8a}$$

$$\left(\widetilde{\boldsymbol{\lambda}}_1, \nabla\cdot\underline{\underline{\sigma}}\right)_\Omega = -\left(\widetilde{\boldsymbol{\lambda}}_1, \mathbf{f}\right)_\Omega, \tag{6.8b}$$

$$\left(\widetilde{\lambda}_2, \nabla\cdot\left(\mathbf{r}\times\underline{\underline{\sigma}}\right)\right)_\Omega = -\left(\widetilde{\lambda}_2, \mathbf{r}\times\mathbf{f}\right)_\Omega. \tag{6.8c}$$

The equations can then be written in a differential notation,

$$\begin{aligned} C\underline{\underline{\sigma}} &= \nabla\boldsymbol{\lambda}_1 - \nabla\begin{bmatrix} y\lambda_2 \\ -x\lambda_2\end{bmatrix} - \begin{bmatrix} 0 & \lambda_2 \\ -\lambda_2 & 0\end{bmatrix} && \text{in } \Omega, \\ \nabla\cdot\underline{\underline{\sigma}} &= -\mathbf{f} && \text{in } \Omega, \\ \nabla\cdot\left(\mathbf{r}\times\underline{\underline{\sigma}}\right) &= -\mathbf{r}\times\mathbf{f} && \text{in } \Omega, \\ \mathbf{u}_P\cdot\mathbf{n} &= g && \text{on } \partial\Omega. \end{aligned}$$

It can be seen that if the first equation is the constitutive law, $C\underline{\underline{\sigma}} = \underline{\underline{\varepsilon}}$, and since $\underline{\underline{\varepsilon}}$ can be rewritten as

$$\underline{\underline{\varepsilon}} = \frac{1}{2}\left(\nabla\mathbf{u} + \left(\nabla\mathbf{u}^T\right)\right) = \nabla\mathbf{u} - \begin{bmatrix} 0 & \omega \\ -\omega & 0\end{bmatrix},$$

the first Lagrange multiplier must be $\boldsymbol{\lambda}_1 = \mathbf{u} + \begin{bmatrix} y\lambda_2 \\ -x\lambda_2\end{bmatrix}$ and the second Lagrange multiplier must be $\lambda_2 = \omega$, such that the equations hold.

6.1.3. The system to be solved

The weak form of the system of equations to be discretised, (6.7), leads to several matrices and right hand side vectors. The complete system that can be solved for $(\underline{\underline{\sigma}}, \boldsymbol{\lambda}_1, \lambda_2)$ is denoted as

$$\begin{bmatrix} \mathbb{M}_\sigma & \mathbb{E}_\sigma^T & \mathbb{Q}^T\left(\mathbb{E}^{(2,1)}\right)^T \\ \mathbb{E}_\sigma & 0 & 0 \\ \mathbb{E}^{(2,1)}\mathbb{Q} & 0 & 0\end{bmatrix}\begin{bmatrix} \boldsymbol{\sigma}^h \\ \left(\boldsymbol{\lambda}_1'\right)^h \\ \left(\boldsymbol{\lambda}_2'\right)^h\end{bmatrix} = \begin{bmatrix} \boldsymbol{b}^h \\ -\boldsymbol{f}^h \\ -\boldsymbol{f}_q^h\end{bmatrix}. \tag{6.10}$$

The sparsity here is due to the fact that the vector- and scalar-valued 2-forms are discretised with the algebraic dual basis, leaving their reconstruction to the post-processing step. This means that the components of the

solution $\boldsymbol{\lambda}_1^h$, and the solution of $\boldsymbol{\lambda}_2^h$ need to be solved for the mass matrix $\mathbb{M}^{(2)}$, i.e.

$$\boldsymbol{\lambda}_1^h = \begin{bmatrix} \boldsymbol{\lambda}_{1_x}^h \\ \boldsymbol{\lambda}_{1_y}^h \end{bmatrix} = \begin{bmatrix} \left(\mathbb{M}^{(2)}\right)^{-1} \left(\boldsymbol{\lambda}'_{1,x}\right)^h \\ \left(\mathbb{M}^{(2)}\right)^{-1} \left(\boldsymbol{\lambda}'_{1,x}\right)^h \end{bmatrix},$$
$$\boldsymbol{\lambda}_2^h = \left(\mathbb{M}^{(2)}\right)^{-1} \left(\boldsymbol{\lambda}'_2\right)^h.$$

In the previous derivations from Lagrangian to weak form, tensors were introduced to represent the stresses. However, so far no mass matrices or incidence matrices have been described that can act as discrete inner product matrices and differential operators for tensors. The derivation and setup of these matrices will therefore be shown in this chapter.

6.1.4. Configuration of stress components

There are multiple configurations possible for assigning the stress components within an element to edges with primal basis. In Fig. 6.1, two possibilities in lowest possible order are shown [2]. The staggered configuration has an overlay alike the standard configuration, but this is drawn apart for both stress directions for clarity.

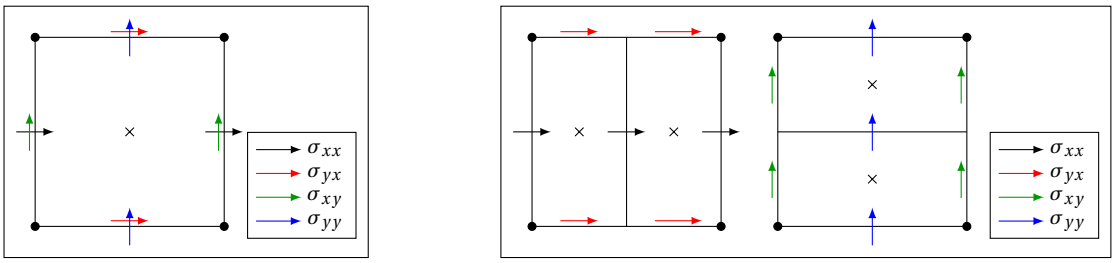

(a) Standard configuration.

(b) Staggered configuration.

Figure 6.1: Assigning the stress tensor components to edges.

The standard configuration assigns both normal and shear stress components along both vertical and horizontal edges at the same order. This means that the polynomial order of the stress components along edges within an element is the same, for a polynomial space $\mathcal{P}^{i,j}$, of order i in x and j in y,

$$\sigma_{xx} \in \mathcal{P}^{1,0}, \quad \sigma_{yx} \in \mathcal{P}^{0,1}, \quad \sigma_{xy} \in \mathcal{P}^{1,0}, \quad \sigma_{yy} \in \mathcal{P}^{0,1}.$$

For the staggered configuration, the polynomial spaces of the stress components are

$$\sigma_{xx} \in \mathcal{P}^{2,0}, \quad \sigma_{yx} \in \mathcal{P}^{1,1}, \quad \sigma_{xy} \in \mathcal{P}^{1,1}, \quad \sigma_{yy} \in \mathcal{P}^{0,2}.$$

For linear momentum conservation, it can be shown that for the standard configuration, the first Lagrange multiplier components $\lambda_{1,x} \in \mathcal{P}^{0,0}$ and $\lambda_{1,y} \in \mathcal{P}^{0,0}$ are positioned in the centre, marked with a cross in Fig. 6.1a. The location is not known exactly due to the use of algebraic dual polynomials. In the staggered configuration, $\lambda_{1,x} \in \mathcal{P}^{1,0}$ and $\lambda_{1,y} \in \mathcal{P}^{0,1}$ are positioned in the centre of the two surfaces, also marked with crosses in Fig. 6.1b. Both configurations have no difficulty in correctly representing the Lagrange multipliers.

For angular momentum conservation, however, the $\mathbf{r}\times$ operator changes the polynomial spaces. In the previously used notation, for instance (6.7), the notation of $\mathbf{r} \times \underline{\underline{\sigma}}$ is used to describe a new quantity, the torque. Writing out all components, for the standard configuration,

$$-y\sigma_{xx} \in \mathcal{P}^{1,1}, \quad -y\sigma_{yx} \in \mathcal{P}^{0,2}, \quad x\sigma_{xy} \in \mathcal{P}^{2,0}, \quad x\sigma_{yy} \in \mathcal{P}^{1,1}.$$

It can be seen that the contributions to the torque components do not match in polynomial spaces. However, performing the same operation for the staggered configuration,

$$-y\sigma_{xx} \in \mathcal{P}^{2,1}, \quad -y\sigma_{yx} \in \mathcal{P}^{1,2}, \quad x\sigma_{xy} \in \mathcal{P}^{2,1}, \quad x\sigma_{yy} \in \mathcal{P}^{1,2},$$

[2] The staggered configuration was proposed by Y. Zhang, PhD candidate at the faculty of Aerospace Engineering of the Delft University of Technology.

the polynomial spaces for **T** do match.

Although this is an argument to use the staggered configuration, for hybridisation this has no advantage, which will be discussed in Section 6.1.9. Hence, in the following, only the derivations and the results for the standard configuration, which is based on the Poisson configuration, are shown.

Note also that the polynomial space for ω is the same as the polynomial space for u and v in the standard configuration, while in the staggered configuration, the polynomial space of ω is one order higher in y direction than u and one order higher in x direction than v.

6.1.5. Mass matrix of a tensor inner product

The derivation of the terms to generate the matrices is elaborate and not documented before. Therefore, the derivation is shown here for completeness. Taking the second order tensor $\underline{\underline{\sigma}}$ and compliance tensor C in two dimensions as given in (6.3) as an example, the inner product between two second order tensor quantities can be written as

$$\left(\underline{\underline{\widetilde{\sigma}}}, C\underline{\underline{\sigma}}\right)_\Omega = \int_\Omega \underline{\underline{\widetilde{\sigma}}}^{(1)} \wedge \star\, C\underline{\sigma}^{(1)}.$$

Here, in terms of differential forms, $\underline{\underline{\sigma}}$ should be taken as a co-vector valued (or alternatively vector valued) $(n-1)$-form [31, p. 618-619]. The implication of this on the balance laws is also elaborated on in [44]. This is denoted in this thesis by $\underline{\sigma}^{(1)}$, such that the edges have two unknowns associated to them. Written out,

$$\underline{\sigma}^{(1)} = \begin{bmatrix} \sigma_x^{(1)} \\ \sigma_y^{(1)} \end{bmatrix} = \begin{bmatrix} \overline{\sigma}_{xx}\mathrm{d}y - \overline{\sigma}_{yx}\mathrm{d}x \\ \overline{\sigma}_{xy}\mathrm{d}y - \overline{\sigma}_{yy}\mathrm{d}x \end{bmatrix}$$

This can also be written as

$$\underline{\sigma}^{(1)} = \mathrm{d}x \otimes \overline{\sigma}_{xx}\mathrm{d}y + \mathrm{d}x \otimes \overline{\sigma}_{yx}\mathrm{d}x + \mathrm{d}y \otimes \overline{\sigma}_{xy}\mathrm{d}y + \mathrm{d}y \otimes \overline{\sigma}_{yy}\mathrm{d}x$$

As the quantities are computed on edges, their bases are given in terms of nodal and edge polynomials in two dimensions for the standard configuration in Fig. 6.1a as

$$\overline{\sigma}_{xx} = \sum_{i=1}^{p+1}\sum_{j=1}^{p} (\sigma_{xx})_{ij}\, h_i(x) e_j(y), \qquad \overline{\sigma}_{yx} = \sum_{i=1}^{p}\sum_{j=1}^{p+1} \left(\sigma_{yx}\right)_{ij} e_i(x) h_j(y),$$
$$\overline{\sigma}_{xy} = \sum_{i=1}^{p+1}\sum_{j=1}^{p} \left(\sigma_{xy}\right)_{ij} h_i(x) e_j(y), \qquad \overline{\sigma}_{yy} = \sum_{i=1}^{p}\sum_{j=1}^{p+1} \left(\sigma_{yy}\right)_{ij} e_i(x) h_j(y).$$

Note that these expansions are the same for the flux $q^{(n-1)}$ in the Poisson and Stokes problem. The bases of the test functions are the same. Writing out in matrix form,

$$\underline{\underline{\widetilde{\sigma}}}^{T} = \begin{bmatrix} \widetilde{\sigma}_{xx} & \widetilde{\sigma}_{yx} & \widetilde{\sigma}_{xy} & \widetilde{\sigma}_{yy} \end{bmatrix},$$
$$C\underline{\underline{\sigma}} = \begin{bmatrix} C_{11} & C_{12} & C_{13} & C_{14} \\ C_{21} & C_{22} & C_{23} & C_{24} \\ C_{31} & C_{32} & C_{33} & C_{34} \\ C_{41} & C_{42} & C_{43} & C_{44} \end{bmatrix} \begin{bmatrix} \overline{\sigma}_{xx} \\ \overline{\sigma}_{yx} \\ \overline{\sigma}_{xy} \\ \overline{\sigma}_{yy} \end{bmatrix}$$

The mass matrix can be denoted in a shortened notation, since there are only two different bases. The first entry can be written out as

$$M^{11}_{ijkl} = \sum_{r=1}^{p+1}\sum_{s=1}^{p+1} (\widetilde{\sigma}_{xx})_{kl}\, C_{11}\, (\sigma_{xx})_{ij}\, h_i(x_r) e_j(y_s) h_k(x_r) e_l(y_s)\, w_r\, w_s,$$

such that in general,

$$M^{ab}_{ijkl} = \sum_{r=1}^{p+1}\sum_{s=1}^{p+1} (\widetilde{\sigma}_a)_{kl}\, C_{ab}\, (\sigma_b)_{ij}\, \varepsilon_b(x_r, y_s) \varepsilon_a(x_r, y_s)\, w_r\, w_s,$$

with $\varepsilon_a(x, y)$ the basis of the a^{th} component of the tensor 1-form. The mass matrix denoted by $\mathbb{M}_\sigma$ is thus formed as a 4 by 4 matrix, resembling the compliance matrix structure,

$$\int_\Omega \underline{\underline{\widetilde{\sigma}}}^{(1)} \wedge \star\, C\underline{\sigma}^{(1)} \approx \left(\widetilde{\boldsymbol{\sigma}}^h\right)^T \mathbb{M}_\sigma \boldsymbol{\sigma}^h,$$

by, setting $N = 2\left(2p(p+1)\right)$ for the standard configuration in Fig. 6.1a,

$$\left(\widetilde{\boldsymbol{\sigma}}^h\right)^T = \left[(\widetilde{\sigma}_{xx})_1, (\widetilde{\sigma}_{xx})_2, ..., (\widetilde{\sigma}_{xx})_{p(p+1)}, \left(\widetilde{\sigma}_{yx}\right)_1, ..., \left(\widetilde{\sigma}_{yy}\right)_{p(p+1)}\right] = [\widetilde{\sigma}_1, \widetilde{\sigma}_2, ..., \widetilde{\sigma}_N],$$
$$\left(\boldsymbol{\sigma}^h\right)^T = \left[(\sigma_{xx})_1, (\sigma_{xx})_2, ..., (\sigma_{xx})_{p(p+1)}, \left(\sigma_{yx}\right)_1, ..., \left(\sigma_{yy}\right)_{p(p+1)}\right] = [\sigma_1, \sigma_2, ..., \sigma_N].$$

For the mapped tensor mass matrix, see Appendix A.1.5.

6.1.6. Torque

The torque is implemented as an operation that maps the components of $\underline{\underline{\sigma}}$ to a single 1-form. Written out,

$$\begin{aligned}\int_\Omega \mathbf{r} \times \underline{\underline{\sigma}}\, \mathrm{d}\Omega &= \int_\Omega \mathbf{r} \times \underline{\sigma}^{(1)} \\ &= \int_\Omega \mathbf{r} \times \begin{bmatrix} \overline{\sigma}_{xx}\mathrm{d}y - \overline{\sigma}_{yx}\mathrm{d}x \\ \overline{\sigma}_{xy}\mathrm{d}y - \overline{\sigma}_{yy}\mathrm{d}x \end{bmatrix} \\ &= \int_\Omega \left\{ \left[X\overline{\sigma}_{xy} - Y\overline{\sigma}_{xx}\right]\mathrm{d}y - \left[X\overline{\sigma}_{yy} - Y\overline{\sigma}_{yx}\right]\mathrm{d}x \right\} \\ &= \int_\Omega \left\{ \overline{T_x}\mathrm{d}y - \overline{T_y}\mathrm{d}x \right\}.\end{aligned}$$

The torque as a 1-form can thus be projected onto edges, where

$$\int_\Omega T^{(1)}\mathrm{d}\Omega \approx \sum_{i=1}^{p+1}\sum_{j=1}^{p} (T_x)_{ij} h_i(x) e_j(y)\mathrm{d}y - \sum_{i=1}^{p}\sum_{j=1}^{p+1} (T_y)_{ij} e_i(x) h_j(y)\mathrm{d}x.$$

The values of the matrix $\mathbb{Q}$ can be obtained for every vertical edge, where $h_i(x_r) = 1$, with matrix components

$$(T_x)_{ijkl} = \sum_{r=1}^{p_f} h_i(x_r) e_j(y_r) w_r \left[X(y_r)\left(\sigma_{xy}\right)_{kl} - Y(y_r)\left(\sigma_{xx}\right)_{kl}\right],$$

and for every horizontal edge, where $h_j(y_r) = 1$, with

$$\left(T_y\right)_{ijkl} = \sum_{r=1}^{p_f} e_i(x_r) h_j(y_r) w_r \left[X(x_r)\left(\sigma_{yy}\right)_{kl} - Y(x_r)\left(\sigma_{yx}\right)_{kl}\right].$$

The terms involving this torque, seen in (6.7c), can then be discretised as

$$\left(\widetilde{\lambda}_2, \nabla\cdot\left(\mathbf{r}\times\underline{\underline{\sigma}}\right)\right)_\Omega = \int_\Omega -\star\,\widetilde{\lambda}_2^{(2)} \wedge \star\,\mathrm{d}\left(\mathbf{r}\times\underline{\sigma}^{(1)}\right) = \int_\Omega \widetilde{\lambda}_2^{(2)} \wedge \mathrm{d}\left(\mathbf{r}\times\underline{\sigma}^{(1)}\right) \approx \left(\left(\widetilde{\boldsymbol{\lambda}}_2'\right)^h\right)^T \mathbb{E}^{(2,1)}\mathbb{Q}\boldsymbol{\sigma}^h.$$

For the mapped torque matrix, see Appendix A.1.5.

6.1.7. Topological divergence of stress

Similar to an incidence matrix acting on a scalar-valued co-chain, the divergence of a tensor can be implemented as an incidence matrix. Writing out the components of the inner product of the first Lagrange multiplier and the divergence of the tensor,

$$\widetilde{\boldsymbol{\lambda}}_1 = \underline{\widetilde{\lambda}}_1^{(2)} = \begin{bmatrix} \star\,\widetilde{\lambda}_{1,x}^{(2)} \\ \star\,\widetilde{\lambda}_{1,y}^{(2)} \end{bmatrix}, \qquad \nabla\cdot\underline{\underline{\sigma}} = \begin{bmatrix} \frac{\partial\sigma_{xx}}{\partial x} + \frac{\partial\sigma_{yx}}{\partial y} \\ \frac{\partial\sigma_{xy}}{\partial x} + \frac{\partial\sigma_{yy}}{\partial y} \end{bmatrix} = \underline{\mathrm{d}}\,\underline{\sigma}^{(1)} = \begin{bmatrix} \mathrm{d}\sigma_x^{(1)} \\ \mathrm{d}\sigma_y^{(1)} \end{bmatrix},$$

where it must be noted that the Lagrange multiplier is taken in the dual complex, such that the inner product becomes metric free. In essence, the operation can be performed using the exterior derivative acting on 1-forms producing 2-forms, or in the discrete setting the incidence matrix $\mathbb{E}^{(2,1)}$, such that

$$\left(\widetilde{\boldsymbol{\lambda}}_1, \nabla\cdot\underline{\underline{\sigma}}\right)_\Omega = \int_\Omega -\star\,\underline{\widetilde{\lambda}_1}^{(2)} \wedge \star\,\underline{\mathrm{d}\sigma}^{(1)} = \int_\Omega \underline{\widetilde{\lambda}_1}^{(2)} \wedge \underline{\mathrm{d}\sigma}^{(1)} \approx \left(\left(\widetilde{\boldsymbol{\lambda}}_1'\right)^h\right)^T \mathbb{E}_\sigma \boldsymbol{\sigma}^h = \begin{bmatrix} \left(\left(\widetilde{\boldsymbol{\lambda}}_1'\right)_{1,x}^h\right)^h \mathbb{E}^{(2,1)}\boldsymbol{\sigma}_x^h \\ \left(\left(\widetilde{\boldsymbol{\lambda}}_1'\right)_{1,y}^h\right)^h \mathbb{E}^{(2,1)}\boldsymbol{\sigma}_y^h \end{bmatrix}.$$

6.1.8. Stress tensor boundary conditions and forcing function

This boundary condition can be implemented by treating the velocity on the boundary as a vector valued 0-form,

$$\int_{\partial\Omega} \underline{\underline{\widetilde{\sigma}}}\,(\mathbf{u}_P \cdot \mathbf{n})\,\mathrm{d}\Gamma = \int_{\partial\Omega} \mathrm{tr}\left(\underline{\widetilde{\sigma}}^{(1)}\right) \wedge -\mathrm{tr}\left(\star\, \underline{\mathrm{u}}_P^{(2)}\right) = \int_{\partial\Omega} \underline{\widetilde{\sigma}}^{(1)} \wedge \underline{\mathrm{u}}_P^{(0)}.$$

Again considering a reference square domain $[-1,1]^2$ with four boundary parts, $\partial\Omega = \partial\Omega_T \cup \partial\Omega_B \cup \partial\Omega_L \cup \partial\Omega_R$, the bottom boundary is written as

$$\begin{aligned}\int_{\partial\Omega} \underline{\widetilde{\sigma}}^{(1)} \wedge \underline{\mathrm{u}}_P^{(0)} &= \int_{\partial\Omega_B} \begin{bmatrix} \left\{\sum_{k=1}^{p+1}\sum_{l=1}^{p}(\widetilde{\sigma}_{xx})_{kl} h_k(x) e_l(-1)\mathrm{d}y - \sum_{k=1}^{p}\sum_{l=1}^{p+1}(\widetilde{\sigma}_{yx})_{kl} e_k(x) h_l(-1)\mathrm{d}x\right\} u(x,-1) \\ \left\{\sum_{k=1}^{p+1}\sum_{l=1}^{p}(\widetilde{\sigma}_{xy})_{kl} h_k(x) e_l(-1)\mathrm{d}y - \sum_{k=1}^{p}\sum_{l=1}^{p+1}(\widetilde{\sigma}_{yy})_{kl} e_k(x) h_l(-1)\mathrm{d}x\right\} v(x,-1) \end{bmatrix} \\ &\approx -\begin{bmatrix} \sum_{r=0}^{p_f}\left\{\sum_{k=1}^{p}\sum_{l=1}^{p+1}(\widetilde{\sigma}_{yx})_{kl} e_k(x) h_l(-1)\mathrm{d}x\right\} u(x_r,-1)\, w_r \\ \sum_{r=0}^{p_f}\left\{\sum_{k=1}^{p}\sum_{l=1}^{p+1}(\widetilde{\sigma}_{yy})_{kl} e_k(x) h_l(-1)\mathrm{d}x\right\} v(x_r,-1)\, w_r \end{bmatrix}.\end{aligned}$$

In the weak formulations discussed, (6.7), there are both vector- and scalar-valued forcing terms. The forcing functions can be written as

$$\mathbf{f} = \underline{\mathrm{f}}^{(2)} = \begin{bmatrix} f_x^{(2)} \\ f_y^{(2)} \end{bmatrix}, \qquad \mathbf{r} \times \mathbf{f} = f_q^{(2)} = x f_y^{(2)} - y f_x^{(2)}.$$

In the case of the former,

$$\left(\widetilde{\boldsymbol{\lambda}}_1, \mathbf{f}\right)_\Omega = \int_\Omega \begin{bmatrix} -\star\, \widetilde{\lambda}_{1,x}^{(2)} \wedge \star\, f_x^{(2)} \\ -\star\, \widetilde{\lambda}_{1,y}^{(2)} \wedge \star\, f_y^{(2)} \end{bmatrix} = \int_\Omega \begin{bmatrix} \widetilde{\lambda}_{1,x}^{(2)} \wedge f_x^{(2)} \\ \widetilde{\lambda}_{1,y}^{(2)} \wedge f_y^{(2)} \end{bmatrix} \approx \left(\left(\boldsymbol{\lambda}_1'\right)^h\right)^T \boldsymbol{f}^h.$$

Similarly,

$$\left(\widetilde{\lambda}_2, \mathbf{r}\times\mathbf{f}\right)_\Omega = \int_\Omega -\star\, \widetilde{\lambda}_2^{(2)} \wedge \star \left(x f_y^{(2)} - y f_x^{(2)}\right) = \int_\Omega \widetilde{\lambda}_2^{(2)} \wedge \left(x f_y^{(2)} - y f_x^{(2)}\right) \approx \left(\left(\boldsymbol{\lambda}_2'\right)^h\right)^T \boldsymbol{f}_q^h.$$

Here, $f_q^{(2)} = x f_y^{(2)} - y f_x^{(2)}$, and $\boldsymbol{f}_q^h$ is the co-chain projection of $f_q^{(2)}$.

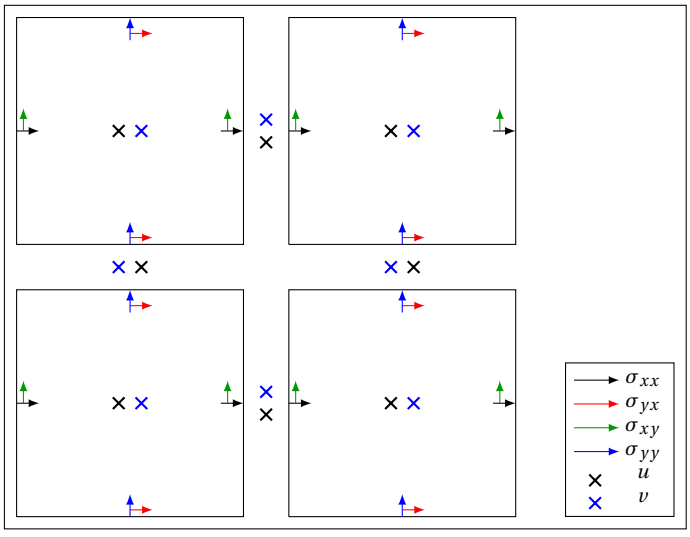

Figure 6.2: Coupling the hybrid elements of lowest order for the primal basis linear elasticity formulation, $K = 2$, $p = 1$.

6.1.9. Note on hybridisation

The system (6.10) cannot be hybridised like the Poisson problem (shown in Section 4.1.5). This can be reasoned as follows. The hybrid elements using this configuration are visualised in Fig. 6.2. The shear stresses and normal stresses are on the boundaries of the elements, and at each interface, they are coupled with a

Lagrange multiplier, such that they are constrained to be equal. However, since within the element, the shear stresses are constrained to be equal as well, there are not enough constraints for the degrees of freedom, and the shear stresses are under-determined. Hence, this system will be singular. This will be the case for both the configurations shown in Fig. 6.1. Only additional constraints, such as one posed on each intersection that sets the sum of four elements, can alleviate this problem, yet it is debatable if this is a physical constraint, since it is arbitrary.

6.2. Results

For this formulation, again a manufactured solution test case is used to test the convergence. Furthermore, the cantilever beam test case is used, in which the body force is zero. Note that for this formulation, the results are generated using continuous elements.

6.2.1. Manufactured solution

For the linear elasticity formulation, the solution for the displacements is taken as

$$u^{\text{ex}}(x,y) = \sin(\pi x)\sin(\pi y),$$
$$v^{\text{ex}}(x,y) = \sin(\pi x)\sin(\pi y).$$

The solution for the rotation, strains and stresses is accordingly derived as

$$\omega^{\text{ex}}(x,y) = \frac{\pi}{2}\left(\cos(\pi x)\sin(\pi y) - \sin(\pi x)\cos(\pi y)\right),$$
$$\underline{\underline{\epsilon}}^{\text{ex}}(x,y) = \pi\begin{bmatrix} \cos(\pi x)\sin(\pi y) & \frac{1}{2}\left[\sin(\pi x)\cos(\pi y) + \cos(\pi x)\sin(\pi y)\right] \\ \frac{1}{2}\left[\sin(\pi x)\cos(\pi y) + \cos(\pi x)\sin(\pi y)\right] & \sin(\pi x)\cos(\pi y) \end{bmatrix},$$
$$\underline{\underline{\sigma}}^{\text{ex}}(x,y) = \frac{\pi E}{1+\nu}\begin{bmatrix} \frac{1}{1-\nu}\left[\cos(\pi x)\sin(\pi y) + \nu\sin(\pi x)\cos(\pi y)\right] & \frac{1}{2}\left[\sin(\pi x)\cos(\pi y) + \cos(\pi x)\sin(\pi y)\right] \\ \frac{1}{2}\left[\sin(\pi x)\cos(\pi y) + \cos(\pi x)\sin(\pi y)\right] & \frac{1}{1-\nu}\left[\sin(\pi x)\cos(\pi y) + \nu\cos(\pi x)\sin(\pi y)\right] \end{bmatrix},$$
$$\mathbf{f}^{\text{ex}}(x,y) = \frac{\pi^2 E}{1-\nu^2}\begin{bmatrix} \frac{1}{2}(2-\nu)\sin(\pi x)\sin(\pi y) - \frac{1}{2}(1+\nu)\cos(\pi x)\cos(\pi y) \\ \frac{1}{2}(2-\nu)\sin(\pi x)\sin(\pi y) - \frac{1}{2}(1+\nu)\cos(\pi x)\cos(\pi y) \end{bmatrix}.$$

This test problem is also seen in [53].

The results for the p- and h-convergence of the solution components are shown in Fig. 6.3. Furthermore, the conservation of linear momentum and the symmetry of the stress tensor are shown in Fig. 6.4 for both p- and h- refinement as well.

The norms are defined by

$$\begin{aligned}
\left\|\epsilon_{\underline{\underline{\sigma}}}\right\|_{[H(\text{div})]^2} &= \left\|\sigma^h_{xx} - \sigma^{\text{ex}}_{xx}\right\|_{L^2} + \left\|\sigma^h_{yx} - \sigma^{\text{ex}}_{yx}\right\|_{L^2} + \left\|\sigma^h_{xy} - \sigma^{\text{ex}}_{xy}\right\|_{L^2} + \left\|\sigma^h_{yy} - \sigma^{\text{ex}}_{yy}\right\|_{L^2} \\
&\quad + \left\|\left(\mathrm{d}\sigma^{(1)}_x\right)^h - f^{ex}_x\right\|_{L^2} + \left\|\left(\mathrm{d}\sigma^{(1)}_y\right)^h - f^{ex}_y\right\|_{L^2}, \\
\|\epsilon_{\mathbf{u}}\|^2_{[H^1]^2} &= \left\|u^h - u^{\text{ex}}\right\|^2_{L^2} + \left\|v^h - v^{\text{ex}}\right\|^2_{L^2} + \left\|\left(\frac{\partial u}{\partial x}\right)^h - \left(\frac{\partial u}{\partial x}\right)^{\text{ex}}\right\|^2_{L^2} + \left\|\left(\frac{\partial u}{\partial y}\right)^h - \left(\frac{\partial u}{\partial y}\right)^{\text{ex}}\right\|^2_{L^2} \\
&\quad + \left\|\left(\frac{\partial v}{\partial x}\right)^h - \left(\frac{\partial v}{\partial x}\right)^{\text{ex}}\right\|^2_{L^2} + \left\|\left(\frac{\partial v}{\partial y}\right)^h - \left(\frac{\partial v}{\partial y}\right)^{\text{ex}}\right\|^2_{L^2}, \\
\|\epsilon_\omega\|_{L^2} &= \left\|\omega^h - \omega^{\text{ex}}\right\|_{L^2}, \\
\left\|\epsilon_{\text{sym}}\right\|_{L^2} &= \left\|\sigma^h_{xy} - \sigma^h_{yx}\right\|_{L^2}.
\end{aligned}$$

Note that for computing the displacement, both $\boldsymbol{\lambda}^h_1$ and λ^h_2 are evaluated point-wise, and the displacement is then computed by simple addition,

$$\mathbf{u}^h(x,y) = \boldsymbol{\lambda}^h_1(x,y) + \begin{bmatrix} -y\lambda^h_2(x,y) \\ x\lambda^h_2(x,y) \end{bmatrix}.$$

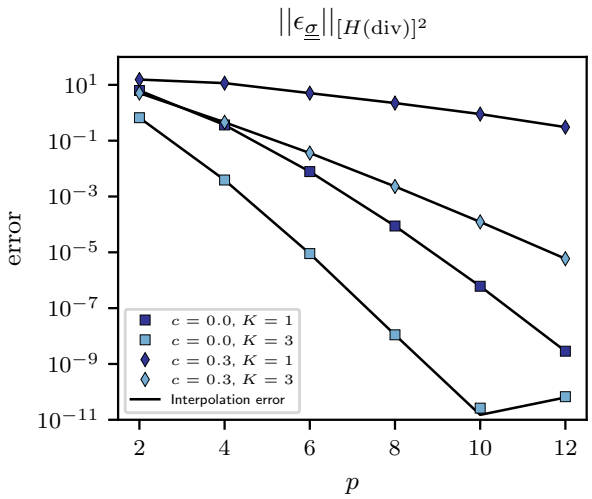

(a) Total error in stress, p-convergence.

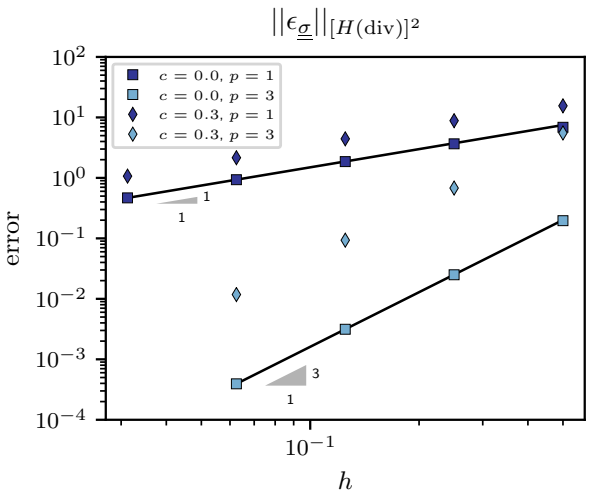

(b) Total error in stress, h-convergence.

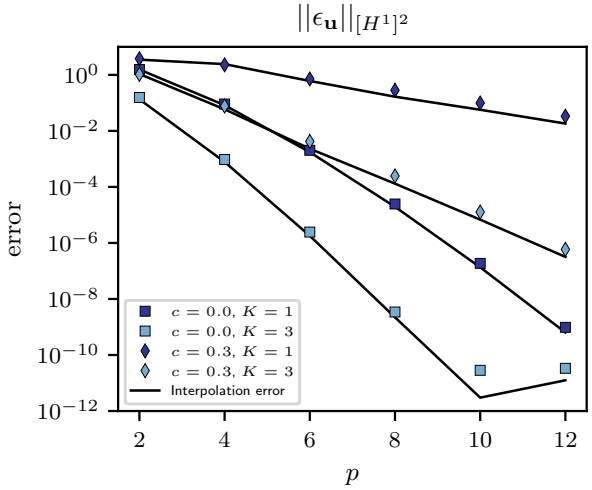

(c) Total error in displacement, p-convergence.

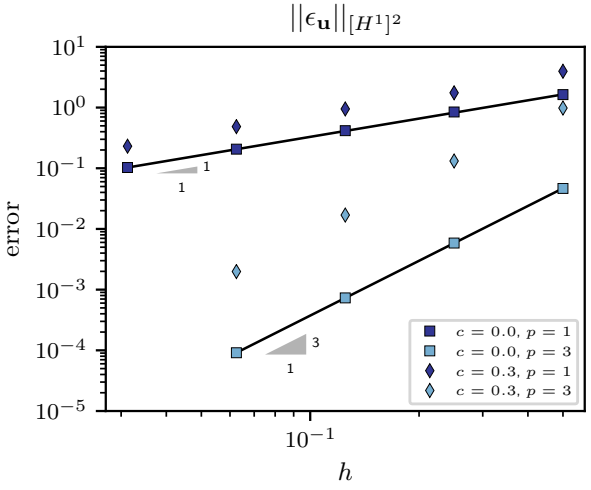

(d) Total error in displacement, h-convergence.

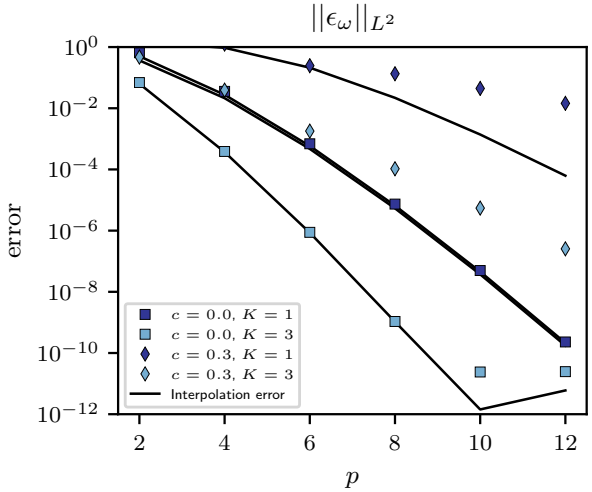

(e) Error in rotation, p-convergence.

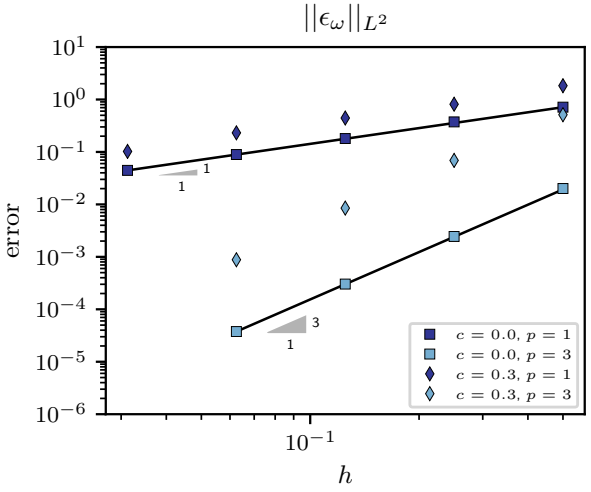

(f) Error in rotation, h-convergence.

Figure 6.3: p- and h-convergence trends for the linear elasticity problem, for the manufactured solution on the domain $[0,1]^2$.

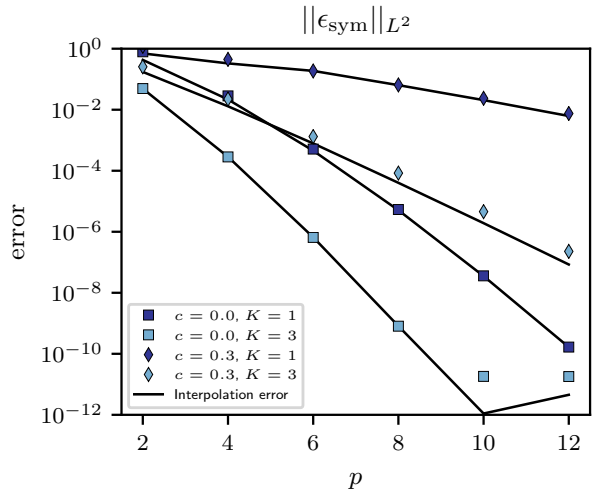

(a) Error in symmetry of the stress tensor, varying p.

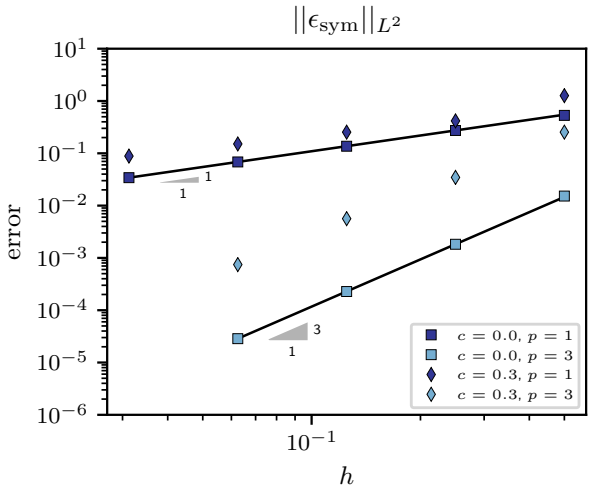

(b) Error in symmetry of the stress tensor, varying h.

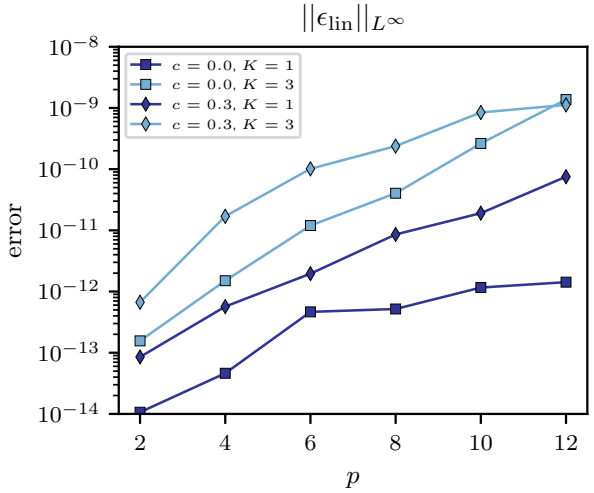

(c) Error in linear momentum, varying p.

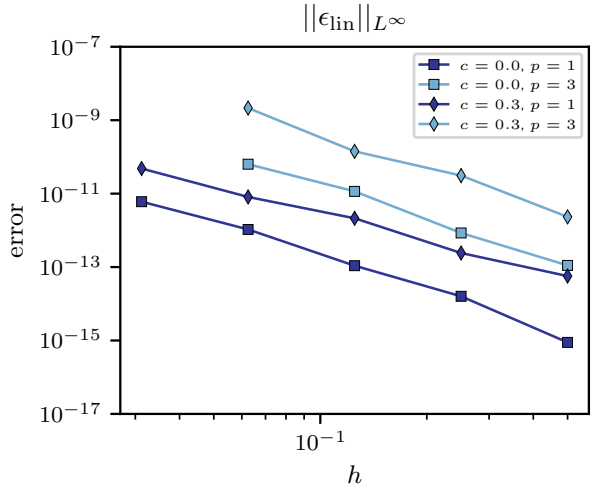

(d) Error in linear momentum, varying h.

Figure 6.4: Properties of the solution for the linear elasticity problem, for the manufactured solution on the domain $[0,1]^2$.

The derivatives in the norm $\|\epsilon_{\mathbf{u}}\|_{H^1}$ are computed by first computing the symmetric part of the displacement gradient tensor, with $\left(\boldsymbol{\epsilon}'\right)^h = \left[\left(\boldsymbol{\epsilon}'_{xx}\right)^h, \left(\boldsymbol{\epsilon}'_{yx}\right)^h, \left(\boldsymbol{\epsilon}'_{xy}\right)^h, \left(\boldsymbol{\epsilon}'_{yy}\right)^h\right]$,

$$\left(\boldsymbol{\epsilon}'\right)^h = -\left(\mathbb{E}_\sigma\right)\left(\boldsymbol{\lambda}'_1\right)^h - \mathbb{Q}^T\left(\mathbb{E}^{(2,1)}\right)^T\left(\boldsymbol{\lambda}'_2\right)^h + \boldsymbol{b}^h$$

Then, using the mass matrix $\mathbb{M}^{(1)}$ for $\mathbb{R}^2$, the primal co-chains are found,

$$\boldsymbol{\epsilon}^h = \begin{bmatrix} \left(\mathbb{M}^{(1)}\right)^{-1} & 0 \\ 0 & \left(\mathbb{M}^{(1)}\right)^{-1} \end{bmatrix}\left(\boldsymbol{\epsilon}'\right)^h$$

The strain components in $\boldsymbol{\epsilon}^h$ can be evaluated with the same expansions as the stress components. Finally, to find the displacement gradient tensor components, the skew-symmetric part needs to be subtracted from the strain tensor, as

$$\nabla\mathbf{u} = \underline{\underline{\epsilon}} + \underline{\underline{\mathrm{W}}} = \begin{bmatrix} \frac{\partial u}{\partial x} & \frac{1}{2}\left(\frac{\partial u}{\partial y} + \frac{\partial v}{\partial x}\right) \\ \frac{1}{2}\left(\frac{\partial u}{\partial y} + \frac{\partial v}{\partial x}\right) & \frac{\partial v}{\partial y} \end{bmatrix} - \begin{bmatrix} 0 & \omega \\ -\omega & 0 \end{bmatrix}.$$

Hence, the vorticity needs to be added or subtracted pointwise for ϵ^h_{xy} and ϵ^h_{yx}. The norm for linear momentum is defined as

$$\|\epsilon_{\mathrm{lin}}\|_{L^\infty} = \max\left(\left\|\left(\mathrm{d}\sigma^{(1)}_x\right)^h - f^h_x\right\|_{L^\infty}, \left\|\left(\mathrm{d}\sigma^{(1)}_y\right)^h - f^h_y\right\|_{L^\infty}\right).$$

This relation is topological, evident from the small maximum error seen in Fig. 6.4, which is considered to be machine precision error.

Optimal convergence is seen in Fig. 6.3, and all errors except for the rotation are of the same magnitude as the interpolation error. It is not clear why the interpolation error for the rotation has a different trend for the deformed mesh, it is possible that this is only the case for this specific problem. However, comparing to the displacements, the error in rotation follows the same trend. The symmetry of the stress tensor is weakly conserved, and converges to zero. Note that the interpolation error for the symmetry is interpreted as the difference in the reduced exact solution of the shear stresses, i.e.

$$\left\|\epsilon_{\mathcal{I},\mathrm{sym}}\right\|_{L^2} = \left\|\left(\sigma^{\mathrm{ex}}_{xy}\right)^h - \left(\sigma^{\mathrm{ex}}_{yx}\right)^h\right\|_{L^2}.$$

This expresses the ability of the solution to represent a symmetric stress tensor. Finally, to reflect on the starting point of this thesis, the error in constitutive law and the total error made are shown in Fig. 6.5. The error in constitutive law is, for the compliance tensor of the problem considered here,

$$\begin{aligned}\|\epsilon_{\mathrm{const}}\|^2_{L^2} &= \left\|C\,\underline{\underline{\sigma}}^h - \underline{\underline{\epsilon}}^{\mathrm{ex}}\right\|^2_{L^2} \\ &= \left\|\frac{1}{E}\left(\sigma^h_{xx} + \nu\sigma^h_{yy}\right) - \epsilon^{\mathrm{ex}}_{xx}\right\|^2_{L^2} + \left\|\frac{1}{E}\left(\nu\sigma^h_{xx} + \sigma^h_{yy}\right) - \epsilon^{\mathrm{ex}}_{yy}\right\|^2_{L^2} + \left\|\frac{1+\nu}{E}\sigma^h_{yx} - \epsilon^{\mathrm{ex}}_{yx}\right\|^2_{L^2} + \left\|\frac{1+\nu}{E}\sigma^h_{xy} - \epsilon^{\mathrm{ex}}_{xy}\right\|^2_{L^2}.\end{aligned}$$

The total error is computed a

$$\|\epsilon_{\mathrm{total}}\|^2_{L^2} = \left\|\underline{\underline{\sigma}}^h - \underline{\underline{\sigma}}^{\mathrm{ex}}\right\|^2_{L^2} + \left\|\mathbf{u}^h - \mathbf{u}^{\mathrm{ex}}\right\|^2_{L^2} + \left\|\omega^h - \omega^{\mathrm{ex}}\right\|^2_{L^2}.$$

It can be seen that these are nearly the same, showing that all the error is concentrated on the constitutive law, while the other relations hold.

6.2.2. Cantilever beam

To show the properties of this formulation without the effects of a forcing function, the cantilever beam problem is used. The algebraic solution of this problem is taken from [62, p. 123-124]. A schematic setup of this problem is shown in Fig. 6.6. In this problem, the height of the beam is taken as $2h_{\mathrm{beam}} = 0.01$, with length $L = 1$. The out-of-plane width of the beam is b_{beam}, in this problem taken as $b_{\mathrm{beam}} = 2h_{\mathrm{beam}}$. This only influences the moment of inertia $I = \frac{2h^3_{\mathrm{beam}}b_{\mathrm{beam}}}{3}$. The load on the left side, $P = 1$, is implemented as a shear stress acting on the boundary. Apart from the rigid connection at $x = L$, where the displacement is set zero, on all

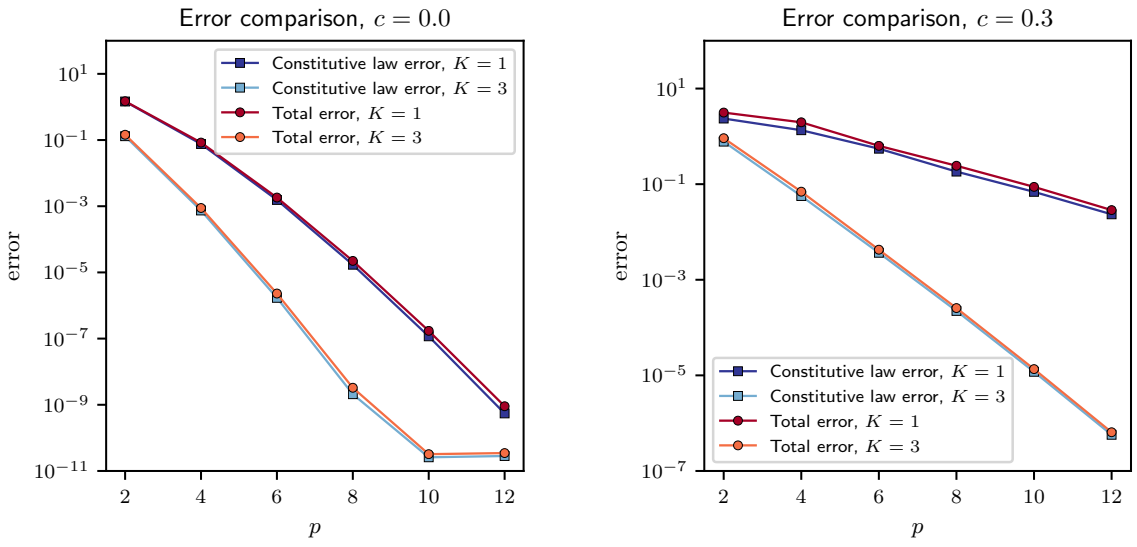

(a) Orthogonal mesh, $c = 0$.

(b) Deformed mesh, $c = 0.3$.

Figure 6.5: Comparison of L^2-error in the constitutive law and the total sum of L^2-error of the solution for the manufactured solution test case on the domain $[0,1]^2$ for p-refinement.

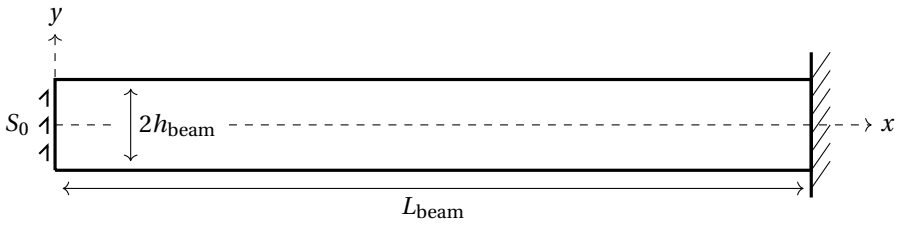

Figure 6.6: Cantilever beam problem setup.

other boundaries the normal and shear stress is prescribed. Finally, as material parameters, $E = 2 \cdot 10^{11}$, and $\nu = 0.3$, (which, if E is in Nm^{-2}, resembles a material like steel).

The exact solution is given for the strains by

$$\epsilon_{xx}^{\text{ex}} = -\frac{Pxy}{EI}, \quad \epsilon_{xy}^{\text{ex}} = \epsilon_{yx}^{\text{ex}} = -\frac{(1+\nu)P}{2EI}\left(h^2 - y^2\right), \quad \epsilon_{yy}^{\text{ex}} = \frac{\nu Pxy}{EI},$$

for the stresses by

$$\sigma_{xx}^{\text{ex}} = \frac{E}{1-\nu^2}\left(\epsilon_{xx}^{\text{ex}} + \nu\epsilon_{yy}^{\text{ex}}\right), \quad \sigma_{xy}^{\text{ex}} = \sigma_{yx}^{\text{ex}} = \frac{E}{1+\nu}\epsilon_{xy}^{\text{ex}}, \quad \sigma_{yy}^{\text{ex}} = \frac{E}{1-\nu^2}\left(\nu\epsilon_{xx}^{\text{ex}} + \epsilon_{yy}^{\text{ex}}\right),$$

and for the displacements and rotation by

$$u^{\text{ex}} = \frac{PL_{\text{beam}}^2 y}{6EI}\left(3\left(1 - \frac{x^2}{L_{\text{beam}}^2}\right) + (2+\nu)\frac{y^2}{L_{\text{beam}}^2} - 3(1+\nu)\frac{h_{\text{beam}}^2}{L_{\text{beam}}^2}\right),$$
$$v^{\text{ex}} = \frac{PL_{\text{beam}}^3}{6EI}\left(2 - 3\frac{x}{L_{\text{beam}}}\left(1 - \nu\frac{y^2}{L_{\text{beam}}^2}\right) + \frac{x^3}{L_{\text{beam}}^3} + 3(1+\nu)\frac{h_{\text{beam}}^2}{L_{\text{beam}}^2}\left(1 - \frac{x^2}{L_{\text{beam}}^2}\right)\right),$$
$$\omega^{\text{ex}} = \frac{1}{2}\left(\frac{\partial v^{\text{ex}}}{\partial x} - \frac{\partial u^{\text{ex}}}{\partial y}\right).$$

The results are shown for two cases. In the first case, the solution is fully resolved with one element of order $p = 3$. This shows that the solution is exactly represented, and in that specific case the stress tensor is

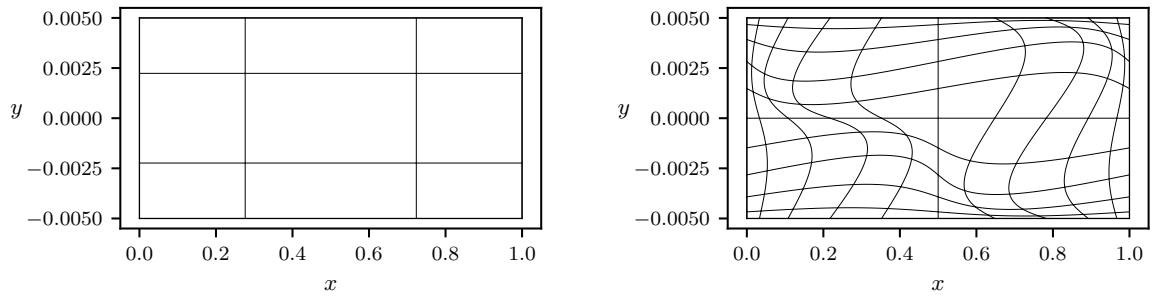

(a) Orthogonal grid, of order $p = 3$, $c = 0$.

(b) Deformed grid, of order $p = 10$, $c = 0.2$.

Figure 6.7: Single element grid used for the cantilever beam problem.

symmetric, see Fig. 6.8. The error in linear momentum is computed as

$$\epsilon_{\text{lin}} = \left(\mathrm{d}\sigma_x^{(1)}\right)^h + \left(\mathrm{d}\sigma_y^{(1)}\right)^h.$$

However, by deforming the mesh using the same mapping as for the manufactured solution test case, the solution becomes underresolved, see Fig. 6.9. Now, exact symmetry clearly breaks down (seen in Fig. 6.9h), while the linear momentum can be said to be still conserved in Fig. 6.9g (the value should be relatively compared to the value of normal stress σ_{xx}). Hence, this formulation conserves only linear momentum strongly, and symmetry of the stress tensor is not strongly satisfied, hence also angular momentum is conserved weakly (since only imposing linear momentum conservation and symmetry of the stress tensor strongly implies imposing angular momentum strongly).

6.3. Summary

This chapter introduced a way of directly implementing continuum mechanics problems with the mimetic spectral element method. By logical choice of the basis of the stresses guided by geometric considerations, the linear momentum relation could be discretised exactly on both an orthogonal and highly deformed grid. However, due to the choice of basis for the shear stresses, the symmetry of the stress tensor and thus the angular momentum could not be conserved strongly but only weakly. This was then also shown in the results for the manufactured solution and cantilever beam test cases. The next chapter addresses a different formulation, which is aimed at satisfying both the linear momentum constraint and symmetry of the stress tensor strongly.

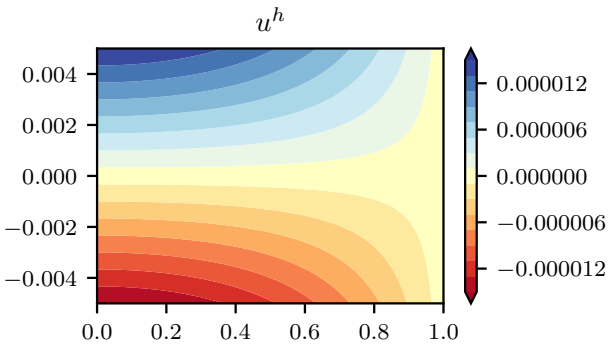

(a) Displacement in x-direction.

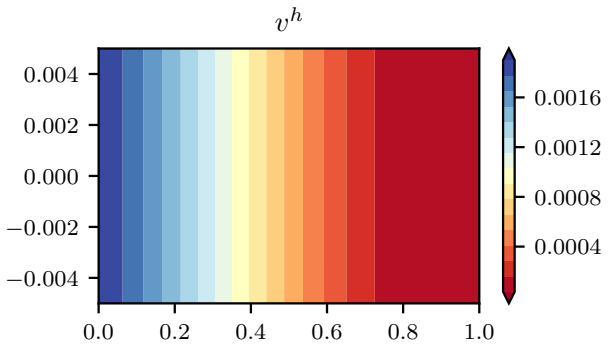

(b) Displacement in y-direction.

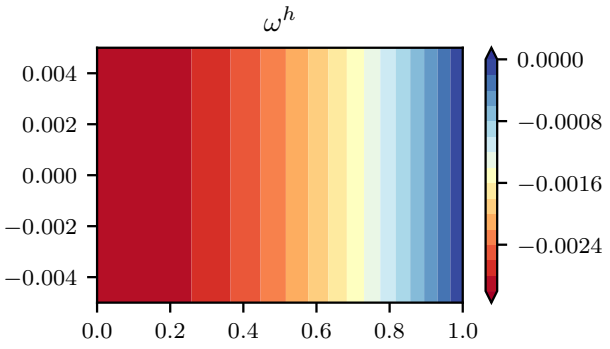

(c) Rotation.

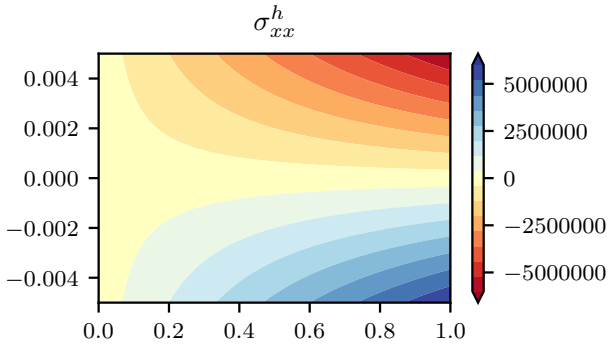

(d) Normal stress in x-direction.

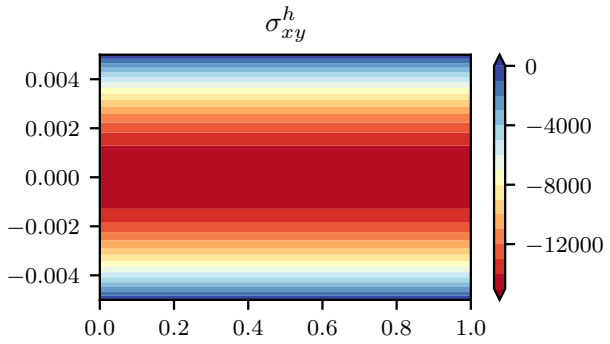

(e) Shear stress in x-direction..

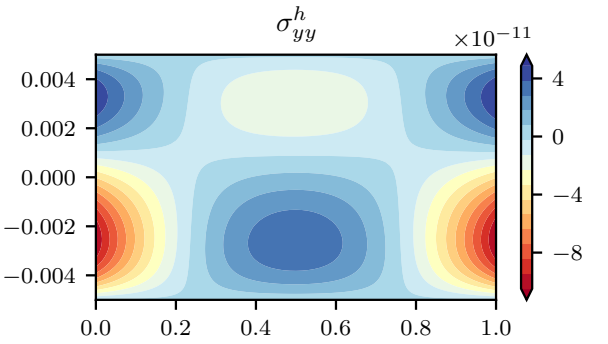

(f) Normal stress in y-direction.

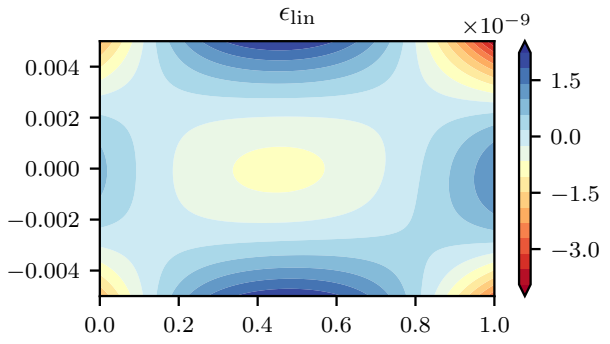

(g) Linear momentum.

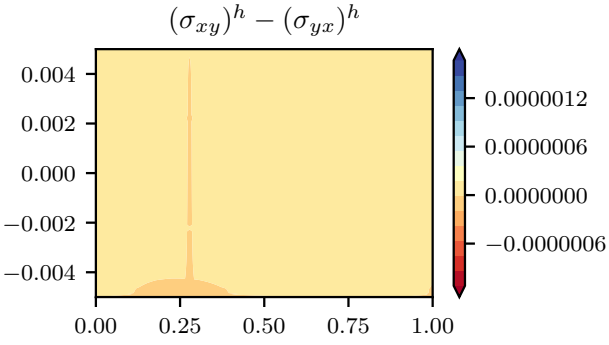

(h) Symmetry of the stress tensor.

Figure 6.8: Fully resolved solution for the cantilever beam on orthogonal grid, single element of order $p = 3$.

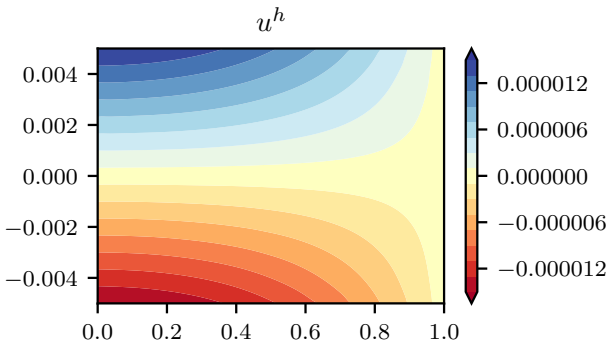

(a) Displacement in x-direction.

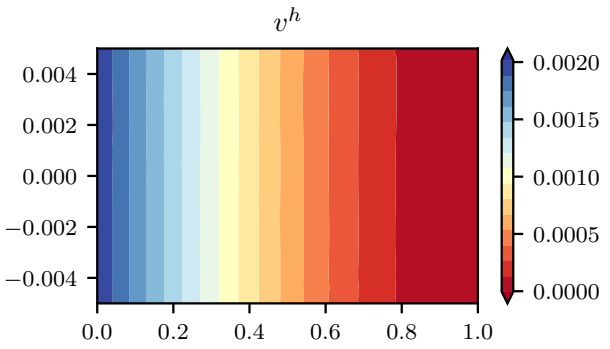

(b) Displacement in y-direction.

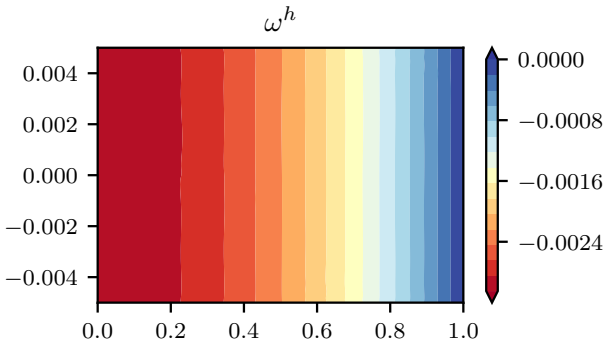

(c) Rotation.

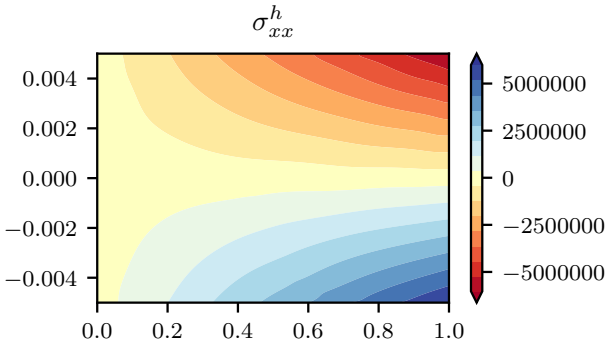

(d) Normal stress in x-direction.

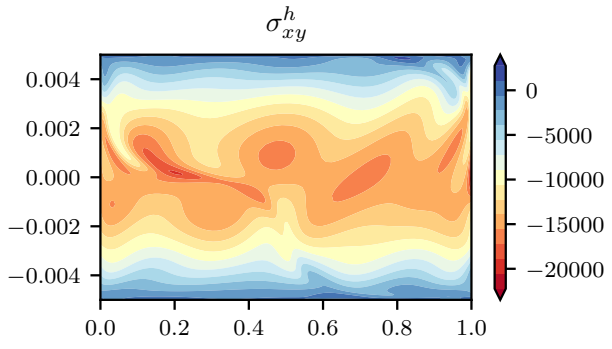

(e) Shear stress in x-direction..

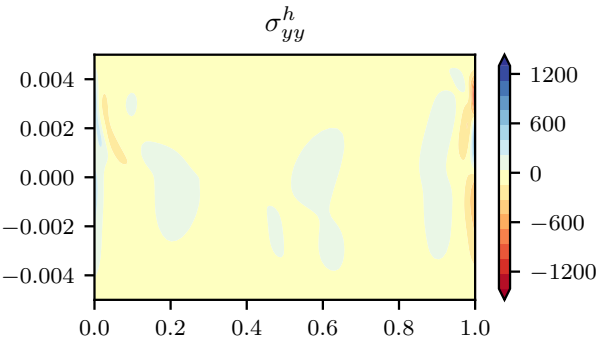

(f) Normal stress in y-direction.

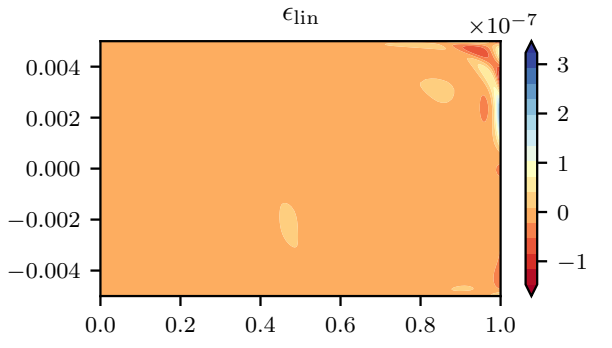

(g) Linear momentum.

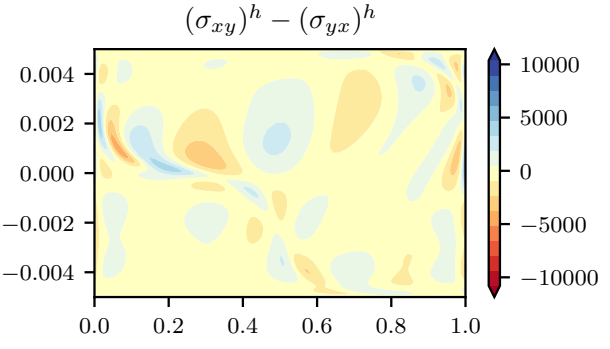

(h) Symmetry of the stress tensor.

Figure 6.9: Underresolved solution for the cantilever beam on deformed grid, single element of order $p = 10$, $c = 0.2$.

7

A New Linear Elasticity Formulation

In the previous formulation for linear elasticity, the stress components were all discretised along the primal edges. This resulted in a configuration with weakly imposed symmetry through the angular momentum conservation constraint. However, to strongly satisfy symmetry and thus angular momentum, a different configuration can be used. In this configuration, the stresses are not assigned on the same edges with primal basis functions only, but are instead assigned to combinations of primal and algebraic dual basis functions. This is not only done to put the shear stresses in the same polynomial space, such that they can be set equal, but also to be able to use hybrid elements.

7.1. Derivation and implementation

In the following, the weak formulation is derived from an altered functional that prescribes the shear stresses on the boundary. Then the mixed basis for the elements is discussed. The reduction of functions for this specific formulation is discussed as well. The last part of this section discusses the hybrid element configuration of this formulation.

7.1.1. Lagrangian and weak formulation

The Lagrangian functional for imposing linear momentum conservation and symmetry of the stress tensor is

$$\mathcal{L}\left(\underline{\underline{\sigma}}, \mathbf{u}, \omega; \mathbf{f}, \mathbf{u}_P\right) = \int_\Omega \frac{1}{2} \underline{\underline{\sigma}}^T C \underline{\underline{\sigma}} \, \mathrm{d}\Omega + \int_\Omega \mathbf{u} \left(\nabla \cdot \underline{\underline{\sigma}} + \mathbf{f}\right) \mathrm{d}\Omega + \int_\Omega \omega \left(\sigma_{xy} - \sigma_{yx}\right) \mathrm{d}\Omega + \int_{\partial\Omega} \underline{\underline{\sigma}} \left(\mathbf{u}_P \cdot \mathbf{n}\right) \mathrm{d}\Gamma.$$

Here, $\underline{\underline{\sigma}} \in [H(\mathrm{div}, \Omega)]^n$, $\mathbf{u} \in \left[L^2(\Omega)\right]^n$, $\omega \in L^2(\Omega)$. The idea[1] is to rewrite the functional such that $\mathbf{u}$ still acts as Lagrange multiplier for the normal stresses, and $\mathbf{u}_P$ is prescribed on the boundary for the normal stresses, while the shear stresses σ_{yx}, σ_{xy} act as Lagrange multipliers for the displacements and $\left(\sigma_{yx}\right)_P, \left(\sigma_{xy}\right)_P$ are prescribed on the boundary for the displacements. In this case, the functional reads in $\mathbb{R}^2$

$$\begin{aligned}\mathcal{L}\left(\underline{\underline{\sigma}}, \mathbf{u}, \omega; \mathbf{f}, \mathbf{u}_p, \left(\sigma_{yx}\right)_P, \left(\sigma_{xy}\right)_P\right) = &\int_\Omega \frac{1}{2} \underline{\underline{\sigma}}^T C \underline{\underline{\sigma}} \, \mathrm{d}\Omega + \int_\Omega u \left(\frac{\partial \sigma_{xx}}{\partial x} + f_x\right) \mathrm{d}\Omega - \int_\Omega \frac{\partial u}{\partial y} \sigma_{yx} \mathrm{d}\Omega \\ &+ \int_\Omega v \left(\frac{\partial \sigma_{yy}}{\partial y} + f_y\right) \mathrm{d}\Omega - \int_\Omega \frac{\partial v}{\partial x} \sigma_{xy} \mathrm{d}\Omega + \int_\Omega \omega \left(\sigma_{xy} - \sigma_{yx}\right) \mathrm{d}\Omega \\ &+ \int_{\partial\Omega} \left[-u_P \sigma_{xx} n_x + u \left(\sigma_{yx}\right)_P n_y + v \left(\sigma_{xy}\right)_P n_x - v_P \sigma_{yy} n_y\right] \mathrm{d}\Gamma.\end{aligned} \tag{7.1}$$

[1] Proposed by Dr. M. I. Gerritsma

Note that the function spaces should now be extended to incorporate the added derivatives, $\underline{\underline{\sigma}} \in [H(\mathrm{div},\Omega)]^2$, $\mathbf{u} \in \left[H^1(\Omega)\right]^2$, $\omega \in L^2(\Omega)$. By taking variations of (7.1), the system will be in the form of

$$\left(\underline{\underline{\widetilde{\sigma}}}, C\underline{\underline{\sigma}}\right)_\Omega + \int_\Omega u\frac{\partial \widetilde{\sigma}_{xx}}{\partial x} - \frac{\partial u}{\partial y}\widetilde{\sigma}_{yx} + v\frac{\partial \widetilde{\sigma}_{yy}}{\partial y} - \frac{\partial v}{\partial x}\widetilde{\sigma}_{xy}\mathrm{d}\Omega + \left(\omega, \left(\widetilde{\sigma}_{xy} - \widetilde{\sigma}_{yx}\right)\right)_\Omega = B_\sigma, \tag{7.2a}$$

$$\int_\Omega \widetilde{u}\frac{\partial \sigma_{xx}}{\partial x} - \frac{\partial \widetilde{u}}{\partial y}\sigma_{yx} + \widetilde{v}\frac{\partial \sigma_{yy}}{\partial y} - \frac{\partial \widetilde{v}}{\partial x}\sigma_{xy}\mathrm{d}\Omega = -\left(\widetilde{\mathbf{u}}, \mathbf{f}\right)_\Omega - B_u, \tag{7.2b}$$

$$\left(\widetilde{\omega}, \left(\sigma_{xy} - \sigma_{yx}\right)\right)_\Omega = 0, \tag{7.2c}$$

where the boundary terms are

$$B_\sigma = \int_{\partial\Omega} \left[u_P \widetilde{\sigma}_{xx} n_x + v_P \widetilde{\sigma}_{yy} n_y\right] \mathrm{d}\Gamma,$$
$$B_u = \int_{\partial\Omega} \left[\widetilde{u}\left(\sigma_{yx}\right)_P n_y + \widetilde{v}\left(\sigma_{xy}\right)_P n_x\right] \mathrm{d}\Gamma.$$

This must hold $\forall\, \underline{\underline{\widetilde{\sigma}}} \in [H(\mathrm{div},\Omega)]^2, \forall\, \widetilde{\mathbf{u}} \in \left[H^1(\Omega)\right]^2, \forall\, \widetilde{\omega} \in L^2(\Omega)$. Assuming a smooth enough solution such that integration by parts can be used,

$$\left(\underline{\underline{\widetilde{\sigma}}}, C\underline{\underline{\sigma}}\right)_\Omega - \left(\underline{\underline{\widetilde{\sigma}}}, \nabla\mathbf{u}\right)_\Omega + \left(\omega, \left(\widetilde{\sigma}_{xy} - \widetilde{\sigma}_{yx}\right)\right)_\Omega = 0,$$
$$\left(\widetilde{\mathbf{u}}, \nabla\cdot\underline{\underline{\sigma}}\right)_\Omega + \left(\widetilde{\mathbf{u}}, \mathbf{f}\right)_\Omega = 0,$$
$$\left(\widetilde{\omega}, \left(\sigma_{xy} - \sigma_{yx}\right)\right)_\Omega = 0,$$

which should hold $\forall\, \underline{\underline{\widetilde{\sigma}}}, \widetilde{\mathbf{u}}, \widetilde{\omega}$, thus

$$C\underline{\underline{\sigma}} = \nabla\mathbf{u} - \begin{bmatrix} 0 & \omega \\ -\omega & 0 \end{bmatrix} = \frac{1}{2}\left(\nabla\mathbf{u} + (\nabla\mathbf{u})^T\right) = 0 \qquad \text{in } \Omega,$$
$$\nabla\cdot\underline{\underline{\sigma}} + \mathbf{f} = 0 \qquad \text{in } \Omega,$$
$$\sigma_{xy} - \sigma_{yx} = 0 \qquad \text{in } \Omega.$$

These equations express the constitutive law, the conservation law of linear momentum, and symmetry of the stress tensor. The system (7.2) can be discretised to

$$\begin{bmatrix} \mathbb{M}_\sigma & \mathbb{E}_\sigma^T & \mathbb{R}^T \\ \mathbb{E}_\sigma & 0 & 0 \\ \mathbb{R} & 0 & 0 \end{bmatrix} \begin{bmatrix} \boldsymbol{\sigma}^h \\ \boldsymbol{u}^h \\ \boldsymbol{\omega}^h \end{bmatrix} = \begin{bmatrix} -\boldsymbol{g}_\sigma^h \\ -\boldsymbol{f}^h - \boldsymbol{g}_u \\ \mathbf{0} \end{bmatrix}. \tag{7.4}$$

The terms in this system will be elaborated on in the following sections.

7.1.2. Expanding into mixed basis

The main idea for this formulation [2] is to discretise the shear stresses, such that the conservation of linear momentum and symmetry can be imposed simultaneously. This can be done if the shear stress components are expressed in the same polynomial spaces, and by making explicit use of the algebraic dual basis functions described in Chapter 3. These are denoted here as

$$e'_k(x_j) = h_i(x_j)\left(\mathbb{M}^{(0)}\right)^{-1}_{ik}, \quad h'_l(x_j) = e_i(x_j)\left(\mathbb{M}^{(1)}\right)^{-1}_{il}.$$

The expansions used to achieve this are

$$\overline{\sigma}_{xx} = \sum_{i=1}^{p+1}\sum_{j=1}^{p+1} (\sigma_{xx})_{ij}\, h_i(x) e'_j(y), \qquad \overline{\sigma}_{yx} = \sum_{i=1}^{p}\sum_{j=1}^{p} \left(\sigma_{yx}\right)_{ij} e_i(x) h'_j(y),$$
$$\overline{\sigma}_{xy} = \sum_{i=1}^{p}\sum_{j=1}^{p} \left(\sigma_{xy}\right)_{ij} h'_i(x) e_j(y), \qquad \overline{\sigma}_{yy} = \sum_{i=1}^{p+1}\sum_{j=1}^{p+1} \left(\sigma_{yy}\right)_{ij} e'_i(x) h_j(y).$$

[2] This idea originated in a discussion by Y. Zhang, V. Jain and M. I. Gerritsma

The stress components are visualised in Fig. 7.1 for an element of order $p = 2$. Since the dual basis functions have different roots than the primal basis, the location of the stress components is only an approximate guess, hence the dashed lines. What should be clear from this visualisation is that the normal components are in $\mathcal{P}^{p,p}$, while the shear stress components are in $\mathcal{P}^{p-1,p-1}$. Furthermore, the shear stresses will be discontinuous between elements, while the normal stresses will be continuous between elements in their respective working direction while discontinuous between elements in the other direction. In order for the linear mo-

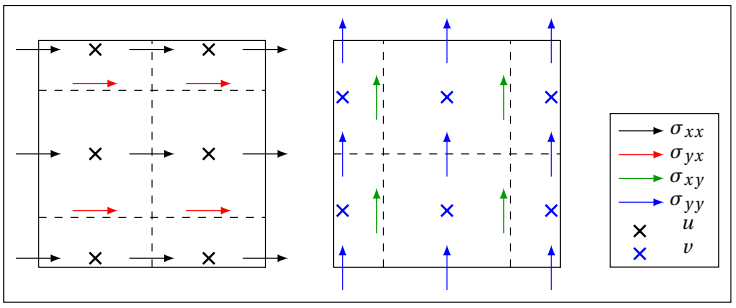

Figure 7.1: Assigning the stress tensor components to an element with mixed basis, $p = 2$.

mentum conservation to be metric independent, the Lagrange multipliers u, v are dual to the components of the divergence of stress. To compute the vector components of the divergence of the stress tensor, the respective derivatives need to be computed. The computation of derivatives of the normal stresses is straightforward,

$$\frac{\partial \overline{\sigma}_{xx}}{\partial x} = \sum_{i=1}^{p} \sum_{j=1}^{p+1} \left[(\sigma_{xx})_{i+1,j} - (\sigma_{xx})_{i,j} \right] e_i(x) e'_j(y),$$
$$\frac{\partial \overline{\sigma}_{yy}}{\partial y} = \sum_{i=1}^{p+1} \sum_{j=1}^{p} \left[(\sigma_{yy})_{i,j+1} - (\sigma_{yy})_{i,j} \right] e'_i(x) e_j(y).$$

To do the same for the shear stress components, the imposed boundary conditions for the shear stresses are necessary. Assigning these to $i = 0$ and $i = p+1$ for σ_{xy} and to $j = 0$ and $j = p+1$ for σ_{yx}, i.e.

$$(\overline{\sigma}_{xy})_{0,j} = (\overline{\sigma}_{xy})_P, \qquad (\overline{\sigma}_{xy})_{p+1,j} = (\overline{\sigma}_{xy})_P,$$
$$(\overline{\sigma}_{yx})_{i,0} = (\overline{\sigma}_{yx})_P, \qquad (\overline{\sigma}_{yx})_{i,p+1} = (\overline{\sigma}_{yx})_P,$$

the derivatives are found to be

$$\frac{\partial \overline{\sigma}_{yx}}{\partial y} = \sum_{i=1}^{p} \sum_{j=1}^{p+1} \left[(\sigma_{yx})_{i,j} - (\sigma_{yx})_{i,j-1} \right] e_i(x) e'_j(y),$$
$$\frac{\partial \overline{\sigma}_{xy}}{\partial x} = \sum_{i=1}^{p+1} \sum_{j=1}^{p} \left[(\sigma_{xy})_{i,j} - (\sigma_{xy})_{i-1,j} \right] e'_i(x) e_j(y).$$

Note that the contributions to linear momentum in both directions have the same expansions, hence the co-chains can simply be added. The forcing function will have the same basis as these derivatives as well, see Section 7.1.5. Thus, the basis functions for the Lagrange multipliers u, v are chosen to be dual to the derivatives of the stress components, such that

$$\overline{u} = \sum_{i=1}^{p} \sum_{j=1}^{p+1} (u)_{ij} h'_i(x) h_j(y), \qquad \overline{v} = \sum_{i=1}^{p+1} \sum_{j=1}^{p} (v)_{ij} h_i(x) h'_j(y).$$

The inner product can then be discretised using

$$\int_\Omega \widetilde{u} \frac{\partial \sigma_{xx}}{\partial x} - \frac{\partial \widetilde{u}}{\partial y} \sigma_{yx} + \widetilde{v} \frac{\partial \sigma_{yy}}{\partial y} - \frac{\partial \widetilde{v}}{\partial x} \sigma_{xy} \mathrm{d}\Omega \approx \boldsymbol{u}^h \mathbb{E}_\sigma \boldsymbol{\sigma}^h,$$

where the components of $\mathbb{E}_\sigma$,

$$\mathbb{E}_\sigma = \begin{bmatrix} (\mathbb{E}_\sigma)_x & 0 \\ 0 & (\mathbb{E}_\sigma)_v \end{bmatrix},$$

are given for $p = 2$, using x-lexicographic numbering as in Section 3.1, as

$$(\mathbb{E}_\sigma)_x = \begin{bmatrix} 1 & -1 & 0 & 0 & 0 & 0 & 0 & 0 & 0 & -1 & 0 & 0 & 0 \\ 0 & 1 & -1 & 0 & 0 & 0 & 0 & 0 & 0 & 0 & -1 & 0 & 0 \\ 0 & 0 & 0 & 1 & -1 & 0 & 0 & 0 & 0 & 1 & 0 & -1 & 0 \\ 0 & 0 & 0 & 0 & 1 & -1 & 0 & 0 & 0 & 0 & 1 & 0 & -1 \\ 0 & 0 & 0 & 0 & 0 & 0 & 1 & -1 & 0 & 0 & 0 & 1 & 0 \\ 0 & 0 & 0 & 0 & 0 & 0 & 0 & 1 & -1 & 0 & 0 & 0 & 1 \end{bmatrix},$$
$$(\mathbb{E}_\sigma)_y = \begin{bmatrix} -1 & 0 & 0 & 0 & 1 & 0 & 0 & -1 & 0 & 0 & 0 & 0 & 0 \\ 1 & -1 & 0 & 0 & 0 & 1 & 0 & 0 & -1 & 0 & 0 & 0 & 0 \\ 0 & 1 & 0 & 0 & 0 & 0 & 1 & 0 & 0 & -1 & 0 & 0 & 0 \\ 0 & 0 & -1 & 0 & 0 & 0 & 0 & 1 & 0 & 0 & -1 & 0 & 0 \\ 0 & 0 & 1 & -1 & 0 & 0 & 0 & 0 & 1 & 0 & 0 & -1 & 0 \\ 0 & 0 & 0 & 1 & 0 & 0 & 0 & 0 & 0 & 1 & 0 & 0 & -1 \end{bmatrix}. \tag{7.5}$$

Finally, also the Lagrange multiplier ω is chosen to be in the dual space of a 2-form, hence

$$\overline{\omega} = \sum_{i=1}^{p} \sum_{j=1}^{p} \omega_{ij} {h'}_i(x) {h'}_j(y).$$

Note that the rotation can also be computed as the curl of the displacement, with components

$$\frac{\partial \overline{u}}{\partial y} = \sum_{i=1}^{p} \sum_{j=1}^{p} \left[(u)_{i,j+1} - (u)_{i,j} \right] {h'}_i(x) e_j(y), \tag{7.6a}$$
$$\frac{\partial \overline{v}}{\partial x} = \sum_{i=1}^{p} \sum_{j=1}^{p} \left[(v)_{i+1,j} - (v)_{i,j} \right] e_i(x) {h'}_j(y). \tag{7.6b}$$

This can be implemented using an incidence matrix $\mathbb{E}_\omega \boldsymbol{u}^h$, with

$$\mathbb{E}_\omega = \begin{bmatrix} (\mathbb{E}_\omega)_u & 0 \\ 0 & (\mathbb{E}_\omega)_v \end{bmatrix},$$

where, for $p = 2$,

$$(\mathbb{E}_\omega)_u = \begin{bmatrix} 1 & 0 & -1 & 0 & 0 & 0 \\ 0 & 1 & 0 & -1 & 0 & 0 \\ 0 & 0 & 1 & 0 & -1 & 0 \\ 0 & 0 & 0 & 1 & 0 & -1 \end{bmatrix}, \quad (\mathbb{E}_\omega)_v = \begin{bmatrix} 1 & -1 & 0 & 0 & 0 & 0 \\ 0 & 1 & -1 & 0 & 0 & 0 \\ 0 & 0 & 0 & 1 & -1 & 0 \\ 0 & 0 & 0 & 0 & 1 & -1 \end{bmatrix}. \tag{7.7}$$

It will be shown in Section 7.2 that for this formulation,

$$\frac{1}{2} \left[\left(\frac{\partial v}{\partial x} \right)^h (x,y) - \left(\frac{\partial u}{\partial y} \right)^h (x,y) \right] = \omega^h(x,y).$$

7.1.3. Deriving the matrices

The derivation of the mass matrix for this formulation for an orthogonal domain is very similar to the derivation in Section 6.1.5. The construction of the incidence matrix for the linear momentum equation is the same. It is noted that the right hand side contains the contributions of the shear stresses at the boundaries, which are not defined inside the elements.

What remains is the derivation of the rotation matrix, $\mathbb{R}$. This matrix forms a projection of the shear stresses, which are expresses in different basis, onto the surface basis that is dual to the basis of the rotation. If the expansion of this common projection is as usual

$$\left(\sigma_{xy} - \sigma_{yx} \right)^{(2)} (x,y) = \sum_{i=1}^{p} \sum_{j=1}^{p} \left(\sigma_{xy} - \sigma_{yx} \right)_{ij} e_i(x) e_j(y).$$

The co-chain denoting the difference of the shear stresses can be found by integration,

$$\left(\sigma_{xy}-\sigma_{yx}\right)_{ij}=\sum_{i=1}^{p}\sum_{j=1}^{p}\sum_{k=1}^{p}\sum_{l=1}^{p}\int_{\Omega}h'_i(x)h'_j(y)\left[\left(\sigma_{xy}\right)_{kl}h'_k(x)e_l(y)-\left(\sigma_{yx}\right)_{kl}e_k(x)h'_l(y)\right]\mathrm{d}x\mathrm{d}y.$$

For an orthogonal domain, the quantities $\int_{\Omega}h'_j(y)e_l(y)\mathrm{d}y=\delta_{jl}$ and $\int_{\Omega}h'_i(x)e_k(x)\mathrm{d}x=\delta_{ik}$ simplify the integral. The components of the rotation matrix $\mathbb{R}=[\mathbb{R}_{xy},\mathbb{R}_{yx}]$ are then found with

$$\left(\mathbb{R}_{xy}\right)_{ijkl}=\sum_{r=1}^{p_f}\sum_{s=1}^{p_f}h'_i(x_r)h'_j(y_s)h'_k(x_r)e_l(y_s)w_r w_s,$$
$$\left(\mathbb{R}_{yx}\right)_{ijkl}=-\sum_{r=1}^{p_f}\sum_{s=1}^{p_f}h'_i(x_r)h'_j(y_s)e_k(x_r)h'_l(y_s)w_r w_s.$$

Then, since the basis of the surface projection of the shear stress components is in the dual space of basis of the rotation, it is possible to set the shear stress components equal point-wise.

7.1.4. Deriving the contributions of boundary conditions

For the boundary conditions, a trick arising from the definition of the dual basis functions leads to the derivation of the components. The boundaries will be considered all in a similar way.

The boundary condition for σ_{xx} requires a projection of u_P on the left boundary. On the boundary, the prescribed velocity is expanded as

$$\int_{\partial\Omega}u^{\mathrm{ex}}(y)\mathrm{d}y\approx\int_{\partial\Omega}\sum_{l=1}^{p+1}(u_P)_l\,h_l(y)\mathrm{d}y.$$

Hence

$$\int_{\partial\Omega}\sum_{j=1}^{p+1}\sum_{l=1}^{p+1}(u_P)_l\,h_l(y)e'_j(y)\mathrm{d}y\approx\int_{\partial\Omega}\sum_{j=1}^{p+1}u^{\mathrm{ex}}(y)e'_j(y)\mathrm{d}y=u_{1,j}.$$

The boundary condition becomes

$$\int_{\partial\Omega_L}u_P\widetilde{\sigma}_{xx}n_x\mathrm{d}\Gamma=\int_{\partial\Omega_L}\sum_{j=1}^{p+1}\sum_{l=1}^{p+1}(\widetilde{\sigma}_{xx})_{1,l}\,u^{\mathrm{ex}}(y)e'_l(y)\mathrm{d}y=\sum_{j=1}^{p+1}\sum_{l=1}^{p+1}(\widetilde{\sigma}_{xx})_{1,l}\,u_{1,j}.$$

This holds also for the other normal stress boundary term $\int_{\partial\Omega}v_P\widetilde{\sigma}_{yy}n_y\mathrm{d}\Gamma$. For instance, the prescribed shear stress on the left and right boundary is given by

$$\int_{\partial\Omega}\widetilde{v}\left(\sigma_{xy}\right)_P n_x\mathrm{d}\Gamma=\int_{\partial\Omega}\sum_{j=1}^{p+1}\sum_{l=1}^{p+1}\widetilde{v}_{1,l}\sigma^{\mathrm{ex}}_{xy}h'_l(y)\mathrm{d}y.$$

7.1.5. Reducing the forcing function

The forcing function components need to have the same basis as the derivatives of the stresses, i. e.

$$f^h_x(x,y)=\sum_{i=1}^{p}\sum_{j=1}^{p+1}\left(f_x\right)_{i,j}e_i(x)e'_j(y),\quad f^h_y(x,y)=\sum_{i=1}^{p+1}\sum_{j=1}^{p}\left(f_y\right)_{i,j}e'_i(x)e_j(y).$$

Similarly to the boundary conditions, the degrees of freedom for the horizontal body forces can be computed using the same property of the basis functions,

$$\left(f_x\right)_{k,l}=\int_{\Omega}\sum_{i=1}^{p}\sum_{j=1}^{p+1}\left(f_x\right)_{i,j}e_i(x)e'_j(y)h'_k(x)h_l(y)\mathrm{d}x\mathrm{d}y=\int_{\Omega}f^{\mathrm{ex}}_x(x,y)h'_k(x)h_l(y)\mathrm{d}x\mathrm{d}y,$$

which can be done in the same way for the vertical body forces. It can be seen that, compared to a reduction on the primal mesh, the integration takes into account the complete basis. In contrast, for the primal mesh, the geometric integration over a predefined cell was taken.

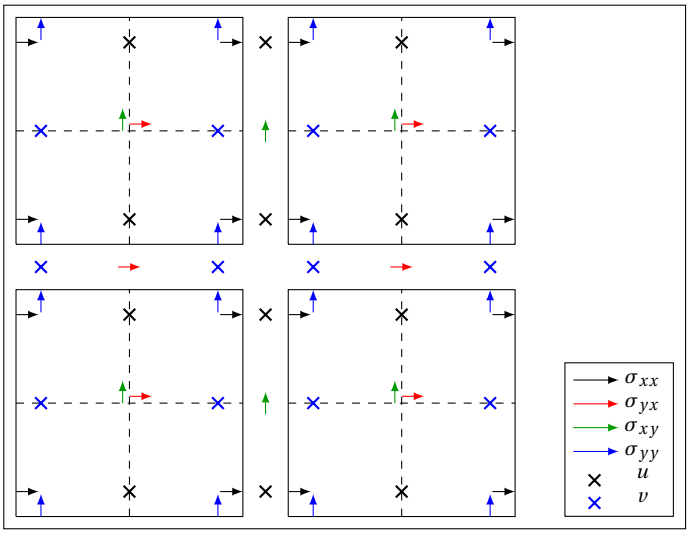

Figure 7.2: Coupling the hybrid elements of lowest order for the new mixed basis linear elasticity formulation, $K = 2$, $p = 1$.

7.1.6. Hybrid elements

Apart from placing the shear stresses in the same polynomial space, this formulation has another advantage over the previously discussed primal formulation. As mentioned before, the mimetic spectral element method can be extended to a hybrid method, that has attractive properties from a computational view. To make the elements hybrid, they are disconnected, and Lagrange multipliers between the elements constrain the values on neighbouring elements to be the same. This is shown schematically in Fig. 7.2. Since the shear stresses are discontinuous between elements, they can be constrained to be equal within the elements. This

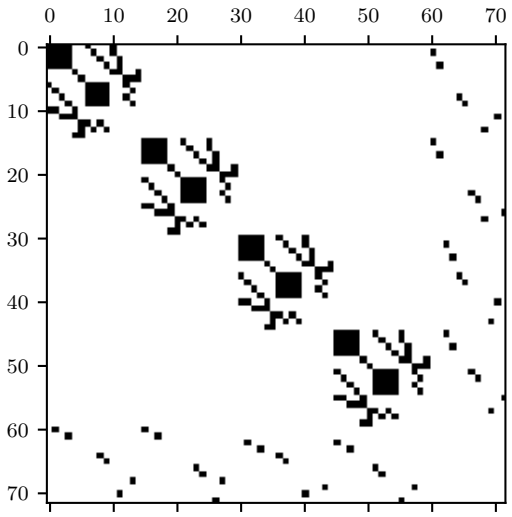

Figure 7.3: The sparsity pattern for the hybrid formulation, $K = 2$, $p = 1$

will result in a system matrix of the form

$$\begin{bmatrix} \mathbb{A} & \mathbb{B}^T \\ \mathbb{B} & 0 \end{bmatrix} \begin{bmatrix} \boldsymbol{x}^h \\ \boldsymbol{\lambda}^h \end{bmatrix} = \begin{bmatrix} \boldsymbol{f}^h \\ \boldsymbol{0} \end{bmatrix}. \tag{7.8}$$

Here, A contains the information of each element. It can be ordered in a block-diagonal matrix containing both the mass matrix and the incidence and rotation matrix. This is also shown in Fig. 7.3, where it is seen

that the elements are really disconnected in the sparsity pattern of the system matrix. Alternatively it can be ordered such that it consists of a block-diagonal of mass matrices and two off-diagonal block-diagonals of incidence and rotation matrices. This system can be solved for $\boldsymbol{\lambda}^h$ by

$$BA^{-1}B^T\boldsymbol{\lambda}^h = BA^{-1}F. \tag{7.9}$$

The system (7.9) is much smaller than the full system (7.8). Noting that A is block diagonal, the setup of a large problem would never involve the direct inversion of A. Instead, each of its blocks can be inverted in parallel separately before construction, such that A^{-1} is constructed instead of A. In the results for this formulation, the system is however directly computed since the number of degrees of freedom is low.

7.2. Results

The same manufactured solution test case will be taken as in Section 6.2.1 with the same exact solution. As discussed in Section 7.1, the displacement component u^{ex} and the shear stress σ^{ex}_{xy} are prescribed on the left and right boundary, and the displacement component v^{ex} and the shear stress σ^{ex}_{yx} are prescribed on the bottom and top boundary. In Fig. 7.4, contour plots of all solution components are shown for a coarse solution to clarify the properties of the solution. The domain is chosen as $[-1,1]^2$ to be able to distinguish more clearly the directions in which the solution components are discontinuous or not. The displacement component u is continuous between elements in y-direction but discontinuous in x-direction. Vice versa, the displacement component v is continuous between elements in x-direction but discontinuous in y-direction. The rotation and shear stresses are discontinuous between elements in both directions. This is why this formulation does allow for the hybridisation of the elements, since no constraint is posed strongly on the shear stresses in between elements. Note that the shear stress component σ_{yx} is not shown, since it is identical (up to machine precision) to σ_{xy}, which will be discussed in the following. Finally, the normal stress σ_{xx} is continuous between elements in x-direction, while the normal stress σ_{yy} is continuous between elements in y-direction.

For this formulation, the aim was to satisfy the conservation laws of linear momentum and angular momentum point-wise. In Section 6.1.1, it was shown that conservation of angular momentum is satisfied when linear momentum and the symmetry of the stress tensor are satisfied. In Fig. 7.5, contour plots of linear momentum and angular momentum conservation, as well as for the symmetry of the stress tensor and curl of the displacements is shown for the same coarse solution as the results in Fig. 7.4. The error in linear momentum and angular momentum is computed here with

$$\begin{aligned}
\epsilon_{\text{lin}} &= \left(\mathrm{d}\sigma_x^{(1)}\right)^h + f_x^h + \left(\mathrm{d}\sigma_y^{(1)}\right)^h + f_y^h, \\
\epsilon_{\text{ang}} &= -Y\left[\left(\mathrm{d}\sigma_x^{(1)}\right)^h + f_x^h\right] + X\left[\left(\mathrm{d}\sigma_y^{(1)}\right)^h + f_y^h\right] + \sigma_{xy}^h - \sigma_{yx}^h.
\end{aligned}$$

Clearly, both the errors are zero up to machine precision. Furthermore, it can be seen that the displacements and rotation are connected through a topological relation as well, as evident from the difference in curl of the displacement and the rotation. The convergence results are summarised in Fig. 7.6 and Fig. 7.8 for p- and h-convergence, respectively. The norms are given by

$$\begin{aligned}
\left\|\epsilon_{\underline{\underline{\sigma}}}\right\|_{L^2} &= \left\|\sigma_{xx}^h - \sigma_{xx}^{\text{ex}}\right\|_{L^2} + \left\|\sigma_{yx}^h - \sigma_{yx}^{\text{ex}}\right\|_{L^2} + \left\|\sigma_{xy}^h - \sigma_{xy}^{\text{ex}}\right\|_{L^2} + \left\|\sigma_{yy}^h - \sigma_{yy}^{\text{ex}}\right\|_{L^2}, \\
\|\epsilon_{\mathbf{u}}\|_{L^2} &= \left\|u^h - u^{\text{ex}}\right\|_{L^2}, \\
\|\epsilon_{\mathbf{v}}\|_{L^2} &= \left\|v^h - v^{\text{ex}}\right\|_{L^2}, \\
\|\epsilon_{\omega}\|_{L^2} &= \left\|\omega^h - \omega^{\text{ex}}\right\|_{L^2}.
\end{aligned}$$

As the mappings of this new formulation have not yet been established, only the convergence results for a non-deformed ($c = 0$) could be computed for now, where a scaling can be applied to compute on the domain $[0,1]^2$. The expected convergence is observed, where the error is close to the interpolation error for p-refinement. For h-refinement, the error clearly follows the expected slopes indicated again by the black lines. The convergence of the error is therefore both optimal for p- and h-refinement.

Furthermore the conservation of linear momentum and the symmetry of the stress tensor is shown in Fig. 7.7 and Fig. 7.9 for both refinements as well, since the values are again considered to be in the order of

machine precision error. The norms are computed as

$$\|\epsilon_{\text{lin}}\|_{L^\infty} = \max\left(\left\|\left(\mathrm{d}\sigma_x^{(1)}\right)^h + f_x^h\right\|_{L^\infty}, \left\|\left(\mathrm{d}\sigma_y^{(1)}\right)^h + f_y^h\right\|_{L^\infty}\right),$$
$$\left\|\epsilon_{\text{sym}}\right\|_{L^\infty} = \left\|\sigma_{xy}^h - \sigma_{yx}^h\right\|_{L^\infty}.$$

As shown in the contour plots, conservation of angular momentum is satisfied point-wise. This is the case because both linear momentum is point-wise conserved and the stress tensor is point-wise symmetric independent of mesh size or polynomial order. Comparing this formulation to the formulation presented in Chapter 6, in particular Fig. 7.7b to Fig. 6.4a and Fig. 7.9b to Fig. 6.4b, this formulation is capable of conserving both linear and angular momentum. Through the choice of basis for the shear stresses, symmetry of the stress tensor can be imposed strongly while conserving linear momentum as well.

7.3. Summary

This chapter introduced a new formulation for the linear elasticity problem. In this formulation, the basis is chosen as pairs of primal and dual basis functions. Furthermore, the shear stresses are prescribed between elements and weakly on the boundary, such that they are discontinuous between elements. This has the important consequence that it is now possible to connect multiple elements with the hybrid method, and still conserve linear momentum and angular momentum in each element. The possibility of hybridisation of this formulation, where the system is non-singular, leads to the great advantage of domain decomposition. After computing the interface operator, the system can be computed for each element separately in parallel. With the convergence results in this section, it is proven that this is possible, and furthermore that linear momentum and angular momentum is still conserved point-wise.

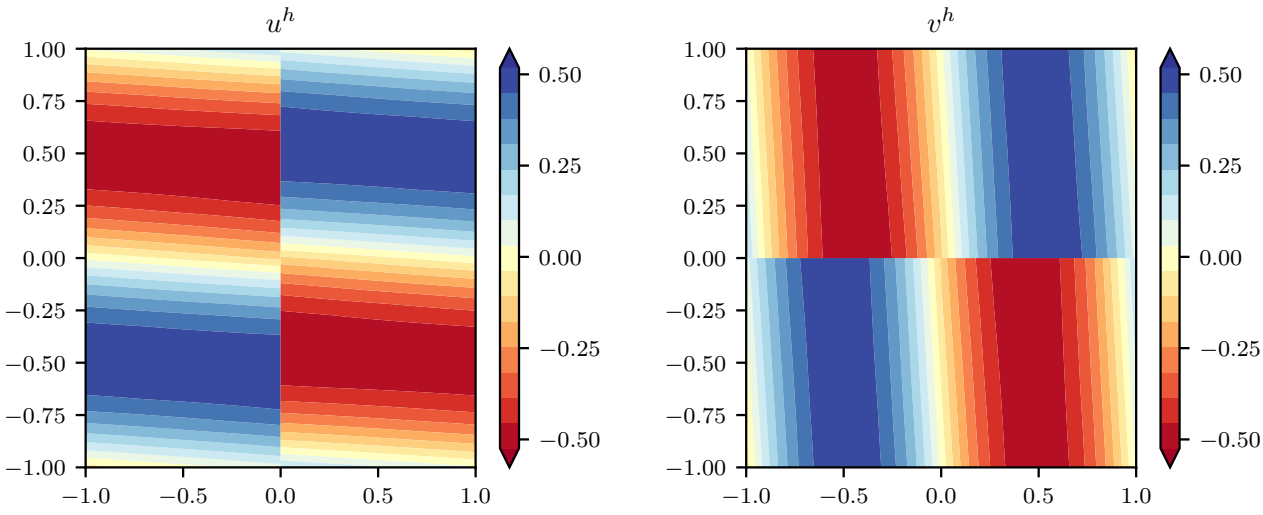

(a) Displacement component u.

(b) Displacement component v.

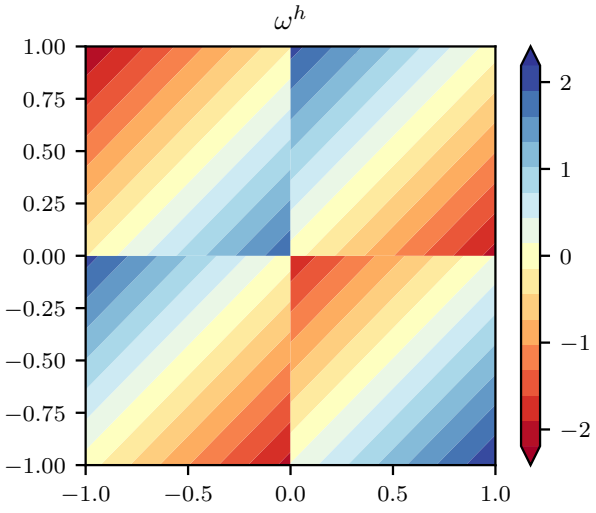

(c) Rotation ω.

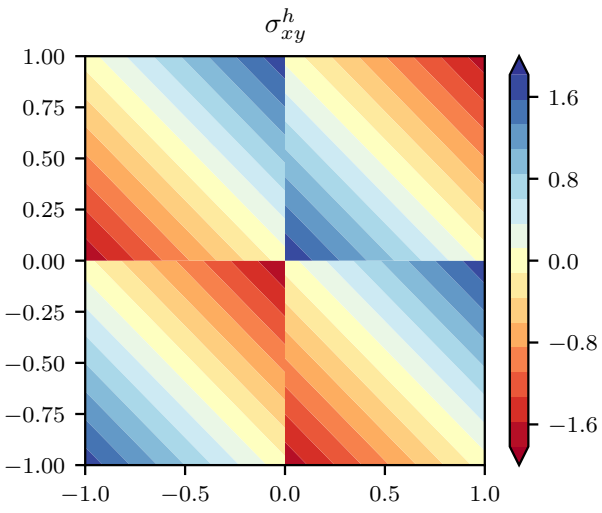

(d) Stress component σ_{xy}.

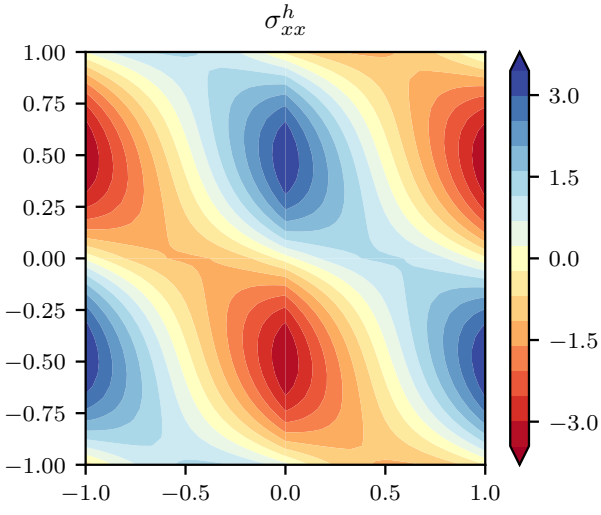

(e) Stress component σ_{xx}.

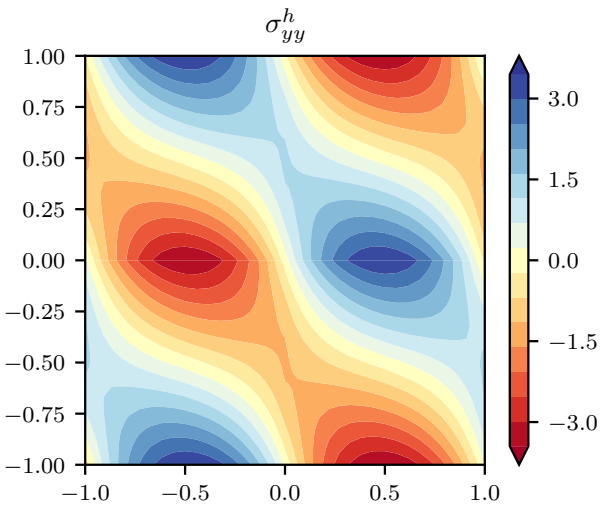

(f) Stress component σ_{yy}.

Figure 7.4: Solution components for the new elasticity formulation for $K^2 = 2^2$ elements on the domain $[-1,1]^2$, $p = 2$.

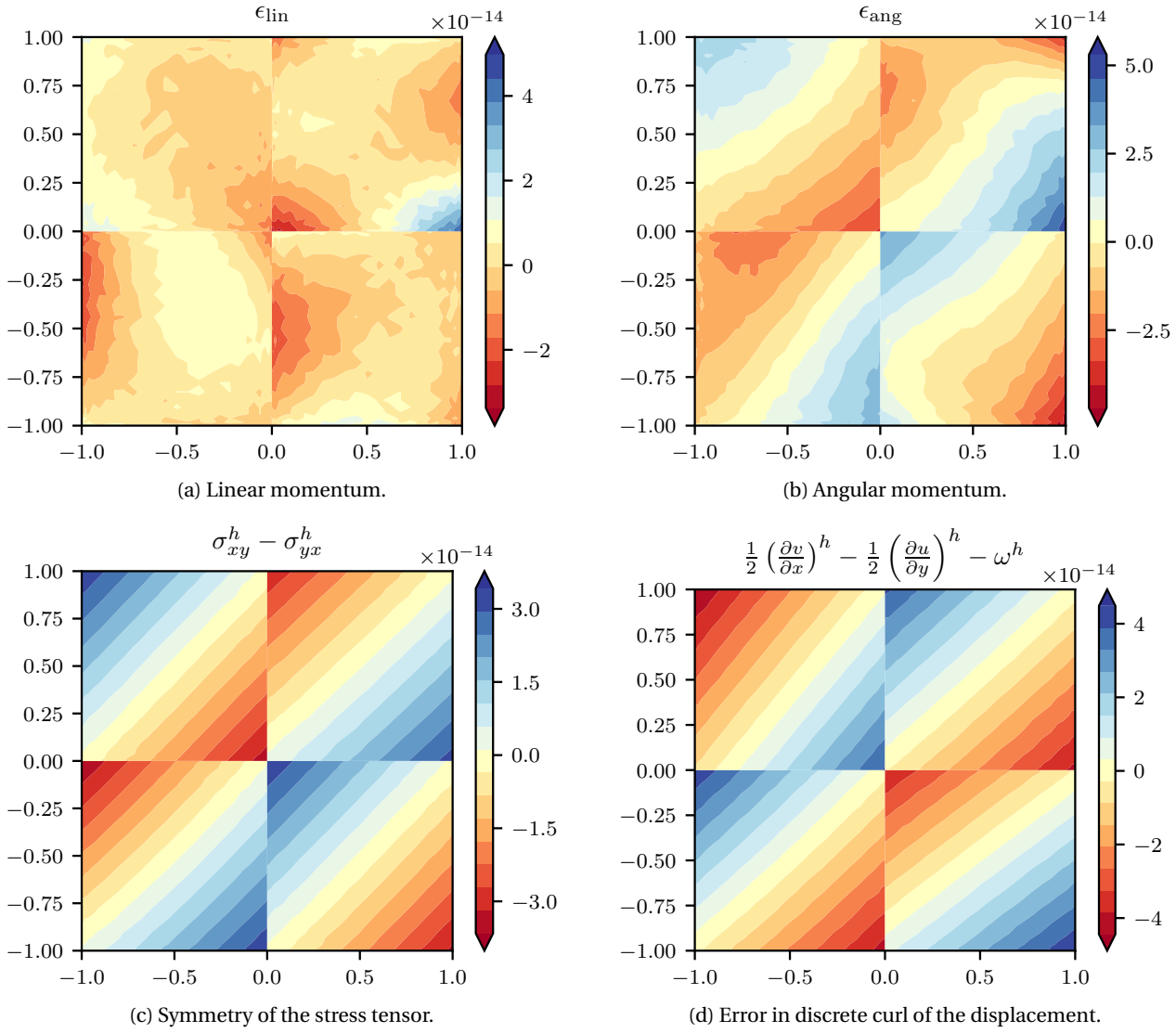

(a) Linear momentum.

(b) Angular momentum.

(c) Symmetry of the stress tensor.

(d) Error in discrete curl of the displacement.

Figure 7.5: Properties of the solution for the new elasticity formulation for $K^2 = 2^2$ elements on the domain $[-1,1]^2$, $p = 2$.

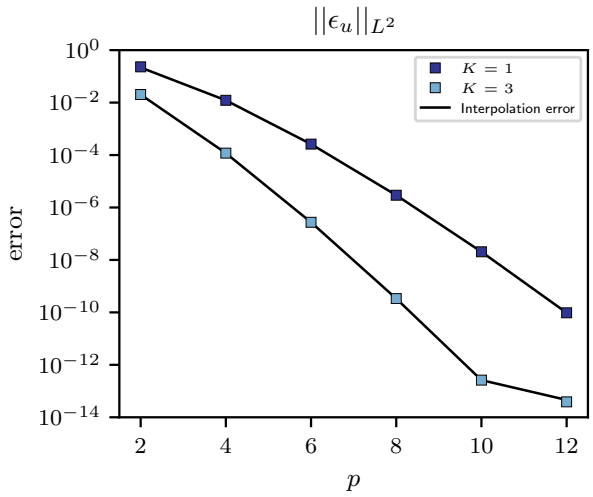

(a) Displacement in x-direction.

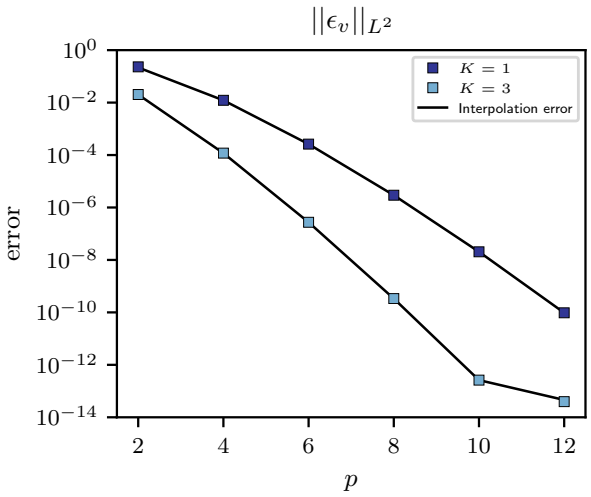

(b) Displacement in y-direction.

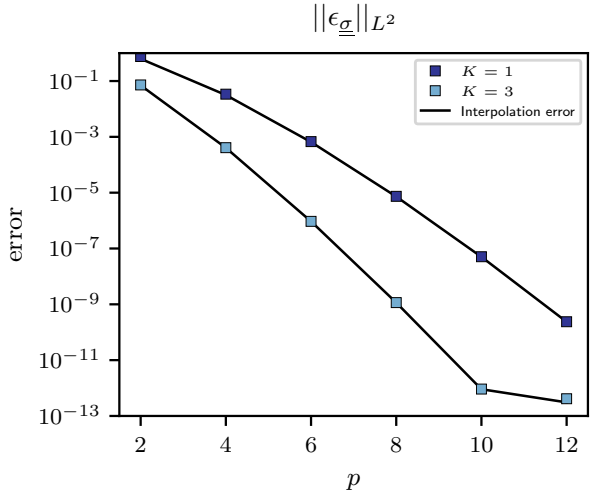

(c) All stress components.

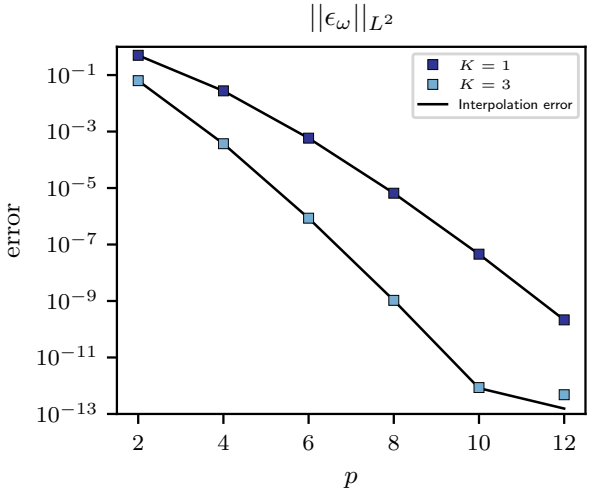

(d) Rotation.

Figure 7.6: p-convergence trends of the new formulation for the manufactured solution on the domain $[0,1]^2$.

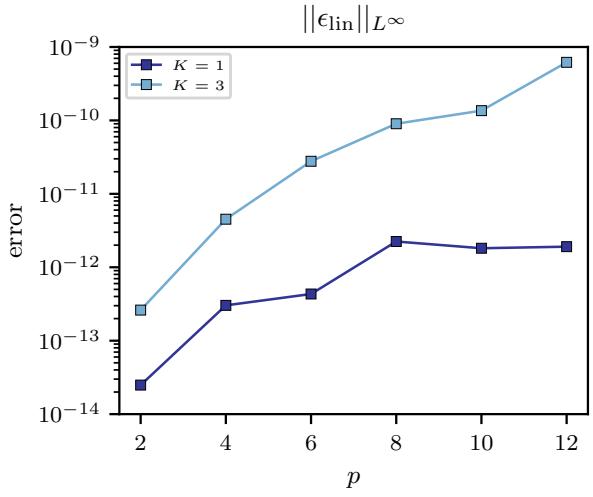

(a) Linear momentum.

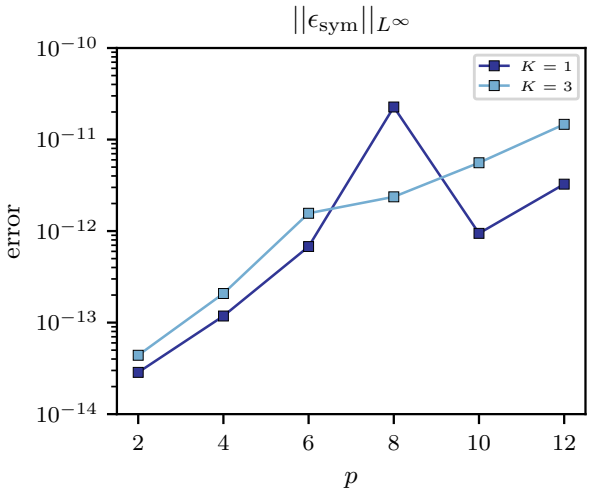

(b) Stress tensor symmetry.

Figure 7.7: Solution properties of the for the new formulation, manufactured solution on the domain $[0,1]^2$ for varying p.

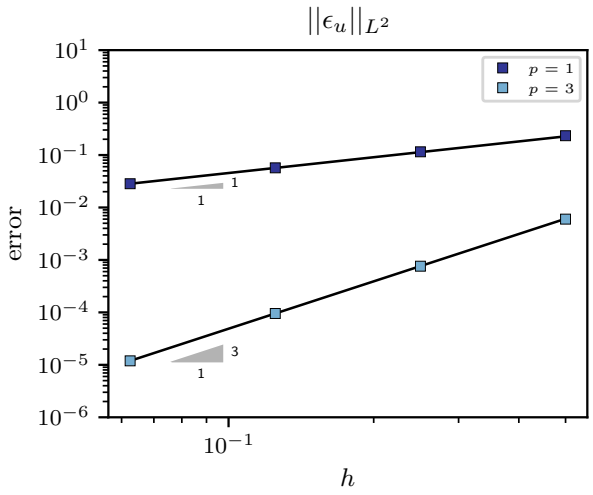

(a) Displacement in x-direction.

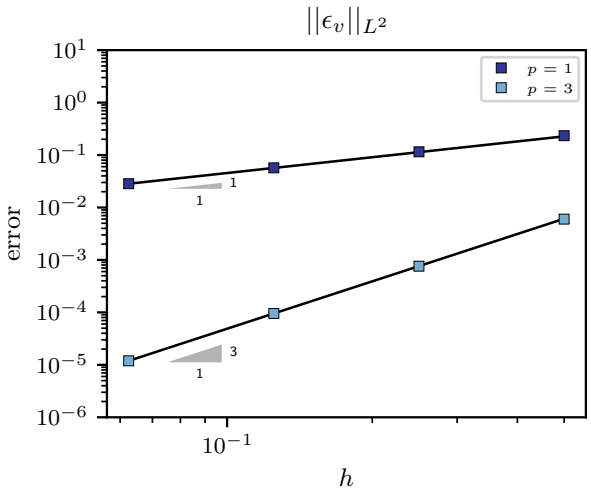

(b) Displacement in y-direction.

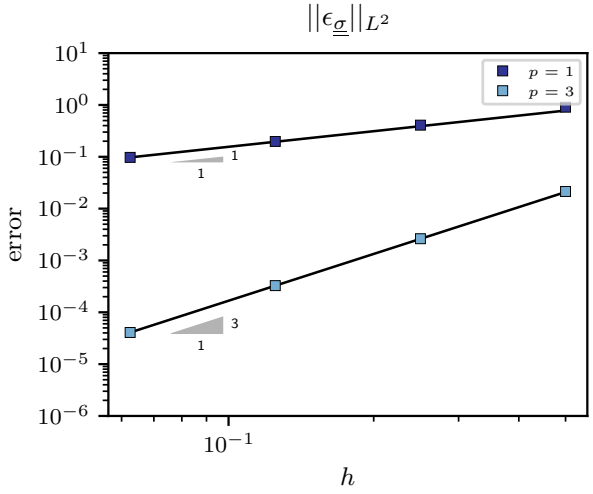

(c) All stress components.

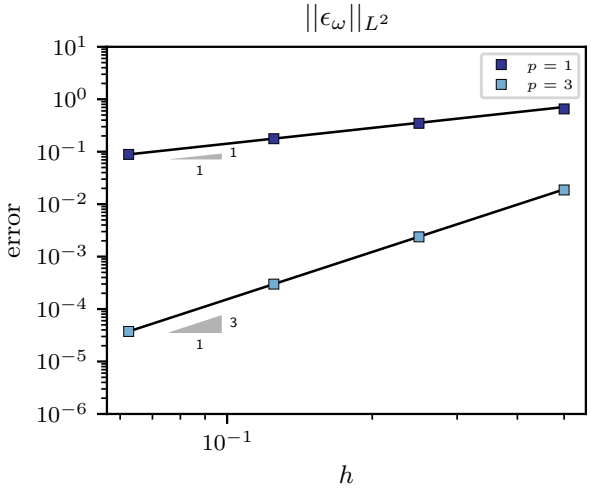

(d) Rotation.

Figure 7.8: h-convergence of the new formulation for the manufactured solution on the domain $[0,1]^2$.

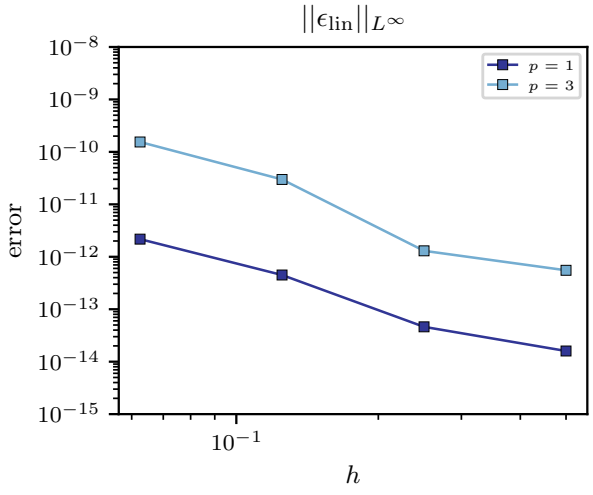

(a) Linear momentum.

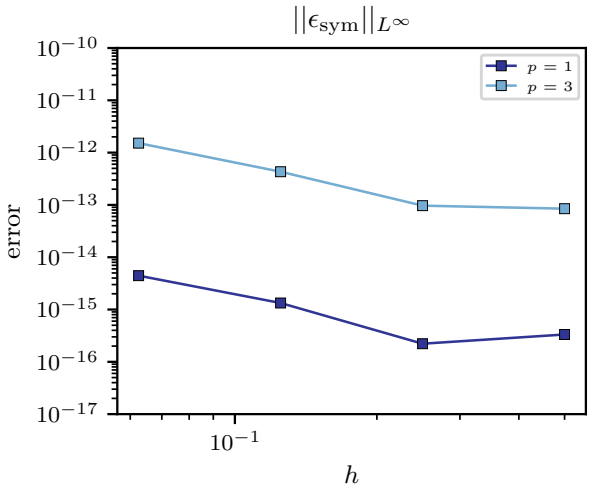

(b) Stress tensor symmetry.

Figure 7.9: Solution properties for the new formulation, manufactured solution on the domain $[0,1]^2$ for varying h.

8

Extension to Fluids

With the previously presented linear elasticity formulation, it is possible to extend the hybrid mimetic spectral element method formulation with mixed basis to fluids. This involves changing the constitutive law, such that velocities instead of displacements are computed, and introducing an extra constraint on these velocities with the pressure.

8.1. Derivation and implementation

In the following, an additional constraint to the Lagrangian formulation is considered, and the implication of the weak form will be shown. Since the formulation shares most of the terms with the new linear elasticity formulation, only the treatment of the additional terms will be discussed.

8.1.1. Lagrangian and weak formulation

The Lagrangian functional for the Stokes problem, that is, imposing linear momentum conservation, symmetry of the stress tensor, and mass conservation, can be denoted by

$$\begin{aligned}\mathcal{L}\left(\underline{\underline{\sigma}}, \mathbf{u}, \omega, p; \mathbf{f}, \mathbf{u}_P\right) = &\int_\Omega \frac{1}{2}\underline{\underline{\sigma}}^T \frac{1}{2\nu}\underline{\underline{\sigma}}\,\mathrm{d}\Omega + \int_\Omega \mathbf{u}\left(\nabla\cdot\underline{\underline{\sigma}} + \mathbf{f}\right)\mathrm{d}\Omega + \int_\Omega \omega\left(\sigma_{xy} - \sigma_{yx}\right)\mathrm{d}\Omega \\ &+ \int_\Omega p\left(\nabla\cdot\mathbf{u}\right)\mathrm{d}\Omega - \int_{\partial\Omega}\underline{\underline{\sigma}}\left(\mathbf{u}_P\cdot\mathbf{n}\right)\mathrm{d}\Gamma.\end{aligned}$$

The function spaces for the unknowns are $\underline{\underline{\sigma}} \in [H(\mathrm{div},\Omega)]^n$, $\mathbf{u} \in H(\mathrm{div},\Omega)$, $\omega, p \in L^2(\Omega)$. Note that here, $\underline{\underline{\sigma}} = 2\nu\underline{\underline{\epsilon}}$, and the compliance tensor becomes the identity tensor which is simply a scalar multiplication. Furthermore, $\mathbf{u}$ is now the velocity. Rewrite the functional again, prescribing the velocity for normal stresses and pressure, and the shear stresses for the velocity, in $\mathbb{R}^2$,

$$\begin{aligned}\mathcal{L}\left(\underline{\underline{\sigma}}, \mathbf{u}, \omega, p; \mathbf{f}, \mathbf{u}_p, \left(\sigma_{yx}\right)_P, \left(\sigma_{xy}\right)_P\right) = &\int_\Omega \frac{1}{2}\underline{\underline{\sigma}}^T \frac{1}{2\nu}\underline{\underline{\sigma}}\,\mathrm{d}\Omega + \int_\Omega u\left(\frac{\partial\sigma_{xx}}{\partial x} + f_x\right)\mathrm{d}\Omega - \int_\Omega \frac{\partial u}{\partial y}\sigma_{yx}\mathrm{d}\Omega \\ &+ \int_\Omega v\left(\frac{\partial\sigma_{yy}}{\partial y} + f_y\right)\mathrm{d}\Omega - \int_\Omega \frac{\partial v}{\partial x}\sigma_{xy}\mathrm{d}\Omega + \int_\Omega \omega\left(\sigma_{xy} - \sigma_{yx}\right)\mathrm{d}\Omega \\ &- \int_\Omega \nabla p\cdot\mathbf{u}\mathrm{d}\Omega + \int_{\partial\Omega} p, \mathbf{u}_P\cdot\mathbf{n}\mathrm{d}\Gamma \\ &+ \int_{\partial\Omega}\left[-u_P\sigma_{xx}n_x + u\left(\sigma_{yx}\right)_P n_y + v\left(\sigma_{xy}\right)_P n_x - v_P\sigma_{yy}n_y\right]\mathrm{d}\Gamma.\end{aligned} \tag{8.1}$$

Now, it is required that $\mathbf{u} \in \left[H^1(\Omega)\right]^2$ and $p \in H^1(\Omega)$. By taking variations of (8.1), the system will be in the form of

$$\begin{aligned}
\left(\underline{\underline{\widetilde{\sigma}}}, \frac{1}{2\nu}\underline{\underline{\sigma}}\right)_\Omega + \int_\Omega \left[u\frac{\partial \widetilde{\sigma}_{xx}}{\partial x} - \frac{\partial u}{\partial y}\widetilde{\sigma}_{yx} + v\frac{\partial \widetilde{\sigma}_{yy}}{\partial y} - \frac{\partial v}{\partial x}\widetilde{\sigma}_{xy}\right] \mathrm{d}\Omega + \left(\omega, \left(\widetilde{\sigma}_{xy} - \widetilde{\sigma}_{yx}\right)\right)_\Omega &= B_\sigma, \\
\int_\Omega \left[\widetilde{u}\frac{\partial \sigma_{xx}}{\partial x} - \frac{\partial \widetilde{u}}{\partial y}\sigma_{yx} + \widetilde{v}\frac{\partial \sigma_{yy}}{\partial y} - \frac{\partial \widetilde{v}}{\partial x}\sigma_{xy}\right] \mathrm{d}\Omega - \left(\widetilde{\mathbf{u}}, \nabla p\right)_\Omega &= -\left(\widetilde{\mathbf{u}}, \mathbf{f}\right)_\Omega - B_u, \\
\left(\widetilde{\omega}, \left(\sigma_{xy} - \sigma_{yx}\right)\right)_\Omega &= 0, \\
\left(\nabla \widetilde{p}, \mathbf{u}\right)_\Omega &= B_p,
\end{aligned} \tag{8.2}$$

where the boundary terms are

$$\begin{aligned}
B_\sigma &= \int_{\partial\Omega} \left[u_P \widetilde{\sigma}_{xx} n_x + v_P \widetilde{\sigma}_{yy} n_y\right] \mathrm{d}\Gamma, \\
B_u &= \int_{\partial\Omega} \left[\widetilde{u}\left(\sigma_{yx}\right)_P n_y + \widetilde{v}\left(\sigma_{xy}\right)_P n_x\right] \mathrm{d}\Gamma, \\
B_p &= \int_{\partial\Omega} \widetilde{p}, \mathbf{u}_P \cdot \mathbf{n} \mathrm{d}\Gamma.
\end{aligned}$$

This must hold $\forall \underline{\underline{\widetilde{\sigma}}} \in [H(\mathrm{div}, \Omega)]^2, \forall \widetilde{\mathbf{u}} \in \left[H^1(\Omega)\right]^2, \forall \widetilde{\omega} \in L^2(\Omega), \forall \widetilde{p} \in H^1(\Omega)$. Using integration by parts, which then leads to

$$\begin{aligned}
\left(\underline{\underline{\widetilde{\sigma}}}, \frac{1}{2\nu}\underline{\underline{\sigma}}\right)_\Omega - \left(\underline{\underline{\widetilde{\sigma}}}, \nabla \mathbf{u}\right)_\Omega + \left(\omega, \left(\widetilde{\sigma}_{xy} - \widetilde{\sigma}_{yx}\right)\right)_\Omega &= 0, \\
\left(\widetilde{\mathbf{u}}, \nabla \cdot \underline{\underline{\sigma}}\right)_\Omega - \left(\widetilde{\mathbf{u}}, \nabla p\right)_\Omega + \left(\widetilde{\mathbf{u}}, \mathbf{f}\right)_\Omega &= 0, \\
\left(\widetilde{\omega}, \left(\sigma_{xy} - \sigma_{yx}\right)\right)_\Omega &= 0, \\
\left(\widetilde{p}, \nabla \cdot \mathbf{u}\right)_\Omega &= 0.
\end{aligned}$$

Then, assuming a smooth solution, as this holds $\forall \left(\underline{\underline{\widetilde{\sigma}}}, \widetilde{\mathbf{u}}, \widetilde{\omega}, \widetilde{p}\right)$, this can be rewritten as

$$\begin{aligned}
\frac{1}{2\nu}\underline{\underline{\sigma}} = \nabla \mathbf{u} - \begin{bmatrix} 0 & \omega \\ -\omega & 0 \end{bmatrix} = \frac{1}{2}\left(\nabla \mathbf{u} + (\nabla \mathbf{u})^T\right) \qquad &\text{in } \Omega, \\
\nabla \cdot \underline{\underline{\sigma}} - \nabla p + \mathbf{f} = 0 \qquad &\text{in } \Omega, \\
\sigma_{xy} - \sigma_{yx} = 0 \qquad &\text{in } \Omega, \\
\nabla \cdot \mathbf{u} = 0 \qquad &\text{in } \Omega.
\end{aligned}$$

which express the constitutive law, conservation of linear momentum, symmetry of the stress tensor, and conservation of mass, respectively. Note that in this formulation, the viscosity ν does not have to be constant, but can vary in the domain. This is a great difference with the velocity-vorticity-pressure formulation, which is based on this assumption.

The weak form (8.2) can be discretised into a system,

$$\begin{bmatrix} \mathbb{M}_\sigma & \mathbb{E}_\sigma^T & \mathbb{R}^T & 0 \\ \mathbb{E}_\sigma & 0 & 0 & (\mathbb{P}\mathbb{E}_{\mathrm{div}\mathbf{u}})^T \\ \mathbb{R} & 0 & 0 & 0 \\ 0 & \mathbb{P}\mathbb{E}_{\mathrm{div}\mathbf{u}} & 0 & 0 \end{bmatrix} \begin{bmatrix} \boldsymbol{\sigma}^h \\ \boldsymbol{u}^h \\ \boldsymbol{\omega}^h \\ \boldsymbol{p}^h \end{bmatrix} = \begin{bmatrix} -\boldsymbol{g}_\sigma^h \\ -\boldsymbol{f}^h - \boldsymbol{g}_u^h \\ \mathbf{0} \\ \boldsymbol{g}_p^h \end{bmatrix}. \tag{8.4}$$

The matrix $\mathbb{E}_{\mathrm{div}\mathbf{u}}$ represent the discrete divergence operation, which will be shown to be topological for the expansions of the velocity components in the next section. The matrix $\mathbb{P}$ is a projection matrix used to project the expansions of the derivatives of $\mathbf{u}$ to the expansion of p. Finally, the system vector $\boldsymbol{g}_p^h$ is constructed in a similar way as $\boldsymbol{g}_\sigma^h$, only the basis changes.

8.1.2. The divergence operator

The pressure must couple the derivatives of the velocity, and its basis is therefore expanded in the primal nodal basis, i.e.

$$p^h(x,y) = \sum_{i=1}^{p+1}\sum_{j=1}^{p+1} p_{ij}\, h_i(x) h_j(y).$$

The velocity components are expanded in the same way as the new linear elasticity formulation,

$$\overline{u} = \sum_{i=1}^{p}\sum_{j=1}^{p+1} (u)_{ij}\, h'_i(x) h_j(y), \qquad \overline{v} = \sum_{i=1}^{p+1}\sum_{j=1}^{p} (v)_{ij}\, h_i(x) h'_j(y).$$

Taking the derivative, $p-1$ points can be found directly in each direction,

$$\frac{\partial \overline{u}}{\partial x} = \sum_{i=2}^{p}\sum_{j=1}^{p+1} \left[u_{i,j} - u_{i-1,j}\right] e'_i(x) h_j(y),$$
$$\frac{\partial \overline{v}}{\partial y} = \sum_{i=1}^{p+1}\sum_{j=2}^{p} \left[v_{i,j} - v_{i,j-1}\right] h_i(x) e'_j(y).$$

This leads to the incidence matrix for the internal part of the element,

$$\mathbb{E}_{\mathrm{div}\mathbf{u}} = \begin{bmatrix} (\mathbb{E}_{\mathrm{div}\mathbf{u}})_u & 0 \\ 0 & (\mathbb{E}_{\mathrm{div}\mathbf{u}})_v \end{bmatrix},$$

where, for $p = 2$,

$$(\mathbb{E}_{\mathrm{div}\mathbf{u}})_u = \begin{bmatrix} -1 & 0 & 0 & 0 & 0 & 0 \\ 1 & -1 & 0 & 0 & 0 & 0 \\ 0 & 1 & 0 & 0 & 0 & 0 \\ 0 & 0 & -1 & 0 & 0 & 0 \\ 0 & 0 & 1 & -1 & 0 & 0 \\ 0 & 0 & 0 & 1 & 0 & 0 \\ 0 & 0 & 0 & 0 & -1 & 0 \\ 0 & 0 & 0 & 0 & 1 & -1 \\ 0 & 0 & 0 & 0 & 0 & 1 \end{bmatrix}, \quad (\mathbb{E}_{\mathrm{div}\mathbf{u}})_v = \begin{bmatrix} -1 & 0 & 0 & 0 & 0 & 0 \\ 0 & -1 & 0 & 0 & 0 & 0 \\ 0 & 0 & -1 & 0 & 0 & 0 \\ 1 & 0 & 0 & -1 & 0 & 0 \\ 0 & 1 & 0 & 0 & -1 & 0 \\ 0 & 0 & 1 & 0 & 0 & -1 \\ 0 & 0 & 0 & 1 & 0 & 0 \\ 0 & 0 & 0 & 0 & 1 & 0 \\ 0 & 0 & 0 & 0 & 0 & 1 \end{bmatrix}. \tag{8.5}$$

The extra u_{ij} ((for $i = 0$, $i = p+1$) and v_{ij} (for $j = 0$, $j = p+1$) will have to be taken from the boundary. In this case, on the left and right side, another u_{ij} is found, and similarly to the top and bottom side, another v_{ij} is found. This is implemented as a boundary condition, with the term $\boldsymbol{g}_p^h$. The final expansions are then

$$\frac{\partial \overline{u}}{\partial x} = \sum_{i=1}^{p+1}\sum_{j=1}^{p+1} \left[(u)_{i,j} - (u)_{i-1,j}\right] e'_i(x) h_j(y), \tag{8.6a}$$
$$\frac{\partial \overline{v}}{\partial y} = \sum_{i=1}^{p+1}\sum_{j=1}^{p+1} \left[(v)_{i,j} - (v)_{i,j-1}\right] h_i(x) e'_j(y). \tag{8.6b}$$

Multiplication with the velocity $\boldsymbol{u}^h$ then results in two times the degrees of freedom of $\boldsymbol{p}^h$, hence this must still be projected onto the expansion of p^h. This is done in the same way as for the shear stress components and the vorticity, expanding the divergence as

$$\left[\left(\frac{\partial \overline{u}}{\partial x} + \frac{\partial \overline{v}}{\partial y}\right)'\right]^{(2)}(x,y) = \sum_{i=1}^{p+1}\sum_{j=1}^{p+1} \left(\frac{\partial \overline{u}}{\partial x} + \frac{\partial \overline{v}}{\partial y}\right)_{ij} e'_i(x) e'_j(y), \tag{8.7}$$

using the inner product definition,

$$\left(\frac{\partial \overline{u}}{\partial x} + \frac{\partial \overline{v}}{\partial y}\right)_{ij} = \sum_{i=1}^{p+1}\sum_{j=1}^{p+1}\sum_{k=1}^{p+1}\sum_{l=1}^{p+1} \int_\Omega h_i(x) h_j(y) \left[\left(u_{k,l} - u_{k-1,l}\right) e'_k(x) h_l(y) + \left(v_{k,l} - v_{k,l-1}\right) h_k(x) e'_l(y)\right] \mathrm{d}x\mathrm{d}y,$$

such that the components of $\mathbb{P} = \left[\mathbb{P}_x, \mathbb{P}_y\right]$ become

$$(\mathbb{P}_x)_{ijkl} = \sum_{r=1}^{p_f}\sum_{s=1}^{p_f} h_i(x_r)h_j(y_s)e'_k(x_r)h_l(y_s)w_r w_s,$$
$$\left(\mathbb{P}_y\right)_{ijkl} = -\sum_{r=1}^{p_f}\sum_{s=1}^{p_f} h_i(x_r)h_j(y_s)h_k(x_r)e'_l(y_s)w_r w_s.$$

A note on the boundary condition for the pressure, following the same line of thinking as in Section 7.1.4, this can be computed with

$$\int_{\partial\Omega_L} u_P \widetilde{p}\mathrm{d}\Gamma = \int_{\partial\Omega_L}\sum_{j=1}^{p+1}\sum_{l=1}^{p+1}\widetilde{p}_{1,l}u^{\mathrm{ex}}(y)h_l(y)\mathrm{d}y = \sum_{j=1}^{p+1}\sum_{l=1}^{p+1}\widetilde{p}_{1,l}u_{1,j}.$$

Note that for the computation of the divergence of the velocity, the co-chain for this is computed with $\mathbb{E}_{\mathbf{u}}\mathbf{u}^h$, where the boundary values need to be introduced as well, which are for the expansion of the components of the divergence of $\mathbf{u}$ computed in the same way as for $\mathbf{g}_\sigma$. These are then expanded with the basis from (8.6a) and (8.6b), respectively. In case of multiple elements, the velocity component part of the result of $B^T\boldsymbol{\lambda}^h$ from (7.8) must be added to the boundary term (acting as the boundary components for neighbouring elements), this part is expanded as in (8.7).

8.1.3. Hybrid elements

The same configuration for the hybrid elements as shown in Fig. 7.2 is used. The only difference is that the pressure is coupled as well by the interface operator, with the same Lagrange multiplier that couples the normal stresses. This relation is given, for instance coupling the left and right normal stress, by

$$-p_{\mathrm{proj}} + \sigma_{xx}\big|_L = -p_{\mathrm{proj}} + \sigma_{xx}\big|_R. \tag{8.8}$$

Since the pressure is expanded with a different basis than the normal stresses, a projection is needed at the interface. This projection is performed by a one-dimensional mass matrix, for instance for the left side,

$$\left(p_{\mathrm{proj}}\right)_{p+1,l} = p_{p+1,j}\left(M^{(0)}_{1D}\right)_{jl}.$$

8.2. Results

The extended new formulation has been implemented as well, and tested with the same manufactured solution test case from Section 5.2.1. The pressure p^{ex} and velocity components u^{ex} and v^{ex} are again taken from (5.16a), (5.16b), and (5.16c), respectively. Furthermore, ω^{ex} here is defined in the same way as rotation,

$$\omega^{\mathrm{ex}}(x,y) = \frac{1}{2}\left(\frac{\partial v^{\mathrm{ex}}(x,y)}{\partial x} - \frac{\partial u^{\mathrm{ex}}(x,y)}{\partial y}\right),$$

which is half the vorticity as used in Section 5.2. To allow for a varying ν, the forcing function can then be expressed as

$$f_x^{\mathrm{ex}}(x,y) = \frac{\partial p^{\mathrm{ex}}(x,y)}{\partial x} + \frac{\partial\left(\nu(x,y)\omega^{\mathrm{ex}}(x,y)\right)}{\partial y},$$
$$f_y^{\mathrm{ex}}(x,y) = \frac{\partial p^{\mathrm{ex}}(x,y)}{\partial y} - \frac{\partial\left(\nu(x,y)\omega^{\mathrm{ex}}(x,y)\right)}{\partial x}.$$

The components for the exact solution of $\underline{\underline{\epsilon}}^{\mathrm{ex}}$ follow directly from the derivatives of u^{ex} and v^{ex}, and similarly, $\underline{\underline{\sigma}}^{\mathrm{ex}} = 2\nu(x,y)\underline{\underline{\epsilon}}^{\mathrm{ex}}$, i.e.

$$\underline{\underline{\epsilon}} = \frac{1}{2}\begin{bmatrix} 2\frac{\partial u^{\mathrm{ex}}(x,y)}{\partial x} & \frac{\partial u^{\mathrm{ex}}(x,y)}{\partial y} + \frac{\partial v^{\mathrm{ex}}(x,y)}{\partial x} \\ \frac{\partial v^{\mathrm{ex}}(x,y)}{\partial x} + \frac{\partial u^{\mathrm{ex}}(x,y)}{\partial y} & 2\frac{\partial v^{\mathrm{ex}}(x,y)}{\partial y}\end{bmatrix}, \qquad \underline{\underline{\sigma}}^{\mathrm{ex}} = \begin{bmatrix} 2\nu(x,y)\epsilon^{\mathrm{ex}}_{xx} & 2\nu(x,y)\epsilon^{\mathrm{ex}}_{yx} \\ 2\nu(x,y)\epsilon^{\mathrm{ex}}_{xy} & 2\nu(x,y)\epsilon^{\mathrm{ex}}_{yy}\end{bmatrix}.$$

In the results, $\nu = 1$ is used. The velocity component u^{ex} and the shear stress $\sigma^{\mathrm{ex}}_{xy}$ are prescribed on the left and right boundary, and the velocity component v^{ex} and the shear stress $\sigma^{\mathrm{ex}}_{yx}$ are prescribed on the bottom

and top boundary. The contour plots for this solution on the domain $[0,1]^2$ are shown in Fig. 8.1 and Fig. 8.2 for the same order solution, $K = 2$ and $p = 2$ as used before in Fig. 7.4. In this formulation, the solution for the velocity, vorticity, and stresses is discontinuous between elements in the same way as discussed in Section 7.2. The pressure is in addition discontinuous between elements in both directions. From Fig. 8.2e, it is clear that even in a very low resolution case, the stress tensor is symmetric point-wise. In addition, Fig. 8.2c shows that linear momentum is satisfied point-wise, which leads to the fact that also angular momentum is point-wise satisfied, seen in Fig. 8.2d. Finally, this solution conserves mass strongly point-wise, evident from Fig. 8.2b.

The conserved relations for both p- and h-refinement are shown in Fig. 8.3. What was seen in the low resolution case is again confirmed, as Fig. 8.3 shows that linear momentum, angular momentum, and mass conservation are point-wise satisfied, evident from the maximum error made in all the cases. The norms computed in the same way as in Section 7.2, only the mass conservation norm is new,

$$\|\epsilon_{\text{mass}}\|_{L^\infty} = \left\| (\text{div}\mathbf{u})^h \right\|_{L^\infty}.$$

where the co-chain of $(\text{div}\mathbf{u})^h$ is computed as explained in Section 8.1.2.

The convergence results are given in Fig. 8.4 and Fig. 8.5. The p-convergence for the velocity and vorticity is optimal, evident from the proximity in value to the interpolation error. For $K \leq 2$, the p-convergence of the stress and pressure follows the interpolation error as well, however, increasing the number of elements to $K > 2$ leads to unexpected high errors. This is also seen clearly in the h- convergence plots, which are sub-optimal for the pressure and stress. This can be attributed to the fact that the relation (8.8) only determines up to a constant, hence it is possible that an additional constraint is needed to set the correct relative value. To further show this interaction, the contour plots of the solution for this test case are compared. The resolutions are a low number of elements of higher order, $K = 2$ and $p = 5$, a higher number of elements of lower order, $K = 5$ and $p = 2$, and a higher number of elements of higher order, $K = 5$ and $p = 5$. The results for the velocity components are compared in Fig. 8.6, for the vorticity and pressure in Fig. 8.7, for the normal stress components in Fig. 8.8, and for the shear stress components in Fig. 8.9. The velocity components and vorticity show expected results for both refinement in K and in p. However, it can be seen that refinement in K while keeping $p = 2$ shows many oscillations in the solution of the pressure and normal stress components. The shear stress components, which should be zero in this case, also contain some of these oscillations. From Fig. 8.2, it was made clear that force equilibrium is maintained, such that only the distribution over the pressure and stress may vary. When refining p, by comparing the last two cases, the oscillations vanish.

8.3. Summary

In this chapter, the constraint of mass conservation was added to the Lagrangian formulation for the new linear elasticity formulation, such that an additional unknown, the pressure, is solved for. The formulation is in addition shown to be hybridisable, with the same setup as for the new linear elasticity formulation. For any number of elements and polynomial order of the solution, linear momentum, angular momentum, and mass conservation is satisfied point-wise by the solution. It also shows good results for the velocity and vorticity. However, due to the simultaneous coupling of the normal stresses and the pressure with the same interface variable, this relation is possibly not represented well in case $K > 2$, which needs to be addressed in future work.

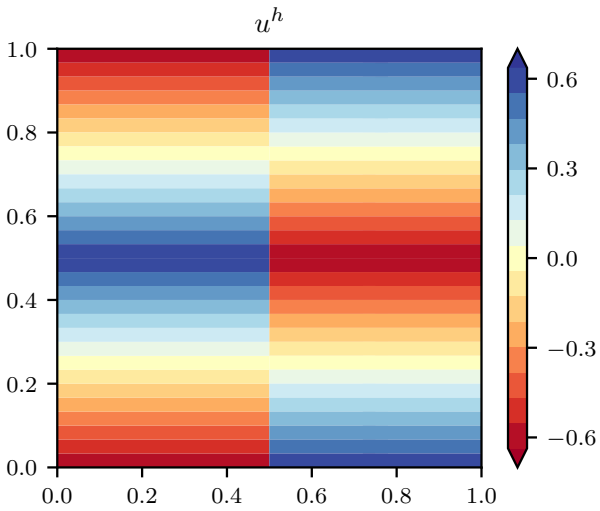

(a) Velocity component u.

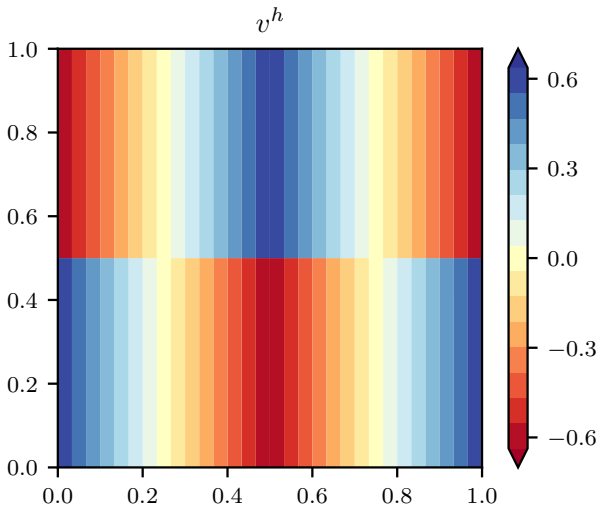

(b) Velocity component v.

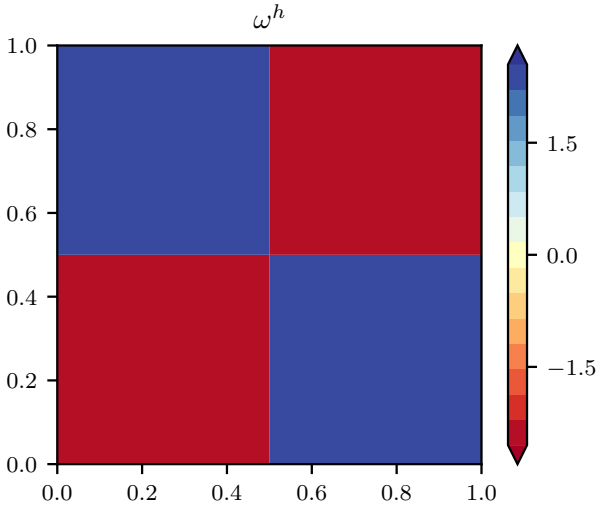

(c) Vorticity ω.

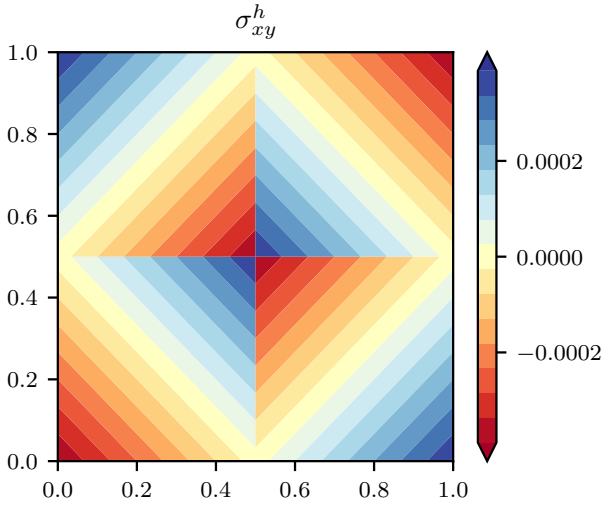

(d) Stress component σ_{xy}.

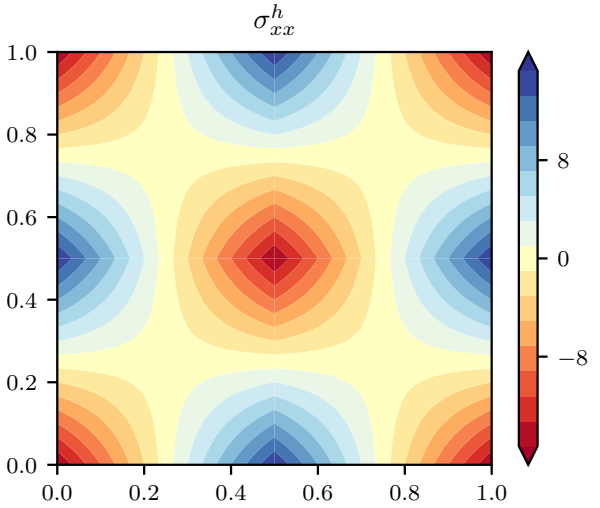

(e) Stress component σ_{xx}.

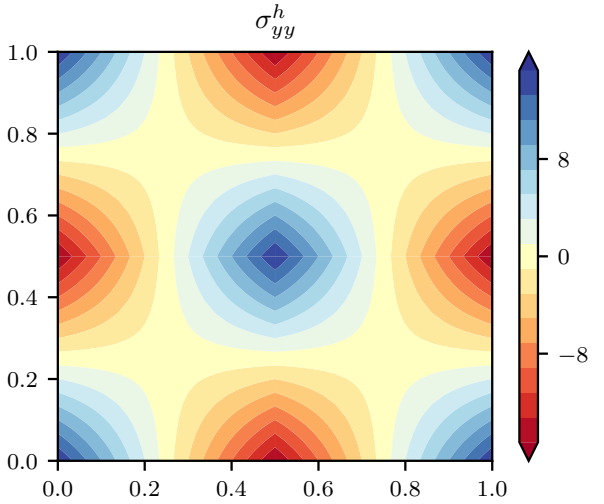

(f) Stress component σ_{yy}.

Figure 8.1: Contour plots for the new Stokes formulation with $K^2 = 2^2$ elements ($c = 0.0$) for the manufactured solution on the domain $[0,1]^2$, $p = 2$.

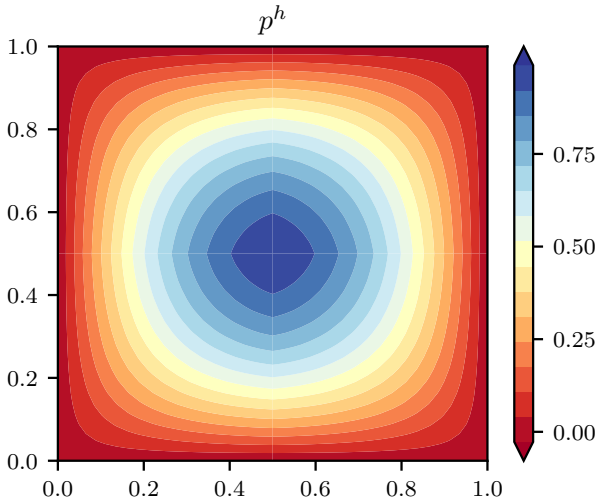

(a) Pressure p.

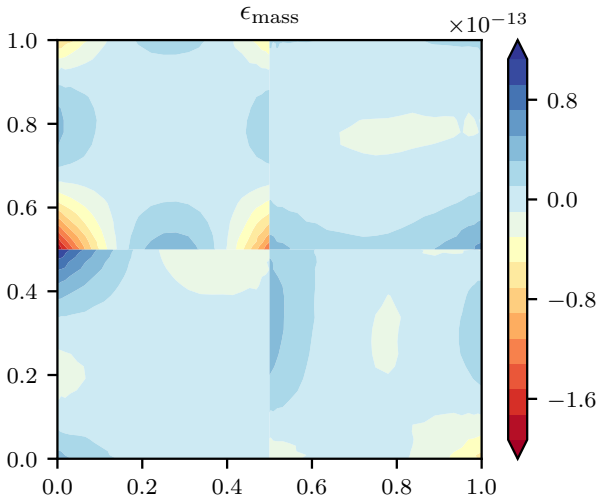

(b) Mass conservation.

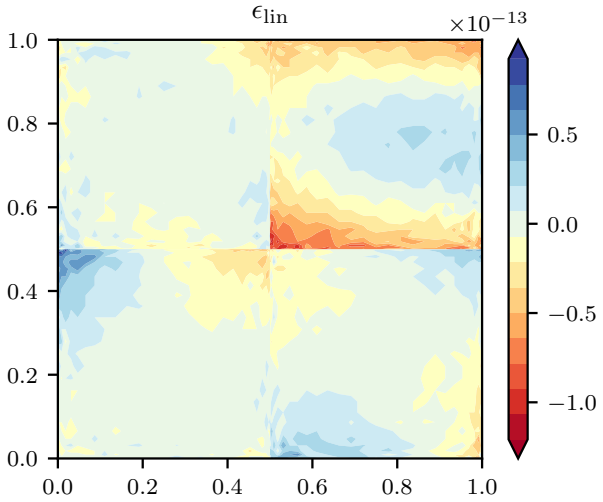

(c) Linear momentum.

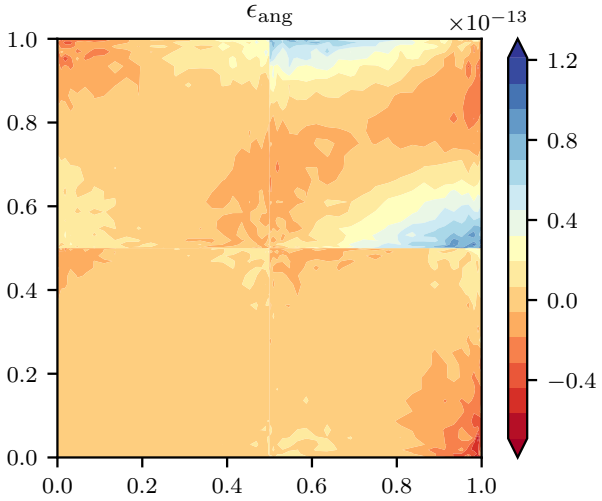

(d) Angular momentum.

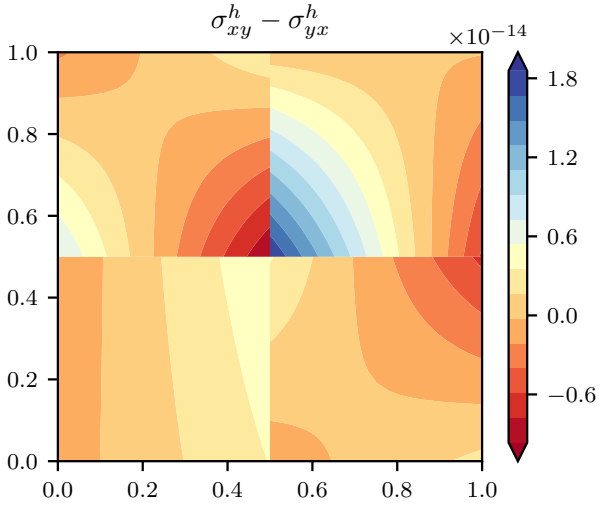

(e) Symmetry of the stress tensor.

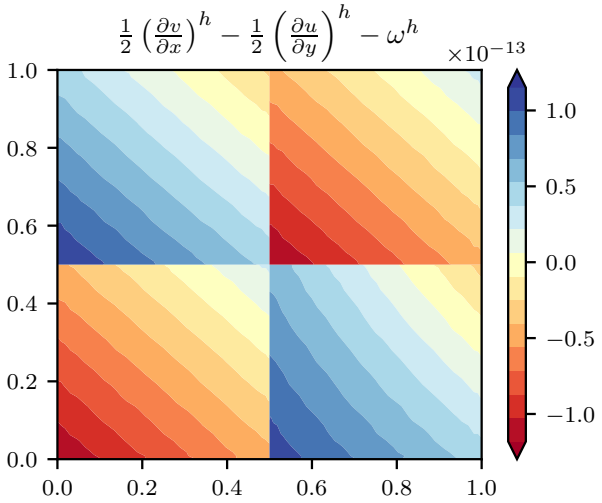

(f) Discrete curl of the displacement.

Figure 8.2: Second part of contour plots for the new Stokes formulation with $K^2 = 2^2$ elements ($c = 0.0$) for the manufactured solution on the domain $[0,1]^2$, $p = 2$.

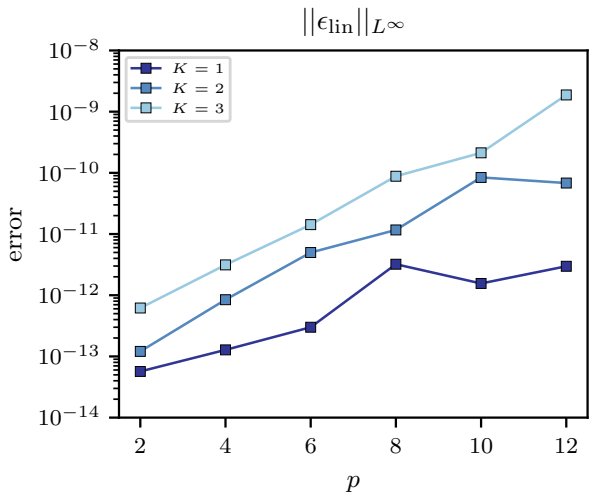

(a) Linear momentum for varying p.

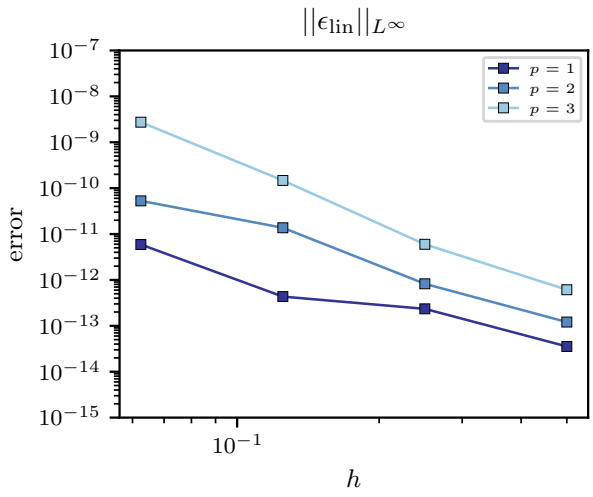

(b) Linear momentum for varying h.

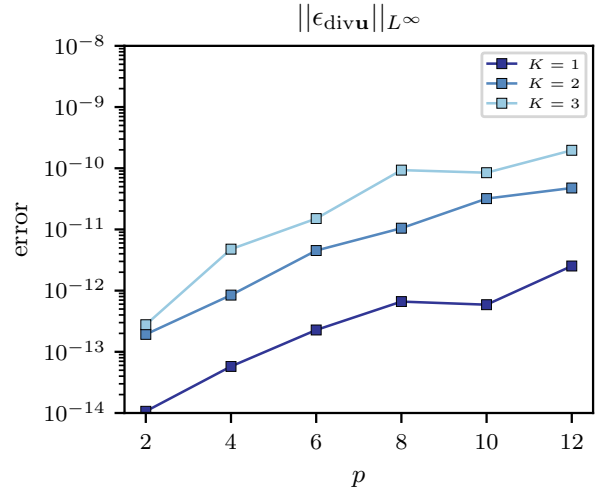

(c) Mass conservation for varying p.

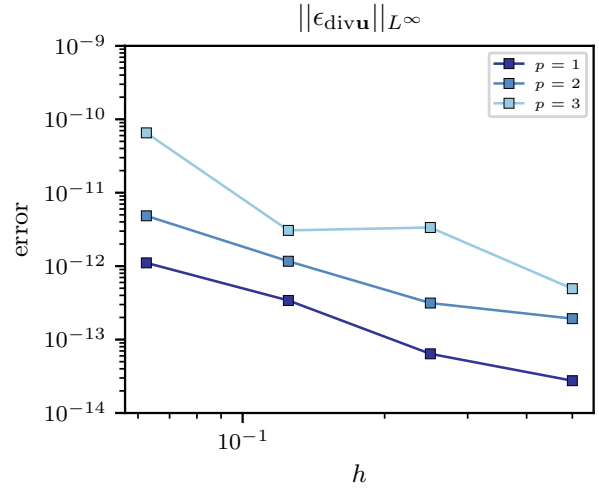

(d) Mass conservation for varying h.

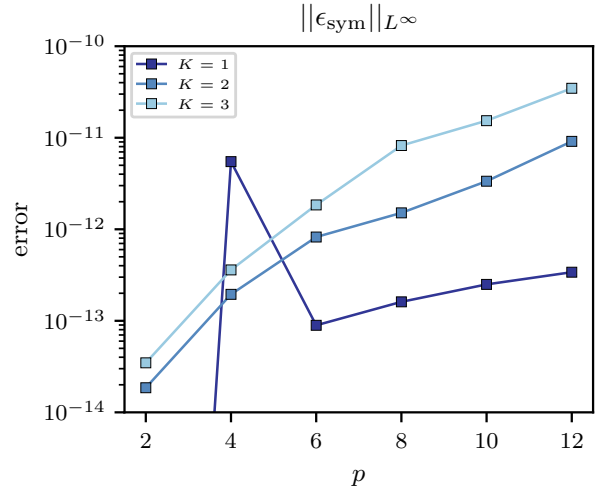

(e) Stress tensor symmetry for varying p.

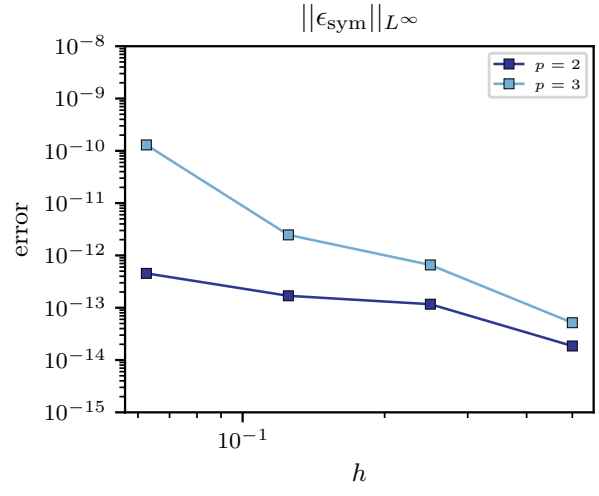

(f) Stress tensor symmetry for varying h.

Figure 8.3: Properties of the solution for new Stokes formulation, for the manufactured solution on the domain $[0,1]^2$ for varying p and h, $c = 0$.

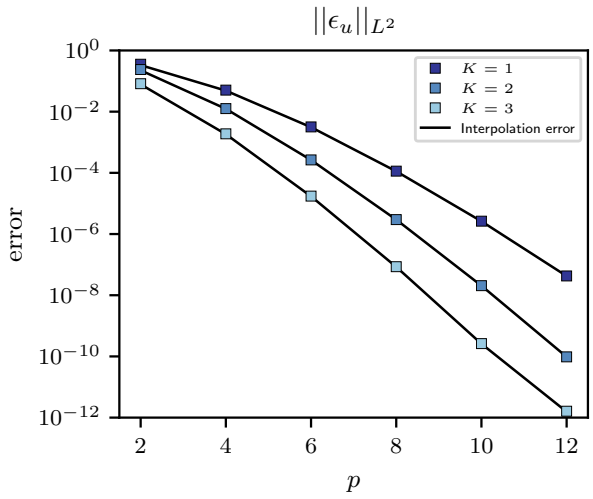

(a) Velocity in x-direction.

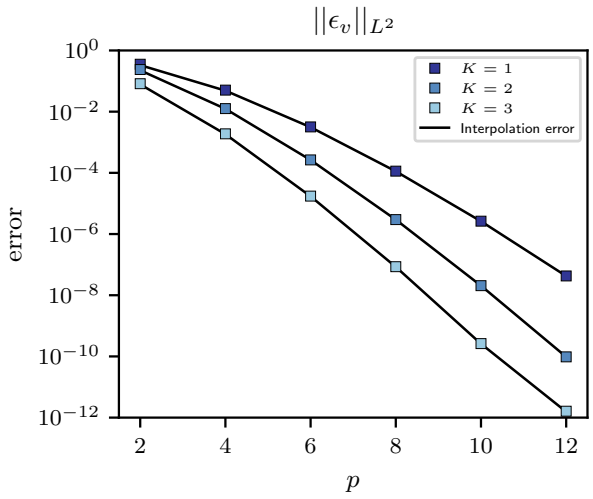

(b) Velocity in y-direction.

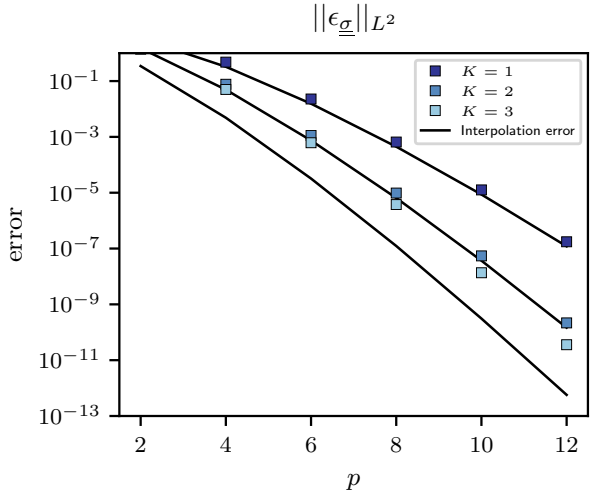

(c) All stress components.

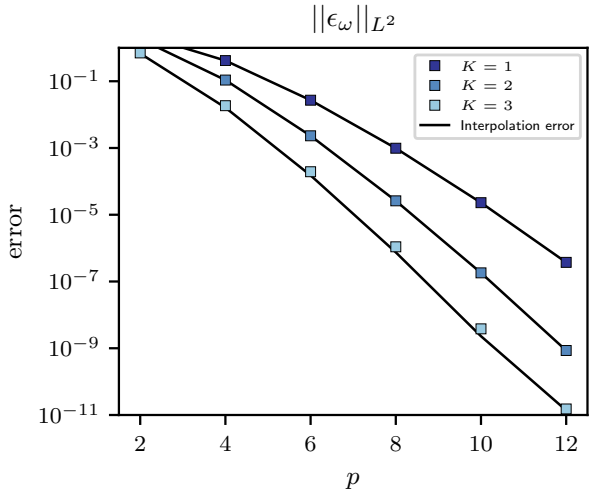

(d) Vorticity.

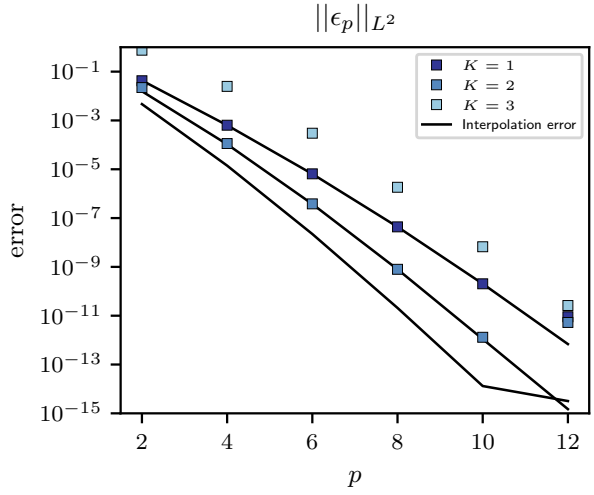

(e) Pressure.

Figure 8.4: p-convergence trends of the new Stokes formulation for the manufactured solution on the domain $[0,1]^2$, $c = 0$.

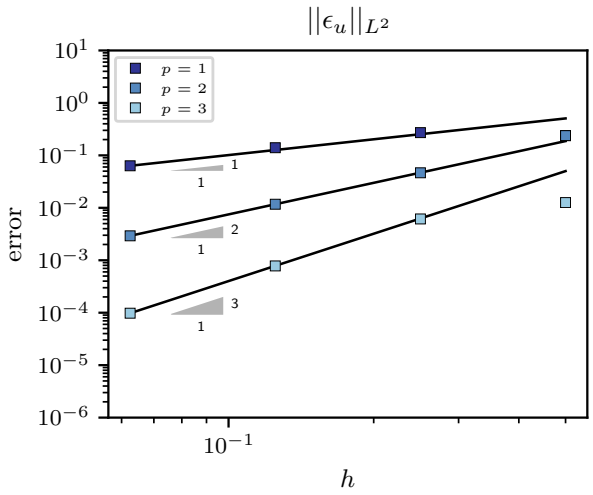

(a) Velocity in x-direction.

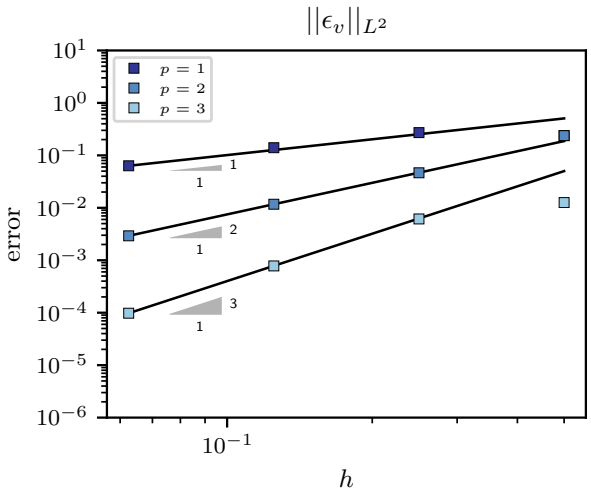

(b) Velocity in y-direction.

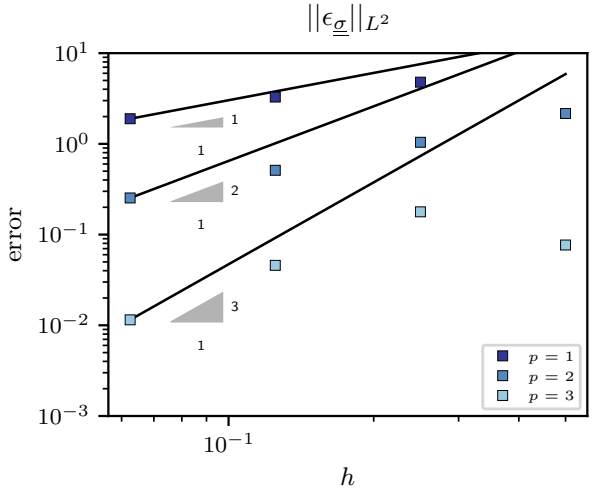

(c) All stress components.

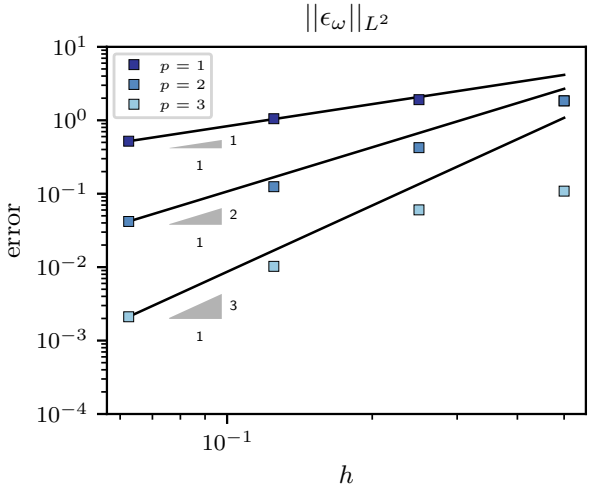

(d) Vorticity.

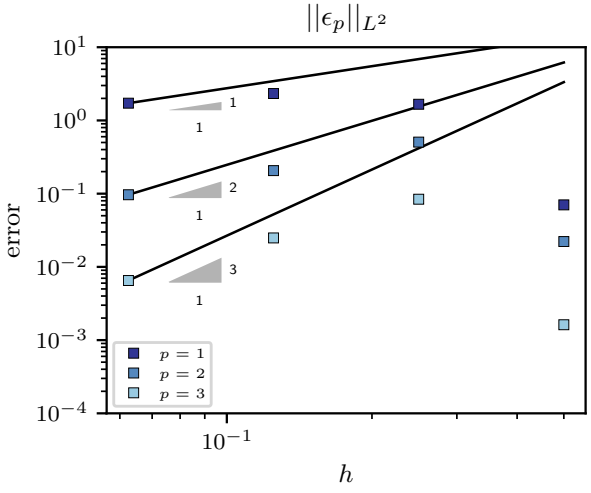

(e) Pressure.

Figure 8.5: h-convergence trends of the new Stokes formulation for the manufactured solution on the domain $[0,1]^2$, $c = 0$.

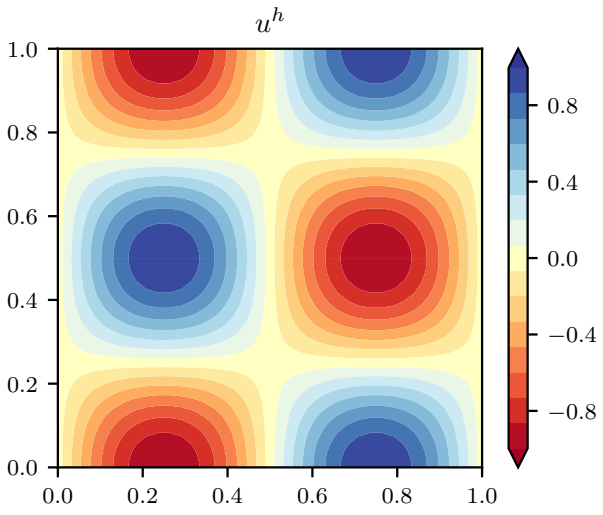

(a) Velocity component u, $K = 2$, $p = 5$.

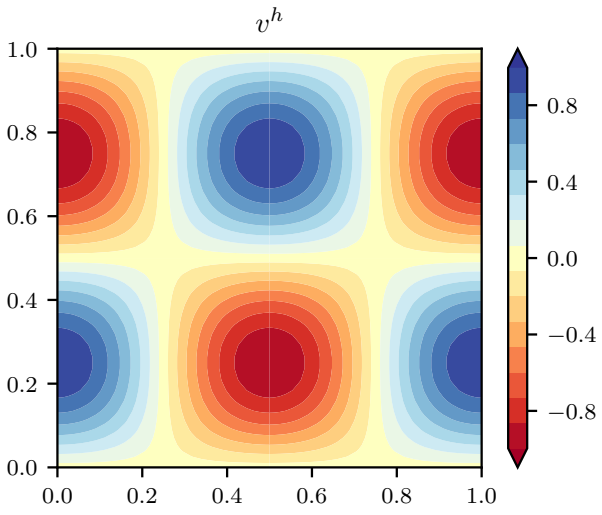

(b) Velocity component v, $K = 2$, $p = 5$.

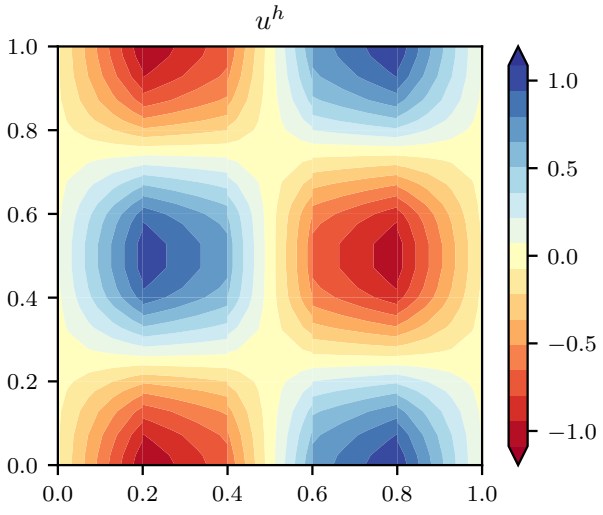

(c) Velocity component u, $K = 5$, $p = 2$.

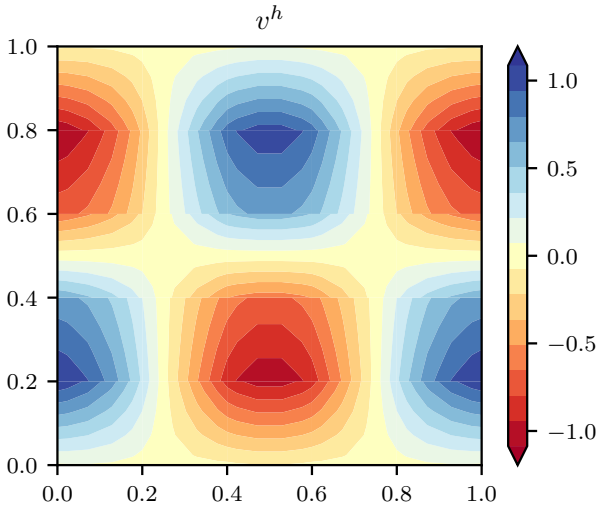

(d) Velocity component v, $K = 5$, $p = 2$.

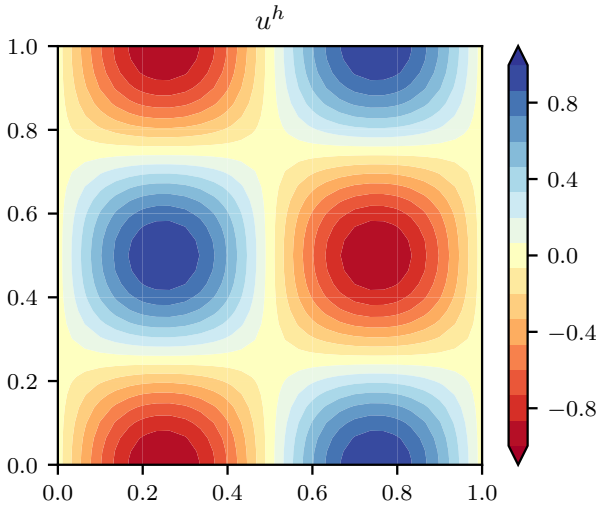

(e) Velocity component u, $K = 5$, $p = 5$.

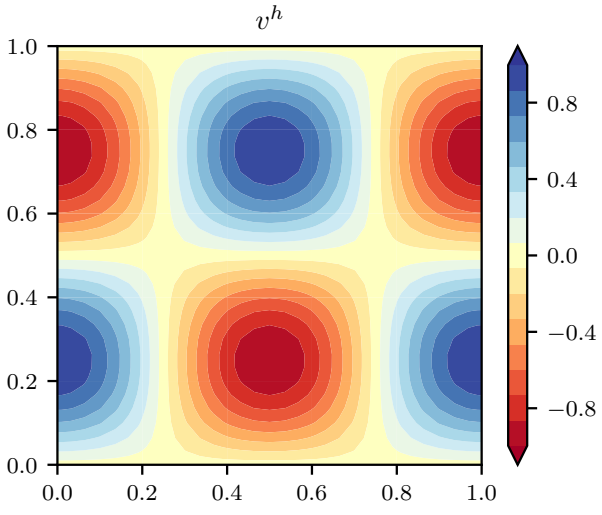

(f) Velocity component v, $K = 5$, $p = 5$.

Figure 8.6: Comparison of velocity components for the manufactured solution ($c = 0$) on the domain $[0,1]^2$.

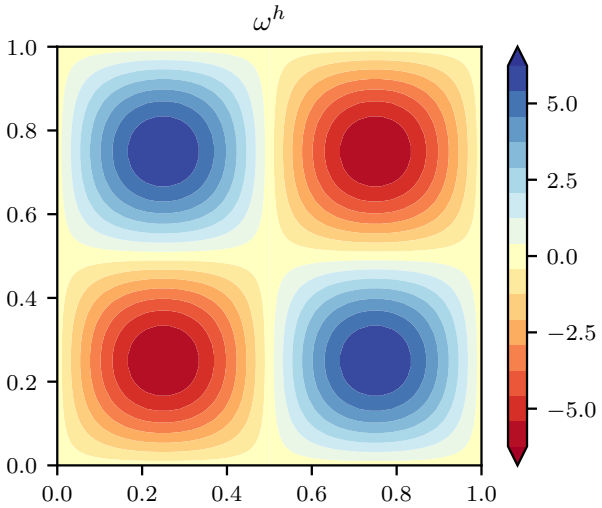

(a) Vorticity ω, $K = 2$, $p = 5$.

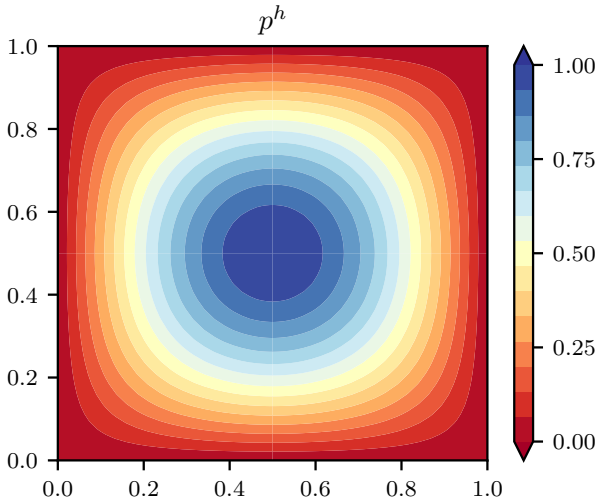

(b) Pressure p, $K = 2$, $p = 5$.

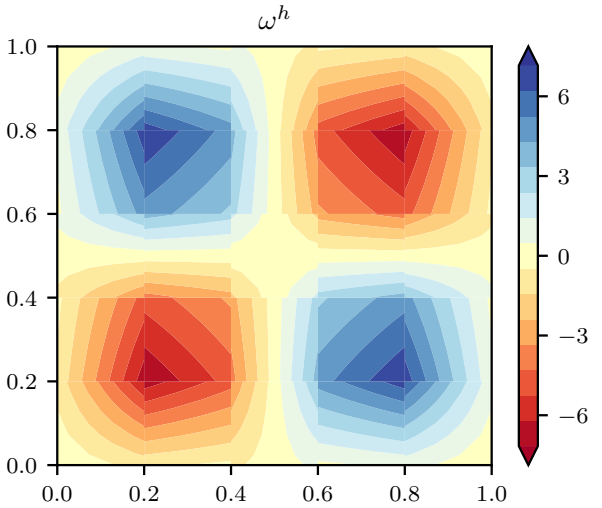

(c) Vorticity ω, $K = 5$, $p = 2$.

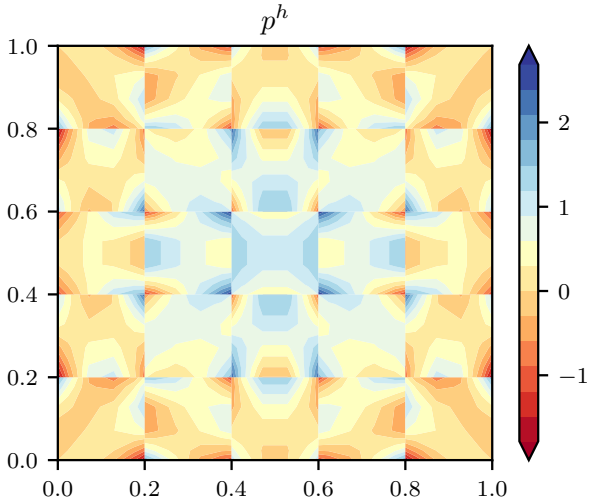

(d) Pressure p, $K = 5$, $p = 2$.

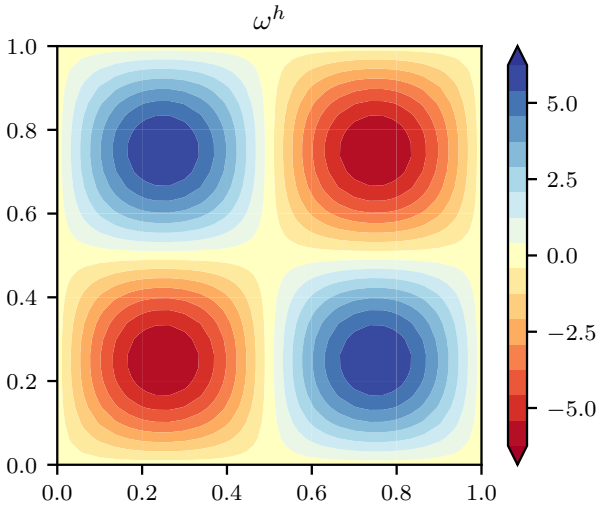

(e) Vorticity ω, $K = 5$, $p = 5$.

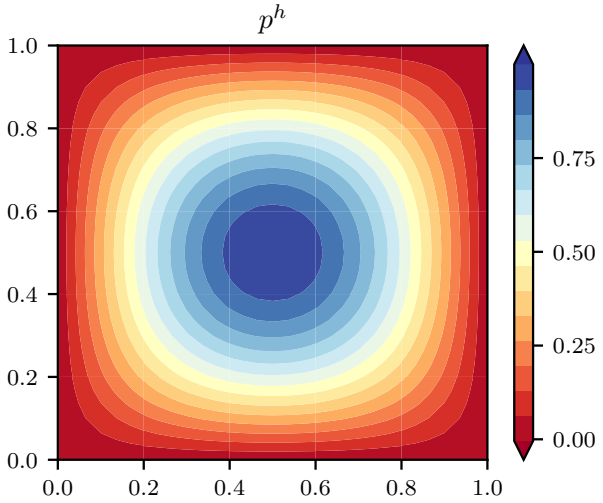

(f) Pressure p, $K = 5$, $p = 5$.

Figure 8.7: Comparison of vorticity and pressure for the manufactured solution ($c = 0$) on the domain $[0,1]^2$.

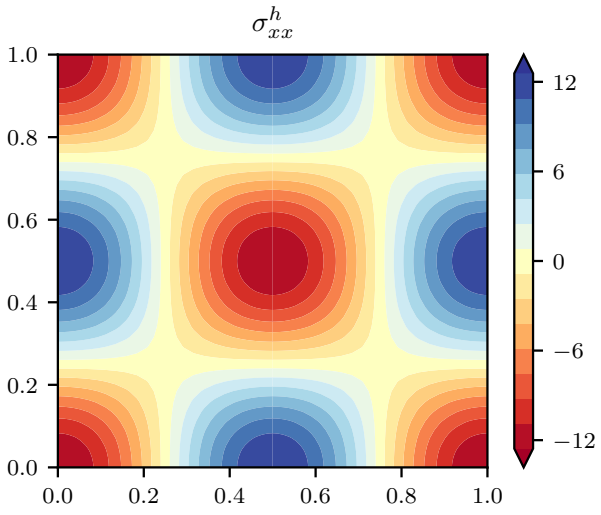

(a) Stress component σ_{xx}, $K = 2$, $p = 5$.

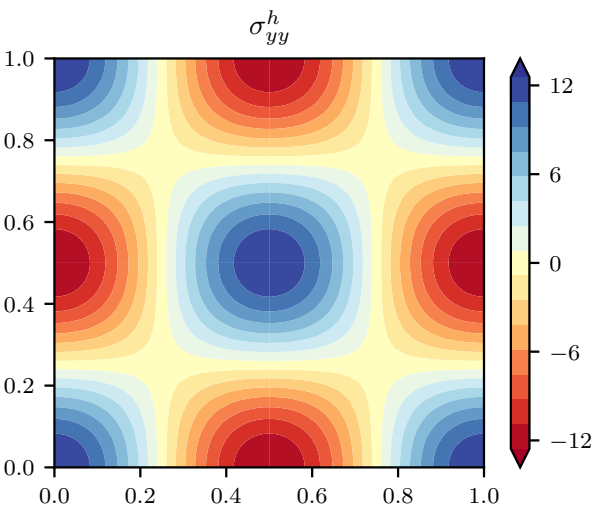

(b) Stress component σ_{yy}, $K = 2$, $p = 5$.

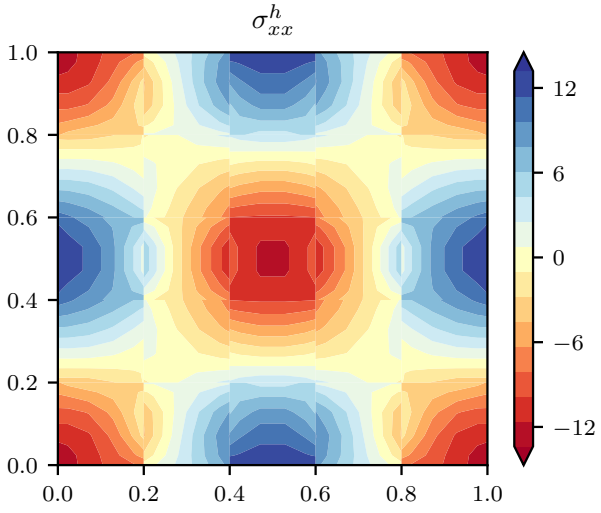

(c) Stress component σ_{xx}, $K = 5$, $p = 2$.

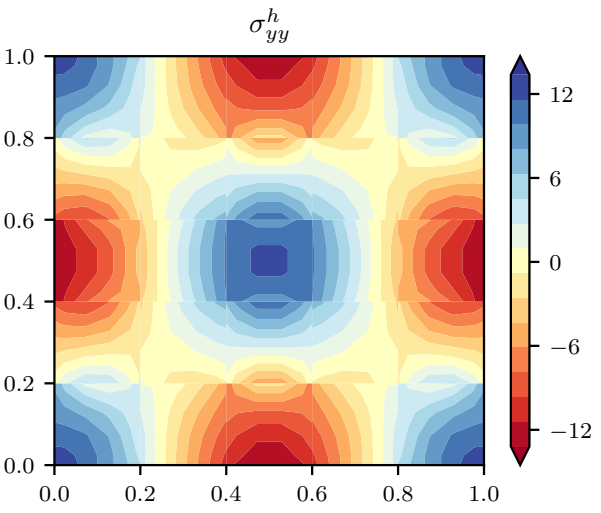

(d) Stress component σ_{yy}, $K = 5$, $p = 2$.

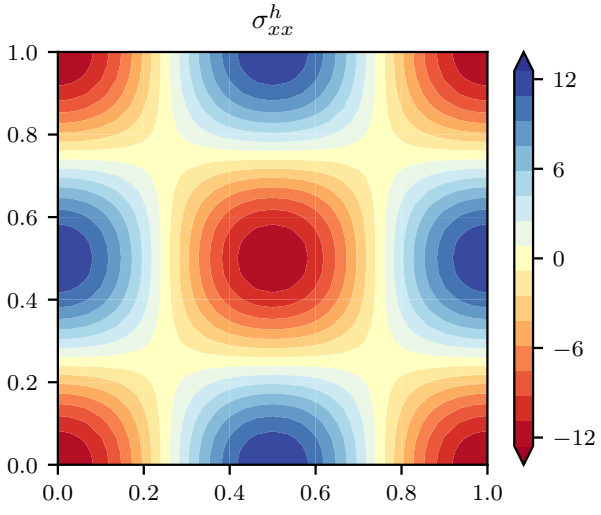

(e) Stress component σ_{xx}, $K = 5$, $p = 5$.

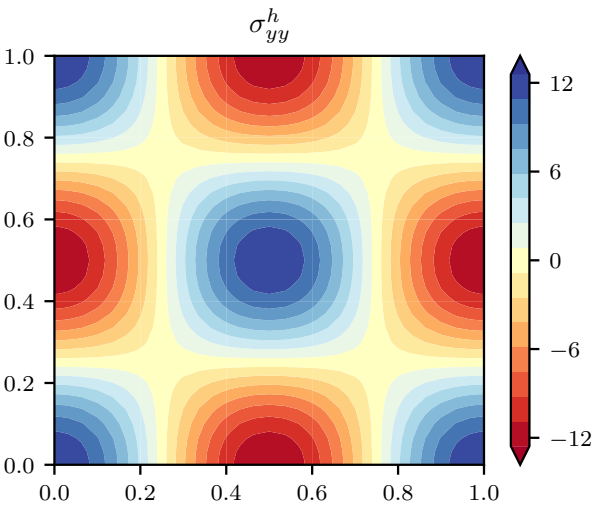

(f) Stress component σ_{yy}, $K = 5$, $p = 5$.

Figure 8.8: Comparison of normal stress components for the manufactured solution ($c = 0$) on the domain $[0,1]^2$.

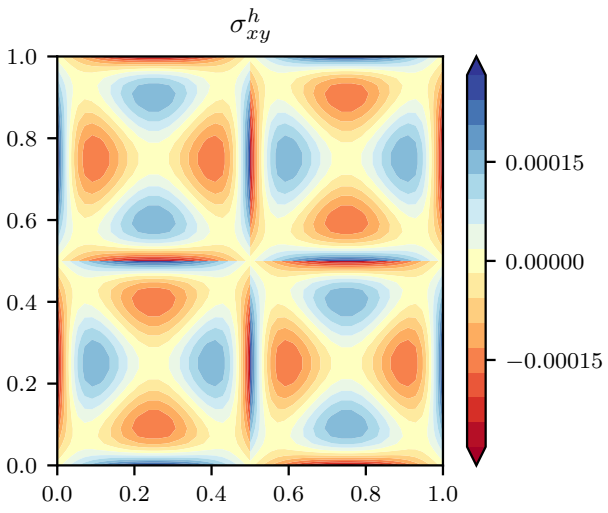

(a) Stress component σ_{xy}, $K = 2$, $p = 5$.

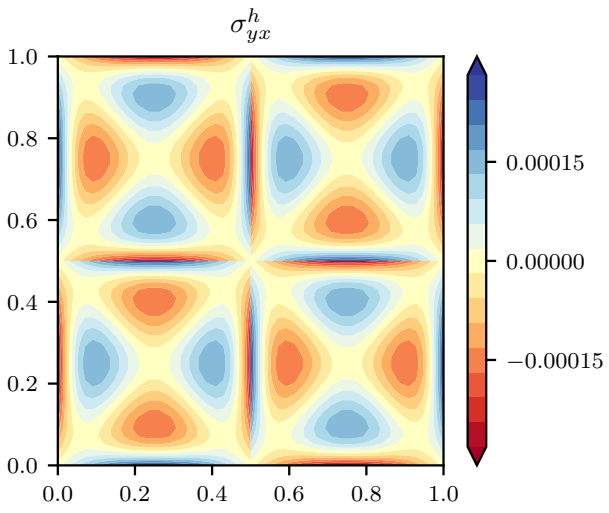

(b) Stress component σ_{yx}, $K = 2$, $p = 5$.

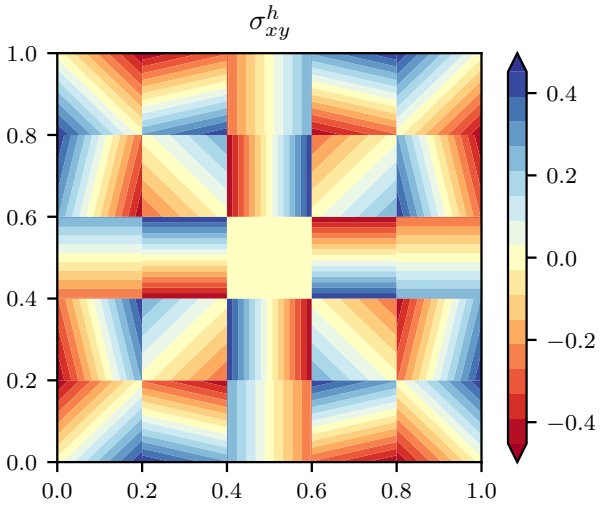

(c) Stress component σ_{xy}, $K = 5$, $p = 2$.

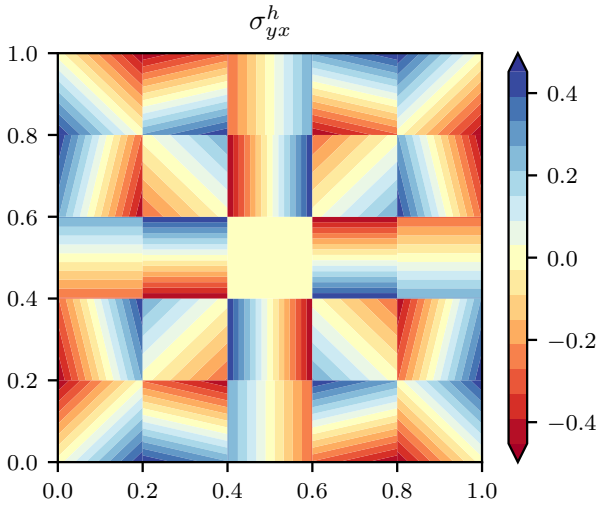

(d) Stress component σ_{yx}, $K = 5$, $p = 2$.

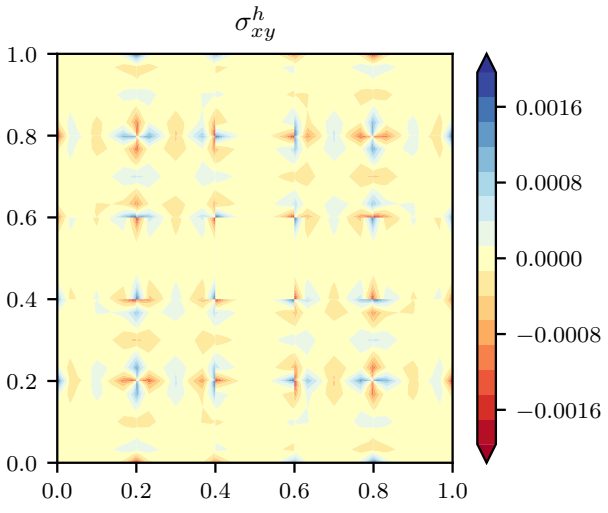

(e) Stress component σ_{xy}, $K = 5$, $p = 5$.

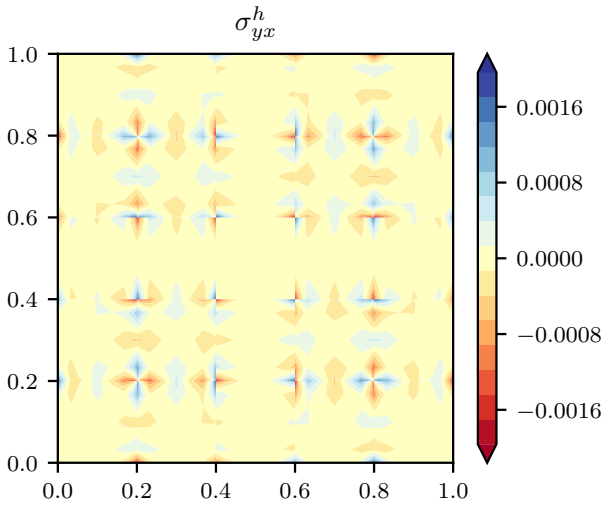

(f) Stress component σ_{yx}, $K = 5$, $p = 5$.

Figure 8.9: Comparison of shear stress components for the manufactured solution ($c = 0$) on the domain $[0,1]^2$.

9

Conclusions and Recommendations

The mimetic spectral element method has been successfully applied to three problems, the Poisson problem, the Stokes problem, and the linear elasticity problem. Using this knowledge, a new formulation for linear elasticity is proposed and the results are shown, which answer the research question: Yes, a formulation for the mimetic spectral element method applied to the linear elasticity problem, that is hybridisable and conserves both linear momentum and angular momentum, is found. To achieve this, several conclusions have been found on the way, that answer the sub-questions posed in Section 1.2.

From the works studied in the literature survey, a motivation and understanding of the mimetic discretisation methods has been found. The origin of these ideas came from the combination of concepts from exterior calculus and the insights of Tonti, leading to a geometric description of physics. The combination of this geometric description with algebraic topology leads to a natural discretisation of the differential forms that describe physics. It is argued that the geometrical description of physics has the advantages of clear separation of metric and topological aspects in a physical problem, which in turn leads to the correct choice in representation of the physical variables and separation of the errors made in a numerical simulation. An overview on the mimetic spectral element method led to the conclusion that to move towards continuum mechanics applications, the problem of linear elasticity needed to be reconsidered, with the extension to a hybrid formulation with attractive properties in mind.

The ingredients of the mimetic spectral element method have been put together to solve the Poisson problem. The system was made more sparse by the introduction of the algebraic dual basis for the expansion of the pressure. The two test problems yielded the expected results. The first was a manufactured solution, that showed the convergence of the error to be optimal for the given basis for both h- and p refinement. The L-shaped domain test case then allowed for showing the point-wise exactness of the divergence operator in the absence of forcing terms.

The second problem that was considered was the Stokes problem, rewritten in a system of first order equations called the vorticity-velocity-pressure formulation. The standard Galerkin procedure was followed to find a weak form. It was tested with the same manufactured solution test case, producing optimal results with point-wise mass conservation. The formulation is also capable of simulating non-smooth cases such as the lid-driven cavity flow and the backwards facing step. Even for these cases, the mass conservation constraint is satisfied point-wise. The conclusion is that the law of conservation of mass is discretised exactly in this formulation, however, the linear momentum balance law cannot be satisfied exactly using this formulation. Furthermore, the formulation is not general due to the assumption of constant viscosity.

This lead to the pursuit of directly implementing continuum mechanics problems with the mimetic spectral element method, with stress as the primary unknown. By a logical choice of the basis of the stresses, the linear momentum balance law can be discretised exactly. However, due to the choice of basis for the shear stresses, the symmetry of the stress tensor and thus the angular momentum could not be conserved strongly but only weakly. This formulation is in addition not directly hybridisable, but requires additional constraints to do so. The results for the manufactured solution and cantilever beam test cases on orthogonal and curvilinear grids showed that linear momentum is strongly conserved by the solution, while the symmetry of the stress tensor and therefore angular momentum are only weakly conserved.

A new formulation has been proposed with the basis chosen as pairs of primal and dual basis functions. Furthermore, the shear stresses are prescribed on the boundary, such that they become discontinuous over

the elements. The implemented formulation is shown to be hybridisable, as the system to solve for the hybrid formulation is non-singular without additional constraints. This new linear elasticity formulation is therefore highly parallelisable. The performance of the method was clear from the convergence results, which prove that linear momentum is still conserved point-wise, as was the case for the previous formulation. In addition, the stress tensor is point-wise symmetric, which was possible due to the choice of polynomial space of the stress components. The combination of the point-wise symmetry of the stress tensor and linear momentum conservation then meant that angular momentum conservation is point-wise satisfied by the solution.

Finally, the mimetic spectral element method has now been applied to the Stokes problem with the stress as explicit unknown, using the new linear elasticity formulation proposed in this work but adding a term where the pressure enforces mass conservation. This is also an improvement on the velocity-vorticity-pressure formulation, since the viscosity does not have to be constant. This formulation is shown to be hybridisable, while satisfying linear momentum, angular momentum, and mass conservation point-wise even for the lowest order cases. The results for the velocity and vorticity are all optimal, while sub-optimal results were obtained for the pressure and stress for a larger number of elements. Further investigation of the interface constraint is necessary.

The aim of this thesis was to document all the steps in the process to arrive at the new formulation for linear elasticity, with the broader continuum mechanics in mind. The first steps in extending the new formulation to fluids have been taken. Some aspects have however still been left untouched and a number of questions still remain. Several recommendations are therefore given here as directions for direct future research.

- Further investigating the coupling of elements for the stress-based Stokes formulation to achieve optimal convergence for the pressure and the stress.
- Testing the stress-based Stokes formulation on a solution with a varying viscosity.
- Comparing the stress-based Stokes formulation formulation to the velocity-vorticity-pressure formulation, for instance using the lid-driven cavity flow problem, to see what the impact of linear momentum conservation is on the solution.
- Mapping the new linear elasticity and Stokes formulations to arbitrary, curvilinear domains.
- Testing the new linear elasticity and Stokes formulations with test problems where the forcing function can be exactly represented.
- Prove the error bounds of the new formulations, and therefore consistency and well-posedness.
- Investigating the performance of computing with the hybrid formulation with different system setup, numbering, and solving techniques.

Further directions for expanding the method are also summarised.

- Three dimensional implementations. Although these should follow in a straightforward manner, considerable effort is needed for the addition of an extra dimension.
- Time dependent problems, such as linear advection and Burgers' equation, starting in one dimension. Eventually, extending the formulation to fluids with convection.
- Extension of the method to triangular elements, which would allow great mesh flexibility. As of now, no edge functions of arbitrary order have been found for these elements.

Bibliography

[1] D. N. Arnold and L. Li. Finite element exterior calculus with lower-order terms. *Mathematics of Computation*, 86(307):2193–2212, 2017.

[2] D. N. Arnold, F. Brezzi, and M. Fortin. A stable finite element for the Stokes equations. *Calcolo*, 21(4): 337–344, 1984.

[3] D. N. Arnold, F. Brezzi, B. Cockburn, and L. D. Marini. Unified analysis of discontinuous Galerkin methods for elliptic problems. *SIAM journal on numerical analysis*, 39(5):1749–1779, 2002.

[4] D. N. Arnold, R. S. Falk, and R. Winther. Finite element exterior calculus, homological techniques, and applications. *Acta numerica*, 15:1–155, 2006.

[5] D. N. Arnold, R. S. Falk, and R. Winther. Finite element exterior calculus: from Hodge theory to numerical stability. *Bulletin of the American mathematical society*, 47(2):281–354, 2010.

[6] P. B. Bochev. A discourse on variational and geometric aspects of stability of discretizations. *33rd Computational Fluid Dynamics Lecture Series, VKI LS*, 5, 2003.

[7] P. B. Bochev and J. M. Hyman. Principles of mimetic discretizations of differential operators. In *Compatible spatial discretizations*, pages 89–119. Springer, 2006.

[8] P. B. Bochev, J. Lai, and L. Olson. A locally conservative, discontinuous least-squares finite element method for the Stokes equations. *International Journal for Numerical Methods in Fluids*, 68(6):782–804, 2012.

[9] D. Boffi, F. Brezzi, and M. Fortin. *Mixed finite element methods and applications*. Springer, 2013.

[10] J. Bonelle and A. Ern. Analysis of compatible discrete operator schemes for elliptic problems on polyhedral meshes. *ESAIM: Mathematical Modelling and Numerical Analysis*, 48(2):553–581, 2014.

[11] A. Bossavit. Whitney forms: A class of finite elements for three-dimensional computations in electromagnetism. *IEE Proceedings A (Physical Science, Measurement and Instrumentation, Management and Education, Reviews)*, 135(8):493–500, 1988.

[12] A. Bossavit. Computational electromagnetism and geometry: Building a finite-dimensional "Maxwell's house"(1): Network equations. *Journal of the Japan Society of Applied Electromagnetics*, 7(2):150–159, 1999.

[13] M. Bouman, A. Palha, J.J. Kreeft, and M. I. Gerritsma. A conservative spectral element method for curvilinear domains. In *Spectral and High Order Methods for Partial Differential Equations ICOSAHOM 2009*, pages 111–119. Springer, 2011.

[14] F. Brezzi, A. Buffa, and K. Lipnikov. Mimetic finite differences for elliptic problems. *ESAIM: Mathematical Modelling and Numerical Analysis*, 43(2):277–295, 2009.

[15] F. Brezzi, R. S. Falk, and L. D. Marini. Basic principles of mixed virtual element methods. *ESAIM: Mathematical Modelling and Numerical Analysis*, 48(4):1227–1240, 2014.

[16] A. Buffa, C. De Falco, and G. Sangalli. Isogeometric analysis: stable elements for the 2D Stokes equation. *International Journal for Numerical Methods in Fluids*, 65(11-12):1407–1422, 2011.

[17] B. Cockburn. Static condensation, hybridization, and the devising of the HDG methods. In *Building bridges: connections and challenges in modern approaches to numerical partial differential equations*, pages 129–177. Springer, 2016.

[18] B. Cockburn, G. E. Karniadakis, and C. Shu. The development of discontinuous Galerkin methods. In *Discontinuous Galerkin Methods*, pages 3–50. Springer, 2000.

[19] C. J. Cotter and J. Thuburn. A finite element exterior calculus framework for the rotating shallow-water equations. *Journal of Computational Physics*, 257:1506–1526, 2014.

[20] L. Beirao Da Veiga, V. Gyrya, K. Lipnikov, and G. Manzini. Mimetic finite difference method for the Stokes problem on polygonal meshes. *Journal of Computational Physics*, 228(19):7215–7232, 2009.

[21] J. P. M. De Almeida and E. A. Maunder. *Equilibrium finite element formulations*. John Wiley & Sons, 2017.

[22] L. F. Demkowicz and J. Gopalakrishnan. Analysis of the DPG method for the Poisson equation. *SIAM Journal on Numerical Analysis*, 49(5):1788–1809, 2011.

[23] L. F. Demkowicz and J. Gopalakrishnan. An overview of the discontinuous Petrov Galerkin method. In *Recent developments in discontinuous Galerkin finite element methods for partial differential equations*, pages 149–180. Springer, 2014.

[24] A. Demlow and A. N. Hirani. A posteriori error estimates for finite element exterior calculus: The De Rham complex. *Foundations of Computational Mathematics*, 14(6):1337–1371, 2014.

[25] M. Desbrun, A. N. Hirani, M. Leok, and J. E. Marsden. Discrete exterior calculus. *arXiv preprint math/0508341*, 2005.

[26] J. Dodziuk. Finite-difference approach to the Hodge theory of harmonic forms. *American Journal of Mathematics*, 98(1):79–104, 1976.

[27] J. Droniou, R. Eymard, T. Gallouët, and R. Herbin. A unified approach to mimetic finite difference, hybrid finite volume and mixed finite volume methods. *Mathematical Models and Methods in Applied Sciences*, 20(02):265–295, 2010.

[28] J. A. Evans and T. J. R. Hughes. Isogeometric divergence-conforming B-splines for the steady Navier–Stokes equations. *Mathematical Models and Methods in Applied Sciences*, 23(08):1421–1478, 2013.

[29] M. Farhloul and M. Fortin. A new mixed finite element for the Stokes and elasticity problems. *SIAM journal on numerical analysis*, 30(4):971–990, 1993.

[30] H. Flanders. *Differential Forms with Applications to the Physical Sciences*. Elsevier, 1963.

[31] T. Frankel. *The Geometry of Physics: An Introduction*. Cambridge University Press, 2004.

[32] M. I. Gerritsma. Edge functions for spectral element methods. In *Spectral and High Order Methods for Partial Differential Equations ICOSAHOM 2009*, pages 199–207. Springer, 2011.

[33] M. I. Gerritsma. An introduction to a compatible spectral discretization method. *Mechanics of Advanced Materials and Structures*, 19(1-3):48–67, 2012.

[34] M. I. Gerritsma, R.R. Hiemstra, J. J. Kreeft, A. Palha, P. P. Rebelo, and D. Toshniwal. The geometric basis of numerical methods. In *Spectral and High Order Methods for Partial Differential Equations ICOSAHOM 2012*, pages 17–35. Springer, 2014.

[35] M. I. Gerritsma, J. Kunnen, and B. de Heij. Discrete Lie derivative. In *Numerical Mathematics and Advanced Applications ENUMATH 2015*, pages 635–643. Springer, 2016.

[36] M. I. Gerritsma, V. Jain, Y. Zhang, and A. Palha. Algebraic dual polynomials for the equivalence of curl-curl problems. *arXiv preprint arXiv:1805.00114*, 2018.

[37] W. J. Gordon and C. A. Hall. Construction of curvilinear co-ordinate systems and applications to mesh generation. *International Journal for Numerical Methods in Engineering*, 7(4):461–477, 1973.

[38] W. J. Gordon and C. A. Hall. Transfinite element methods: blending-function interpolation over arbitrary curved element domains. *Numerische Mathematik*, 21(2):109–129, 1973.

[39] R. R. Hiemstra, D. Toshniwal, R. H. M. Huijsmans, and M. I. Gerritsma. High order geometric methods with exact conservation properties. *Journal of Computational Physics*, 257:1444–1471, 2014.

[40] R. Hiptmair. Discrete Hodge operators. *Numerische Mathematik*, 90(2):265–289, 2001.

[41] T. J. R. Hughes, G. Engel, L. Mazzei, and M. G. Larson. The continuous Galerkin method is locally conservative. *Journal of Computational Physics*, 163(2):467–488, 2000.

[42] J. M. Hyman and M. Shashkov. Natural discretizations for the divergence, gradient, and curl on logically rectangular grids. *Computers & Mathematics with Applications*, 33(4):81–104, 1997.

[43] V. Jain, Y. Zhang, A. Palha, and M. I. Gerritsma. Construction and application of algebraic dual polynomial representations for finite element methods. *arXiv preprint arXiv:1712.09472*, 2017.

[44] E. Kanso, M. Arroyo, Y. Tong, A. Yavari, J. G. Marsden, and M. Desbrun. On the geometric character of stress in continuum mechanics. *Zeitschrift für angewandte Mathematik und Physik*, 58(5):843–856, 2007.

[45] T. Kattelans and W. Heinrichs. Conservation of mass and momentum of the least-squares spectral collocation scheme for the Stokes problem. *Journal of Computational Physics*, 228(13):4649–4664, 2009.

[46] J. J. Kreeft. *Mimetic spectral element method; a discretization of geometry and physics*. PhD thesis, Delft University of Technology, 2013.

[47] J. J. Kreeft and M. I. Gerritsma. Mixed mimetic spectral element method for Stokes flow: A pointwise divergence-free solution. *Journal of Computational Physics*, 240:284–309, 2013.

[48] J. J. Kreeft, A. Palha, and M. I. Gerritsma. Mimetic spectral element method for generalized convection-diffusion problems. In *Proceedings of the V European Conference on Computational Fluid Dynamics ECCOMAS CFD*, 2010.

[49] K. Lipnikov, G. Manzini, and M. Shashkov. Mimetic finite difference method. *Journal of Computational Physics*, 257:1163–1227, 2014.

[50] K. Lipnikov, G. Manzini, J. D. Moulton, and M. Shashkov. The mimetic finite difference method for elliptic and parabolic problems with a staggered discretization of diffusion coefficient. *Journal of Computational Physics*, 305:111–126, 2016.

[51] C. Mattiussi. A reference discretization strategy for the numerical solution of physical field problems. *Advances in imaging and electron physics*, 121(1):143–279, 2002.

[52] R. A. Nicolaides and K. A. Trapp. Covolume discretization of differential forms. In *Compatible spatial discretizations*, pages 161–171. Springer, 2006.

[53] K. Olesen, B. Gervang, J. N. Reddy, and M. I. Gerritsma. A higher-order equilibrium finite element method. *International Journal for Numerical Methods in Engineering*, 114(12):1262–1290, 2018.

[54] A. Palha and M. I. Gerritsma. A mass, energy, enstrophy and vorticity conserving (MEEVC) mimetic spectral element discretization for the 2D incompressible Navier–Stokes equations. *Journal of Computational Physics*, 328:200–220, 2017.

[55] A. Palha, J. J. Kreeft, and M. I. Gerritsma. Numerical solution of advection equations with the discretization of the Lie derivative. In *Proceedings of the V European Conference on Computational Fluid Dynamics ECCOMAS CFD*, 2010.

[56] A. Palha, P. P. Rebelo, and M. I. Gerritsma. Mimetic spectral element advection. In *Spectral and High Order Methods for Partial Differential Equations ICOSAHOM 2012*, pages 325–335. Springer, 2014.

[57] A. Palha, P. P. Rebelo, R. R. Hiemstra, J. J. Kreeft, and M. I. Gerritsma. Physics-compatible discretization techniques on single and dual grids, with application to the Poisson equation of volume forms. *Journal of Computational Physics*, 257:1394–1422, 2014.

[58] J. B. Perot. Discrete conservation properties of unstructured mesh schemes. *Annual review of fluid mechanics*, 43:299–318, 2011.

[59] J. B. Perot and C. J. Zusi. Differential forms for scientists and engineers. *Journal of Computational Physics*, 257:1373–1393, 2014.

[60] A. Quarteroni and A. Valli. Theory and application of Steklov-Poincaré operators for boundary-value problems. In *Applied and Industrial Mathematics*, pages 179–203. Springer, 1991.

[61] P. A. Raviart and J. M. Thomas. Primal hybrid finite element methods for 2nd order elliptic equations. *Mathematics of computation*, 31(138):391–413, 1977.

[62] J. N. Reddy. *An introduction to continuum mechanics*. Cambridge university press, 2013.

[63] N. Robidoux and S. Steinberg. A discrete vector calculus in tensor grids. *Computational Methods in Applied Mathematics*, 11(1):23–66, 2011.

[64] C. J. Roy. Review of code and solution verification procedures for computational simulation. *Journal of Computational Physics*, 205(1):131–156, 2005.

[65] M. Shashkov and S. Steinberg. Solving diffusion equations with rough coefficients in rough grids. *Journal of Computational Physics*, 129(2):383–405, 1996.

[66] T. Tarhasaari, L. Kettunen, and A. Bossavit. Some realizations of a discrete Hodge operator: a reinterpretation of finite element techniques [for EM field analysis]. *IEEE Transactions on magnetics*, 35(3): 1494–1497, 1999.

[67] M. E. Taylor. *Partial Differential Equations I: Basic Theory, Second Edition*. Springer, 2011.

[68] E. Tonti. On the mathematical structure of a large class of physical theories. Technical report, Istituto Di Matematica, Politecnico Di Milano, Italy, 1971.

[69] E. Tonti. *The mathematical structure of classical and relativistic physics*. Springer, 2013.

[70] E. Tonti. Why starting from differential equations for computational physics? *Journal of Computational Physics*, 257:1260–1290, 2014.

[71] D. Toshniwal, R. H. M. Huijsmans, and M. I. Gerritsma. A geometric approach towards momentum conservation. In *Spectral and High Order Methods for Partial Differential Equations ICOSAHOM 2012*, pages 393–402. Springer, 2014.

[72] J. Van Kan, A. Segal, and F. Vermolen. *Numerical Methods in Scientific Computing*. Delft Academic Press, 2008.

[73] Y. Zhang, V. Jain, A. Palha, and M. I. Gerritsma. A high order hybrid mimetic discretization on curvilinear quadrilateral meshes for complex geometries. In *Proceedings to the 6th European Conference on Computational Mechanics and 7th European Conference on Computational Fluid Dynamics-ECCM-ECFD 2018*, 2018.

A

Derivations

A.1. Mass matrices

To compute the terms leading to the mass matrices, the inner product can be written as the wedge product with the Hodge operator on the second term [34, 47]. This can be done for all terms, resulting in three distinct mass matrices in $\mathbb{R}^2$. These will be derived in this section. Also, the mapping terms are derived here, see Section 3.3 for the explanation and notation. The system to solve for mapped domains remains the same, only the mass matrices are affected.

A.1.1. Expansion in basis functions

The 0-forms are expanded in nodal basis functions using

$$\omega^{(0)}(x,y) = \sum_{i=1}^{p+1}\sum_{j=1}^{p+1} \omega_{ij} h_i(x) h_j(y).$$

In two dimensions, it was seen that the outer oriented 1-form can be written as $q^{(1)} = \overline{u}\mathrm{d}y - \overline{v}\mathrm{d}x$, where $\overline{u}$ and $\overline{v}$ are functions that form the vector proxy, and can be projected on basis functions defined in Section 3.2, which leads to

$$\overline{u}(x,y) = \sum_{i=1}^{p+1}\sum_{j=1}^{p} u_{ij} h_i(x) e_j(y), \quad \overline{v}(x,y) = \sum_{i=1}^{p}\sum_{j=1}^{p+1} v_{ij} e_i(x) h_j(y).$$

Hence

$$q^{(1)}(x,y) = \sum_{i=1}^{p+1}\sum_{j=1}^{p} u_{ij} h_i(x) e_j(y)\mathrm{d}y - \sum_{i=1}^{p}\sum_{j=1}^{p+1} v_{ij} e_i(x) h_j(y)\mathrm{d}x.$$

Furthermore, the basis for 2-forms $p^{(n)} = p^{(2)}$ will be

$$p^{(2)}(x,y) = \sum_{i=1}^{p}\sum_{j=1}^{p} p_{ij} e_i(x) e_j(y)\mathrm{d}x \wedge \mathrm{d}y.$$

The test functions $\widetilde{q}^{(n-1)}$ and $\widetilde{p}^{(n)}$ for $n = 2$ are expanded similarly as

$$\begin{aligned}
\widetilde{\omega}^{(0)}(x,y) &= \sum_{k=1}^{p+1}\sum_{l=1}^{p+1} \widetilde{\omega}_{kl} h_k(x) h_l(y), \\
\widetilde{q}^{(1)}(x,y) &= \sum_{k=1}^{p+1}\sum_{l=1}^{p} (\widetilde{q}_x)_{kl} h_k(x) e_l(y)\mathrm{d}y - \sum_{k=1}^{p}\sum_{l=1}^{p+1} (\widetilde{q}_y)_{kl} e_k(x) h_l(y)\mathrm{d}x, \\
\widetilde{p}^{(2)}(x,y) &= \sum_{k=1}^{p}\sum_{l=1}^{p} (\widetilde{p})_{kl} e_k(x) e_l(y)\mathrm{d}x \wedge \mathrm{d}y.
\end{aligned}$$

A.1.2. Mass matrix for 0-forms

The inner product of the two 0-forms can be rewritten as

$$\left(\widetilde{\omega}^{(0)},\omega^{(0)}\right)_\Omega = \int_\Omega \widetilde{\omega}^{(0)} \wedge \star\, \omega^{(0)}.$$

Here, since $\star 1 = \mathrm{d}x \wedge \mathrm{d}y$,

$$\star\, \omega^{(0)} = \sum_{i=1}^{p+1}\sum_{j=1}^{p+1} \omega_{ij} h_i(x) h_j(y) \mathrm{d}x \wedge \mathrm{d}y,$$

the inner product of two 0-forms becomes

$$\int_\Omega \widetilde{\omega}^{(0)} \wedge \star\, \omega^{(0)} \approx \int_\Omega \sum_{i=1}^{p+1}\sum_{j=1}^{p+1}\sum_{k=1}^{p+1}\sum_{l=1}^{p+1} \omega_{ij}\widetilde{\omega}_{kl} h_i(x) h_j(y) h_k(x) h_l(y) \mathrm{d}x \wedge \mathrm{d}y.$$

In the discrete system, this terms becomes $(\widetilde{\boldsymbol{\omega}})^T \mathbb{M}^{(0)} \boldsymbol{\omega}^h$, where the mass matrix is a diagonal matrix with components

$$M^{(0)}_{ijkl} = \sum_{r=1}^{p+1}\sum_{s=1}^{p+1} h_i(x_r) h_j(y_s) h_k(x_r) h_l(y_s) w_r w_s.$$

Here, $\boldsymbol{\omega}$ and $\widetilde{\boldsymbol{\omega}}$ are vectors with components

$$\widetilde{\boldsymbol{\omega}}^h = \left[\widetilde{\omega}_1, \widetilde{\omega}_2, ..., \widetilde{\omega}_{(p+1)^2}\right]^T, \quad \boldsymbol{\omega}^h = \left[\omega_1, \omega_2, ..., \omega_{(p+1)^2}\right]^T.$$

The $\mathbb{M}^{(0)}$ under mapping is obtained by rewriting the inner product of two 0-forms as

$$\begin{aligned}
\left(\widetilde{\omega}^{(0)},\omega^{(0)}\right)_\Omega &= \int_{\Phi(\widehat{\Omega})} \widetilde{\omega}^{(0)} \wedge \star\, \omega^{(0)} \\
&= \int_{\widehat{\Omega}} \Phi^* \left[\widetilde{\omega}^{(0)} \wedge \star\, \omega^{(0)}\right] \\
&= \int_{\widehat{\Omega}} \Phi^* \widetilde{\omega}^{(0)} \wedge \Phi^* \star\, \omega^{(0)} \\
&= \int_{\widehat{\Omega}} \Phi^* \widetilde{\omega}^{(0)} \wedge \Phi^* \star\, \Phi^{-*}\Phi^* \omega^{(0)} \\
&= \int_{\widehat{\Omega}} \widehat{\widetilde{\omega}}^{(0)} \wedge \widehat{\star}\, \widehat{\omega}^{(0)},
\end{aligned}$$

where $\widehat{\omega}^{(0)} = \Phi^* \omega^{(0)}$ and $\widehat{\star} = \Phi^* \star \Phi^{-*}$. In the second to last step, the fact that $\Phi^{-*}\Phi^* = \mathbb{I}$ is used. The last expressions arrive from the fact that the pull-back operator does not commute with the Hodge operator, but it does commute with the wedge product [33, 47]. Considering that the inverse pull-back operator acting on the 0-form does not alter it as it is just a function,

$$\star\, \Phi^{-*}\, \widehat{\omega}^{(0)} = \sum_{i=1}^{p+1}\sum_{j=1}^{p+1} \omega_{ij} h_i(\xi) h_j(\eta) \mathrm{d}x \wedge \mathrm{d}y,$$

hence applying the pull-back gives

$$\begin{aligned}
\Phi^* \star\, \Phi^{-*}\, \widehat{\omega}^{(0)} &= \sum_{i=1}^{p+1}\sum_{j=1}^{p+1} \omega_{ij} h_i(\xi) h_j(\eta) \left[\frac{\partial x}{\partial \xi}\mathrm{d}\xi + \frac{\partial x}{\partial \eta}\right] \mathrm{d}\eta \wedge \left[\frac{\partial y}{\partial \xi}\mathrm{d}\xi + \frac{\partial y}{\partial \eta}\mathrm{d}\eta\right] \\
&= \sum_{i=1}^{p+1}\sum_{j=1}^{p+1} \omega_{ij} h_i(\xi) h_j(\eta) \left[\frac{\partial x}{\partial \xi}\frac{\partial y}{\partial \eta} - \frac{\partial x}{\partial \eta}\frac{\partial y}{\partial \xi}\right] \mathrm{d}\xi \wedge \mathrm{d}\eta \\
&= \sum_{i=1}^{p+1}\sum_{j=1}^{p+1} \omega_{ij} h_i(\xi) h_j(\eta) \left|\boldsymbol{\Phi}^*\right| \mathrm{d}\xi \wedge \mathrm{d}\eta
\end{aligned}$$

The inner product of two 0-forms becomes

$$\int_\Omega \widehat{\widetilde{\omega}}^{(0)} \wedge \widehat{\star}\, \widehat{\omega}^{(0)} \approx \int_\Omega \sum_{i=1}^{p+1}\sum_{j=1}^{p+1}\sum_{k=1}^{p+1}\sum_{l=1}^{p+1} \omega_{ij}\widetilde{\omega}_{kl} J(\xi,\eta) h_i(\xi) h_j(\eta) h_k(\xi) h_l(\eta) \mathrm{d}\xi \wedge \mathrm{d}\eta.$$

Here J is the determinant of the Jacobian matrix at discrete points. The equations become a system $(\widetilde{\boldsymbol{\omega}})^T \mathbb{M}^{(0)} \boldsymbol{\omega}^h$, where the mass matrix is a diagonal matrix with components

$$M^{(0)}_{ijkl} = \sum_{r=1}^{p+1}\sum_{s=1}^{p+1} J(\xi_r,\eta_s) h_i(\xi_r) h_j(\eta_s) h_k(\xi_r) h_l(\eta_s) w_r w_s.$$

A.1.3. Mass matrix for 1-forms

The first term in (4.6) can be computed using

$$\left(\widetilde{q}^{(n-1)}, q^{(n-1)}\right)_\Omega = \int_\Omega \widetilde{q}^{(n-1)} \wedge \star\, q^{(n-1)},$$

where, since $\star\, \mathrm{d}x = \mathrm{d}y$ and $\star\, \mathrm{d}y = -\mathrm{d}x$ as counterclockwise rotation is positive,

$$\star q^{(1)} = -\sum_{i=1}^{p+1}\sum_{j=1}^{p} u_{ij} h_i(x) e_j(y) \mathrm{d}x - \sum_{i=1}^{p}\sum_{j=1}^{p+1} v_{ij} e_i(x) h_j(y) \mathrm{d}y.$$

One of the properties of the exterior product or wedge-product is that it is skew-symmetric. For $n = 2$, this results in the properties $\mathrm{d}y \wedge \mathrm{d}x = -\mathrm{d}x \wedge \mathrm{d}y$ and $\mathrm{d}y \wedge \mathrm{d}y = \mathrm{d}x \wedge \mathrm{d}x = 0$ [33] and thus leads to

$$\begin{aligned}\left(\widetilde{q}^{(1)} \wedge \star\, q^{(1)}\right)_\Omega = \int_\Omega &\sum_{i=1}^{p+1}\sum_{j=1}^{p}\sum_{k=1}^{p+1}\sum_{l=1}^{p} (\widetilde{q}_x)_{ij} u_{ij} h_i(x) e_j(y) h_k(x) e_l(y) \mathrm{d}x \wedge \mathrm{d}y \\ &+ \sum_{k=1}^{p}\sum_{l=1}^{p+1}\sum_{i=1}^{p}\sum_{j=1}^{p+1} (\widetilde{q}_y)_{ij} v_{ij} e_i(x) h_j(y) e_k(x) h_l(y) \mathrm{d}x \wedge \mathrm{d}y,\end{aligned}$$

which can be assembled in a matrix, such that the system becomes $\left(\widetilde{\boldsymbol{q}}^h\right)^T \mathbb{M}^{(1)} \boldsymbol{q}^h$ with, setting $N = 2p(p+1)$,

$$\begin{aligned}\widetilde{\boldsymbol{q}}^h &= \left[\widetilde{q}_{x_1}, \widetilde{q}_{x_2}, ..., \widetilde{q}_{x_{p(p+1)}}, \widetilde{q}_{y_1}, ..., \widetilde{q}_{y_{p(p+1)}}\right] = \left[\widetilde{q}_1, \widetilde{q}_2, ..., \widetilde{q}_N\right]^T, \\ \boldsymbol{q}^h &= \left[u_1, u_2, ..., u_{p(p+1)}, v_1, ..., v_{p(p+1)}\right] = \left[q_1, q_2, ..., q_N\right]^T.\end{aligned}$$

The components of $\mathbb{M}^{(1)}$ can be written as a single sum over the points,

$$M^{(1)}_{ijkl} = \sum_{r=1}^{p+1}\sum_{s=1}^{p+1} \left[h_i(x_r) e_j(y_s) h_k(x_r) e_l(y_s) + e_i(x_r) h_j(y_s) e_k(x_r) h_l(y_s)\right] w_r w_s.$$

For mapping the mass matrix $\mathbb{M}^{(n-1)}$ the first term in (4.6a) is rewritten as

$$\begin{aligned}\left(\widetilde{q}^{(n-1)}, q^{(n-1)}\right)_\Omega &= \int_{\Phi(\widehat{\Omega})} \widetilde{q}^{(n-1)} \wedge \star\, q^{(n-1)} \\ &= \int_{\widehat{\Omega}} \widetilde{q}^{(n-1)} \wedge \star\, q^{(n-1)} \\ &= \int_{\widehat{\Omega}} \Phi^* \widetilde{q}^{(n-1)} \wedge \Phi^* \star\, q^{(n-1)} \\ &= \int_{\widehat{\Omega}} \Phi^* \widetilde{q}^{(n-1)} \wedge \Phi^* \star\, \Phi^{-*} \Phi^* q^{(n-1)} \\ &= \int_{\widehat{\Omega}} \widehat{\widetilde{q}}^{(n-1)} \wedge \widehat{\star}\, \widehat{q}^{(n-1)},\end{aligned}$$

where again $\widehat{\star} = \Phi^* \star \Phi^{-*}$ and $\widehat{q}^{(n-1)} = \Phi^* q^{(n-1)}$. Hence, as now the fluxes $\widehat{q}^{(n-1)}$ are defined on the reference domain, for $n = 2$,

$$\widehat{q}^{(1)} = \overline{u}\mathrm{d}\eta - \overline{v}\mathrm{d}\xi,$$

and applying the inverse pull-back,

$$\begin{aligned}\Phi^{-*}\widehat{q}^{(1)} &= \overline{u}\Phi^{-*}(\mathrm{d}\eta) - \overline{v}\Phi^{*}(\mathrm{d}\xi)\\ &= \frac{1}{|\boldsymbol{\Phi}^*|}\left[\overline{u}\left(-\frac{\partial y}{\partial \xi}\mathrm{d}x + \frac{\partial x}{\partial \xi}\mathrm{d}y\right) - \overline{v}\left(\frac{\partial y}{\partial \eta}\mathrm{d}x - \frac{\partial x}{\partial \eta}\mathrm{d}y\right)\right]\\ &= \frac{1}{|\boldsymbol{\Phi}^*|}\left[-\left(\overline{u}\frac{\partial y}{\partial \xi} + \overline{v}\frac{\partial y}{\partial \eta}\right)\mathrm{d}x + \left(\overline{u}\frac{\partial x}{\partial \xi} + \overline{v}\frac{\partial x}{\partial \eta}\right)\mathrm{d}y\right].\end{aligned}$$

Applying the Hodge operator, $\star\,\mathrm{d}x = \mathrm{d}y$, $\star\,\mathrm{d}y = -\mathrm{d}x$

$$\star\,\Phi^{-*}\widehat{q}^{(1)} = \frac{1}{|\boldsymbol{\Phi}^*|}\left[-\left(\overline{u}\frac{\partial y}{\partial \xi} + \overline{v}\frac{\partial y}{\partial \eta}\right)\mathrm{d}y - \left(\overline{u}\frac{\partial x}{\partial \xi} + \overline{v}\frac{\partial x}{\partial \eta}\right)\mathrm{d}x\right].$$

The final step is then applying the pull-back operator,

$$\begin{aligned}\Phi^{*}\star\,\Phi^{-*}\widehat{q}^{(1)} &= \frac{1}{|\boldsymbol{\Phi}^*|}\left[-\left(\overline{u}\frac{\partial y}{\partial \xi} + \overline{v}\frac{\partial y}{\partial \eta}\right)\Phi^{*}(\mathrm{d}y) - \left(\overline{u}\frac{\partial x}{\partial \xi} + \overline{v}\frac{\partial x}{\partial \eta}\right)\Phi^{*}(\mathrm{d}x)\right]\\ &= \frac{1}{|\boldsymbol{\Phi}^*|}\left[-\left(\overline{u}\frac{\partial y}{\partial \xi} + \overline{v}\frac{\partial y}{\partial \eta}\right)\left(\frac{\partial y}{\partial \xi}\mathrm{d}\xi + \frac{\partial y}{\partial \eta}\mathrm{d}\eta\right) - \left(\overline{u}\frac{\partial x}{\partial \xi} + \overline{v}\frac{\partial x}{\partial \eta}\right)\left(\frac{\partial x}{\partial \xi}\mathrm{d}\xi + \frac{\partial x}{\partial \eta}\mathrm{d}\eta\right)\right]\\ &= \frac{-1}{|\boldsymbol{\Phi}^*|}\left(\left(\left(\frac{\partial x}{\partial \xi}\right)^2 + \left(\frac{\partial y}{\partial \xi}\right)^2\right)\overline{u} + \left(\frac{\partial y}{\partial \xi}\frac{\partial y}{\partial \eta} + \frac{\partial x}{\partial \xi}\frac{\partial x}{\partial \eta}\right)\overline{v}\right)\mathrm{d}\xi\\ &\quad + \frac{-1}{|\boldsymbol{\Phi}^*|}\left(\left(\frac{\partial y}{\partial \xi}\frac{\partial y}{\partial \eta} + \frac{\partial x}{\partial \xi}\frac{\partial x}{\partial \eta}\right)\overline{u} + \left(\left(\frac{\partial x}{\partial \eta}\right)^2 + \left(\frac{\partial y}{\partial \eta}\right)^2\right)\overline{v}\right)\mathrm{d}\eta\\ &= -\Big(\big(G_{11}\overline{u} + G_{12}\overline{v}\big)\,\mathrm{d}\xi + \big(G_{21}\overline{u} + G_{22}\overline{v}\big)\,\mathrm{d}\eta\Big),\end{aligned}$$

where it is noted that $G_{12} = G_{21}$. With $\mathrm{d}\xi\wedge\mathrm{d}\xi = \mathrm{d}\eta\wedge\mathrm{d}\eta = 0$ and $\mathrm{d}\eta\wedge\mathrm{d}\xi = -\mathrm{d}\xi\wedge\mathrm{d}\eta$, and with

$$\begin{aligned}\widehat{\widetilde{q}}^{(1)}(\xi,\eta) &= \sum_{k=1}^{p+1}\sum_{l=1}^{p}(\widetilde{q}_\xi)_{kl}h_k(\xi)e_l(\eta)\mathrm{d}\eta - \sum_{k=1}^{p}\sum_{l=1}^{p+1}(\widetilde{q}_\eta)_{kl}e_k(\xi)h_l(\eta)\mathrm{d}\xi,\\ \overline{u}(\xi,\eta) &= \sum_{i=1}^{p+1}\sum_{j=1}^{p}u_{ij}h_i(\xi)e_j(\eta), \qquad \overline{v}(\xi,\eta) = \sum_{i=1}^{p}\sum_{j=1}^{p+1}v_{ij}e_i(\xi)h_j(\eta),\end{aligned}$$

the wedge product integral in the reference domain becomes

$$\begin{aligned}&\int_{\widehat{\Omega}}\widehat{\widetilde{q}}^{(n-1)}\wedge\widehat{\star}\,\widehat{q}^{(n-1)}\\ &= \int_{\widehat{\Omega}}\sum_{k=1}^{p+1}\sum_{l=1}^{p}(\widetilde{q}_\xi)_{kl}h_k(\xi)e_l(\eta)\left(G_{11}\sum_{i=1}^{p+1}\sum_{j=1}^{p}u_{ij}h_i(\xi)e_j(\eta) + G_{12}\sum_{i=1}^{p}\sum_{j=1}^{p+1}v_{ij}e_i(\xi)h_j(\eta)\right)\mathrm{d}\xi\wedge\mathrm{d}\eta\\ &\quad + \int_{\widehat{\Omega}}\sum_{k=1}^{p}\sum_{l=1}^{p+1}(\widetilde{q}_\eta)_{kl}e_k(\xi)h_l(\eta)\left(G_{21}\sum_{i=1}^{p+1}\sum_{j=1}^{p}u_{ij}h_i(\xi)e_j(\eta) + G_{22}\sum_{i=1}^{p}\sum_{j=1}^{p+1}v_{ij}e_i(\xi)h_j(\eta)\right)\mathrm{d}\xi\wedge\mathrm{d}\eta.\end{aligned}$$

Thus, four submatrices are obtained that can be assembled in the large mass-matrix $\mathbb{M}^{(1)}$, with components

$$\left(\widehat{\widetilde{\boldsymbol{q}}}\right)^T\mathbb{M}^{(1)}\widehat{\boldsymbol{q}} = \begin{bmatrix}\left(\widetilde{\boldsymbol{q}}_\xi\right)^T M_{11}\boldsymbol{u} & \left(\widetilde{\boldsymbol{q}}_\xi\right)^T M_{12}\boldsymbol{v}\\ \left(\widetilde{\boldsymbol{q}}_\eta\right)^T M_{21}\boldsymbol{u} & \left(\widetilde{\boldsymbol{q}}_\eta\right)^T M_{22}\boldsymbol{v}\end{bmatrix}.$$

The components are written out as

$$(M_{11})_{ijkl} = \sum_{r=1}^{p+1}\sum_{s=1}^{p+1} G_{11}(\xi_r,\eta_s)h_i(\xi_r)e_j(\eta_s)h_k(\xi_r)e_l(\eta_s)w_r w_s$$
$$(M_{12})_{ijkl} = \sum_{r=1}^{p+1}\sum_{s=1}^{p+1} G_{12}(\xi_r,\eta_s)e_i(\xi_r)h_j(\eta_s)h_k(\xi_r)e_l(\eta_s)w_r w_s$$
$$(M_{21})_{ijkl} = \sum_{r=1}^{p+1}\sum_{s=1}^{p+1} G_{21}(\xi_r,\eta_s)h_i(\xi_r)e_j(\eta_s)e_k(\xi_r)h_l(\eta_s)w_r w_s$$
$$(M_{22})_{ijkl} = \sum_{r=1}^{p+1}\sum_{s=1}^{p+1} G_{22}(\xi_r,\eta_s)e_i(\xi_r)h_j(\eta_s)e_k(\xi_r)h_l(\eta_s)w_r w_s$$

A.1.4. Mass matrix for 2-forms

Taking the inner product of two n-forms,

$$\left(\widetilde{p}^{(n)}, \mathrm{d}p^{(n)}\right)_\Omega = \int_\Omega \widetilde{p}^{(n)} \wedge \star\, p^{(n)},$$

where, as $\star\left(\mathrm{d}x \wedge \mathrm{d}y\right) = 1$ in $\mathbb{R}^2$, the Hodge-$\star$ maps the 2-form to a 0-form,

$$\star\, p^{(2)} = \sum_{i=1}^{p}\sum_{j=1}^{p} p_{ij}e_i(x)e_j(y),$$

then in general,

$$\int_\Omega \widetilde{p}^{(n)} \wedge \star\, p^{(n)} \approx \left(\widetilde{\boldsymbol{p}}^h\right)^T \mathbb{M}^{(n)}\boldsymbol{p}^h,$$

with $\left(\widetilde{\boldsymbol{p}}^h\right)^T$ a vector of test function weights of size $p^n = p^2$ in $\mathbb{R}^2$ defined as,

$$\widetilde{\boldsymbol{p}}^h = \left[\widetilde{p}_1, \widetilde{p}_2, ..., \widetilde{p}_{p^2}\right]^T, \quad \boldsymbol{p}^h = \left[p_1, p_2, ..., p_{p^2}\right]^T.$$

The components of $\mathbb{M}^{(n)}$ in $\mathbb{R}^2$ are given by

$$M^{(2)}_{ijkl} = \sum_{r=1}^{p+1}\sum_{s=1}^{p+1} e_i(x_r)e_j(y_s)e_k(x_r)e_l(y_s)w_r w_s.$$

Mapping this mass matrix is straightforward. Starting from

$$\begin{aligned}\left(\widetilde{p}^{(n)}, p^{(n)}\right)_\Omega &= \int_{\widehat{\Omega}} \Phi^*\widetilde{p}^{(n)} \wedge \Phi^* \star \Phi^{-*}\Phi^* p^{(n)} \\ &= \int_{\widehat{\Omega}} \widehat{\widetilde{p}}^{(2)} \wedge \widehat{\star}\, \widehat{p}^{(n)},\end{aligned}$$

where again $\widehat{\star} = \Phi^* \star \Phi^{-*}$ and $\widehat{p}^{(n)} = \Phi^* p^{(n)}$. The next step is the inverse-pullback operator, which commutes with the wedge product,

$$\begin{aligned}\Phi^{-*}p^{(n)} &= \overline{p}\Phi^{-*}(\mathrm{d}\xi) \wedge \Phi^{-*}(\mathrm{d}\eta) \\ &= \overline{p}\left[\frac{\partial\xi}{\partial x}\mathrm{d}x + \frac{\partial\xi}{\partial y}\mathrm{d}y\right] \wedge \left[\frac{\partial\eta}{\partial x}\mathrm{d}x + \frac{\partial\eta}{\partial y}\mathrm{d}y\right] \\ &= \overline{p}\left[\frac{\partial\xi}{\partial x}\frac{\partial\eta}{\partial y} - \frac{\partial\eta}{\partial x}\frac{\partial\xi}{\partial y}\right]\mathrm{d}x \wedge \mathrm{d}y \\ &= \overline{p}\left|\boldsymbol{\Phi}^{-*}\right|\mathrm{d}x \wedge \mathrm{d}y \\ &= \overline{p}\frac{1}{|\boldsymbol{\Phi}^*|}\mathrm{d}x \wedge \mathrm{d}y.\end{aligned}$$

Applying first the Hodge operator, with implies that $\star\ \mathrm{d}x \wedge \mathrm{d}y = 1$, then the pullback operator applied to 1 does not change the result, so

$$\widehat{\star}\, p^{(n)} = \overline{p}\frac{1}{|\boldsymbol{\Phi}^*|} = \overline{p}G_0.$$

Then, with

$$\widehat{\widetilde{p}}^{(2)} = \sum_{k=1}^{p}\sum_{l=1}^{p}(\widetilde{p})_{kl}e_k(\xi)e_l(\eta)\mathrm{d}\xi\wedge\mathrm{d}\eta,$$

the term can be written out in $\mathbb{R}^2$ as

$$\int_{\widehat{\Omega}}\widehat{\widetilde{p}}^{(2)}\wedge\widehat{\star}\,\widehat{p}^{(2)} = \int_{\widehat{\Omega}}\sum_{i=1}^{p}\sum_{j=1}^{p}\sum_{k=1}^{p}\sum_{l=1}^{p}(\widetilde{p})_{kl}p_{ij}G_0e_i(\xi)e_j(\eta)e_k(\xi)e_l(\eta)\mathrm{d}\xi\wedge\mathrm{d}\eta$$

In matrix form, this becomes

$$\int_{\widehat{\Omega}}\widehat{\widetilde{p}}^{(2)}\wedge\widehat{\star}\,\widehat{p}^{(2)} \approx \left(\widehat{\widetilde{\boldsymbol{p}}}^{h}\right)^{T}\mathbb{M}^{(2)}\widehat{\boldsymbol{p}}^{h}$$

where the components of $\mathbb{M}^{(2)}$ are

$$M^{(2)}_{ijkl} = \sum_{r=1}^{p+1}\sum_{s=1}^{p+1}G_0(\xi_r,\eta_s)e_i(\xi_r)e_j(\eta_s)e_k(\xi_r)e_l(\eta_s)w_rw_s.$$

A.1.5. Mappings for the tensor mass matrix and torque matrix

For a mapped domain, this inner product can be implemented using

$$\begin{aligned}\left(\underline{\underline{\widetilde{\sigma}}},C\underline{\underline{\sigma}}\right)_{\Phi(\Omega)} &= \int_{\Phi(\Omega)}\underline{\widetilde{\sigma}}^{(1)}\wedge\star\,C\underline{\sigma}^{(1)}\\ &= \int_{\widehat{\Omega}}\Phi^*\left(\underline{\widetilde{\sigma}}^{(1)}\right)\wedge\Phi^*\left(\star\,C\Phi^{-*}\Phi^*\underline{\sigma}^{(1)}\right)\\ &= \int_{\widehat{\Omega}}\underline{\widehat{\widetilde{\sigma}}}^{(1)}\wedge\Phi^*\left(\star\,C\Phi^{-*}\underline{\widehat{\sigma}}^{(1)}\right)\\ &= \int_{\widehat{\Omega}}\underline{\widehat{\widetilde{\sigma}}}^{(1)}\wedge\widehat{\star}_C\,\underline{\widehat{\sigma}}^{(1)}.\end{aligned}$$

Here, $\underline{\widehat{\sigma}}^{(1)} = \Phi^*\underline{\sigma}^{(1)}$ and $\widehat{\star}_C = \Phi^*\star\,C\Phi^{-*}$. Denoting the tensor again as vector valued 1-form,

$$\begin{aligned}\Phi^{-*}\underline{\underline{\widehat{\sigma}}} = \begin{bmatrix}\Phi^{-*}\widehat{\sigma_x}^{(1)}\\ \Phi^{-*}\widehat{\sigma_y}^{(1)}\end{bmatrix} &= \begin{bmatrix}\overline{\sigma}_{xx}\Phi^{-*}\left(\mathrm{d}\eta\right)-\overline{\sigma}_{yx}\Phi^{-*}\left(\mathrm{d}\xi\right)\\ \overline{\sigma}_{xy}\Phi^{-*}\left(\mathrm{d}\eta\right)-\overline{\sigma}_{yy}\Phi^{-*}\left(\mathrm{d}\xi\right)\end{bmatrix}\\ &= \frac{1}{|\boldsymbol{\Phi}^*|}\begin{bmatrix}\overline{\sigma}_{xx}\left(-\frac{\partial y}{\partial\xi}\mathrm{d}x+\frac{\partial x}{\partial\xi}\mathrm{d}y\right)-\overline{\sigma}_{yx}\left(\frac{\partial y}{\partial\eta}\mathrm{d}x-\frac{\partial x}{\partial\eta}\mathrm{d}y\right)\\ \overline{\sigma}_{xy}\left(-\frac{\partial y}{\partial\xi}\mathrm{d}x+\frac{\partial x}{\partial\xi}\mathrm{d}y\right)-\overline{\sigma}_{yy}\left(\frac{\partial y}{\partial\eta}\mathrm{d}x-\frac{\partial x}{\partial\eta}\mathrm{d}y\right)\end{bmatrix}\\ &= \frac{1}{|\boldsymbol{\Phi}^*|}\begin{bmatrix}\left(\overline{\sigma}_{xx}\frac{\partial x}{\partial\xi}+\overline{\sigma}_{yx}\frac{\partial x}{\partial\eta}\right)\mathrm{d}y-\left(\overline{\sigma}_{xx}\frac{\partial y}{\partial\xi}+\overline{\sigma}_{yx}\frac{\partial y}{\partial\eta}\right)\mathrm{d}x\\ \left(\overline{\sigma}_{xy}\frac{\partial x}{\partial\xi}+\overline{\sigma}_{yy}\frac{\partial x}{\partial\eta}\right)\mathrm{d}y-\left(\overline{\sigma}_{xy}\frac{\partial y}{\partial\xi}+\overline{\sigma}_{yy}\frac{\partial y}{\partial\eta}\right)\mathrm{d}x\end{bmatrix}.\end{aligned}$$

The application of the compliance tensor is next. To do so, the vector valued 1-form can be written into four components (for visualisation of the process),

$$\begin{aligned}C\Phi^{-*}\underline{\underline{\widehat{\sigma}}} = &\frac{1}{|\boldsymbol{\Phi}^*|}\begin{bmatrix}C_{11}&C_{12}&0&0\\ C_{21}&C_{22}&0&0\\ 0&0&C_{33}&C_{34}\\ 0&0&C_{43}&C_{44}\end{bmatrix}\begin{bmatrix}\left(\overline{\sigma}_{xx}\frac{\partial x}{\partial\xi}+\overline{\sigma}_{yx}\frac{\partial x}{\partial\eta}\right)\mathrm{d}y\\ -\left(\overline{\sigma}_{xx}\frac{\partial y}{\partial\xi}+\overline{\sigma}_{yx}\frac{\partial y}{\partial\eta}\right)\mathrm{d}x\\ \left(\overline{\sigma}_{xy}\frac{\partial x}{\partial\xi}+\overline{\sigma}_{yy}\frac{\partial x}{\partial\eta}\right)\mathrm{d}y\\ -\left(\overline{\sigma}_{xy}\frac{\partial y}{\partial\xi}+\overline{\sigma}_{yy}\frac{\partial y}{\partial\eta}\right)\mathrm{d}x\end{bmatrix}\\ &+\frac{1}{|\boldsymbol{\Phi}^*|}\begin{bmatrix}0&0&C_{13}&C_{14}\\ 0&0&C_{23}&C_{24}\\ C_{31}&C_{32}&0&0\\ C_{41}&C_{42}&0&0\end{bmatrix}\begin{bmatrix}-\left(\overline{\sigma}_{xx}\frac{\partial x}{\partial\xi}+\overline{\sigma}_{yx}\frac{\partial x}{\partial\eta}\right)\mathrm{d}x\\ \left(\overline{\sigma}_{xx}\frac{\partial y}{\partial\xi}+\overline{\sigma}_{yx}\frac{\partial y}{\partial\eta}\right)\mathrm{d}y\\ -\left(\overline{\sigma}_{xy}\frac{\partial x}{\partial\xi}+\overline{\sigma}_{yy}\frac{\partial x}{\partial\eta}\right)\mathrm{d}x\\ \left(\overline{\sigma}_{xy}\frac{\partial y}{\partial\xi}+\overline{\sigma}_{yy}\frac{\partial y}{\partial\eta}\right)\mathrm{d}y\end{bmatrix},\end{aligned}$$

where the first two rows and last two rows will together form a 1-form again.

For simplicity, the compliance tensor for Hooke's Law is taken (which has 6 of the 16 terms, only the diagonal and off-diagonal entries (1,4) and (4,1)), so in that case, 3 instead of 8 terms per 1-form are non-zero, and the equations become

$$C\Phi^{-*}\,\underline{\underline{\widehat{\sigma}}} = \frac{1}{|\mathbf{\Phi}^*|}\begin{bmatrix} C_{11}\left(\overline{\sigma}_{xx}\frac{\partial x}{\partial \xi}+\overline{\sigma}_{yx}\frac{\partial x}{\partial \eta}\right)\mathrm{d}y - C_{22}\left(\overline{\sigma}_{xx}\frac{\partial y}{\partial \xi}+\overline{\sigma}_{yx}\frac{\partial y}{\partial \eta}\right)\mathrm{d}x + C_{14}\left(\overline{\sigma}_{xy}\frac{\partial y}{\partial \xi}+\overline{\sigma}_{yy}\frac{\partial y}{\partial \eta}\right)\mathrm{d}y \\ C_{33}\left(\overline{\sigma}_{xy}\frac{\partial x}{\partial \xi}+\overline{\sigma}_{yy}\frac{\partial x}{\partial \eta}\right)\mathrm{d}y - C_{44}\left(\overline{\sigma}_{xy}\frac{\partial y}{\partial \xi}+\overline{\sigma}_{yy}\frac{\partial y}{\partial \eta}\right)\mathrm{d}x - C_{41}\left(\overline{\sigma}_{xx}\frac{\partial x}{\partial \xi}+\overline{\sigma}_{yx}\frac{\partial x}{\partial \eta}\right)\mathrm{d}x \end{bmatrix}.$$

Applying the Hodge-$\star$, and then the pullback again, then results in

$$\begin{aligned}\widehat{\star}_C\,\underline{\underline{\widehat{\sigma}}} &= -\frac{1}{|\mathbf{\Phi}^*|}\begin{bmatrix} C_{11}\left(\overline{\sigma}_{xx}\frac{\partial x}{\partial \xi}+\overline{\sigma}_{yx}\frac{\partial x}{\partial \eta}\right)\Phi^*(\mathrm{d}x) + C_{22}\left(\overline{\sigma}_{xx}\frac{\partial y}{\partial \xi}+\overline{\sigma}_{yx}\frac{\partial y}{\partial \eta}\right)\Phi^*(\mathrm{d}y) + C_{14}\left(\overline{\sigma}_{xy}\frac{\partial y}{\partial \xi}+\overline{\sigma}_{yy}\frac{\partial y}{\partial \eta}\right)\Phi^*(\mathrm{d}x) \\ C_{33}\left(\overline{\sigma}_{xy}\frac{\partial x}{\partial \xi}+\overline{\sigma}_{yy}\frac{\partial x}{\partial \eta}\right)\Phi^*(\mathrm{d}x) + C_{44}\left(\overline{\sigma}_{xy}\frac{\partial y}{\partial \xi}+\overline{\sigma}_{yy}\frac{\partial y}{\partial \eta}\right)\Phi^*(\mathrm{d}y) + C_{41}\left(\overline{\sigma}_{xx}\frac{\partial x}{\partial \xi}+\overline{\sigma}_{yx}\frac{\partial x}{\partial \eta}\right)\Phi^*(\mathrm{d}y) \end{bmatrix} \\ &= -\frac{1}{|\mathbf{\Phi}^*|}\begin{bmatrix}\widehat{\overline{\sigma}}_1\mathrm{d}\xi+\widehat{\overline{\sigma}}_2\mathrm{d}\eta \\ \widehat{\overline{\sigma}}_3\mathrm{d}\xi+\widehat{\overline{\sigma}}_4\mathrm{d}\eta\end{bmatrix},\end{aligned}$$

where the abbreviated terms represent

$$\begin{aligned}
\widehat{\overline{\sigma}}_1 &= \left[C_{11}\frac{\partial x}{\partial \xi}\frac{\partial x}{\partial \xi}+C_{22}\frac{\partial y}{\partial \xi}\frac{\partial y}{\partial \xi}\right]\overline{\sigma}_{xx}+\left[C_{11}\frac{\partial x}{\partial \eta}\frac{\partial x}{\partial \xi}+C_{22}\frac{\partial y}{\partial \eta}\frac{\partial y}{\partial \xi}\right]\overline{\sigma}_{yx}+C_{14}\frac{\partial y}{\partial \xi}\frac{\partial x}{\partial \xi}\overline{\sigma}_{xy}+C_{14}\frac{\partial y}{\partial \eta}\frac{\partial x}{\partial \xi}\overline{\sigma}_{yy}, \\
\widehat{\overline{\sigma}}_2 &= \left[C_{11}\frac{\partial x}{\partial \xi}\frac{\partial x}{\partial \eta}+C_{22}\frac{\partial y}{\partial \xi}\frac{\partial y}{\partial \eta}\right]\overline{\sigma}_{xx}+\left[C_{11}\frac{\partial x}{\partial \eta}\frac{\partial x}{\partial \eta}+C_{22}\frac{\partial y}{\partial \eta}\frac{\partial y}{\partial \eta}\right]\overline{\sigma}_{yx}+C_{14}\frac{\partial y}{\partial \xi}\frac{\partial x}{\partial \eta}\overline{\sigma}_{xy}+C_{14}\frac{\partial y}{\partial \eta}\frac{\partial x}{\partial \eta}\overline{\sigma}_{yy}, \\
\widehat{\overline{\sigma}}_3 &= C_{41}\frac{\partial x}{\partial \xi}\frac{\partial y}{\partial \xi}\overline{\sigma}_{xx}+C_{41}\frac{\partial x}{\partial \eta}\frac{\partial y}{\partial \xi}\overline{\sigma}_{yx}+\left[C_{33}\frac{\partial x}{\partial \xi}\frac{\partial x}{\partial \xi}+C_{44}\frac{\partial y}{\partial \xi}\frac{\partial y}{\partial \xi}\right]\overline{\sigma}_{xy}+\left[C_{33}\frac{\partial x}{\partial \eta}\frac{\partial x}{\partial \xi}+C_{44}\frac{\partial y}{\partial \eta}\frac{\partial y}{\partial \xi}\right]\overline{\sigma}_{yy}, \\
\widehat{\overline{\sigma}}_4 &= C_{41}\frac{\partial x}{\partial \xi}\frac{\partial y}{\partial \eta}\overline{\sigma}_{xx}+C_{41}\frac{\partial x}{\partial \eta}\frac{\partial y}{\partial \eta}\overline{\sigma}_{yx}+\left[C_{33}\frac{\partial x}{\partial \xi}\frac{\partial x}{\partial \eta}+C_{44}\frac{\partial y}{\partial \xi}\frac{\partial y}{\partial \eta}\right]\overline{\sigma}_{xy}+\left[C_{33}\frac{\partial x}{\partial \eta}\frac{\partial x}{\partial \eta}+C_{44}\frac{\partial y}{\partial \eta}\frac{\partial y}{\partial \eta}\right]\overline{\sigma}_{yy}.
\end{aligned}$$

Since the operator for the torque is metric dependent, the torque on a mapped domain involves

$$\begin{aligned}
\int_{\Phi(\Omega)}\mathbf{r}\times\underline{\underline{\sigma}}\,\mathrm{d}\Omega &= \int_{\widehat{\Omega}}\Phi^*\left(\mathbf{r}\times\Phi^{-*}\underline{\widehat{\sigma}}^{(1)}\right) \\
&= \int_{\widehat{\Omega}}\Phi^*\left(\mathbf{r}\times\frac{1}{|\mathbf{\Phi}^*|}\begin{bmatrix}\left(\overline{\sigma}_{xx}\frac{\partial x}{\partial \xi}+\overline{\sigma}_{yx}\frac{\partial x}{\partial \eta}\right)\mathrm{d}y-\left(\overline{\sigma}_{xx}\frac{\partial y}{\partial \xi}+\overline{\sigma}_{yx}\frac{\partial y}{\partial \eta}\right)\mathrm{d}x \\ \left(\overline{\sigma}_{xy}\frac{\partial x}{\partial \xi}+\overline{\sigma}_{yy}\frac{\partial x}{\partial \eta}\right)\mathrm{d}y-\left(\overline{\sigma}_{xy}\frac{\partial y}{\partial \xi}+\overline{\sigma}_{yy}\frac{\partial y}{\partial \eta}\right)\mathrm{d}x\end{bmatrix}\right) \\
&= \int_{\widehat{\Omega}}\frac{1}{|\mathbf{\Phi}^*|}\Phi^*\left\{\left[X\left(\overline{\sigma}_{xy}\frac{\partial x}{\partial \xi}+\overline{\sigma}_{yy}\frac{\partial x}{\partial \eta}\right)-Y\left(\overline{\sigma}_{xx}\frac{\partial x}{\partial \xi}+\overline{\sigma}_{yx}\frac{\partial x}{\partial \eta}\right)\right]\mathrm{d}y\right. \\
&\qquad\left.-\left[X\left(\overline{\sigma}_{xy}\frac{\partial y}{\partial \xi}+\overline{\sigma}_{yy}\frac{\partial y}{\partial \eta}\right)-Y\left(\overline{\sigma}_{xx}\frac{\partial y}{\partial \xi}+\overline{\sigma}_{yx}\frac{\partial y}{\partial \eta}\right)\right]\mathrm{d}x\right\} \\
&= \int_{\widehat{\Omega}}\frac{1}{|\mathbf{\Phi}^*|}\left\{\left[X\left(\overline{\sigma}_{xy}\frac{\partial x}{\partial \xi}+\overline{\sigma}_{yy}\frac{\partial x}{\partial \eta}\right)-Y\left(\overline{\sigma}_{xx}\frac{\partial x}{\partial \xi}+\overline{\sigma}_{yx}\frac{\partial x}{\partial \eta}\right)\right]\left(\frac{\partial y}{\partial \xi}\mathrm{d}\xi+\frac{\partial y}{\partial \eta}\mathrm{d}\eta\right)\right. \\
&\qquad\left.-\left[X\left(\overline{\sigma}_{xy}\frac{\partial y}{\partial \xi}+\overline{\sigma}_{yy}\frac{\partial y}{\partial \eta}\right)-Y\left(\overline{\sigma}_{xx}\frac{\partial y}{\partial \xi}+\overline{\sigma}_{yx}\frac{\partial y}{\partial \eta}\right)\right]\left(\frac{\partial x}{\partial \xi}\mathrm{d}\xi+\frac{\partial x}{\partial \eta}\mathrm{d}\eta\right)\right\} \\
&= \int_{\widehat{\Omega}}\frac{1}{|\mathbf{\Phi}^*|}\left\{\left[X\left(\overline{\sigma}_{xy}\left[\frac{\partial x}{\partial \xi}\frac{\partial y}{\partial \eta}-\frac{\partial y}{\partial \xi}\frac{\partial x}{\partial \eta}\right]+\overline{\sigma}_{yy}\left[\frac{\partial x}{\partial \eta}\frac{\partial y}{\partial \eta}-\frac{\partial y}{\partial \eta}\frac{\partial x}{\partial \eta}\right]\right)\right.\right. \\
&\qquad\left.-Y\left(\overline{\sigma}_{xx}\left[\frac{\partial x}{\partial \xi}\frac{\partial y}{\partial \eta}-\frac{\partial y}{\partial \xi}\frac{\partial x}{\partial \eta}\right]+\overline{\sigma}_{yx}\left[\frac{\partial x}{\partial \eta}\frac{\partial y}{\partial \eta}-\frac{\partial y}{\partial \eta}\frac{\partial x}{\partial \eta}\right]\right)\right]\mathrm{d}\eta \\
&\qquad+\left[X\left(\overline{\sigma}_{xy}\left[\frac{\partial x}{\partial \xi}\frac{\partial y}{\partial \xi}-\frac{\partial y}{\partial \xi}\frac{\partial x}{\partial \xi}\right]+\overline{\sigma}_{yy}\left[\frac{\partial x}{\partial \eta}\frac{\partial y}{\partial \xi}-\frac{\partial y}{\partial \eta}\frac{\partial x}{\partial \xi}\right]\right)\right. \\
&\qquad\left.\left.-Y\left(\overline{\sigma}_{xx}\left[\frac{\partial x}{\partial \xi}\frac{\partial y}{\partial \xi}-\frac{\partial y}{\partial \xi}\frac{\partial x}{\partial \xi}\right]+\overline{\sigma}_{yx}\left[\frac{\partial x}{\partial \eta}\frac{\partial y}{\partial \xi}-\frac{\partial y}{\partial \eta}\frac{\partial x}{\partial \xi}\right]\right)\right]\mathrm{d}\xi\right\} \\
&= \int_{\widehat{\Omega}}\frac{1}{|\mathbf{\Phi}^*|}\left\{\left(X\overline{\sigma}_{xy}-Y\overline{\sigma}_{xx}\right)\left|\mathbf{\Phi}^*\right|\mathrm{d}\eta-\left(X\overline{\sigma}_{yy}-Y\overline{\sigma}_{yx}\right)\left|\mathbf{\Phi}^*\right|\mathrm{d}\xi\right\} \\
&= \int_{\widehat{\Omega}}\left(X\overline{\sigma}_{xy}-Y\overline{\sigma}_{xx}\right)\mathrm{d}\eta-\left(X\overline{\sigma}_{yy}-Y\overline{\sigma}_{yx}\right)\mathrm{d}\xi.
\end{aligned}$$

If the torque is written as a 1-form,

$$T^{(1)} = \overline{T_\xi}\mathrm{d}\eta - \overline{T_\eta}\mathrm{d}\xi \approx \sum_{i=1}^{p+1}\sum_{j=1}^{p}\left(T_\xi\right)_{ij} h_i(\xi)e_j(\eta) - \sum_{i=1}^{p}\sum_{j=1}^{p+1}\left(T_\eta\right)_{ij} e_i(\xi)h_j(\eta),$$

then the torque matrix values computed from the stresses for every vertical edge in the reference domain become, where $h_i(\xi_r) = 1$,

$$\left(T_\eta\right)_{ijkl} = \sum_{r=1}^{p_f} h_i(\xi_r)e_j(\eta_r)\,w_r\left\{X(\eta_r)(\sigma_{xy})_{kl} - Y(\eta_r)(\sigma_{xx})_{kl}\right\},$$

and for every horizontal edge, where $h_j(\eta_r) = 1$ for $j = r$ and zero otherwise,

$$\left(T_\xi\right)_{ijkl} = \sum_{r=1}^{p_f} e_i(\xi_r)h_j(\eta_r)\,w_r\left\{X(\xi_r)(\sigma_{yy})_{kl} - Y(\xi_r)(\sigma_{yx})_{kl}\right\}.$$

A.2. Incidence Matrices arising in the weak formulation

In the previous section, the mass matrix $\mathbb{M}^{(2)}$ were derived. It will be shown here that the exterior derivative operator acting on 1-forms leads to an incidence matrix acting on discrete 1-forms. This is also shown for the exterior derivative acting on a 0-form.

A.2.1. Acting on 0-forms

It is seen in (5.13) arises from the first term in the 1-form equation, (5.12b),

$$\left(\widetilde{q}^{(1)}, \mathrm{d}\omega^{(0)}\right)_\Omega = \int_\Omega \widetilde{q}^{(1)} \wedge \star\, \mathrm{d}\omega^{(0)},$$

where the right term of the inner product can be rewritten as, using shorthand for non-varying terms,

$$\begin{aligned}\star\, \mathrm{d}\omega^{(0)} &= \sum_{i=1}^{p}\sum_{j=1}^{p+1}\left(\omega_{i+1,j}-\omega_{i,j}\right) e_i(x)h_j(y)\mathrm{d}x - \sum_{i=1}^{p+1}\sum_{j=1}^{p}\left(\omega_{i,j+1}-\omega_{i,j}\right) h_i(x)e_j(y)\mathrm{d}y \\ &= \delta_i(\omega)\,\mathrm{d}x + \delta_j(\omega)\,\mathrm{d}y.\end{aligned}$$

As $\widetilde{q}^{(1)}$ is

$$\widetilde{q}^{(1)} = \sum_{k=1}^{p+1}\sum_{l=1}^{p}(\widetilde{q}_x)_{kl}h_k(x)e_l(y)\mathrm{d}y - \sum_{k=1}^{p}\sum_{l=1}^{p+1}(\widetilde{q}_y)_{kl}e_k(x)h_l(y)\mathrm{d}x = \overline{\widetilde{q}_x}\mathrm{d}y - \overline{\widetilde{q}_y}\mathrm{d}x,$$

the inner product becomes

$$\int_\Omega \widetilde{q}^{(1)} \wedge \star\, \mathrm{d}\omega^{(0)} = -\left[\overline{\widetilde{q}_x}\partial_j(\omega) + \overline{\widetilde{q}_y}\partial_i(\omega)\right]\mathrm{d}x\wedge\mathrm{d}y.$$

This can be written in a mass-matrix as before, but now the complete matrix multiplied by the incidence matrix $\mathbb{E}^{(1,0)}$,

$$\left(\widetilde{\boldsymbol{q}}^h\right)^T \mathbb{M}^{(1)}\mathbb{E}^{(1,0)}\boldsymbol{\omega}^h = \begin{bmatrix}\widetilde{\boldsymbol{q}}_x^T M_{11} & \widetilde{\boldsymbol{q}}_x^T M_{12}\\ \widetilde{\boldsymbol{q}}_y^T M_{21} & \widetilde{\boldsymbol{q}}_y^T M_{22}\end{bmatrix}\mathbb{E}^{(1,0)}\boldsymbol{\omega}^h,$$

where the submatrices are defined as before.

A.2.2. Acting on 1-forms

The term that will lead to another incidence matrix acting on projected 1-forms can be rewritten as

$$\left(\widetilde{p}^{(n)}, \mathrm{d}q^{(n-1)}\right)_\Omega = \int_\Omega \widetilde{p}^{(n)} \wedge \star\, \mathrm{d}q^{(n-1)},$$

where, as $\star\left(\mathrm{d}x\wedge\mathrm{d}y\right) = 1$ in $\mathbb{R}^2$, as the Hodge-$\star$ maps the n-form to a 0-form,

$$\begin{aligned}\star\, \mathrm{d}q^{(1)} &= \sum_{i=1}^{p}\sum_{j=1}^{p}\left(u_{i+1,j}-u_{i,j}\right)e_i(x)e_j(y)\star\left(\mathrm{d}x\wedge\mathrm{d}y\right) + \sum_{i=1}^{p}\sum_{j=1}^{p}\left(v_{i,j+1}-v_{i,j}\right)e_i(x)e_j(y)\star\left(\mathrm{d}x\wedge\mathrm{d}y\right)\\ &= \sum_{i=1}^{p}\sum_{j=1}^{p}\left(u_{i+1,j}-u_{i,j}+v_{i,j+1}-v_{i,j}\right)e_i(x)e_j(y),\end{aligned}$$

then

$$\int_\Omega \widetilde{p}^{(n)} \wedge \star\, \mathrm{d}q^{(n-1)} \approx \left(\widetilde{\boldsymbol{p}}^h\right)^T \mathbb{M}^{(n)}\mathbb{E}^{(n,n-1)}\boldsymbol{q}^h,$$

A.3. Projection

This section is written to show the steps in deriving the specific mapping terms in reduction and reconstruction operators.

A.3.1. Reduction

For the Poisson problem, the forcing term is assumed to be an exactly known continuous function, but it is required that in $\mathbb{R}^2$, f is represented by a 2-form, an integral value over a surface. As the value of f is assumed exactly known everywhere in this problem, it can be integrated analytically. It is however generally more practical to apply fine quadrature on a fine Gauss-Lobatto grid to approximate this value. To do so on a rectangular reference domain, first, the quadrature points are mapped to a local surface cell, which in the case of the orthogonal physical domain is always a simple scaling and translation. The co-chain values are reduced from the exact function input with

$$f_{ij} = \sum_{r=1}^{p_f} \sum_{s=1}^{p_f} f^{ex}(x_r, y_s) w_r w_s, \tag{A.3}$$

For reconstruction, it then suffices to sum over the weights times the function values at the quadrature nodes in each cell, such that

$$f^h(x,y) = \sum_{i=1}^{p} \sum_{j=1}^{p} f_{ij} e_i(x) e_j(y). \tag{A.4}$$

If f is a 1-form, in the case of the Stokes VVP formulation, this means it will have two components in $\mathbb{R}^2$, so

$$f^{(1)} = \overline{f_x}\mathrm{d}y - \overline{f_y}\mathrm{d}x = \sum_{i=1}^{p+1} \sum_{j=1}^{p} \left(f_x\right)_{ij} h_i(x) e_j(y)\mathrm{d}y - \sum_{i=1}^{p} \sum_{j=1}^{p+1} \left(f_y\right)_{ij} e_i(x) h_j(y)\mathrm{d}x,$$

since the horizontal force acts over a vertical line. The components of the vector $\boldsymbol{f}^h$ are then

$$(f_y)_{ij} \approx -\sum_{r=1}^{p_f+1} f_y^{ex}(x_r, y_j) w_r, \qquad (f_x)_{ij} \approx \sum_{s=1}^{p_f+1} f_x^{ex}(x_i, y_s) w_s$$

The reduction of f involves quadrature, which is inexact and changes when changing coordinates. The mapping of a 2-form is straightforward,

$$\int_\Omega f^{(2)} \approx \int_{\hat{\Omega}} \Phi^* f^{(2)} \approx \sum_{r=1}^{p_f} \sum_{s=1}^{p_f} \sum_{i=1}^{p} \sum_{j=1}^{p} f_{ij} J(\xi_r, \eta_s) e_i(\xi_r) e_j(\eta_s) w_r w_s,$$

with J the determinant of the Jacobian accounting for the mapping, while taking the weights in the reference domain. (A.3) thus alters to include the change,

$$f_{ij} = \sum_{r=1}^{p_f} \sum_{s=1}^{p_f} f^{ex}(x_r, y_s) J(\xi_r, \eta_s) w_r w_s.$$

The reduction of a vector-valued **f** to a 1-form is similarly derived. The mapping of the 1-form is

$$\begin{aligned}\int_\Omega f^{(1)} = \int_{\hat{\Omega}} \Phi^* f^{(1)} &= \int_{\hat{\Omega}} \overline{f_x}\left(\frac{\partial y}{\partial \xi}\mathrm{d}\xi + \frac{\partial y}{\partial \eta}\mathrm{d}\eta\right) - \overline{f_y}\left(\frac{\partial x}{\partial \xi}\mathrm{d}\xi + \frac{\partial x}{\partial \eta}\mathrm{d}\eta\right) \\ &= \int_{\hat{\Omega}} \left(\overline{f_x}\frac{\partial y}{\partial \xi} - \overline{f_y}\frac{\partial x}{\partial \xi}\right)\mathrm{d}\xi + \left(\overline{f_x}\frac{\partial y}{\partial \eta} - \overline{f_y}\frac{\partial x}{\partial \eta}\right)\mathrm{d}\eta.\end{aligned}$$

The components of the vector $\boldsymbol{f}^h$ are then

$$\begin{aligned}(f_y)_{ij} &= \sum_{r=1}^{p_f+1} \left(f_x^{ex}(\xi_r, \eta_j) \left.\frac{\partial y}{\partial \xi}\right|_{\xi_r} - f_y^{ex}(\xi_r, \eta_j) \left.\frac{\partial x}{\partial \xi}\right|_{\xi_r}\right) w_r \\ (f_x)_{ij} &= \sum_{s=1}^{p_f+1} \left(f_x^{ex}(\xi_i, \eta_s) \left.\frac{\partial y}{\partial \eta}\right|_{\eta_s} - f_y^{ex}(\xi_i, \eta_s) \left.\frac{\partial x}{\partial \eta}\right|_{\eta_s}\right) w_s\end{aligned}$$

A.3.2. Solution reconstruction

The reconstruction of the solution requires a mapping as well. Reconstruction from a projected 2-form or 2-cochain in the reference domain is straightforward,

$$\begin{aligned}\int_{\widehat{\Omega}} p^{(2)} &= \left(\Phi^{-*}\widehat{p}^{(2)}\right)_{\Omega} \\ &= \int_{\Omega} \overline{p}\,\Phi^{-*}\left(\mathrm{d}\xi \wedge \mathrm{d}\eta\right) \\ &= \int_{\Omega} \overline{p}\,\frac{1}{|\Phi^*|}\mathrm{d}x \wedge \mathrm{d}y.\end{aligned}$$

For corresponding $(\xi,\eta) \rightarrow (x,y)$, the reconstruction is performed as

$$p^h(x,y) = \sum_{i=1}^{p}\sum_{j=1}^{p} \frac{1}{J}(\xi,\eta)\, p_{ij}\, e_i(\xi)\, e_j(\eta).$$

Similarly, the 1-form projection can be reconstructed or interpolated, but due to the mapping, both the derivatives to ξ and η must be taken into account,

$$\begin{aligned}u^h(x,y) &= \sum_{i=1}^{p}\sum_{j=1}^{p+1} (q_x)_{ij}\, e_i(x)\, h_j(y) \frac{\partial y}{\partial \eta}\frac{1}{J(x,y)} - \sum_{i=1}^{p+1}\sum_{j=1}^{p} (q_y)_{ij}\, h_i(x)\, e_j(y) \frac{\partial y}{\partial \xi}\frac{1}{J(x,y)}, \\ v^h(x,y) &= -\sum_{i=1}^{p}\sum_{j=1}^{p+1} (q_x)_{ij}\, e_i(x)\, h_j(y) \frac{\partial x}{\partial \eta}\frac{1}{J(x,y)} + \sum_{i=1}^{p+1}\sum_{j=1}^{p} (q_y)_{ij}\, h_i(x)\, e_j(y) \frac{\partial x}{\partial \xi}\frac{1}{J(x,y)}.\end{aligned}$$

Finally, the 0-form projection is invariant under mapping (since its basis is 1), such that

$$\omega^h(x,y) = \sum_{i=0}^{p}\sum_{j=0}^{p} \omega_{ij}\, h_i(\xi)\, h_j(\eta).$$

A.4. Boundary conditions

In this section, the derivation of the boundary condition terms leading to right-hand side vectors in a system to solve are shown. Note that these derivations assume the use of primal basis functions for all degrees of freedom.

A.4.1. Pressure boundary condition

This section describes how to evaluate the boundary condition vector $\boldsymbol{g}^h$. This involves the term

$$g = \int_{\partial\Omega} \operatorname{tr}\left(\widetilde{q}^{(n-1)}\right) \wedge \operatorname{tr}\left(p^{(0)}\right) = \int_{\partial\Omega} \widetilde{q}^{(n-1)} \wedge p^{(0)},$$

since it is clear that the trace is taken on the boundary. In the case of a square domain on $(x,y) \in [-1,1]$ for $n=2$, the boundary consists of four parts, hence it can be rewritten using $\partial\Omega = \partial\Omega_T \cup \partial\Omega_B \cup \partial\Omega_L \cup \partial\Omega_R$ as

$$g = \int_{\partial\Omega_T} \widetilde{q}^{(n-1)} \wedge p^{(0)} + \int_{\partial\Omega_B} \widetilde{q}^{(n-1)} \wedge p^{(0)} + \int_{\partial\Omega_L} \widetilde{q}^{(n-1)} \wedge p^{(0)} + \int_{\partial\Omega_R} \widetilde{q}^{(n-1)} \wedge p^{(0)}.$$

Taking the bottom boundary only such that $y=-1$ and $\mathrm{d}y=0$, and rewriting, this gives in this case

$$\begin{aligned}
\int_{\partial\Omega_B} \widetilde{q}^{(1)} \wedge p^{(0)} &= \int_{\partial\Omega_B} \left[\sum_{k=1}^{p+1} \sum_{l=1}^{p} (\widetilde{q}_x)_{kl} h_k(x) e_l(-1)\mathrm{d}y - \sum_{k=1}^{p} \sum_{l=1}^{p+1} (\widetilde{q}_y)_{kl} e_k(x) h_l(-1)\mathrm{d}x \right] p(x,-1) \\
&= \int_{\partial\Omega_B} \sum_{i=1}^{p} (\widetilde{q}_y)_{i1} e_i(x)\, p(x,-1)\mathrm{d}x \\
&\approx \sum_{s=1}^{p+1} \sum_{i=1}^{p} (\widetilde{q}_y)_{i1} e_i(x_s)\, p(x_s,-1)\, w_s.
\end{aligned}$$

Hence each component of $\boldsymbol{g}^h$ is each contribution to the sum over i. This can then be performed for any edge.

A.4.2. Tangential velocity boundary condition

The last derivation concerns the term $\boldsymbol{b}^h$, which introduces the tangential velocity in the equations. Since the flux is related to the circulation with a Hodge star, $\star\, q^{(1)} = u^{(1)}$,

$$\begin{aligned}
\star\, q^{(1)} &= \sum_{i=1}^{p+1} \sum_{j=1}^{p} u_{ij} h_i(x) e_j(y) \star \mathrm{d}y - \sum_{i=1}^{p} \sum_{j=1}^{p+1} v_{ij} e_i(x) h_j(y) \star \mathrm{d}x \\
&= -\sum_{i=1}^{p+1} \sum_{j=1}^{p} u_{ij} h_i(x) e_j(y)\mathrm{d}x - \sum_{i=1}^{p} \sum_{j=1}^{p+1} v_{ij} e_i(x) h_j(y)\mathrm{d}y,
\end{aligned}$$

the term can be written as

$$\begin{aligned}
b = \int_{\partial\Omega} \operatorname{tr}\left(\widetilde{\omega}^{(0)}\right) \wedge \operatorname{tr}\left(\star\, q^{(1)}\right) &= \int_{\partial\Omega} \operatorname{tr}\left(\widetilde{\omega}^{(0)}\right) \wedge \operatorname{tr}\left(u^{(1)}\right) \\
&= -\sum_{k=1}^{p+1} \sum_{l=1}^{p+1} \widetilde{\omega}_{kl} h_k(x) h_l(y)\, u^{ex}(x,y)\mathrm{d}x - \sum_{k=1}^{p+1} \sum_{l=1}^{p+1} \widetilde{\omega}_{kl} h_k(x) h_l(y)\, v^{ex}(x,y)\mathrm{d}y
\end{aligned}$$

Taking again the bottom boundary,

$$\int_{\partial\Omega_B} \operatorname{tr}\left(\widetilde{\omega}^{(0)}\right) \wedge \operatorname{tr}\left(u^{(1)}\right) \approx -\sum_{r=1}^{p+1} \sum_{k=1}^{p+1} \sum_{l=1}^{p+1} \widetilde{\omega}_{kl} h_k(x_r)\, w_r\, u^{ex}(x_r,-1)$$

A.4.3. Normal velocity boundary condition

In the case of natural boundary conditions, $q^{(n-1)}$ is known at the boundary. Hence in (4.8), the row of entries in the left-hand-side matrix corresponding to the boundary contributions are simply set to zero. Only one entry in each of those rows is set to one, such that $q^{(n-1)}|_{\partial\Omega} = \int_{\partial\Omega} g$, where the local value of g must be integrated over the boundary edges, for example the bottom boundary,

$$\boldsymbol{q}^h = \boldsymbol{g}^h = \sum_{s=1}^{p_f} g^{ex}(x_s,-1)\, w_s.$$

B

Note on solving hybrid systems

Considering a hybrid system is in the same form as in [9, p. 429], the procedure called static condensation can be applied. Starting with

$$\begin{bmatrix} A & B^T & C^T \\ B & 0 & 0 \\ C & 0 & 0 \end{bmatrix} \begin{bmatrix} U \\ P \\ \Lambda \end{bmatrix} = \begin{bmatrix} G \\ F \\ 0 \end{bmatrix},$$

the first equation of this system can be rewritten as

$$U = A^{-1}\left(G - B^T P - C^T \Lambda\right).$$

Eliminating the first row, the remaining system is then

$$\begin{bmatrix} -BA^{-1}B^T - BA^{-1}C^T \\ -CA^{-1}B^T - CA^{-1}C^T \end{bmatrix} \begin{bmatrix} P \\ \Lambda \end{bmatrix} = \begin{bmatrix} -BA^{-1}G + F \\ 0 \end{bmatrix}.$$

Since $\left(-BA^{-1}C^T\right)^T = -CA^{-1}B^T$, this can be rewritten as

$$\begin{bmatrix} Q & R^T \\ R & S \end{bmatrix} \begin{bmatrix} P \\ \Lambda \end{bmatrix} = \begin{bmatrix} T \\ 0 \end{bmatrix}.$$

Hence, now this system can be solved for P,

$$P = Q^{-1}\left(T - R^T \Lambda\right)$$

The final system to solve is thus

$$H\Lambda = V,$$

with, for $n = 2$,

$$\begin{aligned} H = -RQ^{-1}R^T + S &= CA^{-1}B^T\left(BA^{-1}B^T\right)^{-1}BA^{-1}C^T - CA^{-1}C^T \\ &= \mathbb{N}\left(\mathbb{M}^{(1)}\right)^{-1}\mathbb{E}^{(2,1)\,T}\left(\mathbb{E}^{(2,1)}\left(\mathbb{M}^{(1)}\right)^{-1}\mathbb{E}^{(2,1)\,T}\right)^{-1}\mathbb{E}^{(2,1)}\left(\mathbb{M}^{(1)}\right)^{-1}\mathbb{N}^T - \mathbb{N}\left(\mathbb{M}^{(1)}\right)^{-1}\mathbb{N}^T \\ &= \mathbb{N}\left(\mathbb{M}^{(1)}\right)^{-1}\left(\mathbb{E}^{(2,1)\,T}\left(\mathbb{E}^{(2,1)}\left(\mathbb{M}^{(1)}\right)^{-1}\mathbb{E}^{(2,1)\,T}\right)^{-1}\mathbb{E}^{(2,1)} - \mathbb{M}^{(1)}\right)\left(\mathbb{M}^{(1)}\right)^{-1}\mathbb{N}^T, \end{aligned}$$

and

$$\begin{aligned} V = -RQ^{-1}T &= -CA^{-1}B^T\left(BA^{-1}B^T\right)^{-1}\left(-BA^{-1}G + F\right) \\ &= -\mathbb{N}\left(\mathbb{M}^{(1)}\right)^{-1}\mathbb{E}^{(2,1)\,T}\left(\mathbb{E}^{(2,1)}\left(\mathbb{M}^{(1)}\right)^{-1}\mathbb{E}^{(2,1)\,T}\right)^{-1}\left(-\mathbb{E}^{(2,1)}\left(\mathbb{M}^{(1)}\right)^{-1}\boldsymbol{g}^h + \boldsymbol{f}^h\right). \end{aligned}$$

Here, $\boldsymbol{g}^h$ and $\boldsymbol{f}^h$ are the vectors from (4.9). Note that for square matrices A and B, $Q^{-1} = \left(BA^{-1}B^T\right)^{-1} = \left(B^T\right)^{-1}AB^{-1}$, but the matrix $\mathbb{E}^{(2,1)}$ is not square and thus not invertible. If it was, the terms in determining the matrix H would cancel out.

C

Program implementation

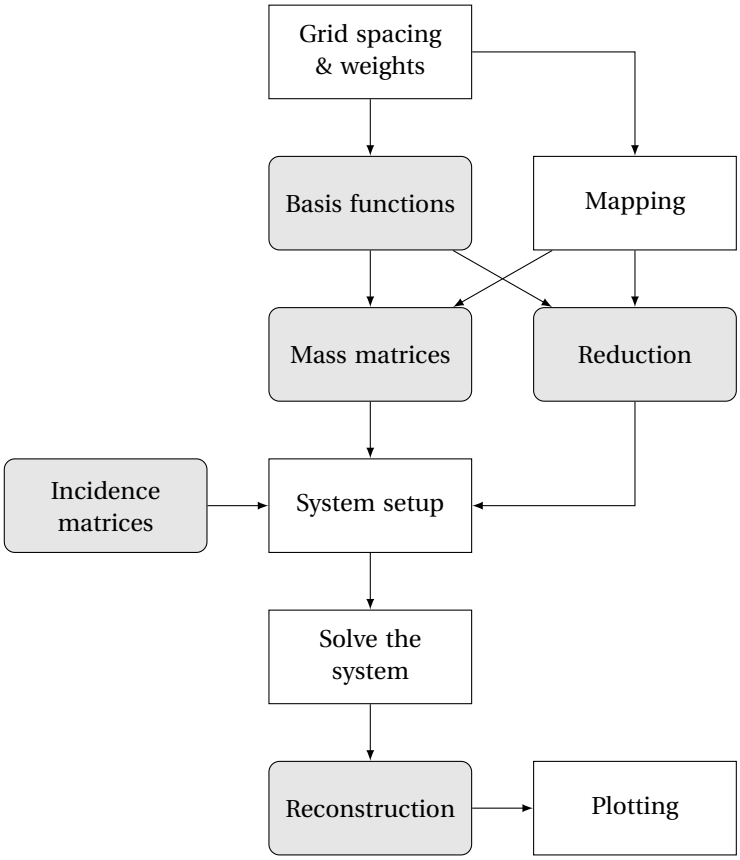

Figure C.1: Schematic flow diagram of the implementation of the mimetic spectral element method. The white square blocks are not specific for the method, as opposed to the grey rounded blocks.